Nonlinear Dynamics, Synchronisation and Chaos in Coupled FHN Cardiac and Neural Cells.

Sepanda Pouryahya

NUI MAYNOOTH

Ollscoil na hÉireann Má Nuad

Thesis presented for the degree of

Doctor of Philosophy

to the

National University of Ireland Maynooth

Department of Mathematical Physics

February 2013

Research Supervisor

Professor Daniel M. Heffernan

Abstract

Physiological systems are amongst the most challenging systems to investigate from a mathematically based approach. The field of mathematical biology is a relatively recent one when compared to physics. In this thesis I present an introduction to the physiological aspects needed to gain access to both cardiac and neural systems for a researcher trained in a mathematically based discipline. By using techniques from nonlinear dynamical systems theory I show a number of results that have implications for both neural and cardiac cells. Examining a reduced model of an excitable biological oscillator I show how rich the dynamical behaviour of such systems can be when coupled together. Quantifying the dynamics of coupled cells in terms of synchronisation measures is treated at length. Most notably it is shown that for cells that themselves cannot admit chaotic solutions, communication between cells be it through electrical coupling or synaptic like coupling, can lead to the emergence of chaotic behaviour. I also show that in the presence of emergent chaos one finds great variability in intervals of activity between the constituent cells. This implies that chaos in both cardiac and neural systems can be a direct result of interactions between the constituent cells rather than intrinsic to the cells themselves. Furthermore the ubiquity of chaotic solutions in the coupled systems may be a means of information production and signaling in neural systems.

Contents

List of Figures

List of Tables

Chapter 1

The Cardiac and Neural System: Physiology and Modeling

1.1 Chapter Introduction and Aim.

The aim of this chapter is to introduce the reader to the biological systems under study, namely the cardiac and neural systems. This chapter outlines the physiological aspects relevant to the creation and propogation of action potentials. The mechanisms involved in cardiomyocyte action potential production and propagation is discussed. Attention is spent on the various regions of the cardiac system and how the cardiac system regulates the flow of action potentials through its conduction system to the bulk muscle mass.

The action potentials of neurons is also discussed with an emphasis placed on what is physiologically known concerning the conduction action potentials through neurons, the ionic mechanisms involved and a brief discussion of ion channel kinetics and structure. This chapter serves as a basis for readers to gain an insight into the complexity of both the central nervous system and the cardiac system. The various technical physiological terms are defined and explored such that future mathematically based researchers will be able to access a number of the key ideas presented in biomedical research concerning both neural and cardiac systems.

1.2 Physiology of the heart.

1.2.1 A General Introduction

The heart is an organ

Definition 1.2.1 (Organ)**.** An organ is a collection of connected *tissue* which serve a common function.

Definition 1.2.2 (Tissue)**.** Tissues are collections of *cells*, which may not be identical, that share the same origins and collectively carry out a specific function.

Definition 1.2.3 (Cell)**.** A cell is the smallest unit of life and is the basic functional unit of all living organisms.

The hearts function as a pump is two fold

- pump oxygenated blood received from the lungs to the rest of the body
- pump deoxygenated blood, along with waste products such as carbon dioxide, received from the rest of the body to the lungs for re-oxygenation.

In order to effectively pump blood around the body, information in the form of waves of electrical potential are used by the heart to effectively trigger cells into contracting.

These electrical impulses are termed *action potentials* and provide a form of communication between the muscle cells, (*myocytes*) within the heart's structure. The dynamical properties of the cardiac cells themselves, such as conduction delays or periods of non stimulability, provide the necessary feedback-response in communication between cells to provide the heart with a robust, dynamic and adaptable structure with respect to stimulus.

It is however the abnormal conduction of the cardiac action potential or equivalently the abnormal propagation of the "excitation wave" that the fundamental function of the heart, pumping blood, is compromised. This abnormal propagation of the action potential can in many cases lead to what is termed *cardiac arrhythmia*.

A cardiac arrhythmia, loosely defined, is any disturbance from the 'normal' propagation of the excitation wave in the heart. Such disturbances can have a dramatic range of effects on the functionality of the heart as a pump. Arrhythmias do also occur in healthy humans, these arrhythmia manifest themselves as an increase in heart rate that do not

greatly effect the efficiency of the heart and can be considered as part of the normal functionality of the heart. There are however arrhythmias that have dangerous consequences which comprise of a large percentage of the number one cause of death in the industrialised world, cardiovascular disease [147]. The most dangerous of the arrhythmias are Ventricular Fibrillation (VF) and Ventricular Tachycardia (VT). The ventricular chamber in the heart is responsible for pumping blood from the heart to the lungs as well as to the body. As it is the ventricles that must produce the force to push blood around the entire body the ventricular muscle structure is the most built up in the heart, we will later go into more detail of the structure of heart muscle in subsequent sections. For now it suffices to know that the ventricles are areas of the heart responsible for the largest part of the hearts realisation as a pump. As such abnormal propagation of excitation waves in the ventricular muscle structure can quickly have large repercussions on the rest of body. This being the reason why ventricular arrhythmias can cause fatality within minutes of its genesis.

1.2.2 The Structure of the Heart

The human heart is made up of four separate chambers, the two chambers at the top are the left and right *atria* while the two chambers at the bottom are the left and right *ventricles*. The left and right sides of the heart are separated by the *septum* which is a collection of collagenous fibres which are more rigid that the rest of the cardiac tissue. There are four main valves in the human heart as shown in figure 1.1 these are the

1. mitral valve
    - located between the left atrium and left ventricle
    - ensures no oxygenated blood is pushed back into the ventricle while it is being pumped through the aorta to every cell in the body.
2. tricuspid valve
    - located between the right atrium and right ventricle
    - ensures deoxygenated blood does not flow into the right atrium from the right ventricle when it is being pumped to the lungs for re-oxygenation.
3. aortic valve
    - located between the left ventricle and the aorta

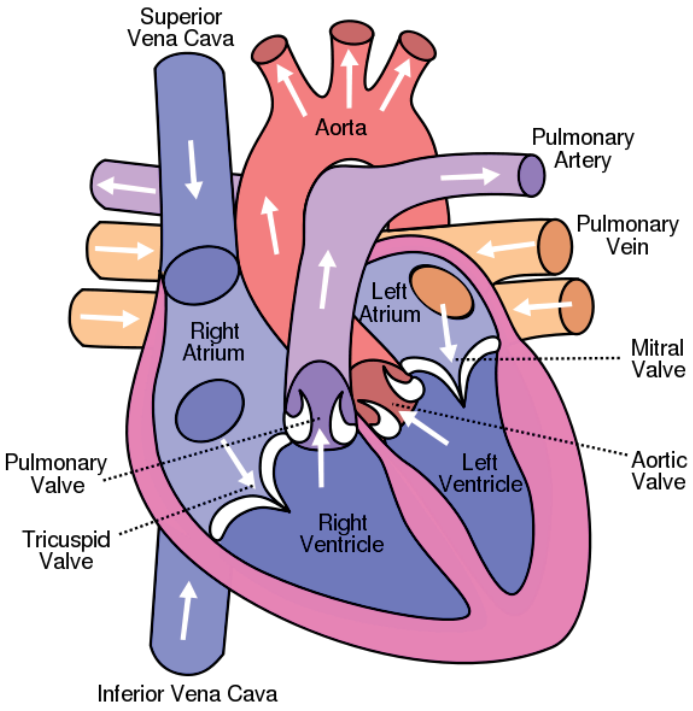

Figure 1.1: The heart, its main chambers, valves and blood flow.

- ensures that oxygenated blood does not flow back into the left ventricle after it has contracted.

4. pulmonary valve

   - located between the right ventricle and the pulmonary artery
   - ensures that the deoxygenated blood being sent to the lungs does not reenter the right ventricle after it has contracted.

These valves are remarkably elegant in the simple manner in which they are designed, their opening and closing being entirely dictated by the blood pressure in the ventricles. The compartmentalisation of the heart is a necessity unique to complex organisms in contrast to the basic tubular hearts of mollusks and insects. To understand the need for this level of complexity in what is essentially a pump one can gain a great deal of insight by looking at the blood pressure in each of the chambers. In humans the atrial pressure at rest (given in units of torr[1]) are given in table 1.1
while in the ventricles the pressures needed to pump blood through the body (left ventricle) and to the lungs (right ventricle) are given in table 1.2.
Not only do the left and right sides of the heart keep the oxygenated and de-oxgenated bloods from mixing, they also pump the blood with different pressure. The right ventricle

[1] 1 Torr is defined as $\frac{1}{760}$ of a standard atmosphere. Using SI units we have 1 Torr = 133.3224 pascal.

Atrial Pressure	
Left	Right
10 mm Hg	0-8 mm Hg

Table 1.1: Typical human atrial pressures.

Ventricles Pressure	
Left	Right
118-138 mm Hg	15-30 mm Hg

Table 1.2: Typical human ventricular pressures.

sends blood to the lungs at which point the waste products in the blood are exchanged for oxygen by osmosis in delicate structures known as *alveoli*. At which point it should be clear why the pressure from the contraction of the right ventricle is relatively small as higher pressures could rupture the alveoli leading to bleeding in the lungs. On the other side of the heart the left ventricle is responsible for sending the oxygenated blood throughout the entire systemic[2] system. Thus in order to push the blood through the entire organism the left ventricle must be capable of producing higher force which leads to increased pressure. A fact which is made clear when one examines the tickness of the ventricular muscle walls, known as *myocardium*, of the human heart

Ventricular myocardial thickness	
Left	Right
15 mm	2mm

Table 1.3: Typical human ventricular myocardial thickness.

The pressures found in the ventricles can be understood well from the function of the chambers. The atria however serve as prechambers for the ventricles, why the ventricles require prechambers is a consequence of the *Frank-Starling Mechanism*[38, p 81.] named after Otto Frank[3] and Ernest Henry Starling[4]

Definition 1.2.4. Frank-Starling Mechanism The ventricular contractile force is related to the amount of stretching the ventricle is exposed to prior to contraction. Hence the

[2]This being the system which carries oxygenated blood away from the heart to the body
[3]German Physiologist 1865-1944
[4]British Physiologist 1866-1927

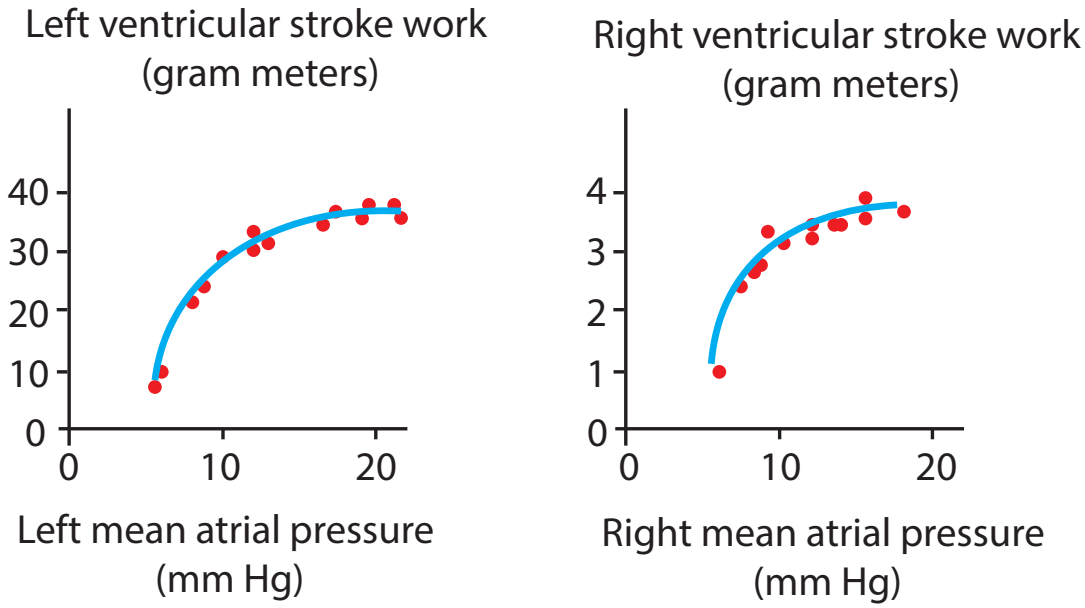

Figure 1.2: The Frank-Starling law showing that increased atrial pressure results in more forcible contractions of the ventricles. Figure recreated from [69, p 112] based on data from [151].

force of contraction in the heart is dependant on the volume of blood present (which stretches the ventricular muscle tissue) in the ventricle.

As an interesting consequence of the Frank-Starling mechanism it is worth noting the remarkable design feature that this mechanism imposes on the heart. We know that pumping a greater amount of blood into the ventricle results in a more forceable 'beat' from the ventricle[5]. This mechanism's design is simple and effective in situations of emergency. In behavioral situations of rage and/or fear where adrenaline is injected into the blood stream, adrenaline results in arterial contraction and pulse rate increase. This contraction and increase causes blood pressure to rise and the atria to pump more blood into the ventricles. The increased blood introduces an increased stretching of the ventricles and by the Frank-Starling mechanism a larger beat. This increase in ejection force overcomes the increased atrial back pressure and pumps more blood around the system increasing the circulation rate and providing an increase in energy available to the organism, thus providing the organism with an effective means to cope in its environment.

[5]There is an upper limit to this mechanism as is with all real systems. At large stretching of the ventricle the Frank-Starling mechanism breaks down, as is the case in high blood pressure patients that receive sudden sock, the heart may in fact entirely fail to beat, or beat with only a small force that can result in cardiac failure

1.2.3 The cardiac muscle fibre and their orientation

The chambers of the heart are made up of fibres of muscles. These fibers are oriented in twists and curves about each other in order to optimize their pumping action. This twisted orientation allows the ventricles to have an additional twist to the upward pressure which directs the blood to either the pulmonary or systemic circuit outflow depending on which side of the heart the blood is in. Muscle fibres are chains of cardiac muscle cells connected in series predominantly in the longitudinal direction via communicating junctions known as *gap junctions*

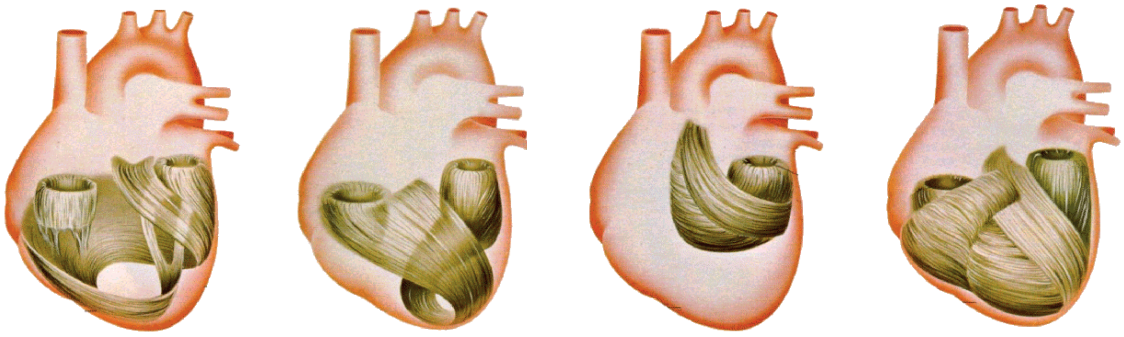

Figure 1.3: The fibre orientation of the canine heart from [110, p167].

Relating fibre orientation, Figures 1.3 and 1.4, to cardiac function is a difficult task that pushes both theoretical and experimental investigation [61, 30, 175].

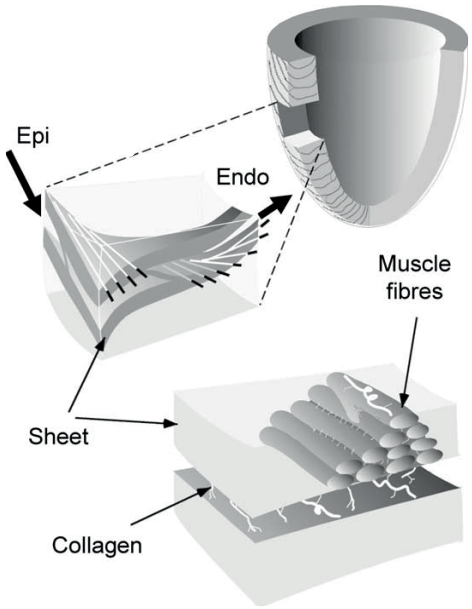

Figure 1.4: Idealised transmural block cut from the ventricular wall showing the change in fibre orientation. Figure from [175]

The current imaging techniques are based on Diffusion Tensor Magnetic Resonance Imag-

ing (DT-MRI). DT-MRI measures the diffusion of water in tissue, cardiac fibres contain microstructure that influence the direction of diffusion, thus making them detectable. The corresponding diffusion information that is gained in the imagining using the techniques of traditional magnetic resonance imaging is stored in a tensor, this change from analog-to-digital (scanning-to-tensor) information allows the data to be more readily manipulated for observation and interpretation. From the tensor the corresponding eigenvectors and eigenvalues can be extracted[13] to yield the directions of least and greatest diffusion. The method is to examine the data in terms of three directions, leading to three eigenvectors with three corresponding eigenvalues. The largest eigenvalue indicates that its eigenvector is the primary direction which follows the fibre direction. The other two eigenvalues also give their corresponding eigenvectors significance, the secondary points in the transmural direction while the tertiary is found parallel to the epicardial tangent plane [154, 80]. Implementing methods to calculate the eigenvectors and to conclude the tracts from the DT-MRI data is still an active area of research with applications in neural imaging where the hope is to visualize and study the neural pathways in vivo [12].

1.2.4 The Cardiac conduction system

The Cardiac Conduction System, Figure 1.5, is responsible for initiating, synchronising, timing and propagating the contraction signal to the myocardial cells in the heart. The conduction system transmits information by creating a propagating wave containing the "contract" signal known as the *Action Potential* (AP). The primary structures responsible for the conduction of action potentials are shown in figure 1.5

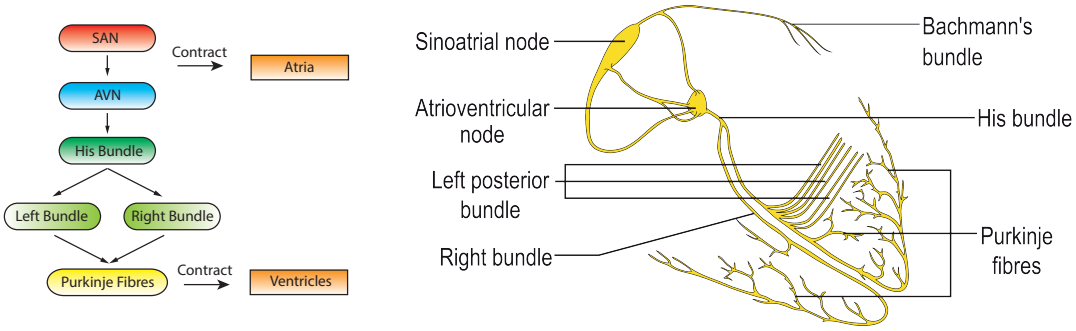

(a) Flow chart of the cardiac conduction system

(b) Anatomical representation of the hearts conduction system

Figure 1.5: The cardiac conduction system.

The Genesis of the heart beat: The Sinoatrial Node

The heart beat begins with the genesis of an Action Potential. This is the signal, in the form of a wave of electrical potential, whereby the cells through out the cardiac myocardium will be instructed to contract. The action potential is created in a cluster of *pacemaker cells* found in the right atrium near the vena cavae known as the sinoatrial node (SAN)[6].

The sinoatrial node itself is made up of excitable cells that have the property of *automaticity*.

Definition 1.2.5 (Excitable Cell)**.**
This is a cell that when stimulated is capable of producing an action potential.

Definition 1.2.6 (Automaticity)**.**
An excitable cell possessing this property is capable of producing an action potential without the need of an external stimulus.

Each cell in the sinoatrial node spontaneously creates a current of a certain frequency by energy consuming biochemical processes intrinsic to the cell.

It's important to note that these cells are not absolutely identical, as is the case with all real systems, as such each cell individually produces a current at its own natural frequency. This however leads to a problem when we consider the effect of action potential signals of multiple frequencies spreading over the hearts myocardium.

As stated previously the action potential is the "contraction signal" that is transmitted to all of the cells in the hearts muscle structure. It necessarily needs to be a coherent wave of uniform frequency if it is to ensure the optimal spread of contraction throughout the heart. The accurate triggering of cells to contract results in the effective pumping of blood throughout the cardiovascular system.

Thus the problem is such; with the SAN being made up of cells that together produce a spread of AP frequencies how does the heart translate these multiple contraction signals into the well timed and effective contractions that makes up the normal heart beat?
The answer may lie in a physical phenomenon termed *synchronisation* which is due to the dynamical restraints on each cell that intercellular coupling imposes.

[6]We note that this is the case in healthy hearts. In some cases the SAN is dominated over by different regions of self sustained excitable cells, this in many cases is a life threatening condition.

Definition 1.2.7 (Synchronisation)**.**
Synchronization is an adjustment of rhythms of oscillating objects due to their weak interaction. [134, p 8]

Pacemaker synchronisation in the SAN has been extensively studied theoretically and experimentally to great effect [116, 115, 194, 183, 65]. In some cases it has lead to performing man made coupling between between SAN cells [183] which may lead to a means of physically controlling this phenomena in "biological oscillators". The theoretical treatment of pacemaker synchronization is still an open problem. The difficulties lie in examining the property of synchronization when the inhomogeneous nature of the pacemaker frequencies is taken into account, though an elegant theory of N coupled homogenous cells has been formulated [118] and progress has been made concerning the introduction of inhomogeneity to the theoretical models [78].

The SAN

Fibre diameter	Conduction Velocity	Intrinsic Firing rate	Rest Voltage
3-5 μ m	$\sim$2 cm/s	70-80 bpm	-55 to -65 mV

Table 1.4: Properties os the SAN [69, p 116-120][109, vol 1, p150].

Atrial Contraction and AP Delay: The Atrioventricular Node

The production of the "contraction signal", action potential, originating from the SAN is dynamically linked to the physical process of synchronisation. The pumping of blood around the body is directly linked to the propagation of the wave of the action potential to the myocardial cells in the heart. The SAN is located in the right atrium and the genesis of the AP wave causes the atria to contract. This is achieved by the rapid conduction of the AP through Bachmann's bundle[7] to the the myocardial mass comprising the wall of the left atrium. Simultaneously the AP wave from the SAN is conducted to the right atrium [8] leading to simultaneous contraction of both the left and right atria.

The conduction of AP through the atria is rapid. After atrial stimulation the AP finds its way through the muscle mass to the *atrioventricular node* (AVN) junction. The AVN

[7]This is the only conduction pathway, known as a *tract*, to the left atrium.

[8]It was believed in the 1970-1980s that there were three tracts that conducted the AP to the right atrium the *Anterior*, *Middle* and *Posterior Internodal tracts*[88]. In more recent times however it is believed that the conduction from SAN through the atria is conducted through *preferential conduction due to anisotropic properties of cardiac muscle.* For a more in depth discussion the reader is referred to [109, vol 1, p 151]

The Atrial Muscle Mass

Fibre diameter	Conduction Velocity	Intrinsic Firing rate	Rest Voltage
	0.3 - 1 m/s	bpm	-85 to -90 mV

Table 1.5: Properties of the Atrial muscle mass [69, p 116-120].

junction is made up of a dense network of cells which delay the conduction of the AP to the rest of the heart. No single factor is responsible for the slowing of the impulse in this area, some of the factors involved in the slowing of AP are [109, Vol 1. p 155]

- The small size of AV nodal cells.
- The scarcity of intercellular connections
- The complex network of small bundles separated by connective tissue where summation and collision of impulses occur.

The role of the AVN junction is delay the AP signal from reaching the ventricles of the heart long enough so that the mechanical process of pumping blood from the contracting atria fills the ventricles. After the ventricles are filled the AP is rapidly passed through the remainder of the conduction system.

An interesting point to note is that there is no backward conduction of AP from the AVN to the atria. This remarkable specialisation of AVN junctional cells is due to the length of their *refractory period*.

Definition 1.2.8 (Refractory Period)**.**
The refractory period of a cell is the amount of time that an excitable cell requires before it is capable of producing a second action potential response from a second stimulus after it has produced a response from an initial stimulus.

The AV node also plays an important role as a **secondary pacemaker** where the SAN is the **primary pacemaker**. The key is that AV nodal cells have the property of automaticity and are capable of producing action potentials without stimulus. The natural frequency of AP production in isolated AVN cells is lower than that of the SAN. The coupling between the SAN and the AVN through the atria ensures that the AVN cells are *entrained* or *locked*[9] to the frequency of the SAN.

[9]In this thesis the terms entrainment and locking are used synonymously.

The AV Node Junction

Fibre diameter	Conduction Velocity	Intrinsic Firing rate
7 μ m	$\sim< 5cm/s$	40-60 bpm

Table 1.6: AV Node junction properties [109, Vol. 1, p 155].

Definition 1.2.9 (Frequency entrainment/locking)**.**
Given two nonidentical oscillators with their own frequencies that are coupled. The coincidence of their frequencies is referred to as frequency entrainment.

Automaticity in the AVN gives the heart a back up means of propagating the contraction signal to the heart should the SAN fail to produce an AP response.

Definition 1.2.10 (Ectopic beat)**.**
A contraction of the heart due to an action potential response not originating for the sinoatrial node.

Ventricular Contraction: The Purkinje Fibres

After the ventricles of the heart have been filled by blood entering via the atria, the AP signal is conducted through the AVN, the bundle of His [10] and the bundle branches to the apex of the heart. At the apex of the heart the bundle branches spread into a fractal-like structure known as the Purkinje network where the conduction system finally makes a direct interface with the ventricular myocytes. This specialised set of cells from the AVN to the ventricles is composed of Purkinje myocytes, longitudinally oriented in bundles, packed by dense connective tissue. [109, vol 1, p109]

The Purkinje Fibre

Fibre diameter	Conduction Velocity	Intrinsic Firing rate
50 μ m	$\sim 2-4m/s$	25-40 bpm

Table 1.7: Purkinje Fibre properties [109, Vol. 1, p 156].

The formation of irregularities in the contraction of the ventricles can lead to *ventricular fibrillation*. Fibrillation, which can also occur in the atria, is a form of contraction of a cardiac chamber which is a chaotic fluttering of the the muscle mass. The action potential wave is seen to break up into *reentrant waves* of smaller size until the heart no longer effectively pumps blood through the system. Ventricular fibrillation is a type of cardiac

[10] Named after the Swiss cardiologist Wilhelm His Jr. whom discovered the His-bundle in 1893.

arrest, know as sudden cardiac death it is the leading cause of death in the industrialised world[199].

The Ventricular Muscle Mass

Fibre diameter	Conduction Velocity	Intrinsic Firing rate	Rest Voltage
m	∼60cm/s	bpm	-85 to -90 mV

Table 1.8: Properties of the Ventricular muscle mass [69, p 116][109, vol 1, p150].

1.3 The Cardiac Action Potential

Cardiac action potentials are potential differences across the muscle cell membrane known as the *sarcolemma*.
Excitable cells, such as are found in the heart, at rest maintain a constant nonzero potential[11]. This nonzero *rest potential* is a result of the intracellular and extracellular concentrations a fact that shall be discussed shortly. When stimulated[12] (electrically) a cell will not produce an exciton response if the the stimulus is not large enough, such a stimuls is termed a *subthreshold stimulus*. If the stimulus is large enough the stimulus is termed *superthreshold*, shown in Figure 1.6, and the cell produces an action potential consisting of 5 phases.

1.3.1 Phases of the Cardiac Action Potential

Action potentials created/transmitted through different regions of the heart have different shapes and amplitudes. The *morphology* of the action potential varies with differing cardiomyocyte types. This is due to the variety of different ionic currents typically found in myocytes in different regions of the heart.

The flow of ions along electrochemical gradients is the mechanism by which potential differences are maintained across a myocytes cell membrane. For 'typical' action potentials[13] these phases are easily distinguishable on the action potential's voltage vs. time profile.

[11] We are here purposefully not taking automaticity into account here.
[12] by means of an external current - this could be an AP from another cell or simply an electrode
[13] Typical here is referred to as any non-pacemaker action potential. The Purkinje network is however not excluded from the 'typical' class as its action potential is similar to that of the non-pacemaker regions of the heart.

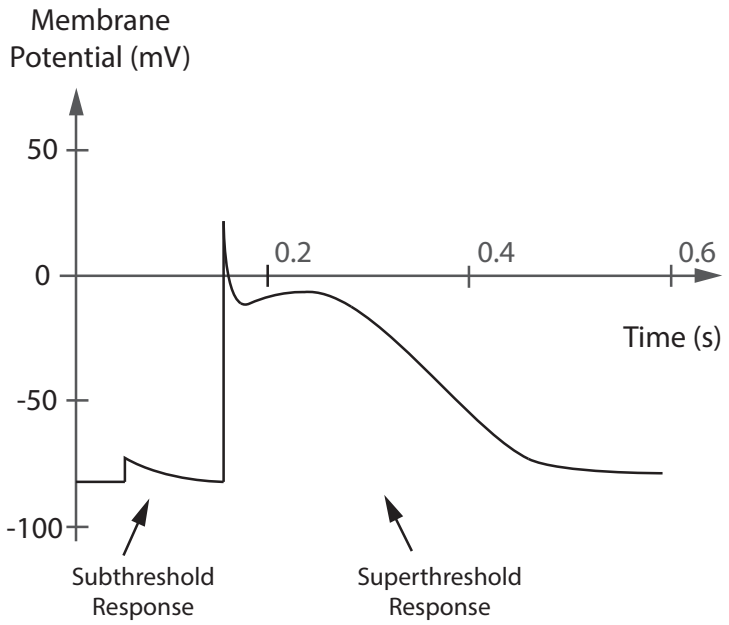

Figure 1.6: Subthreshold and superthreshold responses to stimulus.

The phases are, shown in Figure 1.7

Phase 0. Upstroke: Rapid Depolarisation.

Phase 1. Notch: Early repolarisation.

Phase 2. Plateau: Balance between inward and outward currents.

Phase 3. Rapid repolarisation.

Phase 4. Return to rest potential.

Action potential phases are mediated by different ion movements producing ionic currents I_{ion}. These ionic currents flow both inward and outward along electrochemical gradients while the release of ions is subject to various gates that allow or inhibit their flow. The ionic currents flow in two directions, *inward currents* correspond to the flow of positive ions into the cell causing depolarisation while *outward currents* correspond to the outward flow of positive ions from the cell resulting in repolarisation.

The major ion fluxes composing the action potential are mediated by Na^+, K^+ and Ca^{2+}. The rapid upstroke, that corresponds to the rapid depolarisation of the cell, is a result of the *fast inward sodium current* I_{Na}

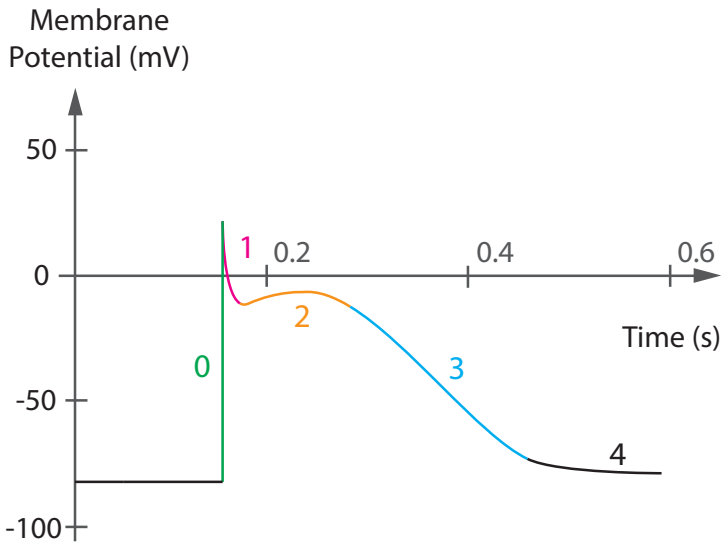

Figure 1.7: The phases of a typical (Purkinje) cardiac action potential.

Phase 0

The upstroke, or autoregenative deoplarisation, when a suprathreshold stimulus is applied to an excitable cell, occurs when the stimulus activates sodium (Na), calcium (Ca) and potassium (K) gates. Phase 0 is predominantly due to the rapid inward movement of Na ions (inward sodium current I_{Na}) causing the cell to depolarise[14], the inward movement of Ca ions (inward sodium current I_{Ca}) into the cell, which also depolarises the cell, results in an abundance of Ca^{2+} ions which is required to trigger myocyte contraction[15].

After depolarisation the potential triggers the closing of the Na and Ca gates and activates the outward K gates resulting in the outward transient current I_{to}, which marks the end of Phase 0.

Phase 1

[14]It is typical in the literature concerning action potentials to refer to depolarisation as an positive charge of charge across a cell membrane and repolarisation as a negative change in charge.

[15]The process by which this electrical potential translates into a mechanical contraction is termed Excitation - Contraction coupling[16]. E-C coupling itself is a cellular process where by the depolarization of the sarcolemma overlying the terminal cisternae of the sarcoplasmic reticulum (SR) induces the release of Ca(2+) from the SR. This calcium release binds itself to a binding subunit found in the protein troponin which activates the cellular contraction.

Phase 1 is characterised by the outward movement of K^+ ions from the cell which results in an early repolarisation through the I_{to} current. This current is quickly activated and inactivated in a manner similar to the I_{Na} current present in phase 0.

Phase 2

The plateau phase is composed of the algebraic sum of both inward and outward moving currents. The effect being that the net change in membrane potential is small. The predominant currents are due to the delayed rectifier current[17] I_{K}, residual outward I_{Na} and the L-type calcium current I_{Ca}. There is also an *exchange* current where the cell physically exchanges sodium ions for calcium ions within this phase $I_{\text{Na-Ca}}$ which also contributes to Phase 2.

Phase 3

The rapid repolarisation present in phase three is mediated by the two delayed rectifier currents I_{Kr} and I_{Kl}. I_{Kr} is responsible for the initial repolarisation while I_{Kl} brings the cell to its rest potential toward the end of the Phase 3.

Phase 4

The final stage describes the myocyte during its noncontracting, relaxed, phase. This phase depends on the final current from phase 3, namely the delay rectifier current I_{Kl}. For cells expressing a significant I_{Kl} (such as in atrial and ventricular myocytes) the rest potential is stablised close to the Nernst potential ensuring that only a significant stimulus will produce an AP response. Cells that have a less pronounced I_{Kl} current (Purkinje cells) or absent I_{Kl} current (nodal cells) have a more unstable rest potential, allowing small stimuli to trigger action potentials.

[17] This is actually the sum of two outward potassium currents I_{Kr}, the rapid rectifier current and I_{Ks}, the slow rectifier current.

Summary of major ion fluxes involved in the AP phases

Current	Selective Ion	Current Direction	AP Phase	Effect
I_{Na}	Na^+	Inward	0	Depolarising
I_{CaT}	Ca^{2+}	Inward	0	Depolarising
I_{to}	K^+	Outward	1	Early repolarising
I_{CaL}	Ca^{2+}	Inward	2	Plateau
I_{Kr}	K^+	Outward	3	Repolarising
I_{Ks}	K^+	Outward	3	Repolarising
I_{Kl}	K^+	Outward	4	Return to rest potential
I_{t}	K^+/Na^+	Inward	4	Depolarising/pacemaking

Table 1.9: Table of major currents contributing to the phases of the action potential, taken from [159, p 48]

1.3.2 Action potentials and Ion Channels.

The production of action potentials in an excitable cell, be it a neuron or cardiomyocyte, is regulated by the influx or efflux of ions through the cells membrane.

Definition 1.3.1 (**Cell Membrane**)**.** This is a membrane consisting of phospholipids (in a bilayer) which acts as an insulator. The cell membrane ensures that the various proteins, ions and organelles are kept separate from the extracellular space and provide the cell with a physical structure.

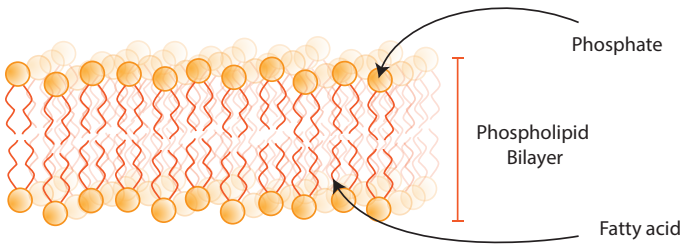

Figure 1.8: The Phospholipid bilayer making up the cell membrane.

The movement of ions across the cell is mediated by structures found in the phospholipid cell membrane known as

Definition 1.3.2 (**Ion Channels**)**.** Ion channels are proteins made up of long chains of amino acids, that are laced through the cell membrane of an excitable cell. Ion channels

are pores which have selective permittivity to in influx and/or efflux of ions through the membrane [50].

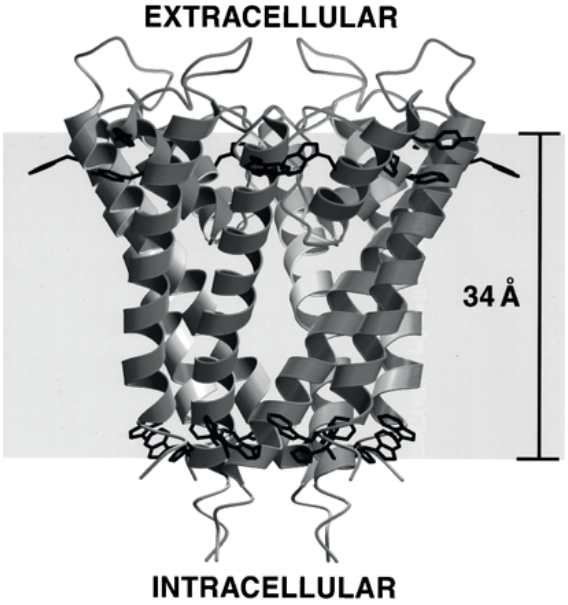

Figure 1.9: Ion channel protein representation [50]

Ion channels allow the passage of thousands of specifically selected ions per second. They do this by bringing about changes in their *conformational shape* via energy consuming processes. The changes of conformational shape are sensitive to both voltages and ligand[18] concentration making them **voltage gated** and **ligand gated** ion channels. The 'gating process' (opening and closing of the ion channel) takes place on the millisecond timescale the details of which are still open problems in the field of *ion channel kinetics*. This topic is not considered here in any detail, however the interested reader is referred to [28, 201] and references therein for an introduction.

It is estimated a typical neuron has on the order of 10,000 ion channels [25], the number of different ion channels are extensive however for excitable cells found in the heart or central nervous system, the channels that regulate the movement of Na^+ (sodium ions), K^+ (potassium ions) and Ca^{2+} (calcium ions) are the most influential in dictating the shape of an action potential. Different ions induce different potential responses across the cell membrane. The interaction of ion channels, pumps and exchangers in excitable cells and their relation to the morphology of the action potential is an extensively studied area of cardiac and neural electrophysiology. The range of ionic based models for cardiac systems alone is extensive

[18] A collective term for ions and molecules.

Table 1.10: Cardiac Ion Models.

Model	Species	Parent Model
Ventricular cell models		
Noble et al.[124]	Guinea Pig	Earm and Noble[51]
Luo and Rudy[107]	Guinea pig	Beeler and Reuter[15]
Nordin[126]	Guinea pig	-
Luo and Rudy[108]	Guinea pig	Luo and Rudy[107]
Jafri et al.[87]	Guinea pig	Luo and Rudy[108]
Noble et al.[125]	Guinea pig	Noble et al.[124]
Priebe and Beuckelmann[138]	Human	Luo and Rudy[108]
Winslow et al[198]	Canine	Jafri et al.[87]
Pandit et al.[129]	Rat	Demir et al.[42]
Puglisi and Bers[139]	Rabbit	Luo and Rudy[108]
Bernus et al.[17]	Human	Priebe and Beuckelmann[138]
Fox et al.[58]	Canine	Winslow et al[198]
Greenstein and Winslow[68]	Canine	Winslow et al[198]
Cabo and Boyden[27]	Canine	Luo and Rudy[108]
Matsuoka et al.[114]	Guinea pig	-
Bondarenko et al.[19]	Mouse	-
Shannon et al.[156]	Rabbit	Puglisi and Bers[139]
ten Tusscher et al.[169]	Human	-
Iyer et al[85]	Human	-
Hund and Rudy[83]	Canine	Luo and Rudy[108]
ten Tusscher et al.[170]	Human	ten Tusscher et al.[169]
Atrial Cell Models		
Earm and Noble[51]	Rabbit	Hilgemann and Noble[74]

Continued on Next Page...

Table 1.10 – Continued

Model	Species	Parent Model
Lindblad et al.[103]	Rabbit	-
Courtemanche et al.[39]	Human	Luo and Rudy[108]
Nygren et al.[127]	Human	Lindblad et al.[103]
Ramirez et al.[143]	Canine	Courtemanche et al.[39]
Sinoatrial Cell models		
Noble et al[122]	Rabbit	Noble and Noble[123]
Wilders et al.[195]	Rabbit	Noble and Noble[123]
Demir et al.[42]	Rabbit	-
Dekos et al.[48]	Rabbit	Wilders et al.[195]
Dokos et al.[49]	Rabbit	Dekos et al.[48]
Demir et al.[43]	Rabbit	Demir et al.[42]
Endresen et al.[53]	Rabbit	-
Zhang et al.[202]	Rabbit	-
Boyett et al.[21]	Rabbit	Zhang et al.[202]
Zhang et al.[203]	Rabbit	Zhang et al.[202]
Kurata et al.[99]	Rabbit	-
Sarai et al.[150]	Rabbit	-
Lovell et al.[1]	Rabbit	-
Mangoni et al.[111]	Rabbit	Zhang et al.[202]

To gain a basic insight into the formation of the action potential in relation to ion channels, it is sufficient to consider an ion channel as being a simple gate which is capable of switching between an open and a closed state.

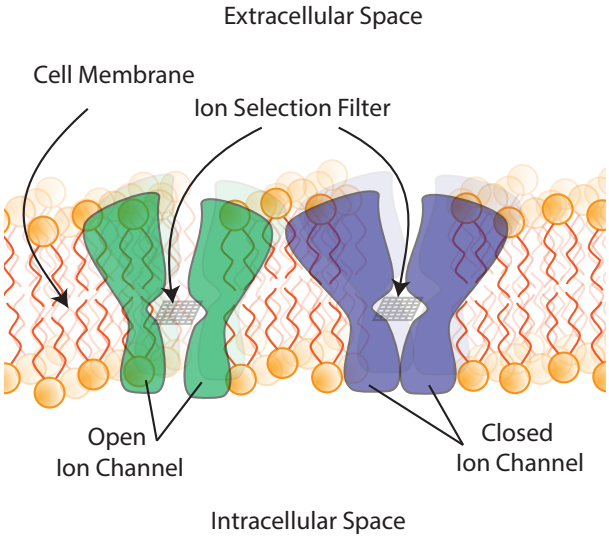

Figure 1.10: A basic representation of an open (green) and closed (blue) ion channel

The rest potential and the chemical gradient

Typical cardiomyocytes and neurons have negative rest potentials in vivo, $-60 - -70\text{mV}$. This potential difference is measured between the intercellular and extracellular space of a cell. The rest potential is produced by means of active transport of ions into and out of the cell in an energy consuming process due mainly to $\mathbf{Na^+}$–$\mathbf{K^+}$ **pumps**. The sodium-potassium pump[19] is an enzyme found laced through a cells membrane.

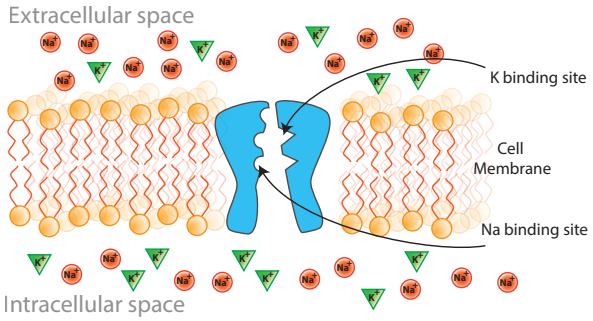

Figure 1.11: The sodium-potassium pump.

This enzyme is capable of moving three Na^+ ions from the cytoplasm of a cell into the extracellular space and two K^+ ions from the extracellular space into the cells cytoplasm. The pump moves ions from a low concentration to regions of high concentration, ie against the potential gradient, making it an *active transport* mechanism. To counter the forces due to the potential gradient the pump requires energy to change its conformational

[19]also referred to as an exchanger.

shape, which it receives from the metabolic process of converting ATP to ADP.

The exchangers lowest energy conformation exposes the regions along its protein chain which have a high affinity for sodium ions, these are *sodium binding sites*. This conformational state allows the binding of sodium from within the cell. This state also suppresses the binding of potassium ions to the potassium binding sites. Thus sodium, and only sodium, binds to the Na-K pump from inside the cell. At this point the pump also has the availability of ATP (also bound to the pump) for energy release.

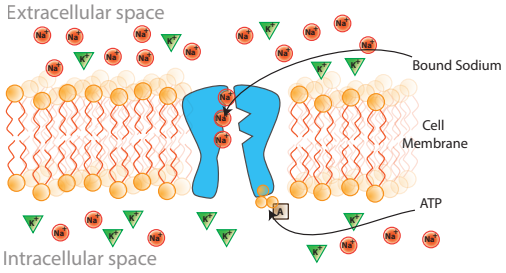

(a) The sodium-potassium pump, with bound sodium and ATP.

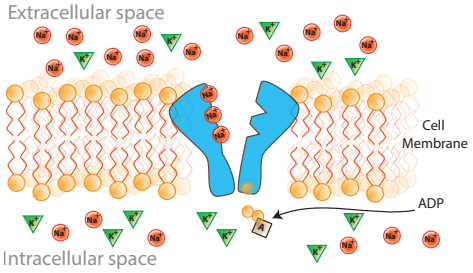

(b) The sodium-potassium pump in a high energy state after the conversion of ATP to ADP.

Figure 1.12: The sodium-potassium pump, from low energy to high energy state.

Through the metabolic process of converting ATP[20] to ADP[21] the Na-K pump has enough energy to change its conformational shape and move the sodium ions from an area of low sodium concentration[22] (intracellular) to a region of high sodium concentration (extracellular), thus doing work against the *chemical gradient*.

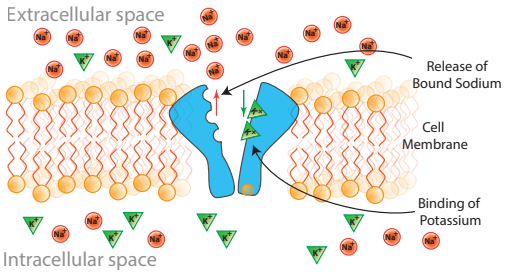

(a) In the high energy state the Na^+ ions do not bind well with the new conformation of the pump, the K^+ binding sites are now active and available for binding.

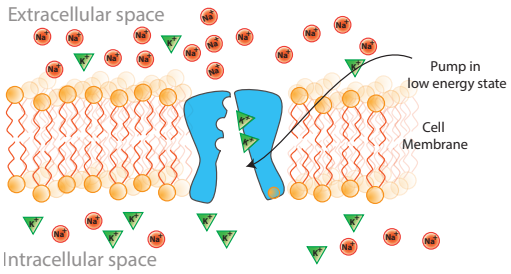

(b) The pump returns to its low energy state with the bound K^+ ions from the extracellular space for release into the intracellular space.

Figure 1.13: The sodium-potassium pump, from high energy to low energy state.

[20] Adenosine triphosphate.
[21] Adenosine diphosphate.
[22] This is low relative to the extracellular space.

The new conformation is weakly binding with sodium and the sodium binding sites release the sodium ions into the extracellular space. This high energy state however exposes the potassium binding sites and potassium is bound the channel from the extracellular space.

After potassium binding the pump returns to its low energy state which is again weakly binding to potassium allowing the release of potassium into the intracellular space.

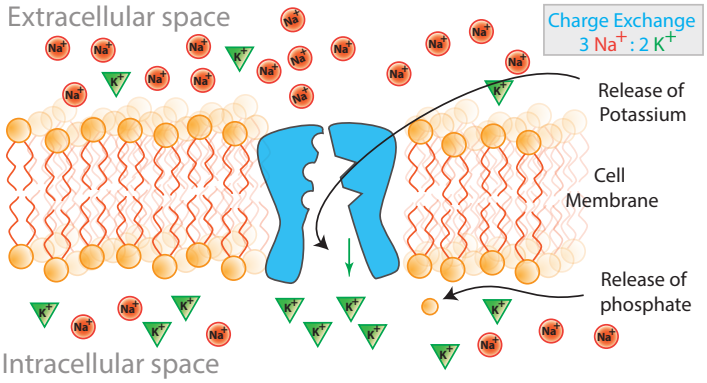

Figure 1.14: After the exchange of 3 Na^+ ions for 2 K^+ ions the effect is a net change in potential across the cell membrane of -1.

The 3 : 2 exchange of positive ions across the cell membrane results in the cell becoming *repolarised*. This process continues typically keeping the cell at its *rest potential*. Furthermore as a direct consequence of the transport due to the Na-K pump there is **an abundance of potassium ions within an excitable cell** and **an abundance of sodium ions outside of an excitable cell**. As is shown in Table 1.11 taken from [69, p 60]

Table 1.11: Potassium and Sodium concentration of a nerve membrane.

Ion	Location	Concentraction
Na^+	Outside	142 mEq/L
Na^+	Inside	14 mEq/L
K^+	Outside	4 mEq/L
K^+	Outside	140 mEq/L

The maintenance of these concentration gradients is vital for the production of action potentials.

The sodium ion channel: The number of different ion channels in humans is still an open problem of discussion, however all ion channels have a simple function - to allow the selective flow of ions across the cell membrane. In order to achieve this function the ion channel has a selectivity filter and a gating mechanism which may be sensitive to, voltage, temperature, ion concentration and mechanical force. The sodium ion channel possesses two voltage-dependant gates. The gates are known as the *activation* and *inactivation* gates. At the sodium gates equilibrium potential (approx -90mV) the gate is inactive.

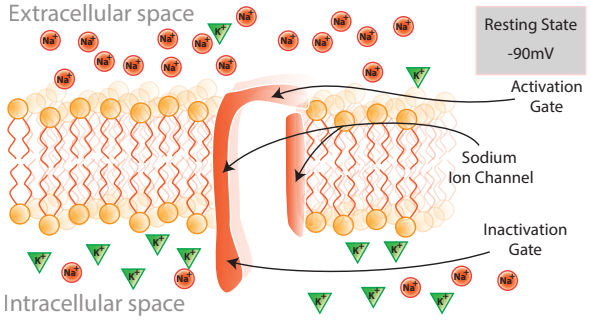

Figure 1.15: The sodium channel while at a rest. Adapted from [69, p 62].

Depolarisation from the rest state causes the (protein) channel to undergo a change in shape. This change in conformational shape puts it in an "activated" state. The filtering mechanism ensures that only sodium ions pass through the sodium channel from the extracellular space (where there is a relative abundance of sodium) into the cell. This movement is due to the sodium (chemical) gradient maintained by the Na-K pump and doesn't require any further energy.

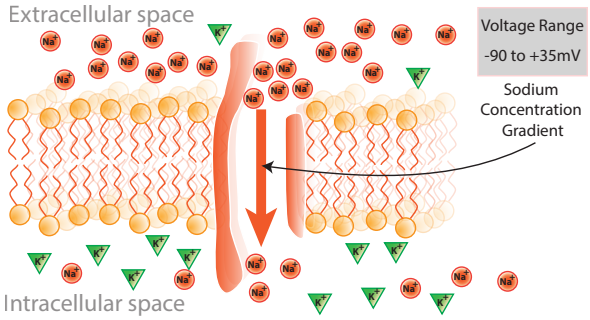

Figure 1.16: The activated sodium channel. Adapted from [69, p 62].

The rapid movement of sodium into the cell causes a sharp increase in the potential difference across the cells membrane. Depolarisation [23] doesn't cause a conformational change in the channels arrangement until the channel has a potential difference of approximately +35mV across its structure at which point the conformation changes until the channel reaches an *inactive* state.

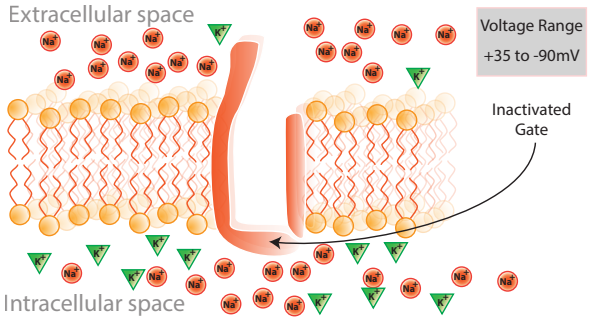

Figure 1.17: The inactivated sodium channel. Adapted from [69, p 62].

Once in this state the channel will remain inactive until the channel returns to its rest potential, at which point the process is capable of repeating itself.

The potassium ion channel: The voltage gated potassium ion channel unlike the sodium channel has a single gate. It remains at its rest state which impairs the outflux of potassium ions from the cell until activation,

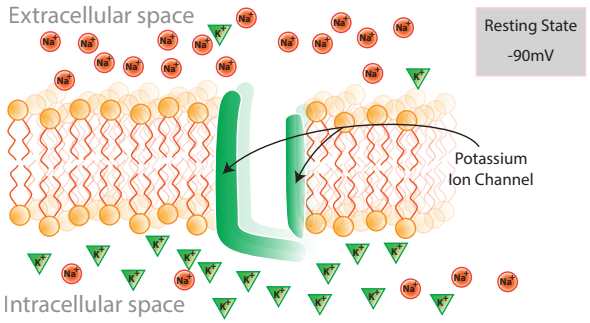

Figure 1.18: The potassium channel. Adapted from [69, p 62].

Once the potential reaches a voltage of approximately +35mV the potassium channel becomes active resulting in the flow of potassium ions due to the potassium (chemical) gradient across the cell membrane. The outward movement of positive charge causes a negative potential difference across the membrane which *repolarises* the cell. This process

[23] This is a local depolarisation; in other words depolarisation across the cell membrane where the sodium channel is located.

of repolarisation returns the cell to its rest potential[24] and inactivates the potassium gate once it reaches -90mV.

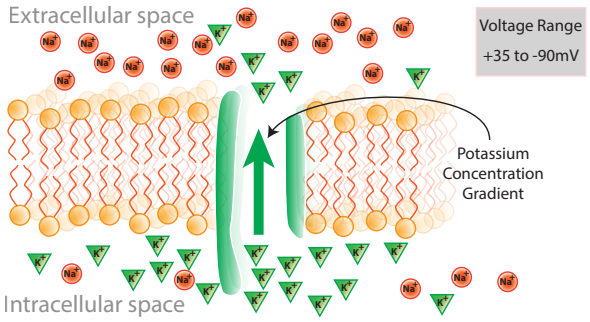

Figure 1.19: The active potassium channel and the outward potassium current. Adapted from [69, p 62].

Variety of ion channels There are a multitude of different ion channels involved in the processes which govern excitable cells. There exist ion channels that are part of the internal structures of cell as opposed to ion channels on the cell membrane. These are not discussed in this thesis however the reader is referred to [75] for a readable text on the subject of ion channels.

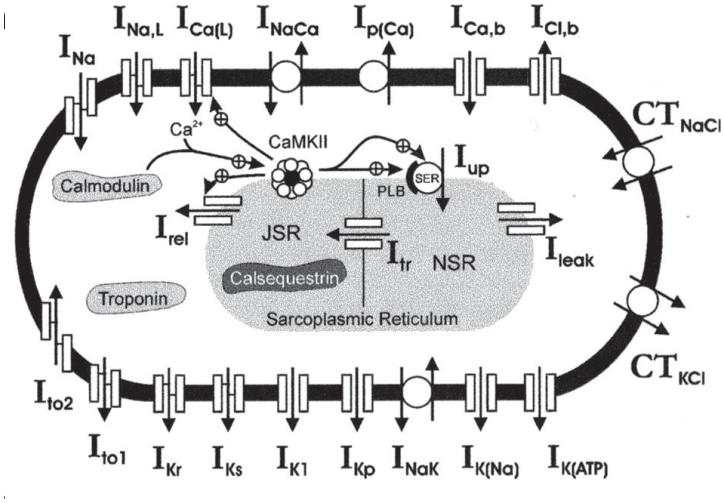

Figure 1.20: Variety of ionic currents in a typical electrophysiological model of a cardiac ventricular cell [82].

[24]The cell can in fact become more negative than its rest potential a situation which is typical but omitted here for the sake of simplicity. This 'extra' repolarisation is known as the *hyperpolarisation* when looking at the profile of an action potential.

1.3.3 Action Potential Morphology

As stated earlier the shape and amplitude of an AP depends on the magnitude and types of ionic currents flowing into and out of a myocardial cell. The myocardial cells regulate the flow of ions differently depending on where in the heart they are found. This gives rise to a variability in the AP forms found in the heart, an illustration of which is shown in figure 1.21.

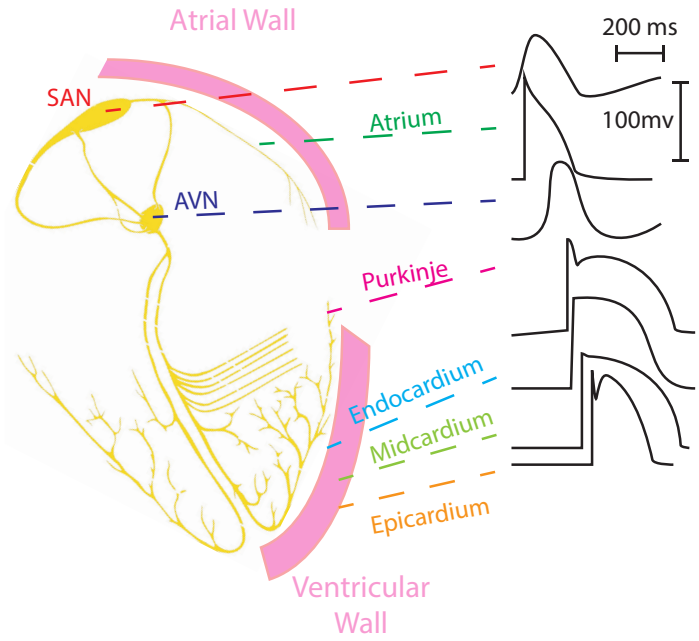

Figure 1.21: Illustration of the morphology of the cardiac action potential.

1.3.4 Excitability and Refractoriness

Excitability is the ease at which a response may be triggered from a cell[22, 84]. Properties such as threshold valueV_{th}, membrane resistance R_{m} and conductance g_{ion} of a cell are directly related to cells excitability.

The excited state of a cell can be seen in the cell's action potential profile, this state being the region of the action potential after the upstroke and ending when the cell has returned (or is near) to its resting potential. During the excited period the cell is found in a *refractory* state. In a refractory state a cell is unable to produce a response from stimulus even though the cell may be at its rest potential[93]. Refractoriness is a result of a cell's ionic channels recovering from a prior excited state, while Na channels in the cell are recovering the cell is unable to produce an upstroke response to a stimulus that is above its threshold value. This behaviour is an example of a cell being refractory.

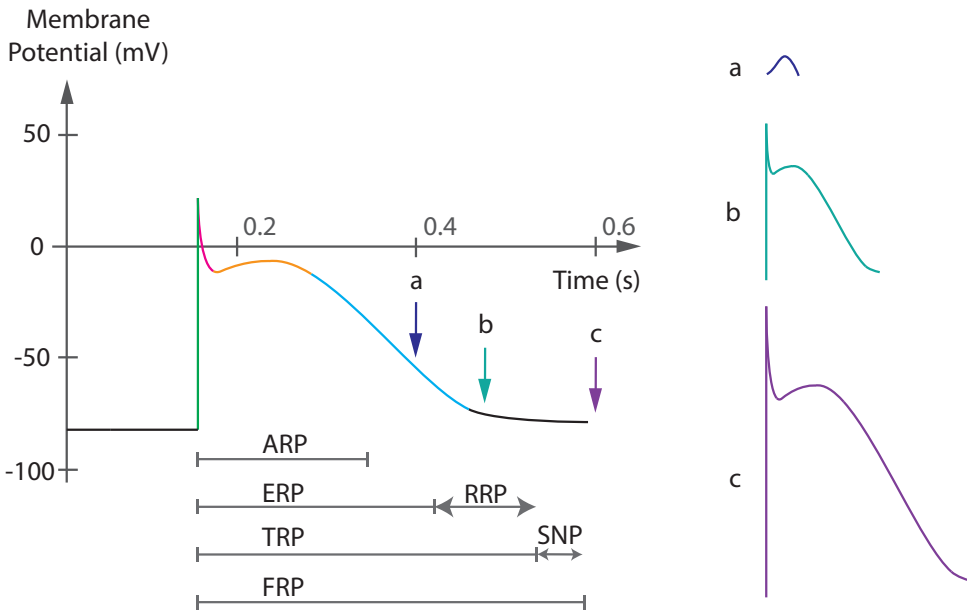

Figure 1.22: Illustration of the refractory periods associated with the action potential. To the right are illustrations of the AP response of stimulating a cell with a suprathreshold stimulus at various points during the cells refractory period.

The transient behaviour of refractoriness is divided into three refractory periods in an action potential's profile; these three distinctions are made based on the cells responsiveness during its refractory state. These three periods are *the absolute refractory period* (ARP), *the effective refractory period* (ERP) and *the relative refractory period* (RRP). The distinctions of these periods becomes more apparent and important when investigating possible mechanisms involved in arrhythmia genesis and considering possible measures that can be taken when developing arrhythmia treatments. The ARP is the duration of time from the depolarization of the cell (the action potentials upstroke) and terminates before the cell is able to produce a local nonconducted response to a stimulus. This is the absolute minimum time required after the depolarization of a myocyte until it is able to produce any response to another stimulus. During the ARP the myocyte is unable to produce any response to a stimulus no matter how large the magnitude of the stimulus. The ERP includes the ARP and is extended until the point in time in which the cell is able to produce a nonconducted stimulus to an external stimulus. This is thus the minimum time a cell needs between two stimuli to produce a response. The RRP begins at the end of the ERP and is the period of time that a cell is able to produce a propagating response to a stimulus that exceeds the normal threshold value of the completely recovered cell. Another period, often used in the literature, before the cell is completely repolarized that has a unique property to stimulus, this is the *supranormal period.* (SNP). The SNP is the period of time that a cell is able to elicit a propagated response to an external stimulus

that is slightly below that of the normal threshold, and is found after the RRP. Although during both the RRP and the SNP a cell is able to produce a propagating action potential, this response differs to the *normal action potential* produced by normal threshold stimulus from a cell that has been given sufficient time to recover, this period is known as the *Full recovery time* (FRT). The difference is that action potential's produced during the RRP and SNP have a reduced amplitude compared to those produced after the FRT [92, 40].

1.3.5 Intercellular Communication - Gap Junctions

The heart's ability to conduct action potential depends on cells communicating with their neighbours. The communication is mediated by *Gap Junctions*[160], which are a form of intercellular coupling of cellular membranes. It has been found that gap junctions play a crucial role in cardiovascular pathiophysiology[46]. Gap junctions are themselves a subcategory of a larger set of cellular connective structures known simply as *cell junctions*. Cell junctions are categorised functionally into *Occluding junctions*[a], *Anchoring junctions*[b] and *Communicating junctions* of which gap junctions are considered a member.

Occluding Junctions
1. tight junctions (vertebrates only)
2. septate junctions (invertebrates only)
Anchoring junctions
Actin filament attachment sites
1. cell-cell junctions (adherens junctions)
2. cell-matrix junctions (focal adhersions)
Intermediate filament attachment sites
1. cell-cell junctions (desmosomes)
2. cell-matrix junctions (hemidesmosomes)
Communicating junctions
1. gap junctions
2. chemical synapses
3. plasmodesmata (plants only)

[a] These provide an intercellular connection that limits/prevents the passage of molecules between cells and the loss of solutes to the intercellular space

[b] These junctions connect cell membranes to cytoskeletal elements (these being networks of protein filaments enabling a cell to maintain its shape and ability for cellular movements.)

Gap junctions provide cells with a communication junction via the passage of small ions[25] between cells and by a process of passive diffusion. Furthermore gap junctions inhibit the passage of nucleic acid and proteins between cells.
Structurally, gap junctions are clusters of intercellular channels between cells which are themselves made of proteins. Vertibrate gap junctions are made up of the *connexin*[26] family of proteins that have evolved from the *innexin* gene family found in invertibrates[132].

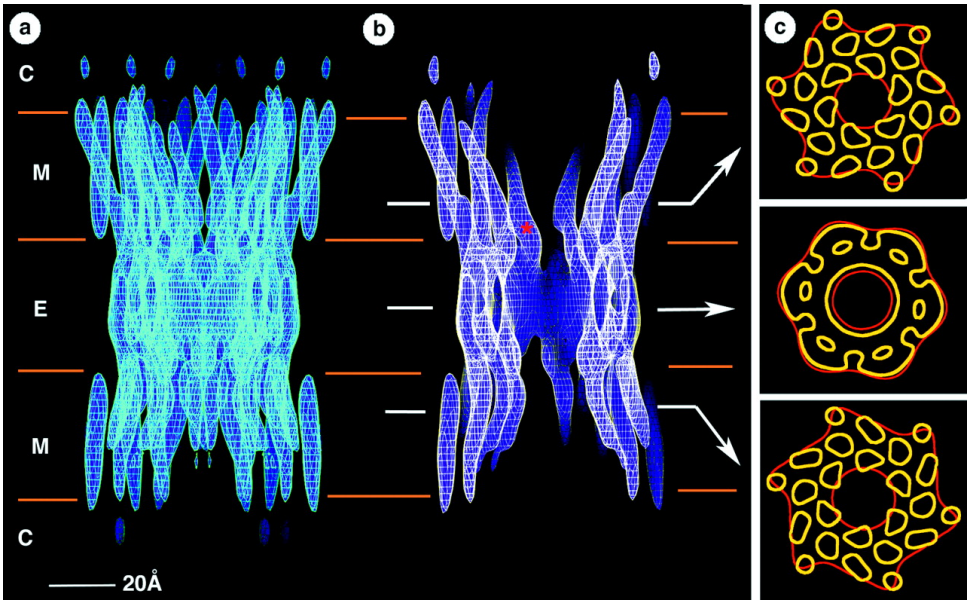

Figure 1.23: The full profile of a gap junction (a), (b) shows the figure (a) with the density cropped to allow for better viewing of the connexin arrangement. Also indicated are the approximate boundaries of the cells cytoplasm (C), the membrane bilayer (M) and the extracellular space (E) [179].

Although connexins express great variation in their properties, they are identified by their similarities in protein sequences and transmembrane topology. There are variations in their lengths but all connexin have four membrane crossing domains (M1-M4), see Figure 1.24, which result in three loops. Two loops occur in the extracellular space E1 and E2 resulting from the connection of the M1-M2 and M3-M4 domains. The third loop occurs within the cells cytoplasm, the cytoplasm loop (CL), and is the region connecting the M2-M3 domains [72].
In situ[27] two cells are separated by intercellular fluid, the membranes of the cells are

[25]Gap junctions also mediate intercellular movement of cytoplasmic molecules and show a rich ability of selective permeability that are not further discussed here, as our main focus here is on the electrical properties of gap junctions, the reader is referred to [71] and references therein for a comprehensive review.

[26]We note that there is another family of proteins, the pannexins, which are present in both chordates and invertibrates which will not be discussed here, the reader is referred to [128] for further reading.

[27]This is a laten term, meaning 'in place' which in the medical sciences referes to observing an object or phenomena in the place where it occurs without moving it elsewhere.

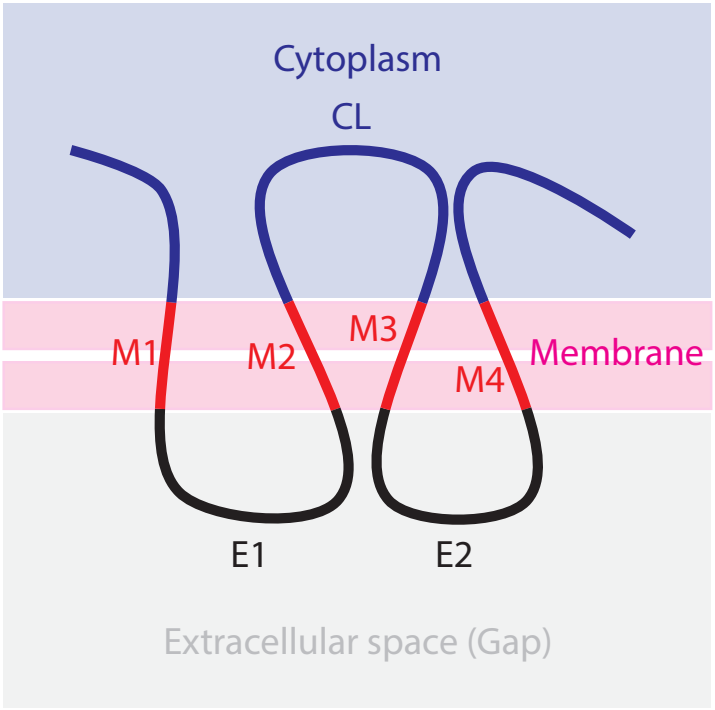

Figure 1.24: The looping of the connexin protein through the cell membrane, figure adapted from [62].

connected with one another by a series of *connexons*. Connexons, see Figure 1.25, are docking locations found on a cell membrane made of connexin proteins arranged in a hexameric structure. Once a connexon of a cell has docked ono the connexon of the adjacent cell a *gap junction channel* is formed. The gap junction channel provides the cells with a means to communicate with another. Multiple gap junction channels together form a structure known as a *gap junction plaque* connecting a cell to its neighbor through multiple locations.

Connexons, and hence gap junctions as a whole, have varied properties and sensitivities depending on their constituent connexin expressions. Connexons have the ability to select what molecules and atomic ions they will allow to be transmitted from a cell as well as what molecules and ions they will accept into a cell. This selective property is known as *permeant selectivity*. Connexons also show *gating*[28] dependencies on *pH* and *voltage* and the ability to rectify unitary conductance[181, 73, 72].

There have been at least 21 connexin genes (Cx23, Cx25, Cx26, Cx30, Cx30.2, Cx30.3, Cx32, Cx31.1, Cx31.9, Cx32, Cx36, Cx37, Cx40, Cx40.1, Cx43, Cx45, Cx46, Cx47, Cx50, Cx59, Cx62) [29] discovered in human gap junctions [149]. Of the 21 connexin there are three main connexin found in the heart. These are connexin 40 (Cx40), connexin

[28]This is the process of opening and closing of the connexon pores to influence.
[29]There are also three pannexin genes identified Px1, Px2, Px3

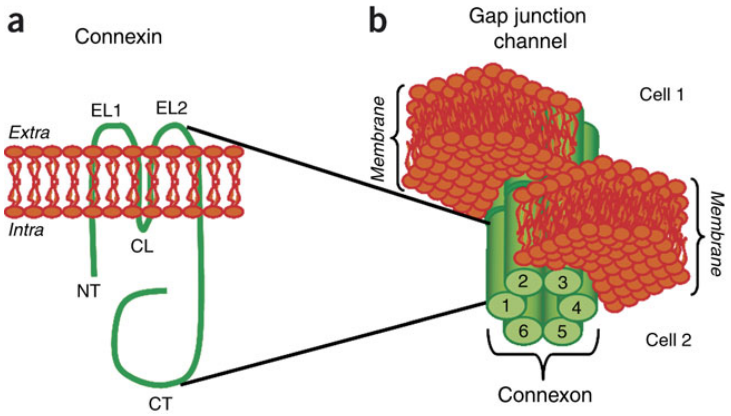

Figure 1.25: (a) shows the membrane topology of the connexin protein, CT is the carboxyl terminus. (b) shows the the joining of two connexons to form a complete gap junction channel [41].

43 (Cx43), and connexin 45 (Cx45). The numbering system used to identify between connexin is based on their molecular weight (measured in kDa, the atomic mass unit) [45]. Cx43 is found in most regions of the heart and is the main connexin expressed in all mammalian ventricles, it is also found in atrial muscle and the His-Purkinje system [67, 184]. Cx40 is mainly found in the atria and the conduction system, abundantly in the SAN and the AVN, and is not expressed in the ventricles see [155] and references therein. Cx45 which is found predominantly in embryonic development is also found in the conduction system of mice and rats [36]. Cx45 is largely absent in the myocardium [35] but is found in the SAN, AVN and BoH [37, 104]. The connexin have a spatial organization about the heart's structure and are summarized in the table below for an adult human[180]

Region Vs. Connexin	Cx40	Cx43	Cx45
SAN	✓	x	✓
Atrial myocardium	✓	✓	x
AVN	x	x	✓
AV Bundle	✓	x	✓
Bundle Branches	✓	x	✓
Ventricular myocardium	x	✓	x
Purkinje Fibres	✓	✓	✓

It is worth noting at this point that the nomenclature used to identify cardiac connexins can lead to some confusion when interpreting results in various species. For example

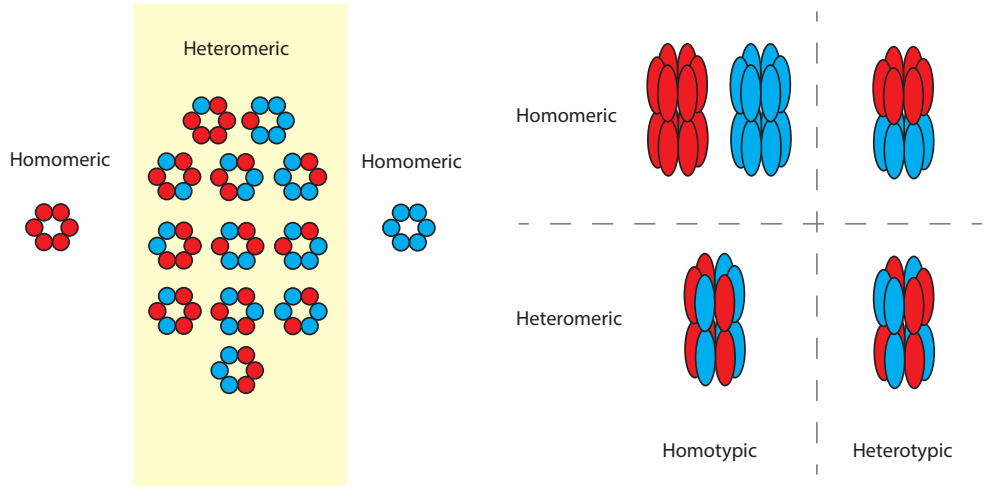

(a) Figure showing the 14 different configurations that a connexon can have if there are two different connexin proteins available for expression. When there are at least two different connexin expressed in connexon the connexon is said to be heteromeric. If the connexon is made up of only one connexin type then it is said to be homomeric.

(b) Figure showing the diversity of gap junctions when two connexon dock.

Figure 1.26: (a) Possible configurations of connexons when there are two connexins. (b) The categorised types of gap junctions that can be formed from the hommomeric and heteromeric connexons. Figures both adapted from [45].

Cx57 in mice have the same function as Cx62 in humans, making Cx57 in mice orthologous to human Cx62[149], thus experimental results found from connexinX from speciesX should not be suggested to hold true for connexinX from speciesY but can be suggested to hold for connexinY in speciesY if connexinX in speciesX is orthologous to connexinY in speciesY. Furthermore *orthologous connexin pairs* may not be express in the same tissue or cell type between the two species [163] and thus a prior knowledge to species dependent connexin orthologous is necessary for comparative work between connexin in different species.

All gap junctions express voltage sensitivity which is a result of the voltage dependant processes found in connexons. In the cardiac system these voltage dependencies influence how action potentials propagate from one cell to the next. Factors such as the distribution and number of gap junctions between cells (which varies across different cardiac regions), the locally dependant orientation of cell relative to its neighbour and a cell's size [164, 81] all effect the conduction velocity. The coupling itself, between cells, has voltage dependencies to consider when trying to build a full dynamical picture of the cardiac system.

Connexin Voltage Sensitivities

1. V_j gating - Macroscopic junction conductance has a dependency on the magnitude of transjunctional voltage [72].

2. Loop-gating - mechanism that can slowly open or close a junctional channel, dependant on transjunctional voltage [176].

3. V_m gating - The steady state of the junctional channel is dependant on the membrane potential of the cells. (distinct from V_j gating)[11]

4. V_m has sensitivity to the initial and instantaneous conductance of the cell. The case when initial conductance is monotonically dependant on V_m has been termed *fast* V_m voltage dependance.[72, 152, 52]

Due to the variations in conductance properties, molecular permittivity and gating properties of connexins the ability to produce heterotypic junctions results in areas of specialization and control in communication between cells in neighboring regions of the heart. This suggests that the spatial distribution of gap junction type is significant for the regional separations of heart functions, such as the separability of the conduction system from the bulk myocardium. The question of how specific hemichannels form the connexin configurations is still an ongoing and active area of research. However there are insights into the types of heterotypic hemichannels that can form between Cx40, Cx43, Cx45, as well as other mammalian and insect connexins that have not been discussed [191, 26, 10, 79, 140]. The variety of possible junctions between cells though diverse shows preference in connexin combination. This has been observed using HeLa cells[30] transfected with Cx40, Cx43 and Cx45. The results shown that heterologous cell pairings of Cx40/Cx43 do not form junction plaques between contacting Cx40 and Cx43 transfected HeLa cells, but form cell couplings between HeLa cells with weak conductance properties. It has been further suggested this is the result of intermediate coupling stages with Cx45 connexins forming heterotypic Cx40/Cx45 and Cx43/Cx45 junctions, for details the reader is referred to [140].

[30]HeLa cells are an immortal cell line derived from cervical cancer cells that are mass cultured for used in medical research.

1.4 Physiology of the brain.

1.4.1 A General Introduction

The brain like the heart is an organ with various regions of specialisation. Here the reader is given a brief overview of the functional aspects of the neural system and its various constituent parts.

1.4.2 Structure of the Central Nervous system

The central nervous system is made up of the **brain** and the **spinal cord**.
The brain itself can be coarsely divided into three basic units; the **forebrain**, the **midbrain** and the **hindbrain**. The forebrain[31], consisting primarily of the **cerebrum**, is the largest and most developed part of of the human brain. The cerebrum is responsible for the higher order functions of the brain such as **cognition**[188, p 2]. This region is greatly effected by diseases such as **Alzheimer's** [192].
The midbrain[32] is responsible for functions such as vision, motor control and sleep wake cycles[23, p 45]. The **thalamus** which is considered a part if the forebrain is found near the midbrain and also contributes to the regulation of consciousness sleep and alertness[33].
The hindbrain[34] is the region of the brain which is most responsible for the control of muscle movement[35].

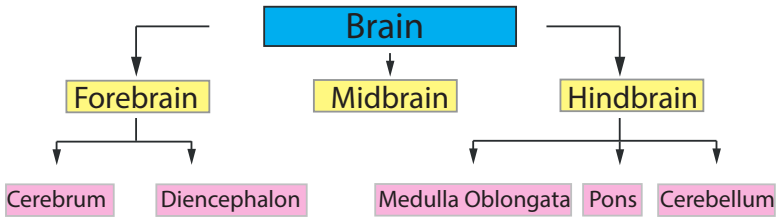

Figure 1.27: Basic division of the brain into the forebrain, midbrain and hindbrain. Adapted from [162, p 5].

Typically there is a complex interplay between the various regions of the brain from stimulus to thought and then action, which is well illustrated by the somatosensory

[31] In the medical literature this region is also referred to as the posencephalon when an organism is in its developmental stage.
[32] In the medical literature this region is also referred to as the mesencephalon when an organism is in its developmental stage.
[33] The thalmus is located between the midbrain and the cerebral cortex and thus also contributes to the relay of motor signals and spatial awareness.
[34] referred to as the rhombencephalon in an organisms development stage.
[35] This excludes the movement of the eyes which is controlled by the midbrain.

system show in Fig 1.28

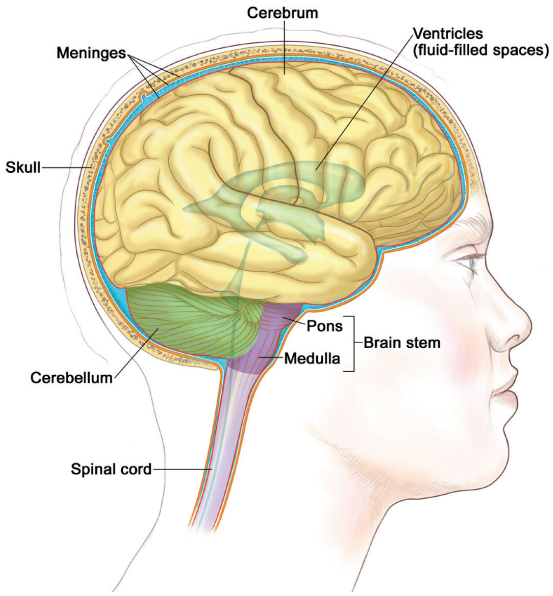

(a) Schematic showing the location of the Cerebrum (forebrain), the (hindbrain) Cerebellum, Pons, Medulla and the Spinal cord.

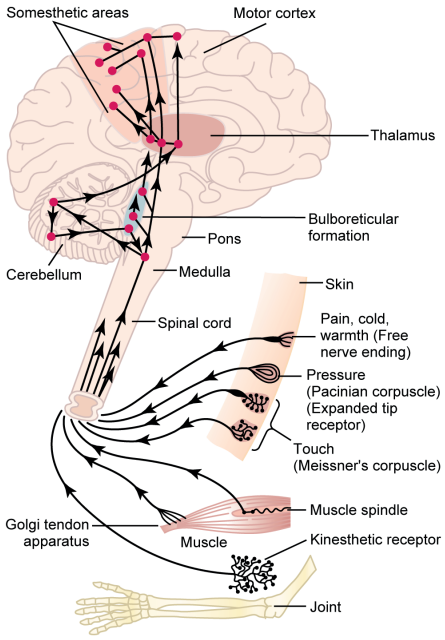

(b) The somatosensory system.

Figure 1.28: The Central Nervous system and the somatosensory system.

A thorough introduction to the function and role of the various compartments and structures present in the brain is not the focus of this thesis and thus the reader is referred to the following texts [14, 162, 23] for further reading.

1.4.3 The Neuron

The central nervous system is made up of two main classes of cells; **neurons** and **glia**. Though there are on the order order of $10^9 - -10^{11}$ neurons in the human brain, glial cells vastly outnumber neurons [14, p 24]. The distinction between these cells is important to note; neurons are cells that sense changes in the environment, communicate the changes and send response commands to the body. Glial cells are thought to contribute to the brain function by insulating, supporting and nourishing neighbouring cells [14, p 24]. The role of glial cells still play a significant role when one considers the response of the central nervous system to disease and immune interactions with sensory systems such as pain, a review of which can be found in [187].

Within the class of cells known as *neurons* and *glia* there is a large variety of different categories of cells, based on function, structure, size and chemistry. It is however believed

that neurons are the cells through which the majority of the brains information processing is conducted. Neurons, like cardiomyocytes, are excitable cells. Unlike cells found in the rest of the body, neurons do not undergo cell division and replication [69, p 39]. Neuroscientists are still unable to categorise all neurons in a complete manner, the hope being that one can study the effect of a complete group of similar neurons and draw conclusions regarding the other members of the category [153].

The structure of a neuron

Neurons can be found in the central nervous system in a variety of different sizes and shapes. However all neurons possess a structure known as a **cell body** from which a number of structures, known as **neurites**, project.

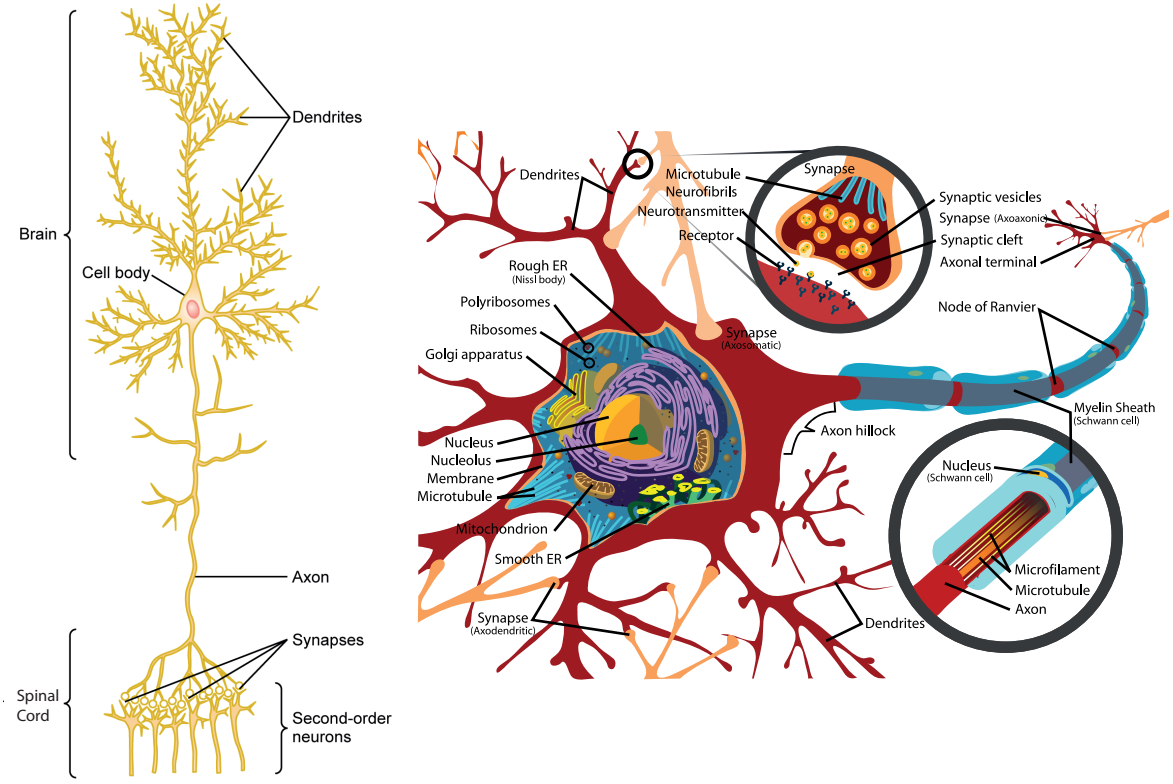

(a) Figure depicting a large neuron in the brain, taken from [69, p 556]

(b) Detailed depiction of a neuron

Figure 1.29: The structure of a neuron.

The main components of a neuron are:

Definition 1.4.1 (**The Soma**)**.** This is is the region of the neuron which contains the cell's nucleus and hence DNA. The soma is also often referred to as the **cell body**. The soma is also the region from which a cells neurites project.

From the soma we have the neurites that make up the

Definition 1.4.2 (**Dendrites**)**.** These are nerve fibres which are responsible for recieving information from a neuron and conducting it toward the cell body.

A further neurite that makes up a typical cell is

Definition 1.4.3 (**Axon**)**.** The axon is a single long tubular neurite which conducts information away from the cell body.

The intracellular fluid of a cell is predominantly made up of a gel like substance known as *cytoplasm*. This allows suspension of the various cell *organelles* which are necessary for the metabolic processes that support the cell.
The axon, which is connected to the soma at the *axon hillock*, is covered by a layer of insulating material known as

Definition 1.4.4 (**Myelin sheath**)**.** This is an electrical insulating material that covers the axon, allowing for the rapid conduction of ions through the axon via *saltatory conduction*. The Myelin sheath is a tubular case and is made up of glial cells called *Schwann cells*.

Damage to the myelin sheath can lead to paralysis, sensory disturbances, visual impairment and multiple sclerosis [167]. The Myelin sheath reduces the flow of ions through the cell membrane by approximately 5000-fold compared to the axon of a nonmyelinated axon[69, p68]. The Myelin sheath around the axon has a number of openings that are approximately 2 - 3 μm in length known as the

Definition 1.4.5 (**Nodes of Ranvier**)**.** The nodes of ranvier are points along the axon at the openings in the myelin sheath that allow the movement of ions between the extracellular and intracellular space. Along the axon the nodes of ranvier are the only place where action potentials occur.

The nodes of ranvier in essence act as a signal boost through which the ion movements due to saltatory conduction can be supplemented with an action potential which draws upon ions in the extracellular fluid. The advantage to having myelinated fibres is that they allow for more rapid conduction of potential through long nerve fibres, myelinated fibres have a conduction velocity that is 5 - 50 times greater than their non myelinated counterparts[69, p69].

The axon terminates at the *axon terminus* leading to a number of *synapses*.

Definition 1.4.6 (**synapse**)**.** A synapse is a structure which allows the flow of electrical charge or chemicals from one neuron to another cell.

Synapses come in two types, electrical or chemical. Electrical synapses are infact *gap junctions* which have been discussed earlier. Chemical synapses however transmit information from a neuron to another neuron by a more intricate nature than gap junctions. The transmission occurs via a complex chemical known as a *neurotransmitter*. The neuron is capable of producing neurotransmitters and stores them in the synapse within a structure known as a *vesicle*. The vesicle is a small structure within the cytoplasm which is made of phospholipid bilayer and serves as a container. The process of moving neurotransmitters into a vesicle is known as *vesicular transport*.

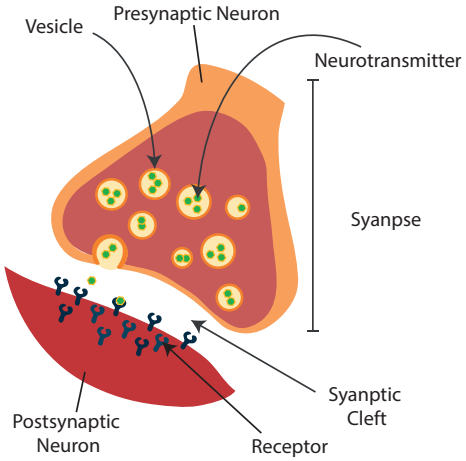

Figure 1.30: The main substructures associated with a chemical synapse.

Conduction of Action Potential Through a Neuron

Typically neurons communicate with one another by the movement of neurotransmitters from the synapse of the the presynaptic neuron to the soma and dendrites of the post synaptic neuron. The post synaptic neuron produces action potentials in this manner by allowing the passage of ions through ion channels in the cell membrane that are neurotransmitter gated. Once the potential difference reaches the activation potential of the sodium channels, previously described, located at or near the axon hillock the transmission of electrical activity through the axon of a myelinated neuron is governed by *saltatory conduction*.

Definition 1.4.7 (Saltatory conduction)**.** This is the mechanism by which action potentials jump from one node of ranvier along a myelinated neuron to another node of ranvier.

The axon of a myelinated cell is covered in insulating cells, in the peripheral nervous system these are known as Schwann cells while in the central nervous system the myelin

is made up of oligodendrocytes. Both these cells that act as myelin have similar electrical properties namely, they are both poor capacitors and excellent resistors. The myelin however does not cover the entire length of a myelinated neuron. The points along the axon that are not covered by the myelin are the nodes of ranvier. It is only at the nodes of ranvier that the myelinated axon possesses ion channels that are capable of passing ions into and out of the cell membrane. The movement of charge through the axon between the nodes of ranvier is via the passive movements of ions due to an *electrotonic potential*.

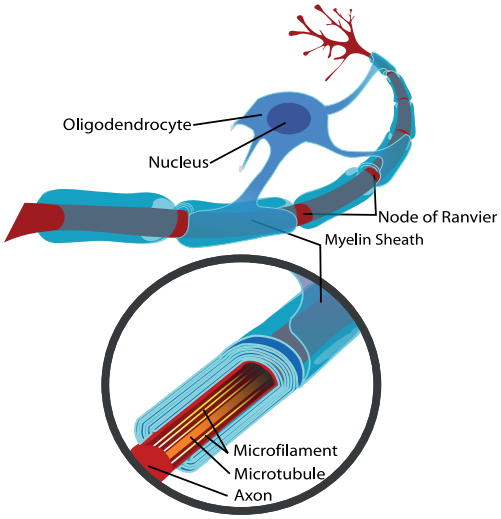

(a) Oligodendrocyte covering the axon of a myelinated neuron in the central nervous system.

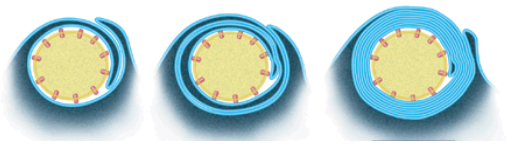

(b) Cross section of a myelinated axon showing how a Schwann cell (blue) wraps around the axon (yellow) of a neuron [56].

Figure 1.31: Myelinated neurons in the CNS and PNS.

The electrotonic conduction through the myelinated axon occurs in the following manner

1. Voltage gated ion channels are activated (due to AP conduction from another neuron or from electrotonic conduction from a prior section of the myelinated axon) allowing the influx of positive ions (Na) into the axon.

2. The influx of positive charge causes a local build up of positive charge within the axon at the node of ranvier. This local positive charge induces ions within the axon to be electrostatically pushed, producing a current. This current also activates gates responsible for the efflux of ions through the membrane (K) producing the action potential response at the node of ranvier.

3. The electrotonic pressure causes the influx channels at the next node to become activated thereby triggering the mechanism to repeat itself.

There are a number of consequences of saltatory conduction in myelinated neurons as opposed to action potential conduction through demyelinated cells [188, p23]

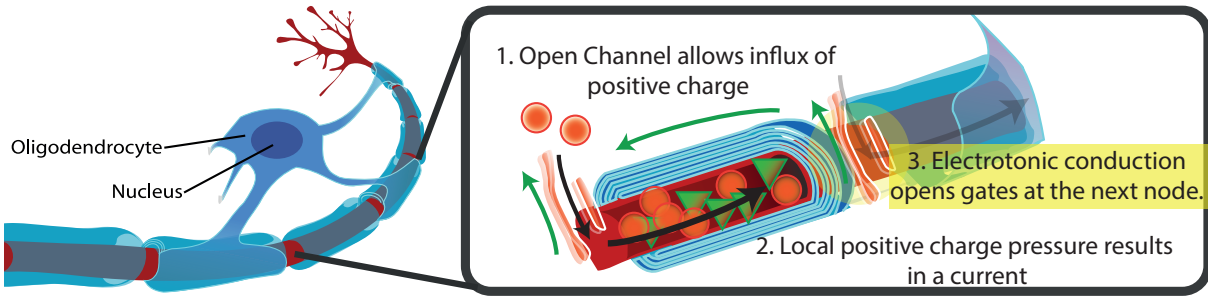

Figure 1.32: Electrotonic conduction through a myelinated axon.

1. Energy requirements for impulse conduction for myelinated fibres is lower, thus the metabolic cost of conduction is lower.

2. Myelination results in increased conduction speed. Thus signals can be sent more rapidly through long axons which of vital importance for reflexive activities and rapid information processing.

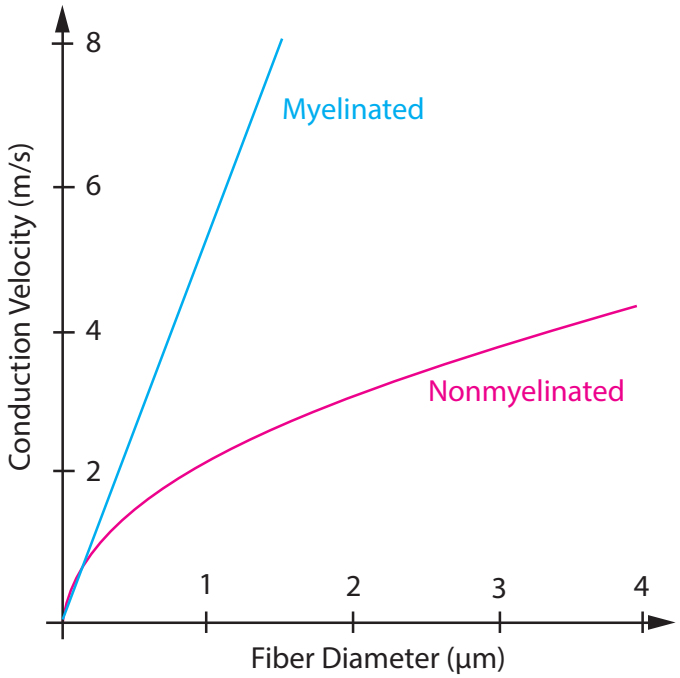

Figure 1.33: Conduction velocity of a myelinated fibre and a nonmyelinated fibre, reproduced from [188, p23]

Conduction of Action Potential From Neuron to Neuron Via a Chemical Synapse

Chemical synapses are the main means by which a neuron communicates with other neurons. Synapses can be divided into two broad classes based on their effect on the postsynaptic neuron,

- **Excitatory:** This type of neuron increases the probability of firing in the postsynaptic neuron [inducing depolarization].
- **Inhibitory:** This type of neuron decreases the probability of firing in the postsynaptic neuron [inducing hyperpolarization].

Communication between a presynaptic and postsynaptic neuron takes place across an extension of the extracellular space (approx 30μm) know as the *synaptic cleft*. The communication is achieved via the diffusion of molecules known as *neurotransmitters*.

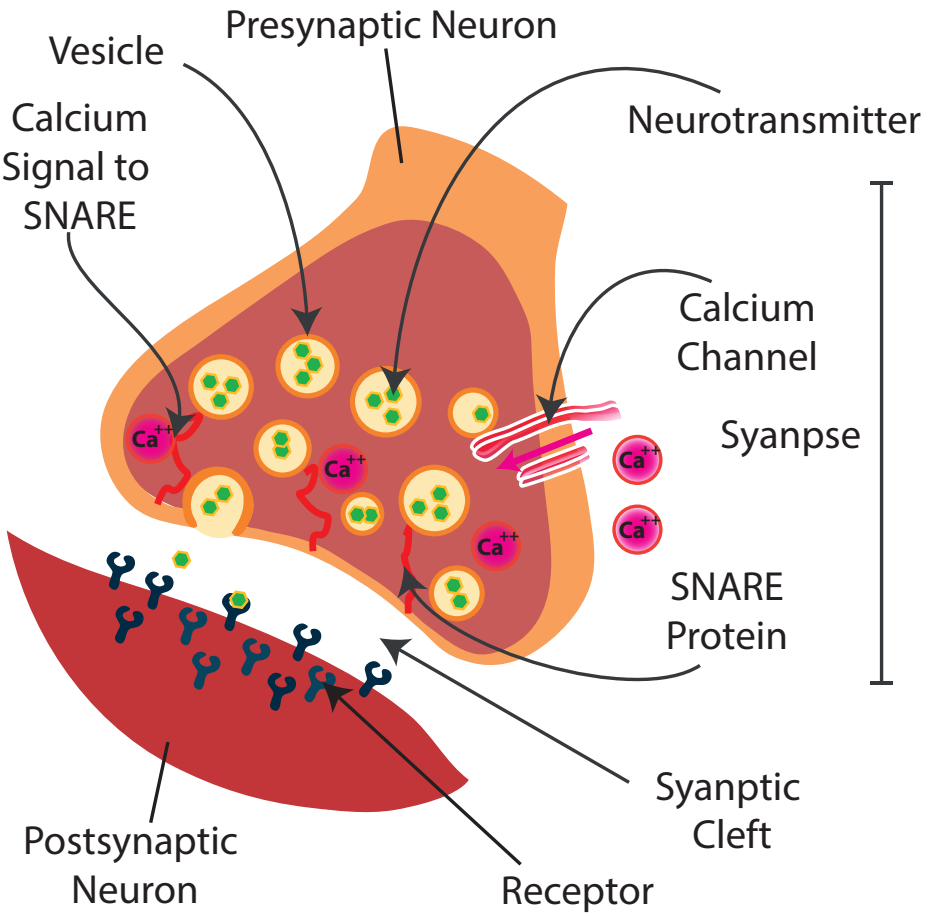

Figure 1.34: The chemical synapse, illustration shows a calcium channel, the influx of calcium ions and signaling to the SNARE proteins.

The neurotransmitter is contained in the presynaptic neuron within a vesicle. Vesicles are themselves connected to cell membrane of the synapse by SNARE[36] proteins. SNARE proteins are themselves intensively studied structures are capable of fusion cell membranes together, a topic not here discussed however the reader is referred to [178] for further reading.

Activation of the SNARE proteins occurs due to the presence of calcium ions in the synapse. The result is the release of neurotransmitter into the synaptic cleft. The neurotransmitters bind to receptors on the postsynaptic neuron. This binding triggers the operation of present **ligand-gated channels**. These channels allow the flow of sodium and potassium ions much like their voltage gated counterparts, they are however triggered by the presence of neurotransmitter.

After conformational changes of the ligand-gated channels have taken place, the neurotransmitter is re-released into the synaptic cleft from the receptor site. At this point *reuptake proteins* return the neurotransmitter to the presynaptic neuron.

[36] Acronym from **SNA**P soluble NSF attachment protein and **RE**ceptor.

1.5 Chapter Summary

- Both neural and cardiac systems are composed of cells with are capable of producing *action potentials*. These cells are *neurons* and *cardiopmyocytes* respectively.
- Action potentials are potential differences measured across a cells membrane.
- The shape of an action potential is dictated by the movement of ions into and out of a cell. The movement of ions is mediated by chemical gradients maintained by the active process of *ion pumps* and the selective passage of ions through *ion channels*.
- There are cells in both the cardiac and neural system which can intrinsically produce action potentials without the need for stimulus. Such cells are said to have the property of *automaticity*. Action potentials are more typically produced by neurons and cardiomyocytes in response to a voltage based stimulation. There is a threshold voltage required to stimulate an excitable cell to produce an action potential.
- Action potentials are produced by cells which are stimulated by an external voltage. This is due to the ion channels being *voltage gated*, i.e. they can change conformational shape when stimulated by an external current.
- Once a cell is stimulated to produce an action potential, intrinsically or otherwise, there is a period of time over which the cell will not produce an action potential even if stimulated with a suprathreshold stimulus. This period is known as the *refractory period*.
- Physiologically, the refractory period is the time that the cell requires in order to set up the ionic gradients required to produce an action potential.
- Action potentials are transmitted from cardiomyocyte to cardiomyocyte via protein structures known as *gap junctions*. Gap junction connections are physical connections between cell membranes and can also be found between neurons.
- Neurons predominantly transmit action potentials through a *synapse*. Synaptic transmission of action potentials is achieved when a presynaptic neuron releases *neurotransmitter* into the gap between the neighbouring neurons and the postsynaptic neurons *ligand gated* ion channels are stimulated to open.

Chapter 2

Fitzhugh-Nagumo Single Cell Dynamical Analysis

2.1 Chapter Introduction and Aim

The aim of this chapter is to introduce the reader to the Fitzhugh-Nagumo (FHN) system of ordinary differential equations and to explore their dynamical behaviour using techniques from nonlinear dynamical systems theory.

Before treating the FHN system the reader is introduced to the Electrophysiological model due to Hodgkin and Huxley[77]. The FHN system is a reduction of the HH model for a neuron. This introduction also serves as a bridge between the physiological information in the previous chapter and mathematical modeling of action potentials.
The FHN system is introduced to the reader with reference to its historical formulation and context. After defining the FHN system a phase plane analysis is conducted and the systems parameters are interpreted in terms of the effect they have on the existence and stability of dynamical equilibrium points. The flow of trajectories in phase space are treated with particular attention to the systems nullclines and a number of results concerning the existence of equilibria are found.

The FHN system is shown to be a Lienard type differential equation which allows a theorem stating sufficient conditions on the system parameters in order to admit unique limit cycle solutions.

The fast-slow dynamics of the FHN system are explored after introducing the relevant results from classical perturbation theory. The result of the perturbation analysis is in finding the fold points of the FHN system, the systems slow manifold the fast-foliation.

This brings analytic insight into the approximate shape and of the limit cycles that are produced in the phase space of the FHN system.

A mechanism for limit cycle production through a Hopf bifurcation is treated. The conditions under which the FHN system undergoes a Hopf bifurcation are analytically treated and the stability of the resulting limit cycle oscillations are also derived.

Finally the phase space of the FHN system is probed using numerical continuation methods with greater emphasis on investigating the bifurcation structure of the system with respect to its parameters.

2.2 From Biological System to Mathematical Model - The Hodgkin-Huxley (HH) Model.

The invention of the *voltage-clamp* experimental method by Cole and Marmont[112] in the 1940s, led two researchers, Hodgkin and Huxley, studying the action potential of the squid's giant axon (a very large neuron which made experimentation practical). In a series of five papers published in 1952[77], Hodgkin and Huxley presented the relationship between the sodium, potassium and leak (mainly carried by chlorine ions) ionic currents on the action potential. Their model will be described in detail in the next chapter. The two won the Nobel Prize in 1963 for this ground-breaking work.

The Squid Giant Axon:
The giant *axon* of the squid is part of a neuron that runs down the length of the squid *mantel*. When the squid wishes to move quickly it sends a number of action potentials down the length of it's giant axon to initiate the contraction of muscles in it's mantel. The muscle contractions cause the ejection of a fluid jet, propelling the squid in the opposite direction; this being the squid's main defense mechanism from predators. The *conduction velocity* of the action potentials within this axon is rather quick with a pulse traveling at $20ms^{-1}$.

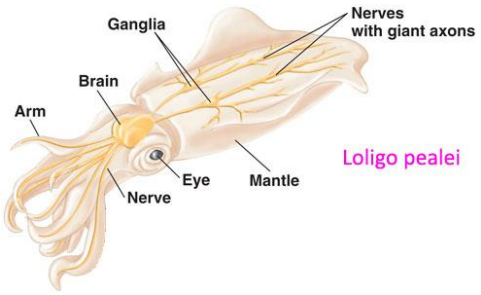

Figure 2.1: Squid and giant axon.

The pioneering work in the field of *electrophysiology* describing the firing of action poten-

tials was conducted in the 1940-50s by Cole, Curtis, Hodgkin and Huxley. In a series of four papers Hodgkin and Huxley presented both their experimental findings concerning the conductivity properties of the squid axon and their theoretical model of the action potential. Their experiments involved recording the response of the squid neuron in various chemical baths (Na and K) and recording the response of the neuron to electrical stimulus. This in itself was a never before conducted piece of science, however H & H continued to produce a complete theoretical framework for their findings based on a system of ordinary differential equations. This formulation of the system is now the fundamental framework governing the majority of research in the field of electrophysiology.

When formulating their model for action potential generation HH considered the phospholipid bilayer which makes up a neurons membrane as a capacitor, with capacitance C_m. The total transmembrane current, I_m, is related to the sum of all the ionic currents I_{ion} which move across the cells membrane, see Figure 2.2, and the rate of change of current across the membrane V_m, according to Ohm's law we have

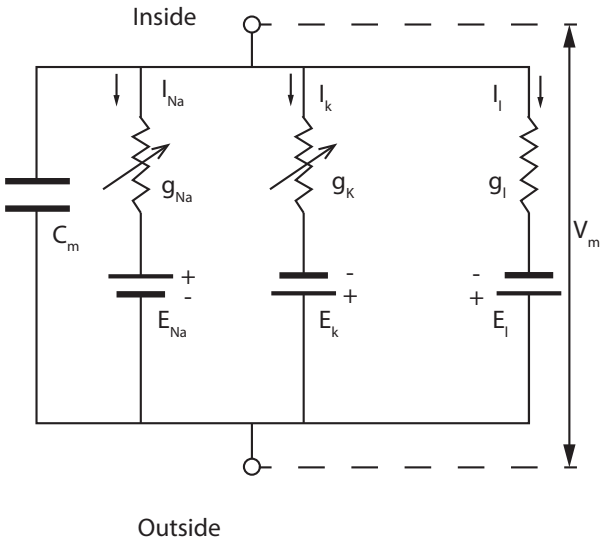

Figure 2.2: Circuit representation of Hodgkin and Huxley's model of a squid giant axon.

$$I_m = C_m \frac{V_m}{dt} + \sum I_{\text{ion}}.$$

From Kirchoff's loop rule, the sum of all the currents going into and out of the cell is

zero, $I_m = 0$ and

$$\frac{V_m}{dt} = -\frac{1}{C_m} \sum I_{\text{ion}}.$$

This forms the basic frame of Hodgkin and Huxley's model, what is required is an expression for each of the ionic currents involved in the sum. Each of the ion currents are modeled in terms of the channels conductance[1] g_{ion}, the cell's membrane voltage V_m and E_{ion}, the *Nernst reverse potential*.

$$I_{\text{ion}} = g_{\text{ion}}(V_m - E_{\text{ion}})$$

The Nernst potential acts as a voltage source, the source is related to the semipermeable nature of the cell membrane which allows the flow and build up of ions inside and outside of the membrane. More specifically the Nernst potential is the voltage required to oppose the concentration-gradient flow across the semipermiable membrane for a particular ion:

$$E_{\text{ion}} = \frac{RT}{z_{\text{ion}}F} \ln\left(\frac{[\text{ion}]_o}{[\text{ion}]_i}\right)$$

where R is the universal gas constant, T is the temperature in Kelvin, z_{ion} is the valency of the ion, F is Farady's constant, $[\text{ion}]_o$ is the concentration of 'ion' outside the cell and $[\text{ion}]_i$ is the concentration of 'ion' inside the cell.

Another complication arises when considering the conductance of a particular ion channel. The conductance not a constant as the flow of ions (via the ion channels) is related to the voltage across the cell membrane. Thus it is necessary to specify how the "gating" of ion channels behaves dynamically. The study of ion channels and their changes in conformation is still an intensive area of research referred to as *ion channel kinetics*, we however H& H took a rather simplistic view on the ion channel[2], which is here described. An ion channel is considered a simple gate on the cell membrane that can either allow or block the entrance of a specific ion. In this view the gate can either be in an Open state or a Closed state. The transitions of state from Closed $\rightarrow$ Open or Open $\rightarrow$ Closed occur at different rates

$$C \underset{\beta}{\overset{\alpha}{\rightleftharpoons}} O$$

where α and β are the transition rate constants which are themselves functions of voltage.

[1] Conductance being the reciprocal of the resistance.
[2] first order kinetics.

A gating variable is introduced to the model which can be interpreted as the fraction of gates that are open or equivalently as *the probability that a given gate will be open*[3]. For the potassium (K^+) current this gating probability is given by n and is modeled by

$$\frac{dn}{dt} = \alpha_n(1-n) - \beta_n n$$

From their experiments H&H found that one gate isn't sufficient to specify the dynamics of the sodium current, as such H&H used two gating probabilities: m the activation variable and h the inactivation variable.

$$\frac{dm}{dt} = \alpha_m(1-m) - \beta_m m, \quad \frac{dh}{dt} = \alpha_h(1-h) - \beta_h h$$

These gating variables lead to the replacement of the ion channel's conductance $g_{ion}(t,V)$ with the product of the channels maximal conductance $\bar{g}_{ion}$, which is a constant, and the fraction of open channels[4] of that specific ion throughout the cell membrane.

Hodgkin-Huxley Equations:
We have the following set of 4 coupled ODEs:

$$\begin{aligned}
\frac{dV}{dt} &= -\frac{1}{C}[\bar{g}_{Na}m^3h(V-E_{Na}) + \bar{g}_K n^4(V-E_K) + \bar{g}_L(V-E_L) - I_{stim}] \\
\frac{dm}{dt} &= \alpha_m(1-m) - \beta_m m \\
\frac{dh}{dt} &= \alpha_h(1-h) - \beta_h h \\
\frac{dn}{dt} &= \alpha_n(1-n) - \beta_n n
\end{aligned}$$

where the maximum conductances are experimentally obtained to be

$$\bar{g}_{Na} = 120\ mS\ cm^{-2},\ \bar{g}_K = 36\ mS\ cm^{-2},\ \bar{g}_l = 0.3\ mS\ cm^{-2}$$

and the reversal potentials are obtained to be

[3]H&H did not make this interpretation, they believed that there existed carrier particles n, m and h that moved the ion across the cell membrane. The probabilistic interpretation was brought forward after a better understanding of ion channels developed.

[4]One will notice that in the H&H equations the fraction of open channels or the probability of having an open channel are raised to certain powers; these powers had been deduced by experimentation, in fact higher powers fit the data better but H&H did not have access to computers during their work having to do all the 'curve' fitting by hand calculation!

$$E_{Na} = +55mV,\ E_K = -72mV,\ E_l = -49.387mV$$

the cells capacitance (ability to hold electrical charge) is taken to be $C = 1\,\mu F$. The α_* and β_* functions are exponential functions that are fit appropriately from experimental data

$$\alpha_m = 0.1\left(\frac{V+35}{1-\exp(-(V+35)/10)}\right) \qquad \beta_m = 4\exp\left(\frac{-(V+60)}{18}\right)$$

$$\alpha_h = 0.07\exp\left(\frac{-(V+60)}{20}\right) \qquad \beta_h = \frac{1}{\exp\left(\frac{-(V+30)}{10}\right)+1}$$

$$\alpha_n = 0.01\left(\frac{V+50}{1-\exp\left(\frac{-(V+50)}{10}\right)}\right) \quad \beta_n = 0.125\exp\left(\frac{-(V+60)}{80}\right).$$

2.3 The FHN System

The Fitzhugh-Nagumo (FHN) equations where introduced as a reduction of the HH-model[77] of the squid giant axon. The FHN model is a modified set of equations based around the Van der Pol oscillator[5] which itself was used as a cardiac model [136, 135].

Another influence on Fitzhugh's work was the experimental work conduced Bonhoeffer [20] concerning the activation of iron in an acid solution. Fitzhugh modified Van der Pols oscillator to take into account Bonhoeffer's results and named the equations the Bonhoeffer-van der Pol equations[57]. Nagumo and colleagues working on circuit representations of electrical transmission in nerves, the circuit is shown in Figure 2.3, arrived at the same set of equations publishing a paper in the following year[119].

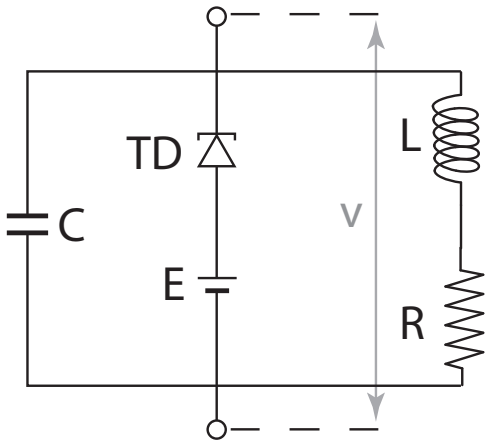

Figure 2.3: The Nagumo circuit [119]. C is a capacitor, E a (battery) voltage source, R a resistor, L an inductor, TD is a tunneling diode and v is the potential that represents the nerve action action potential.

This lead to the what is currently known as the FitzHugh-Nagumo equations. The FHN

[5]this being a relaxation type oscillator

equations fall under the class of *excitable systems*. The main properties of excitable systems are [133, p. 93]

- In response to superthreshold stimulus they generate a spike called an action potential. Subthreshold stimuli do not cause any response, or the response is negligibly small.
- Immediately after the action potential excitable systems are refractory, i.e. they do not respond to stimuli of any amplitude.

FitzHugh's original paper uses the specific form

$$\begin{aligned} \dot{x} &= c(y + x - x^3/3 + z) \\ \dot{v} &= -(x - a + by)/c \end{aligned} \tag{2.3.0.1}$$

Here the two dynamical variables, x and y, are the known as the *activator* and *inhibitor* respectively in a general dynamical systems context. In terms of physiology (of neural and cardiac systems) the variables are, qualitatively, related to the *transmembrane voltage* and *recovery*. The resulting system is a reduction of the 4-Dimensional system of equations formulated by Hodgkin and Huxley in 1952[77]. z represents an injected current, in its most general form is a function of time $z = z(t)$ while a,b and c are parameters. The special case of parameter values $a = b = I = 0$ corresponds to the van der Pol oscillator. Typical parameter values used by Fitzhugh[57]

$$a = 0.7 \quad b = 0.8 \quad c = 3.0$$

with constraints

$$1 - 2b/3 < a < 1, \qquad 0 < b < 1, \qquad b < c^2.$$

There are a number of variants of the form of the equations used in the literature; throughout this thesis however we will be concerned with the following form of the equations

$$\begin{aligned} \dot{x} &= x - x^3/3 - y + I \\ \dot{y} &= \epsilon(x + a - by). \end{aligned} \tag{2.3.0.2}$$

This form being preferred as it introduces the small parameter ϵ which can later be exploited when examining the asymptotic structure of the FHN system.

Though this system can be further simplified by absorbing a parameter (such as 'a') into the definition of one of our variables, we choose to omit doing so to maintain the interpretable features of a neuron (such as negative rest potentials).

2.3.1 Phase Plane Analysis

The predominant advantage the FHN model offers over more complex models from electrophysiology (see table 1.10) is that it is a two variable system whose phase space can be visually realised and investigated. Fitzhugh's original work suggested and showed that projecting the HH-model on $\mathbb{R}^2$ produces a qualitatively similar phase space as that of the van der Pol oscillator. This reduction was made possible as the 4D system of ODEs could be reduced into a 2D system of ODEs when one took into account that there are variables that track each other during an action potential[6].

Nullclines

We begin the phase plane analysis by examining the nullclines of the FHN system,

Definition 2.3.1 (Nullcline)**.**
Given a dynamical system

$$\dot{\mathbf{x}} = f(\mathbf{x})$$

where $\mathbf{x} \in \mathbb{R}^n$. The **nullclines** of the dynamical system are given by the curves defined by

$$\dot{x_i} = 0$$

There are two nullclines from (2.3.0.2) which satisfy the nullcline condition.

The **Nullclines** of the FHN system are given by

$$y = x - x^3/3 + I \tag{2.3.1.1}$$

$$y = \frac{x + a}{b} \tag{2.3.1.2}$$

[6]FitzHugh found that the V and m variables tracked each other and thus one could be expressed as an algebraic expression of the other, the same was also found to be true for the variables h and n.

provided $b \neq 0$.[7]
We refer to (2.3.1.1) and (2.3.1.2) as the 'x-nullcline' and the 'y-nullcline' respectively. Given the polynomial form of the nullclines we can make some observations concerning their shape with little effort.

The x-nullcine:

- Intercepts the x-axis at most three times which occur whenever $x^3 - 3x - 3I = 0$.
- Intercepts the y-axis at $(x, y) = (0, I)$.
- Has a maxima at $(x_{mx}, y_{mx}) = \left(1, \frac{2}{3} + I\right)$ and a minima at $(x_{mn}, y_{mn}) = \left(-1, -\frac{2}{3} + I\right)$.

The y-nullcline:

- Intercepts the x-axis at $(x, y) = \left(0, \frac{a}{b}\right)$.
- Intercepts the y-axis at $(x, y) = (-a, 0)$.
- Is a monotonic increasing function if $b > 0$ and a monotonic decreasing function if $b < 0$.

This allows us to produce the following qualitative picture of the nullclines, an example of which is shown in Figure 2.4

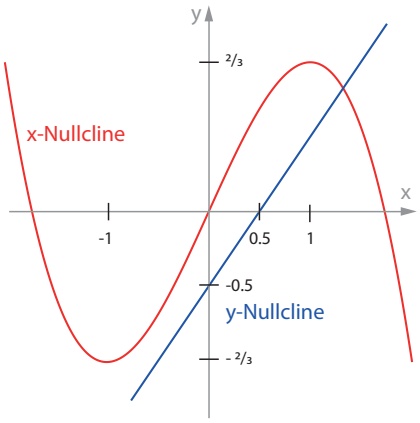

Figure 2.4: The Nullclines of the FHN system; parameters $I = 0$, $a = 0.5$ and $b = 1$.

[7] if $b = 0$.

$$y = x - x^3/3 + I, \quad \text{and} \quad x = -a.$$

These curves define the regions in space where the vector field defined by the right hand side (RHS) of the FHN system (2.3.0.2) is made up of purely vertical (x-nullcline) and horizontal (y-nullcline) vectors.

Nullcline Parameter dependance

The equations for the nullclines given by (2.3.1.1) and (2.3.1.2) clearly depend on the system parameters a, b and I. The x-nullcline with equation given by (2.3.1.1)

$$y = x - x^3/3 + I$$

depends on I the external current; taking I to be constant (which corresponds to examining an excitable cell under voltage clamp) it is clear that variation of I result in translation of the x-nullcline in the y-direction.

Pictorially, we have

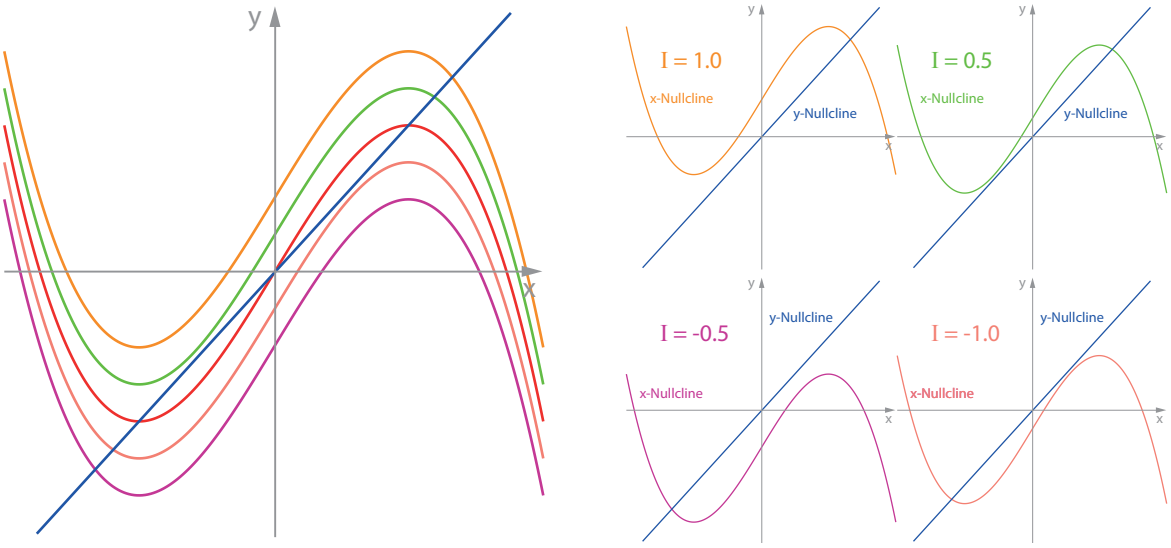

Figure 2.5: The nullclines of the FHN system on variation of the parameter I. The fixed parameters are $a = 0$ and $b = 1$.

The y-nullcline, given by

$$y = \frac{x + a}{b}$$

is a straight line whose slope varies with b.

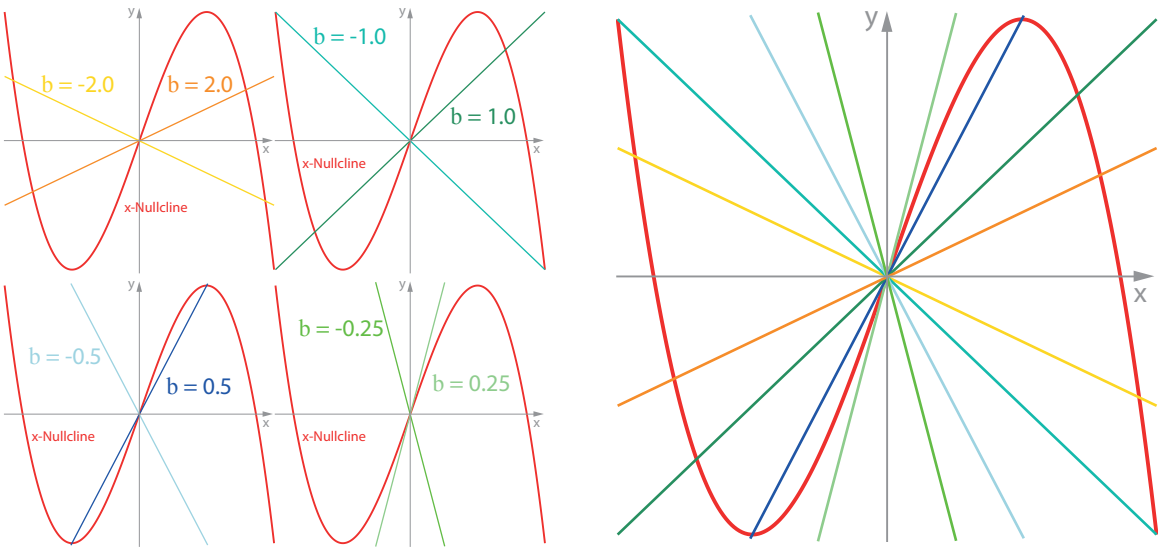

Figure 2.6: The nullclines of the FHN system on variation of the parameter b. The fixed parameters are $a = 0$ and $I = 0$.

Variation of the parameter a, for constant b, results in translation of the y-nullcline in the x-direction.

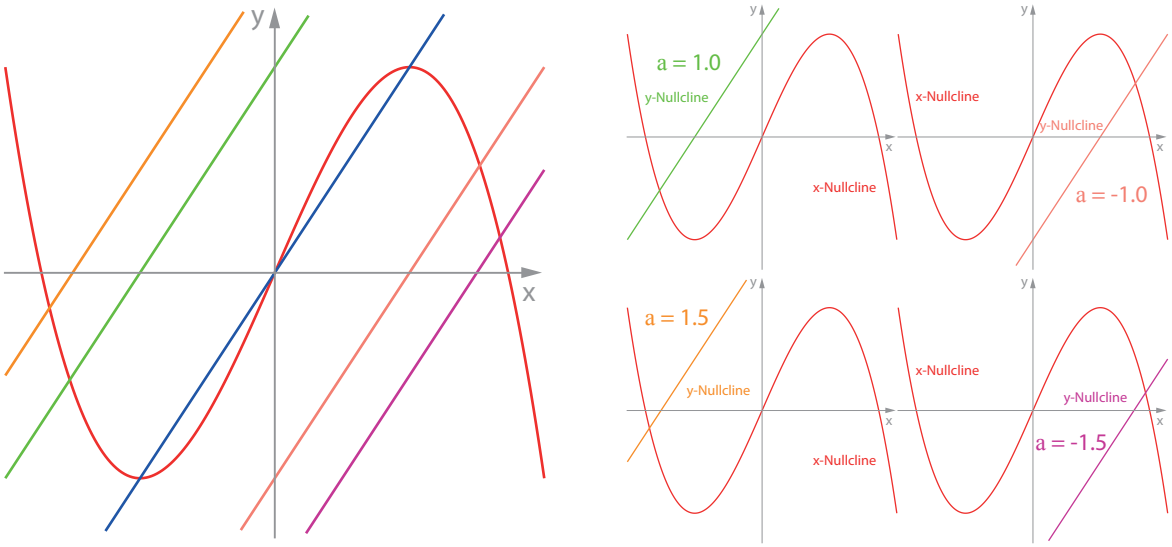

Figure 2.7: The nullclines of the FHN system on variation of the parameter a. The fixed parameters are $I = 0$ and $b = 0.5$.

Equilibrium points and nullclines

The first note of interest concerning the nullclines of a system is that all the systems equilibrium points are found precisely at points in space where all the nullclines intersect.

Definition 2.3.2 (Equilibrium point)**.**
An equilibrium point of a dynamical system

$$\dot{\mathbf{x}} = f(\mathbf{x})$$

where $\mathbf{x} \in \mathbb{R}^n$, is a point $\bar{\mathbf{x}} \in \mathbb{R}^n$ such that

$$f(\bar{\mathbf{x}}) = 0$$

Fixed points are points of no dynamical change in a system, in other words points at which a system will never escape from in time unless acted upon by an external agent. The fact that this occurs at the intersection of all the nullclines should be clear as at the nullcline intersections

$$\dot{\mathbf{x}} = 0.$$

Now from (2.3.1.1) and (2.3.1.2) we have

The fixed points of the FHN system given by (2.3.0.2) must satisfy

$$b\bar{x}^3 + 3(1-b)\bar{x} + 3(a - bI) = 0 \tag{2.3.1.3}$$

$$\bar{y} = \frac{\bar{x} + a}{b} \tag{2.3.1.4}$$

From virtue of (2.3.1.3) being a cubic polynomial and (2.3.1.4) being a linear equation it is clear that there exists at most three fixed points in the system for any combination of parameters. This could also have been seen from the graphs of both nullclines and realising that any combination of translations of the x-nullcline and translations plus rotations of the y-nullcline can only produce at most three intersections.

Flows and nullclines

In the previous subsection we briefly saw that nullclines can be useful when looking for fixed points which are a static dynamical state. Nullclines also provide information on the behaviour of trajectories that venture near the nullclines. Since the nullclines are points where the rate of change of one of the state variables is zero. Thus the vector flow

on a nullcline should have zero direction in at least one dimension in state space.

Since the FHN system is only a two dimensional system of autonomouos ODEs, this means that the flow on the nullclines point 'vertically' or 'horizontally'. The flow thus is pictorially representable as

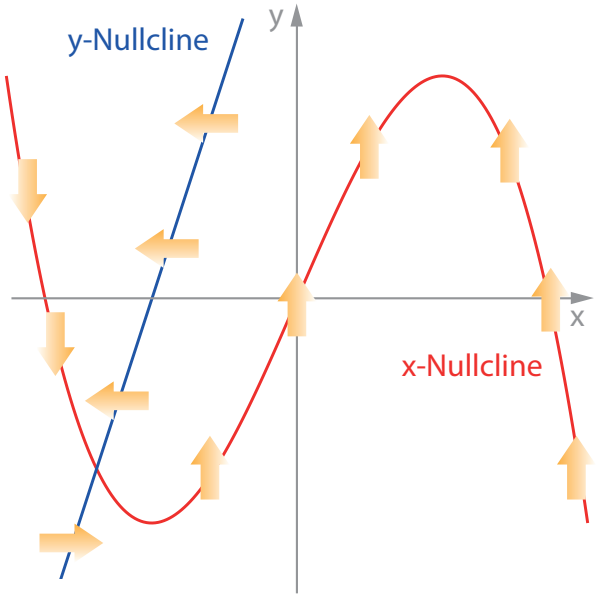

Figure 2.8: Arrows representing the vector field defined by the FHN system on the nullclines.

Equilibrium points

We have seen from the previous section that the system can have one, two or three equilibria, in this section we set about deriving conditions for their existence and finally provide an expression for the equilibria.

The number of equilibrium points

We begin by finding the *resultant* associated with the cubic given by (2.3.1.3)

$$p(x) = bx^3 + 3(1-b)x + 3(a - bI).$$

The resultant of $p(x)$ is the determinant of the Sylvester matrix of $p(x)$ and its derivative [137, p 20]

$$p'(x) = 3bx^2 + 3(1-b).$$

The Sylvester matrix of interest is given by

$$S(p,p') = \begin{pmatrix} b & 0 & 3(1-b) & 3(a-bI) & 0 \\ 0 & b & 0 & 3(1-b) & 3(a-bI) \\ 3b & 0 & 3(1-b) & 0 & 0 \\ 0 & 3b & 0 & 3(1-b) & 0 \\ 0 & 0 & 3b & 0 & 3(1-b) \end{pmatrix} \tag{2.3.1.5}$$

The Resultant can now be computed by taking the determinant of (2.3.1.5)

$$R(p,p') = \det\left(S(p,p')\right)$$

$$= (-1)^{2+5}3(a-bI)\det\begin{vmatrix} b & 0 & 3(1-b) & 3(a-bI) \\ 3b & 0 & 3(1-b) & 0 \\ 0 & 3b & 0 & 3(1-b) \\ 0 & 0 & 3b & 0 \end{vmatrix} + \dots$$

$$+ (-1)^{5+5}3(1-b)\det\begin{vmatrix} b & 0 & 3(1-b) & 3(a-bI) \\ 0 & b & 0 & 3(1-b) \\ 3b & 0 & 3(1-b) & 0 \\ 0 & 3b & 0 & 3(1-b) \end{vmatrix}$$

$$= -9b(a-bI)(-1)^{3+2}\det\begin{vmatrix} b & 3(1-b) & 3(a-bI) \\ 3b & 3(1-b) & 0 \\ 0 & 3b & 0 \end{vmatrix} + \dots$$

$$+ 3^2(1-b)^2\left\{(-1)^{1+3}\det\begin{vmatrix} 0 & b & 3(1-b) \\ 3b & 0 & 0 \\ 0 & 3b & 3(1-b) \end{vmatrix} + (-1)^{3+3}\det\begin{vmatrix} b & 0 & 3(a-bI) \\ 0 & b & 3(1-b) \\ 0 & 3b & 3(1-b) \end{vmatrix}\right\}$$

$$= 27b(a-bI)^2(-1)^{1+3}(3b)^2 + 3^2(1-b)^2\left\{3b(-1)^{2+1}\left(-6b(1-b)\right) + (-1)^{1+1}b\left(-6b(1-b)\right)\right\}$$

$$= 27b(a-bI)^2(3b)^2 + 3^2 12b^2(1-b)^3$$

$$= 3^3b^2\left\{9b(a-bI)^2 + 4(1-b)^3\right\}$$

Which can finally be used to obtain an expression for the discriminant[8] ,

$$D(p) = = (-1)^3 \frac{R(p,p')}{b}$$

$$= -\frac{3^3 b^2 \left\{ 9b(a-bI)^2 + 4(1-b)^3 \right\}}{b}$$

The equilibria of the FHN system satisfy the equation

$$p(x) = bx^3 + 3(1-b)x + 3(a-bI) = 0$$

given in (2.3.1.3). The discriminant of $p(x)$ is given by

$$D(p) = -3^3 b \left\{ 9b(a-bI)^2 + 4(1-b)^3 \right\} \tag{2.3.1.6}$$

The discriminant of a polynomial is simply made up of the product of the difference between its roots squared; that is for a polynomial

$$P(x) = a_n x^n + a_{n-1} x^{n-1} + \cdots + a_0$$

the discriminant is

$$D(P) = a_n^{2(n-1)} \prod_{\forall i<j} (x_i - x_j)^2$$

where the x_i and x_js are the roots of $P(x)$. Thus it is clear that for a cubic polynomial

- $D < 0$ Tells us that there is 1 real root and a pair of complex conjugate roots.
- $D = 0$ Tells us that there is at least one repeated root.
- $D > 0$ Tells us that there are three distinct real roots.

[8]The discriminant of a polynomial

$$p(x) = a_n x^n + a_{n-1} x^{n-1} + \cdots + a_0$$

is given by

$$D(p) = (-1)^{\frac{1}{2}n(n-1)} \frac{R(p,p')}{a_n}$$

where $R(p,p')$ is the resultant, which is equivalent to the determinant of the Sylvester matrix, of the polynomial and its derivative.

For the FHN system we have the following result concerning the fixed points

From the discriminant

$$D = -3^3 b \left\{ 9b(a - bI)^2 + 4(1 - b)^3 \right\}$$

one can conclude that the FHN system (2.3.0.2) has

- 1 equilibrium point if $D < 0$
- At least 1 equilibrium and definitely not 3 equilibrium points if $D = 0$ and
- 3 equilibrium points if $D > 0$.

An inspection of (2.3.1.3)

$$b\bar{x}^3 + 3(1 - b)\bar{x} + 3(a - bI) = 0$$

shows that we have a triply repeated real root under the following condition

The FHN system (2.3.0.2) has only **one equilibrium point** when

$$b = 1 \quad \text{and} \quad a = I$$

Furthermore the system has only one distinct equilibrium point when

$$\begin{aligned} D &< 0 \\ -3^3 b \left\{ 9b(a - bI)^2 + 4(1 - b)^3 \right\} &< 0 \end{aligned}$$

assuming that $b \neq 0$ and dividing through by b^2 we have

$$-3^3 \left(9(a - bI)^2 + \frac{4(1 - b)^3}{b} \right) < 0$$

The FHN system (2.3.0.2) has **one equilibrium point** if

$$0 < b \leq 1$$

One can make these assertions concerning the number of equilibrium points as we necessarily require them to be *real* and thus disregard the complex conjugate solutions that are possible.

The stability of equilibrium points

Given an equilirbium point $\bar{\mathbf{x}} = (\bar{x}, \bar{y})$ of a 2D dynamical system[9]

$$\dot{x} = f(x, y)$$
$$\dot{y} = g(x, y)$$

the behaviour of solutions "near" an equilibrium point can be approximated by looking at the *linearised* system. To see this one begins by Taylor expanding the vector field defined by $f(x, y)$ and $g(x, y)$ about an equilibrium point $\bar{\mathbf{x}}$ which yields

$$f(x,y) = f(\bar{x},\bar{y}) + \left.\frac{\partial f}{\partial x}\right|_{(\bar{x},\bar{y})} (x-\bar{x}) + \left.\frac{\partial f}{\partial y}\right|_{(\bar{x},\bar{y})} (y-\bar{y}) + \mathcal{O}\left((x-\bar{x})^2\right) + \mathcal{O}\left((y-\bar{y})^2\right) + \dots$$

$$g(x,y) = g(\bar{x},\bar{y}) + \left.\frac{\partial g}{\partial x}\right|_{(\bar{x},\bar{y})} (x-\bar{x}) + \left.\frac{\partial g}{\partial y}\right|_{(\bar{x},\bar{y})} (y-\bar{y}) + \mathcal{O}\left((x-\bar{x})^2\right) + \mathcal{O}\left((y-\bar{y})^2\right) + \dots$$

In order to turn the problem/system into a relatively straightforward one it is desirable to remove the nonlinear terms. One can safely neglect the nonlinear terms when

$$(x-\bar{x})^2 << |(x-\bar{x})| \quad \text{and} \quad (y-\bar{y})^2 << |(y-\bar{y})|$$

this being precisely what is meant by "near" an equilibrium point. Furthermore making a change of variables

$$X = x - \bar{x}$$
$$Y = y - \bar{y}$$

which is equivalent to translating the system so that the fixed point of interest is located at the origin

$$\begin{pmatrix} \dfrac{dX}{dt} \\ \dfrac{dY}{dt} \end{pmatrix} = \begin{pmatrix} \left.\dfrac{\partial f}{\partial x}\right|_{(\bar{x},\bar{y})} & \left.\dfrac{\partial f}{\partial y}\right|_{(\bar{x},\bar{y})} \\ \left.\dfrac{\partial g}{\partial x}\right|_{(\bar{x},\bar{y})} & \left.\dfrac{\partial g}{\partial y}\right|_{(\bar{x},\bar{y})} \end{pmatrix} \begin{pmatrix} X \\ \\ Y \end{pmatrix}$$

$$= J(\bar{x},\bar{y}) \begin{pmatrix} X \\ \\ Y \end{pmatrix} \tag{2.3.1.7}$$

[9]The generalisation to higher dimensions is the natural one.

Where the symbol J has been introduced for the Jacobian matrix. Equation (2.3.1.7) is known as **the linearised system**. The eigenvalues of the Jacobian matrix provides insight into the nature of solution trajectories to the linearised system. The attraction and repulsion of trajectories in the full nonlinear system in a small neighbourhood around the equilibrium points, and hence the stability of the equilibrium point, is given by the eigenvalues of the linearised system.

Building a little notation let

$$A = \frac{\partial f}{\partial x}, \qquad B = \frac{\partial f}{\partial y}, \qquad C = \frac{\partial g}{\partial x} \quad \text{and} \quad D = \frac{\partial g}{\partial x}$$

thus the Jacobian can be written as

$$J = \begin{pmatrix} A & B \\ C & D \end{pmatrix}$$

The characteristic equation for the eigenvalues λ_1 and λ_2 can be written as

$$\lambda^2 - (A + D)\lambda + (AD - BC) = 0 \tag{2.3.1.8}$$

which alternatively can be written as

$$\lambda^2 - \tau\lambda + \Delta = 0 \tag{2.3.1.9}$$

where, $\tau = \text{tr}(J) = A + D$ is the trace of the Jacobian and $\Delta = \det(J) = AD - BC$ is the Jacobian determinant.

The characteristic equation has solutions, after a little simplification

$$\lambda_{1,2} = \frac{(A + D) \pm \sqrt{(A - D)^2 + 4BC)}}{2} \tag{2.3.1.10}$$

this can also be written in terms of the trace and determinant of the Jacobian as

$$\lambda_{1,2} = \frac{\tau \pm \sqrt{\tau^2 - 4\Delta}}{2} \tag{2.3.1.11}$$

The equilibrium points are thus categorised as shown in Figure 2.9

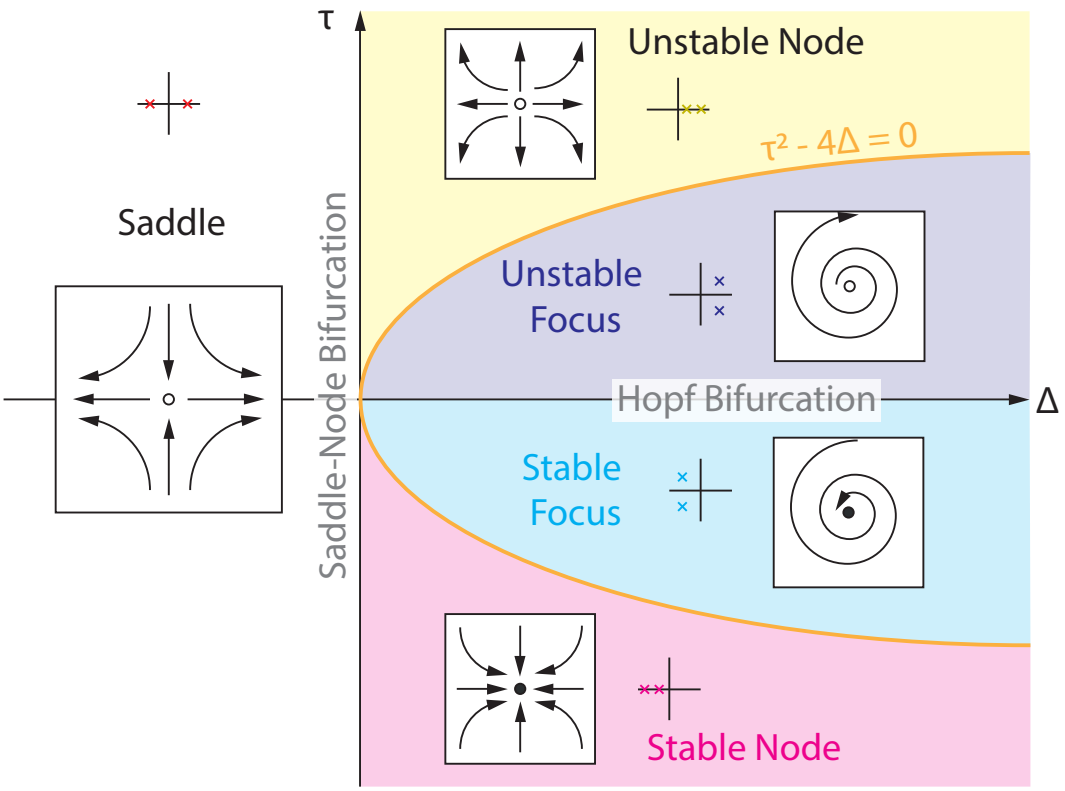

Figure 2.9: Division of the different local behaviour that a 2D system can have in terms of the trace, τ, and the determinant δ of the system's Jacobian matrix. The x's signify the sign and nature of the eigenvalues in the complex plane associated with each local phase portrait. The figure is a modified one based on[86, p 104.]

Stability of the FHN equilibrium points

To examine the stability conditions of the FHN system we begin by finding the Jacobian of the FHN system given by

$$\dot{x} = x - x^3/3 - y + I$$
$$\dot{y} = \epsilon(x + a - by)$$

which when evaluated at an equilibrium point (2.3.1.3) is given by

$$J(\bar{x}, \bar{y}) = \begin{pmatrix} \left.\frac{\partial f}{\partial x}\right|_{(\bar{x},\bar{y})} & \left.\frac{\partial f}{\partial y}\right|_{(\bar{x},\bar{y})} \\ \left.\frac{\partial g}{\partial x}\right|_{(\bar{x},\bar{y})} & \left.\frac{\partial g}{\partial y}\right|_{(\bar{x},\bar{y})} \end{pmatrix} = \begin{pmatrix} 1 - \bar{x}^2 & -1 \\ \epsilon & -\epsilon b \end{pmatrix}. \tag{2.3.1.12}$$

Implementing (2.3.1.10) we have

The stability coefficient of the equilibrium points of the FHN system (2.3.0.2) are

$$\lambda_1 = \frac{(1-\bar{x}^2-\epsilon b)+\sqrt{(1-\bar{x}^2+\epsilon b)^2-4\epsilon)}}{2} \tag{2.3.1.13}$$

$$\lambda_2 = \frac{(1-\bar{x}^2-\epsilon b)-\sqrt{(1-\bar{x}^2+\epsilon b)^2-4\epsilon)}}{2} \tag{2.3.1.14}$$

The trace of the Jacobian is given by

$$\mathrm{tr}(J(\bar{x},\bar{y})) = 1-\bar{x}^2-\epsilon b \tag{2.3.1.15}$$

and the determinant is given by

$$\det(J(\bar{x},\bar{y})) = \epsilon b\bar{x}^2+\epsilon(1-b) \tag{2.3.1.16}$$

Looking for stable equilibrium points requires

$$\mathrm{tr}(J(\bar{x},\bar{y})) < 0 \tag{2.3.1.17}$$

$$\det(J(\bar{x},\bar{y})) > 0. \tag{2.3.1.18}$$

Interestingly, these are rather strict conditions on the system's equilibrium points. From (2.3.1.17) we find that

$$1-\bar{x}^2-\epsilon b < 0$$

$$\Rightarrow \bar{x} < -\sqrt{1-\epsilon b} \quad \text{or} \quad \bar{x} > \sqrt{1-\epsilon b}$$

and from (2.3.1.18) we have

$$\epsilon b\bar{x}^2+\epsilon(1-b) > 0$$

$$\Rightarrow \bar{x} < -\sqrt{\frac{1}{b}-1} \quad \text{or} \quad \bar{x} > \sqrt{\frac{1}{b}-1}$$

Thus we have the following result

Theorem 2.3.1.1. The FHN system (2.3.0.2) possess a stable equilibrium point when-

ever a solution to (2.3.1.3)

$$b\bar{x}^3 + 3(1-b)\bar{x} + 3(a - bI) = 0$$

satisfies one of the conditions from A and B given by

$$\text{Condition A} \qquad \begin{cases} \bar{x} < -\sqrt{1-\epsilon b}, & \text{or} \\ \\ \bar{x} > \sqrt{1-\epsilon b} \end{cases}$$

and

$$\text{Condition B} \qquad \begin{cases} \bar{x} < -\sqrt{1-\dfrac{1}{b}}, & \text{or} \\ \\ \bar{x} > \sqrt{1-\dfrac{1}{b}} \end{cases}$$

Our previous result is dependant on the square roots being real. However when the roots are complex we can return to the basic requirements of (2.3.1.17) and (2.3.1.18) find the special case

Given the FHN system (2.3.0.2) with

$$\epsilon b > 1 \quad \text{and} \quad 0 < b \leq 1$$

the system **always** contains at least **one stable equilibrium point**, provided

$$b\bar{x}^3 + 3(1-b)\bar{x} + 3(a - bI) = 0$$

has at least one real solution.

Stability of the branches of the x-nullcline The result found in Theorem 2.3.1.1 dictates when equilibrium points are stable in the FHN system and in fact there are two intervals over which the equilibrium point is stable

$$\bar{x} \in \left(-\infty, -\sqrt{1-\epsilon b}\right) \cup \left(\sqrt{1-\epsilon b}, \infty\right).$$

It has also been shown that the equilibrium point(s) must be on the nullclines; the equations of which are given by (2.3.1.1) and (2.3.1.2). A closer examination of the

x-nullcline

$$y = x - \frac{1}{3}x^3 + I$$

reveals that the maxima and minima occur at the points $(1, I)$ and $(-1, I)$ respectively. Defining the follow sets

Definition 2.3.3 (Nullcline branches)**.** Define the sets

$$L = \left\{ (x, y) : x < -1 \quad \text{and} \quad y = x - \frac{1}{3}x^3 + I \right\}$$

$$C = \left\{ (x, y) : -1 \leq x \leq 1 \quad \text{and} \quad y = x - \frac{1}{3}x^3 + I \right\}$$

$$R = \left\{ (x, y) : 1 < x \quad \text{and} \quad y = x - \frac{1}{3}x^3 + I \right\}$$

then the x-nullcline of the FHN system is simply a union of these three sets which will be referred to as the *Left*, *Center* and *Right* branches of the x-nullxline

Now we have

Theorem 2.3.1.2. If an equilibrium point of the FHN system falls on the left or right branch of the x-nullcline then it must be stable.

The stability of the fixed point is not exactly lost (gained) on entering (leaving) the center branch of the x-nullcline, however when looking at systems with $|\epsilon b| \to 0$ the stability is exactly lost (gained) on entering (leaving) the center branch from the left.[10]

[10]Taking ϵ to be a small parameter is essential if one is interested in excitable dynamics, it is in fact the interplay between the two effective times scales which produces action potential like dynamics.

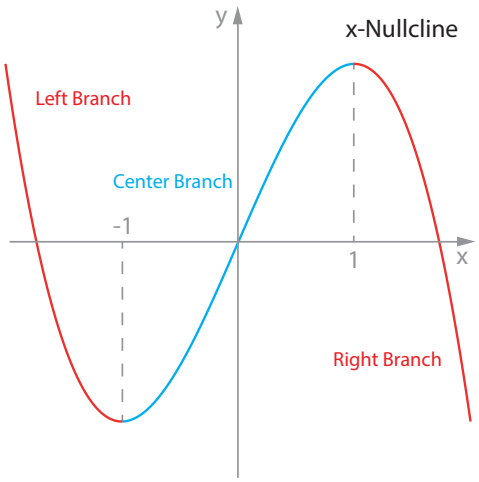

Figure 2.10: The branches of the x-nullcline. In the limit as $\epsilon b \to 0$ the red branches are the 'stable' branches on which one would find a stable fixed point if y-nullcline would interest there, which the blue curve is where there would be an unstable equilibrium.

The saddle node

The FHN system (2.3.0.2) is capable of having a saddle node equilibrium point, these are points at which the Jacobian matrix has a negative determinant. In other words one requires

$$\Delta = \det\left(J\left(\bar{x}, \bar{y}\right)\right) < 0.$$

From (2.3.1.16) the condition is

$$\epsilon b \bar{x}^2 + \epsilon(1 - b) < 0$$

and thus

A saddle node equilibrium point will occur in the FHN system (2.3.0.2) only when

$$b > 1$$

The eigenvalues of the system's Jacobian given by (2.3.1.13) and (2.3.1.14) are

$$\lambda_1 = \frac{(1 - \bar{x}^2 - \epsilon b) + \sqrt{(1 - \bar{x}^2 + \epsilon b)^2 - 4\epsilon)}}{2}$$

$$\lambda_2 = \frac{(1 - \bar{x}^2 - \epsilon b) - \sqrt{(1 - \bar{x}^2 + \epsilon b)^2 - 4\epsilon)}}{2}$$

and have respective eigenvectors [11]
These being the directions along which the stable and unstable manifolds evolve from the saddle node.

$$v_1 = \begin{bmatrix} -1 \\ \lambda_1 - (1 - \bar{x}^2) \end{bmatrix} \quad \text{and} \quad v_2 = \begin{bmatrix} -1 \\ \lambda_2 - (1 - \bar{x}^2) \end{bmatrix}$$

2.4 Fitzhugh-Nagumo As a Lienard System

2.4.1 Transforming The FHN system to Lienard Form.

Given the FHN system

$$\begin{aligned} \dot{x} &= x - x^3/3 - y + I \\ \dot{y} &= \epsilon(x + a - by) \end{aligned} \tag{2.4.1.1}$$

We wish to transform the system into a Lienard system which is a second order ODE system given by the following form

$$\ddot{x} + f(x)\dot{x} + g(x) = 0 \tag{2.4.1.2}$$

where we have overloaded the role of the variable x to keep standard notation for (2.4.1.1) and (2.4.1.2).

Firstly we eliminate the constant term appearing in the right hand side of the $\dot{y}$ in (2.4.1.1)

[11] A arbitrary 2x2 matrix

$$M = \begin{pmatrix} a & b \\ c & d \end{pmatrix}$$

has eigenvalues

$$\lambda_{1,2} = \frac{\tau \pm \sqrt{\tau^2 - 4\Delta}}{2}$$

where $\tau = a + d$ and $ad - bc$. Eigenvectors corresponding to these eigenvalues are given by

$$v_1 = \begin{bmatrix} b \\ \lambda_1 - a \end{bmatrix} \qquad v_2 = \begin{bmatrix} b \\ \lambda_2 - a \end{bmatrix}$$

by making the change of variables

$$y \to z + \frac{a}{b}. \tag{2.4.1.3}$$

Equation (2.4.1.1) can now be expressed as

$$\begin{aligned} \dot{x} &= x - x^3/3 - z - \frac{a}{b} + I \\ \dot{z} &= \epsilon(x - bz). \end{aligned} \tag{2.4.1.4}$$

Now relabeling

$$\begin{aligned} z &\to y \\ \frac{a}{b} + I &\to I' \end{aligned}$$

we have a more compact expression for the FHN system given by

$$\begin{aligned} \dot{x} &= x - x^3/3 - y + I' \\ \dot{y} &= \epsilon(x - by). \end{aligned} \tag{2.4.1.5}$$

In order to rewrite the (2.4.1.5) in the form of equation (2.4.1.2) we start by taking the derivative of the $\dot{x}$ equation found in (2.4.1.5) which on application of the chain rule yields

$$\ddot{x} = \dot{x} - x^2\dot{x} - \dot{y} + \dot{I}'$$

now want to eliminate reference to $\dot{y}$ and so substitute the expression for $\dot{y}$ found in (2.4.1.5)

$$\ddot{x} = \dot{x} - x^2\dot{x} - \epsilon x + \epsilon by + \dot{I}'.$$

The Lienard system however demands that we have functions of only one variable appearing in the second order equation and thus we remove reference to y by noticing that

$$y = x - x^3/3 - \dot{x} + I'$$

which finally allows us to expression the FHN system as

$$\ddot{x} = \dot{x} - x^2\dot{x} - \epsilon x + \epsilon b\left(x - x^3/3 - \dot{x} + I'\right) + \dot{I'}. \tag{2.4.1.6}$$

After a little simplification this can be expressed as

Theorem 2.4.1.1. FHN System in Lienard form

$$\ddot{x} + f(x)\dot{x} + g(x) = 0 \tag{2.4.1.7}$$

where

$$f(x) = x^2 + \epsilon b - 1 \tag{2.4.1.8}$$

$$g(x) = \frac{\epsilon b}{3}x^3 + \epsilon x(1-b) - \epsilon b I' - \dot{I'} \tag{2.4.1.9}$$

As is standard in the literature when dealing with Lienard systems we define

The function,

$$F(x) = \int_0^x f(\omega)\, d\omega = \frac{x^3}{3} + (\epsilon b - 1)x \tag{2.4.1.10}$$

and the variables

$$\mathbf{x} = \begin{bmatrix} x_1 \\ x_2 \end{bmatrix} = \begin{bmatrix} x \\ \dot{x} + F(x) \end{bmatrix}$$

This allows us to write (2.4.1.7) as a pair of first order differential equations of the form

$$\dot{\mathbf{x}} = \begin{bmatrix} \dot{x_1} \\ \dot{x_2} \end{bmatrix} = \begin{bmatrix} x_2 - F(x_1) \\ -g(x_1) \end{bmatrix}$$

2.4.2 Existence of Limit cycles in Lienard Systems

We begin with a theorem concerning limit cycles in Lienard type systems

Theorem 2.4.2.1. The equation

$$\ddot{x} + f(x)\dot{x} + g(x) = 0$$

has a unique periodic solution if f and g are continuous, and

(i) $F(x)$ is an odd function.

(ii) $F(x)$ is zero only at $x = 0$, $x = a$, $x = -a$, for some $a > 0$.

(iii) $F(x) \to \infty$ as $x \to \infty$ monotonically for $x > a$.

(iv) $g(x)$ is an odd function and $g(x) > 0$ for $x > 0$

A proof of Theorem 2.4.2.1 can be found in [89, p. 395].

For the FHN system we found

$$f(x) = x^2 + \epsilon b - 1$$

$$g(x) = \frac{\epsilon b}{3}x^3 + \epsilon x(1 - b) - \epsilon b I' - \dot{I}'$$

which are both continuous functions as they are of polynomial type. Furthermore we have also found that

$$F(x) = \frac{x^3}{3} + (\epsilon b - 1)x.$$

The first condition stated by Theorem 2.4.2.1 concerns the symmetry of $F(x)$, which we can show is odd $\forall x \in \mathbb{R}$

$$F(-u) = \frac{(-u)^3}{3} + (\epsilon b - 1)(-u) = -\left(\frac{u^3}{3} + (\epsilon b - 1)u\right) = -F(u)$$

as required.

$$F(x) \text{ is an odd function.}$$

The second requirement concerns the roots of $F(x)$. Solving

$$\frac{x^3}{3} + (\epsilon b - 1)x = 0$$

one finds the three roots

$$x_1 = 0, \quad x_2 = -\sqrt{-3(\epsilon b - 1)} \quad \text{and} \quad x_3 = \sqrt{-3(\epsilon b - 1)}$$

$F(x)$ has three roots that are given by,

$$x_1 = 0, \quad x_2 = -\sqrt{-3(\epsilon b - 1)} \quad \text{and} \quad x_3 = \sqrt{-3(\epsilon b - 1)}$$

The third requirement asks us to show that

$$F(x) \to \infty, \quad \text{when} \quad x > \sqrt{-3(\epsilon b - 1)} \quad \text{and} \quad x \to \infty$$

Beginning with

$$\sqrt{-3(\epsilon b - 1)} \in \mathbb{R}^+$$

so that $F(x)$ has three distinct real roots, we have the constraint

$$\epsilon b < 1.$$

defining the quantity

$$\eta = \sqrt{-3(\epsilon b - 1)} + \delta, \quad \delta > 0$$

We want

$$F(\eta) \to \infty, \quad \text{when} \quad \eta \to \infty$$

Now,

$$F(\eta) = 2\delta - 2\epsilon b\delta + \sqrt{-3(\epsilon b - 1)}\delta^2 + \frac{\delta^3}{3}$$

The constraint $\epsilon b < 1$ tells us that $2\delta - 2\epsilon b\delta > 0$ and thus we can conclude

$$F(x) \to \infty$$

monotonically when

$$x > \sqrt{-3(\epsilon b - 1)} \quad \text{and} \quad x \to \infty$$

provided

$$\epsilon b < 1.$$

Finally we examine the situation where $I = 0$ though this can be somewhat relaxed [12] Thus we require

$$g(x) = \frac{\epsilon b}{3}x^3 + \epsilon x(1-b).$$

to be odd and $g(x) > 0$ when $x > 0$. We can say

$g(x)$ is clearly odd and is positive definite for all $x > 0$ if one constrains the parameter

$$b \leq 1.$$

Finally we have covered all the requirements for 2.4.2.1 and state the following existence theorem for the FHN system

Theorem 2.4.2.2. FHN Limit Cycle Existence 1
The FHN system (2.4.1.1) has **one unique** limit cycle if

- $I = 0$
- $b \leq 1$
- $\epsilon b < 1$

[12] One can examine the case where there are no current (I) terms in the expression for $g(x)$. What is required is a time varying external current that satisfies

$$\dot{I}' = \epsilon b I'$$

Leaving the expression

$$g(x) = \frac{\epsilon b}{3}x^3 + \epsilon x(1-b).$$

2.5 Fast Slow Dynamics in the FHN system

In this section the aim is to derive a number of results concerning the interplay between *fast* and *slow* dynamics in the FHN system. This is thus a departure from the study of equilibrium points in the system but is nevertheless related to the nullclines of the system.

2.5.1 Classical Perturbation Method

Before starting the analysis of the FHN system it is useful to state a number of useful definitions,

Definition 2.5.1 (Smooth Manifold)**.**
Let $\mathbb{R}^p$ be a p dimensional Euclidean space. A set of points $U \subset \mathbb{R}^p$ is said to be a *smooth* or *differentiable manifold* of dimension q with $q \leq p$ if there exists a neighbourhood around every point $P \in U$ that is C^∞ diffeomorphic to $\mathbb{R}^q$.

Given the *fast* variables $\mathbf{x} \in \mathbb{R}^n$, the *slow* variables $\mathbf{y} \in \mathbb{R}^m$ and the parameter ϵ, the system

$$\begin{aligned} \dot{\mathbf{x}} &= F(\mathbf{x}, \mathbf{y}, \epsilon) \\ \dot{\mathbf{y}} &= \epsilon G(\mathbf{x}, \mathbf{y}, \epsilon) \end{aligned} \tag{2.5.1.1}$$

along with a full set of initial conditions is known as the *full system* with asymptotic structure (m, n). The *fast* system is defined by setting ϵ to zero,

Definition 2.5.2 (Fast system)**.**
The *fast* system associated with the full system (2.5.1.1) is given by

$$\begin{aligned} \dot{\mathbf{x}} &= F(\mathbf{x}, \mathbf{y}, 0) \\ \dot{\mathbf{y}} &= 0 \end{aligned} \tag{2.5.1.2}$$

For sufficiently small ϵ and time intervals the full system (2.5.1.1) and the fast system (2.5.1.2) differ only "slightly" for every choice of $\mathbf{x}$ and $\mathbf{y}$. In fact solutions of the full system (2.5.1.1) converge to the corresponding initial value problem in the fast system (2.5.1.2) as $\epsilon \to 0$ for an appropriately short interval of time, this is a consequence of

the Theorem of Continuous Dependence on Parameters [95, p 87]. Thus one can view the full system as being the fast system subject to continuous perturbation [7, p 64]. To study the behaviour of the full system over longer time intervals than those over which the fast system is comparable one introduces the change of variables

$$\tau = \epsilon t$$

where τ is referred to as the *slow time*. The change of variables to slow time transforms the full system (2.5.1.1) to

$$\begin{aligned} \epsilon \dot{\mathbf{x}}_\tau &= F(\mathbf{x}, \mathbf{y}, \epsilon) \\ \dot{\mathbf{y}}_\tau &= G(\mathbf{x}, \mathbf{y}, \epsilon) \end{aligned}$$

where the overdot and tau subscript mean differentiation with respect to the slow time tau. The slow time scale defines the *slow* or *reduced system* by taking the small parameter ϵ to zero[13]

Definition 2.5.3 (Slow system)**.**
The *slow* system associated with the full system (2.5.1.1) is given by

$$\begin{aligned} F(\mathbf{x}, \mathbf{y}, 0) &= 0 \\ \dot{\mathbf{y}}_\tau &= G(\mathbf{x}, \mathbf{y}, 0) \end{aligned} \tag{2.5.1.3}$$

Reducing the generalisation from an (n+m)-dimensional system to a system in $\mathbb{R}^2$. The slow system given by (2.5.1.3) defines the *slow manifold* if one assumes there exists at least one real root to

$$F(x, y) = 0$$

for every y. Which gives us

$$x = \phi(y)$$

the equation of the slow manifold. This allows us to further rewrite the equations governing the slow manifold using (2.5.1.3)

[13]If the small parameter is not well approximated by zero we can still find an approximation to the slow manifold with higher order terms of epsilon represented and make a truncation at whatever order is reasonable $\mathcal{O}(\epsilon)$, $\mathcal{O}(\epsilon^2)$, etc. For the FHN system such an expression has been shown in the appendix.

$$\begin{aligned} \dot{y}_\tau &= G(x, y, 0) \\ x &= \phi(y) \end{aligned} \tag{2.5.1.4}$$

Important features of the slow manifold occur at *fold points*:

Definition 2.5.4 (Fold Points)**.**
Fold points are points on the slow manifold where the linearisation of the fast variable has at least one zero eigenvalue.

The fold points are thus points where the slow manifold switches from being attractive to repulsive or viceversa.
Finally one comes to an important theorem concerning slow-fast systems due to Tikhonov [173, 182]. Before we can state the theorem and its underling assumptions we require the following definitions:

Definition 2.5.5 (Lyapunov Stability of Equilibrium Points)**.**
Given the system

$$\dot{\mathbf{z}} = H(\mathbf{z}, t)$$

with H being a vector field and $\dot{z}$ denoting the derivative with respect to t. A point $z = z_0$ is called a Lyapunov stable equilirbium point of the system if

- $H(\mathbf{z}_0, t) = 0, \quad \forall t \geq 0$
- For every given $\mu > 0$ there exists a $\delta = \delta(\mu)$ such that for any solution $\mathbf{z}(t)$ of the given system satisfying

  $$|\mathbf{z}_0 - \mathbf{z}(t_0)| < \delta$$

  then

  $$|\mathbf{z}_0 - \mathbf{z}(t)| < \epsilon, \quad \forall\, t > t_0,\, t_0 \in \mathbb{R}.$$

Further more an equilibrium point is said to be asymptotically stable if:

Definition 2.5.6 (Asymptotic Stability of Equilibrium Point)**.**
Given the system

$$\dot{\mathbf{z}} = H(\mathbf{z}, t)$$

A point $\mathbf{z} = \mathbf{z}_0$ is called an asymptotically stable equilibrium point of the system if

- It is a Lyapunov stable equilibrium point.
- There exists a constant $\eta > 0$ such that, if

  $$|\mathbf{z}_0 - \mathbf{z}(t_0)| < \eta$$

  then,

  $$\lim_{t\to\infty} |\mathbf{z}_0 - \mathbf{z}(t)| = 0$$

Now the Tikhonov theorem states,

For the system given by (2.5.1.1)

$$\dot{\mathbf{x}} = F(\mathbf{x}, \mathbf{y}, \epsilon)$$
$$\dot{\mathbf{y}} = \epsilon G(\mathbf{x}, \mathbf{y}, \epsilon)$$

subject to the following conditions

1. F and G are continuous
2. There exists a continuous function $\phi(y)$ such that

   $$F(\phi(y), y, 0) = 0$$

3. There exists $\eta > 0$, such that

   $$|x - \phi(y)| < \eta, \quad x \neq \phi(y)$$

   implies

   $$F(x, y) \neq 0$$

4. The equilibrium point $x = \phi(y)$ of the fast system (2.5.1.2) is asymptotically stable.

5. The full system (2.5.1.1) and the slow system (2.5.1.3) have unique solutions in an interval

$$0 \leq \tau \leq T$$

for any choice of ϵ.

Theorem 2.5.1.1 (Tikhonov's Theorem)**.** Given that the above conditions hold for a given system. Let (x_0, y_0) be a point in the basin of attraction of the equilibrium $(\phi(y_0), y_0)$ of the fast system (2.5.1.2), which is assumed to exist for the interval of time $[0, T]$. Then the solution $(x(\tau, \epsilon), y(\tau, \epsilon))$ to the full system (2.5.1.1) for sufficiently small ϵ on the interval $[0, T]$ is related to the solution of the slow system

$$(x_s(\tau), y_s(\tau)), \qquad x_s(\tau) = \phi(y_s)$$

by the relations,

$$\begin{aligned} &\lim_{\epsilon \to 0} x(\tau, \epsilon) = x_s(\tau) = \phi(y_s(\tau)), \\ &\lim_{\epsilon \to 0} y(\tau, \epsilon) = y_s(\tau), \quad 0 < \tau < T_0 \end{aligned}$$

where $0 < T_0 \leq T$.

The structure of the FHN system

In order to look at the asymptotic structure of the FHN system

$$\begin{aligned} \dot{x} &= x - \frac{x^3}{3} - y + I \\ \dot{y} &= \epsilon(x + a - by) \end{aligned}$$

it is necessary to make a small parameter assumption on ϵ,

$$0 < \epsilon \ll 1$$

which imposes two times scales on the system. Thus the fast subsystem is given by

The **fast system** associated with the FHN equations is given by

$$\begin{aligned} \dot{x} &= x - \frac{x^3}{3} - y + I \\ y &= \text{constant} \end{aligned} \tag{2.5.1.5}$$

The slow system is obtained by switching the full system to the slow time, $t = \epsilon\tau$,

$$\begin{aligned} \epsilon\dot{x}_\tau &= x - \frac{x^3}{3} - y + I \\ \dot{y}_\tau &= x + a - by \end{aligned}$$

and setting the small parameter $\epsilon = 0$. [14]

The **slow system** associated with the FHN equations is given by

$$\begin{aligned} y &= x - \frac{x^3}{3} + I \\ \dot{y}_\tau &= x + a - by \end{aligned} \tag{2.5.1.6}$$

The slow manifold is given by the equation for the x-nullcline

$$y = x - \frac{x^3}{3} + I$$

Which has fold points wherever the derivative

$$\frac{dy}{dx} = 1 - x^2 + I$$

vanishes. Thus

The fold points of the FHN system occur at

$$x_{\text{fold}} = \pm\sqrt{1 + I}$$

At the fold points the branches of the stable slow manifold looses stability at which point the dynamics are approximated by the fast system. The fast system (2.5.1.5) shows that

[14] If the small parameter is not negligibly small but can be considered negligibly small at higher orders one can still find an expression for the invariant slow manifold as is shown in the appendix.

the dynamics move along lines where

$$y = \text{constant}$$

These curves (lines) of the fast system partition the full system's phase space and are referred to in the literature as the *fast foliation*. After moving along the fast foliation a trajectory of the full system will again meet a branch of the stable slow manifold, shown in Figure 2.11, along which it will again flow until it reaches a point where the slow manifold is unstable again or an equilibrium point of the system.

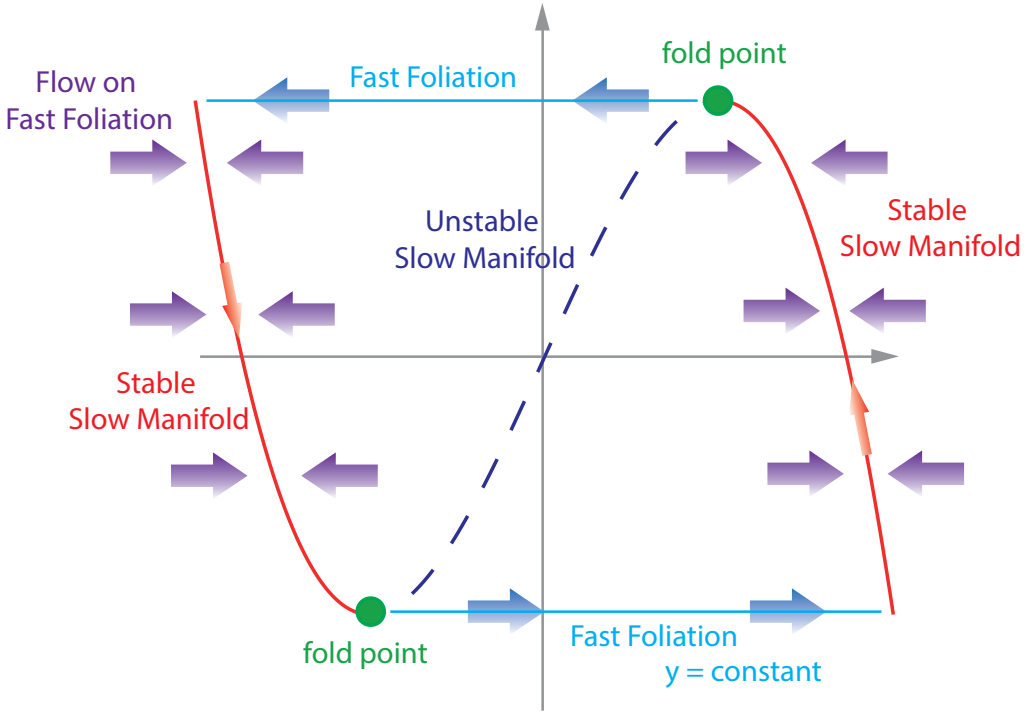

Figure 2.11: A schematic diagram showing the slow manifold and fast flow across representative lines on the fast foliation. If the only equilibrium present in the system is an unstable one the system will undergo the cycle from slow manifold to fast foliation to slow manifold repeatedly giving rise to limit cycles/oscillations.

2.6 Andronov-Hopf Bifurcation in the FHN system

This section looks at the formation of limit cycles in the FHN system through an Andronov-Hopf bifurcation. The formation of limit cycles are of central importance in the study of biological systems as they are they are the structures which introduce oscillation into the system.

2.6.1 The Hopf Bifurcation

Definition 2.6.1 (Bifurcation of an equilibrium point)**.**
An equilibrium point $\mathbf{x} = \bar{\mathbf{x}}$ of a vector field is said to undergo a bifurcation at the parameter $\mu = \bar{\mu}$ if the flow near $\bar{\mathbf{x}}$ when $\mu \simeq \bar{\mu}$ is qualitatively different to the flow near $\bar{\mathbf{x}}$ when $\mu = \bar{\mu}$.

As a consequence of the above definition there are a number of useful remarks to make that can be found in [193, p 363], one of which is concerned about the *hyperbolicity* of an equilibrium point:

Definition 2.6.2 (Hyperbolic Point)**.**
An equilibrium point, $\bar{\mathbf{x}}$ of a dynamical system

$$\dot{\mathbf{x}} = f(\mathbf{x})$$

is said to be *hyperbolic* if the, linearised system, Jacobian at the equilibrium point only has eigenvalues with nonzero real parts.

Now we make the remark found in [193, p 363] that states:

The condition that an equilibrium point is *nonhyperbolic* is a necessary but not sufficient condition for a bifurcation to occur in one-parameter families of vector fields.

A Hopf bifurcation is defined as follows [63, p 66–67]:

Definition 2.6.3 (Hopf Bifurcation)**.**
Given a set of ODEs with state variables $\mathbf{x} \in \mathbb{R}^n$ and parameter $\mu \in \mathbb{R}$

$$\dot{\mathbf{x}} = \mathbf{F}(\mathbf{x}, \mu)$$

Then given

- An equilibrium point of the system $\bar{\mathbf{x}}$ dependent on μ.
- The linearised system at the equilibrium point $\bar{\mathbf{x}}$ has a pair of complex conjugate eigenvalues

$$\lambda_{1,2} = \alpha(\mu) \pm i\omega(\mu)$$

such that

1. at a critical bifurcation parameter $\mu = \mu_c$

$$\alpha(\mu_c) = 0 \quad \text{and} \quad \left.\frac{d\alpha}{d\mu}\right|_{\mu=\mu_c} \neq 0$$

2. the remaining $n-2$ eigenvalues of the Jacobian have strictly negative real parts

The system is said to undergo a *Hopf-bifurcation* at $\mu = \mu_c$ and there appears a limit cycle from the equilibrium point $\bar{\mathbf{x}}$.

2.6.2 The Hopf point in the FHN system

We begin with the now familiar FHN system

$$\dot{x} = x - \frac{x^3}{3} - y + I$$
$$\dot{y} = \epsilon(x + a - by)$$

The equilibrium points have been shown to be solutions to

$$b\bar{x}^3 + 3(1-b)\bar{x} + 3(a - bI) = 0, \qquad \bar{y} = \frac{\bar{x} + a}{b}$$

they are dependant on all of the parameters in the system and their existence and stability have been discussed earlier. As such we simply take an equilibrium of the system to be

$$\bar{\mathbf{x}} = (\bar{x}, \bar{y})$$

and assume it adheres to the various existence criteria. The second requirement for the Hopf bifurcation from definition 2.6.3 is that the linearised system has complex conjugate

eigenvalues. Recalling the Jacobian evaluated at the equilibrium point is given by

$$J(\bar{x}, \bar{y}) = \begin{pmatrix} 1 - \bar{x}^2 & -1 \\ \\ \epsilon & -\epsilon b \end{pmatrix}$$

with trace

$$\tau = 1 - \bar{x}^2 - \epsilon b$$

and determinant

$$\Delta = \epsilon b \bar{x}^2 + \epsilon(1 - b)$$

The eigenvalues are given by

$$\lambda_{1,2} = \frac{\tau \pm \sqrt{\tau^2 - 4\Delta}}{2}.$$

To have purely imaginary eigenvalues one requires

$$\tau = 0 \quad \text{and} \quad \Delta > 0$$

which yields

$$\bar{x}^2 = 1 - \epsilon b \quad \text{and} \quad b\bar{x}^2 + (1 - b) > 0$$

Substituting the expression for $\bar{x}^2$ into the inequality we have the condition for nonzero imaginary part of the eigenvalue being

$$\epsilon^2 b^3 - 2\epsilon b^2 + 1 > 0.$$

The transitivity condition asks us to examine

$$\frac{d}{d\bar{x}} \left(\text{Real} \left(\lambda_{1,2} \right) \right) \Big|_{\bar{x} = \pm\sqrt{1-\epsilon b}} = -2\bar{x}|_{\bar{x} = \pm\sqrt{1-\epsilon b}} = \pm 2(1 - \epsilon b)$$

which is nonzero provided

$$\epsilon b \neq 1.$$

Thus the equilibrium point $\bar{x}$ undergoes a Hopf bifurcation. The Hopf bifurcation point

occurs at

$$\bar{x}^2 = 1 - \epsilon b.$$

It has already been shown that when

$$\bar{x} < -\sqrt{1-\epsilon b} \quad \text{or} \quad \bar{x} > \sqrt{1-\epsilon b}$$

the equilibrium point is stable as it is on the stable branch of the x-Nullcline. Thus a Hopf bifurcation occurs in the system when the equilibrium point is moved to the unstable branch of the x-Nullcline from a stable branch.

A Hopf bifurcation occurs in the FHN system when

$$\bar{x} = \pm\sqrt{1-\epsilon b}$$

whenever the equilibrium point $\bar{x}$ moves from a stable branch of x-Nullcline to the unstable branch.

2.6.3 The stability of the limit cycle resulting from the Hopf bifurcation

Even thought the conditions for a Hopf bifurcation are satisfied by the FHN system, one does not know if the resulting limit cycle is stable or unstable. In order to infer the stability of the resulting limit cycle we continue the analysis and calculate the first Lyapunov exponent associated with the formed limit cycle. We use the methods outlined in [100, 96–104] and begin by transforming the system so that the equilibrium point $\bar{x}$ occurs at the origin by introducing the change of variables

$$x = \bar{x} + h_1 \quad \text{and} \quad y = \bar{y} + h_2$$

which transforms the FHN system

$$\begin{aligned} \dot{x} &= x - \frac{x^3}{3} - y + I \\ \dot{y} &= \epsilon(x + a - by) \end{aligned}$$

to the system

$$\dot{h_1} = (\bar{x} + h_1) - \frac{1}{3}(\bar{x} + h_1)^3 - (\bar{y} + h_2) + I$$

$$\dot{h_2} = \epsilon(\bar{x} + h_1 + a - b\bar{y} - bh_2)$$

which when expanded yields

$$\dot{h_1} = \left\{\bar{x} - \frac{1}{3}\bar{x}^3 - \bar{y} + I\right\} + h_1 - \frac{1}{3}\left(3\bar{x}^2 h_1 + 3\bar{x}h_1^2 + h_1^3\right) - h_2$$

$$\dot{h_2} = \left\{\epsilon(\bar{x} + a - b\bar{y})\right\} + \epsilon(h_1 - bh_2)$$

The terms in the curly brackets however are both equal to zero as $(\bar{x}, \bar{y})$ is an equilibrium point of the FHN system[15], thus the translated system is given by

$$\dot{h_1} = h_1 - \frac{1}{3}\left(3\bar{x}^2 h_1 + 3\bar{x}h_1^2 + h_1^3\right) - h_2 \equiv F_1(h_1, h_2)$$

$$\dot{h_2} = \epsilon(h_1 - bh_2) \equiv F_2(h_1, h_2) \tag{2.6.3.1}$$

Which now has the equilibrium point of interest translated to the origin. Equation (2.6.3.1) can be expressed an terms of symmetric multilinear vector functions that result from the multidimensional Taylor expansion of F_1 and F_2 as [100, p 93]

$$\dot{\mathbf{h}} = A\mathbf{h} + \frac{1}{2}B(\mathbf{h}, \mathbf{h}) + \frac{1}{6}C(\mathbf{h}, \mathbf{h}, \mathbf{h}) + \mathcal{O}(|\mathbf{h}|^4)$$

where $\mathbf{h} = [h_1, h_2]$, A is the Jacobian matrix at the Hopf point
The multilinear function $B(x, y)$ is given by

$$B_i(x, y) = \sum_{i,j=1}^{2} \frac{\partial^2 F_i(h_1, h_2)}{\partial h_j \partial h_k} x_j y_k$$

Which for (2.6.3.1) yields

[15]These are infact the equations of the x and y-nullclines which are points in which there the curves upon which the flow reduces to having at most one dimension.

$$B(x,y) = \begin{pmatrix} 2\bar{x}x_1y_1 \\ \\ 0 \end{pmatrix}$$

$C(x,y,u)$ is given by

$$C_i(x,y,u) = \sum_{i,j,l=1}^{2} \frac{\partial^3 F_i(h_1,h_2)}{\partial h_j \partial h_k \partial h_l} x_j y_k u_l.$$

Which for (2.6.3.1) yields

$$C(x,y,u) = \begin{pmatrix} 2x_1y_1u_1 \\ \\ 0 \end{pmatrix}$$

The Jacobian matrix of (2.6.3.1) at the Hopf point $\mathbf{h} = (0,0)$, $\bar{x}^2 = 1 - \epsilon b$ is

$$A = \begin{pmatrix} \epsilon b & -1 \\ \\ \epsilon & -\epsilon b \end{pmatrix} \tag{2.6.3.2}$$

which has purely imaginary eigenvalues

$$\lambda_{1,2} = \pm i\omega = \pm\sqrt{\epsilon^2 b^2 - \epsilon} \tag{2.6.3.3}$$

The complex eigenvector associated with the eigenvalue $\lambda_1 = i\omega$ from (2.6.3.3) of (2.6.3.2) can be given as

$$q \sim \begin{pmatrix} 1 \\ \\ \epsilon b - i\omega \end{pmatrix}$$

It is also necessary to find the eigenvector of A^T associated with the eigenvalue $\lambda_2 = -i\omega$

$$p \sim \begin{pmatrix} \epsilon \\ \\ -\epsilon b - i\omega \end{pmatrix}$$

these are proper eigenvectors such that

$$Aq = i\omega q, \qquad A^T p = -i\omega p.$$

Before using these vectors as the basis to find the first Lyapunov exponent of the Hopf bifurcation one needs to ensure that the vectors are normalised such that

$$\langle p, q\rangle = 1$$

where $\langle p, q\rangle$ is the usual inner product in $\mathbb{C}^2$

$$\langle p, q\rangle = \bar{p_1} q_1 + \bar{p_2} q_2$$

here the overbar means complex conjugate. For the p and q given

$$\begin{aligned}\langle p, q\rangle &= \epsilon - \epsilon^2 b^2 + 2\epsilon b\omega i + \omega^2 \\ &= 2\omega^2 + 2\epsilon b\omega i\end{aligned}$$

and thus taking the eigenvectors to be

$$q = \begin{pmatrix} 1 \\ \epsilon b - i\omega \end{pmatrix}, \qquad p = \frac{1}{2\omega^2 + 2\epsilon b\omega i} \begin{pmatrix} \epsilon \\ -\epsilon b - i\omega \end{pmatrix} \tag{2.6.3.4}$$

yields the desired normalised eigenvectors. The difficult work is complete and all that is left is to find an expression for the first Lyapunov exponent which is given by [100, p 99]

$$l = \frac{1}{2\omega^2} \mathrm{Re}\left(i g_{20} g_{11} + \omega g_{21}\right)$$

where

$$g_{20} = \langle p, B(q, q)\rangle, \quad g_{11} = \langle p, B(q, \bar{q})\rangle, \quad \text{and} \quad g_{21} = \langle p, C(q, q, \bar{q})\rangle$$

with a little work these quantities are

$$g_{20} = \left\langle \frac{1}{2\omega^2 + 2\epsilon b\omega i} \begin{pmatrix} \epsilon \\ -\epsilon b - i\omega \end{pmatrix}, \begin{pmatrix} 2\bar{x} \\ 0 \end{pmatrix} \right\rangle = \frac{\epsilon \bar{x}}{\omega^2 - \epsilon b\omega i}$$

Recall that $\bar{x}$ is the x-coordinate of the equilibrium undergoing a Hopf bifurcation and is given by $\bar{x} = \pm\sqrt{1-\epsilon b}$, this is in contrast to $\bar{p}$ which signifies the complex conjugate of p, now noticing that $B(q,q) = B(q,\bar{q})$ we have

$$g_{11} = \left\langle \frac{1}{2\omega^2 + 2\epsilon b\omega i} \begin{pmatrix} \epsilon \\ -\epsilon b - i\omega \end{pmatrix}, \begin{pmatrix} 2\bar{x} \\ 0 \end{pmatrix} \right\rangle = \frac{\epsilon\bar{x}}{\omega^2 - \epsilon b\omega i}$$

lastly

$$g_{21} = \left\langle \frac{1}{2\omega^2 + 2\epsilon b\omega i} \begin{pmatrix} \epsilon \\ -\epsilon b - i\omega \end{pmatrix}, \begin{pmatrix} 2 \\ 0 \end{pmatrix} \right\rangle = \frac{\epsilon}{\omega^2 - \epsilon b\omega i}$$

The quantity that requires some simplification in order to extract its real part is

$$ig_{20}g_{11} + \omega g_{21} = \frac{i\epsilon^2\bar{x}^2}{\left(\omega^2 - \epsilon b\omega i\right)^2} + \frac{\epsilon\omega}{\omega^2 - \epsilon b\omega i}$$

Making use of the conjugate of the denominator offers a little more simplification

$$ig_{20}g_{11} + \omega g_{21} = \frac{\epsilon\omega^3}{\omega^4 + \epsilon^2 b^2\omega^2} - \frac{2\epsilon^3 b\bar{x}^2\omega^3}{\left(\omega^4 + \epsilon^2 b^2\omega^2\right)^2} + \left(\frac{\epsilon^2\bar{x}^2\omega^4 - \epsilon^4 b^2\bar{x}^2\omega^2}{\left(\omega^4 + \epsilon^2 b^2\omega^2\right)^2} + \frac{\epsilon^2 b\omega^2}{\omega^4 + \epsilon^2 b^2\omega^2}\right) i$$

Finally we have the first Lyapunov number for the FHN systems Hopf bifurcations

$$l = \frac{1}{2\omega^2}\left\{\frac{\epsilon\omega^3}{\omega^4 + \epsilon^2 b^2\omega^2} - \frac{2\epsilon^3 b\bar{x}^2\omega^3}{\left(\omega^4 + \epsilon^2 b^2\omega^2\right)^2}\right\} \tag{2.6.3.5}$$

where,

$$\omega^2 = \epsilon - \epsilon^2 b^2 > 0 \quad \text{and} \quad \bar{x}^2 = 1 - \epsilon b > 0$$

ϵ and b are real. A plot of l vs. b is show in Figure 2.12 for a fixed value of ϵ.

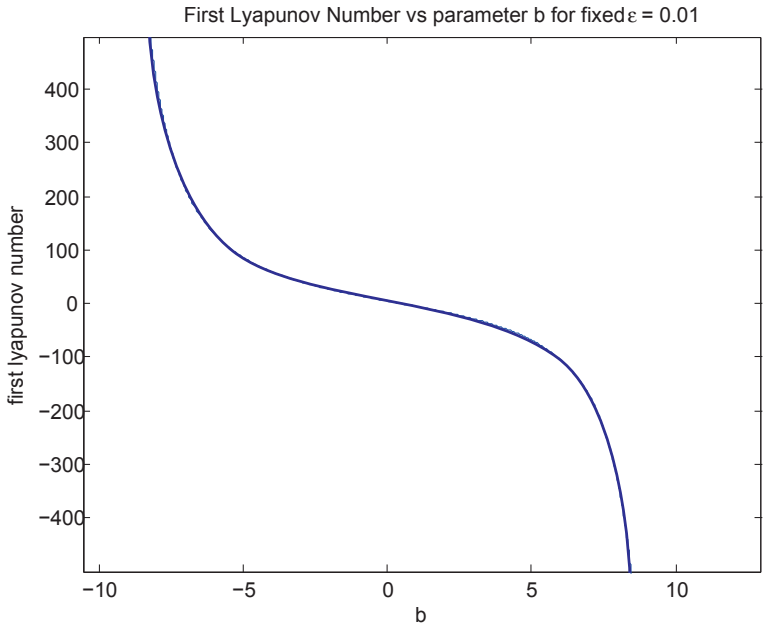

Figure 2.12: Typical plot of the first lyapunov number of the FHN system resulting from the Hopf bifurcation, $\epsilon = 0.01$. Notice that depending on the parameter b one can have stable ($l_1 < 0$) or unstable ($l_1 > 0$) limit cycle appearing. Of further note is the point at which $l_1 = 0$ where one can find Generalised Hopf/Bautin Bifurcations.

2.7 Bifurcations of the FHN system: Numerical

In this section we examine the bifurcation structure of the FHN system using numerical methods offered by continuation packages available for the study of nonlinear systems. The majority of results shown here involve using the MATCONT toolbox which is available as an extension to the MatLab environment. The package has been further set to utilise the symbolic mathematics toolbox which is based on the MAPLE engine. The simulations utilised the following

- MatLab R2011a - 64-bit edition
- MAPLE 15
- Microsoft Visual C++ 2010 Express
- Matcont 4.1

The simulations have been run on a 64-bit machine running Windows 7 with the following hardware

- Processor: Intel i7-920xm 8M Cache, 2.00GHz-3.20GHz, 4 cores and 8 threads.
- RAM: 16Gb DDR3.

The default ODE solver used throughout this thesis is MatLabs *ode*45 solver. This is an adaptive timestep solver utilising a fourth order Runga-Kutta scheme. An adaptive solver is particularly useful when looking at the FHN system due to the presences of the small parameter ϵ. The smaller this parameter is made the "stiffer" the set of ODEs that require solving, this leading to increased computational times.
Unless stated otherwise the simulations in this thesis use $\epsilon = 0.1$. This value of ϵ has been chosen as it maintains the essential "excitable dynamics" that one is interested in when looking at the FHN systems in a biological context while offering little stiffness in the ODE system.

2.7.1 The Hopf Bifurcation Curve

Locating an equilibrium

In order to examine the Hopf bifurcation curve in the system it is necessary to find a particular instance of a Hopf bifurcation occurring in the system as a starting point. To achieve this for a set of parameters one finds an equilibrium point of the system. Numerically one picks an initial condition within an equilibrium points basin of attraction and numerically solves the system of ODEs until one arrives at the equilibrium.

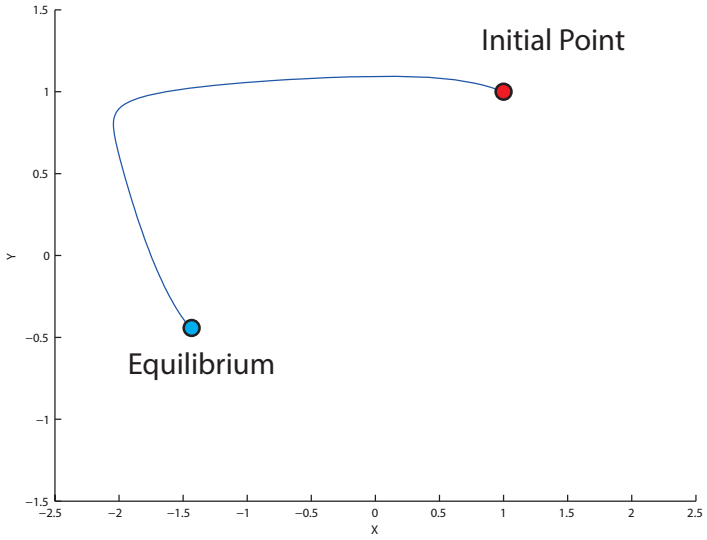

Figure 2.13: Convergence to the equilibrium point of the FHN system

The parameters used to generate figure 2.13 are

$$\epsilon = 0.1, \quad a = 1.0, \quad b = 1.0 \quad \text{and} \quad I = 0.$$

The initial point was chosen to be

$$\mathbf{x}_0 = \begin{bmatrix} 1 \\ 1 \end{bmatrix}$$

and the equilibrium point is found after 1000 time units to be

$$\bar{\mathbf{x}} = \begin{bmatrix} -1.441746686 \\ -0.4423078901 \end{bmatrix}.$$

Locating Hopf bifurcations upon variation of a single parameter

After converging to an equilibrium of the system one is now in a position to vary a particular parameter of the system while tracing the location of the equilibrium and computing the eigenvalues of the linearised system about the equilibrium point.

The MatCont toobox provides a simple means to achieve this. One selects the equilibrium point and the appropriate bifurcation parameter, the (parameter) increment size and the option to track the changes in the systems eigenvalues.

The result of incrementing the parameter both forward and backward (positive and negative increments respectively) are shown in Figure 2.14 for variation of the parameter 'a'.

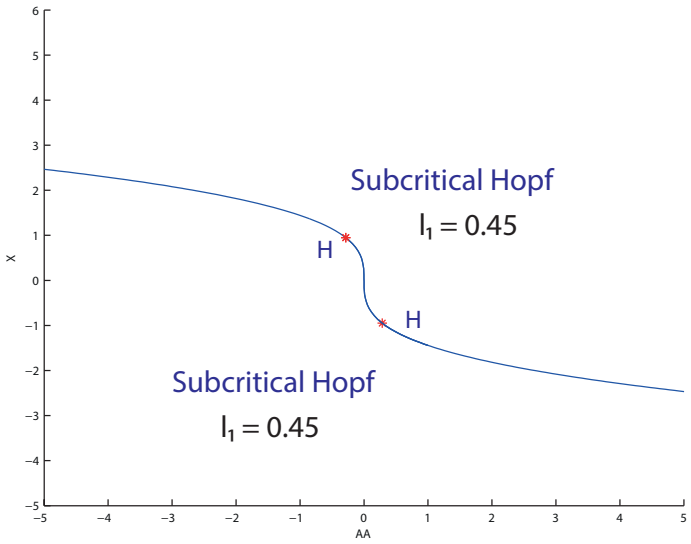

Figure 2.14: The subcritical Hopf bifurcations when $\epsilon = 0.1$, $b = 1$ and a is allowed to vary. Axes show the value of x in the FHN system against the parameter a.

The Hopf bifurcations in figure 2.14 occur at the points

$$\bar{\mathbf{x}}_1 \approx \begin{bmatrix} -0.95 \\ -0.66 \end{bmatrix}, \qquad a \approx 0.28$$

and

$$\bar{\mathbf{x}}_2 \approx \begin{bmatrix} 0.95 \\ 0.66 \end{bmatrix}, \qquad a \approx -0.28$$

The first Lyapunov coefficient for these Hopf bifurcations are given by

$$l_1 = 4.545543 \times 10^{-1} \quad \text{and} \quad l_2 = 4.545419 \times 10^{-1}$$

indicating that the bifurcation limit cycle is unstable making the Hopf bifurcations subcritical.

The Hopf Curve

Once a Hopf point has been located one can find the curve over which Hopf Bifurcations will occur on variation of two free parameters. This is achieved by again tracking the eigenvalues of the system when varying the two parameters and following the direction which admits only imaginary eigenvalues.

While tracking the Hopf curve through parameter space one can also locate codimension-2 bifurcations such as

- The Bogdanov-Takens Bifurcation
- The Generalised (Bautin) Hopf Bifurcation

by checking for their relevant conditions and nondegeneracy conditions.
The bifurcations shown in figure 2.15 have the following properties from bottom to top

1. The first bifurcation and last are labeled BT signifying Bogdanov-Takens bifurcation, these points are

$$\mathbf{x}_1 \approx \begin{bmatrix} -1.147271 \\ -0.643913 \end{bmatrix} \quad a \approx 3.18 \quad b \approx -3.16$$

   and

$$\mathbf{x} \approx \begin{bmatrix} 1.147271 \\ 0.643913 \end{bmatrix} \quad a \approx -3.183516 \quad b \approx -3.162298$$

   However the 'Normal Form' coefficients of the bifurcations cannot be computed signifying that they are both **degenerate** BT bifurcations.

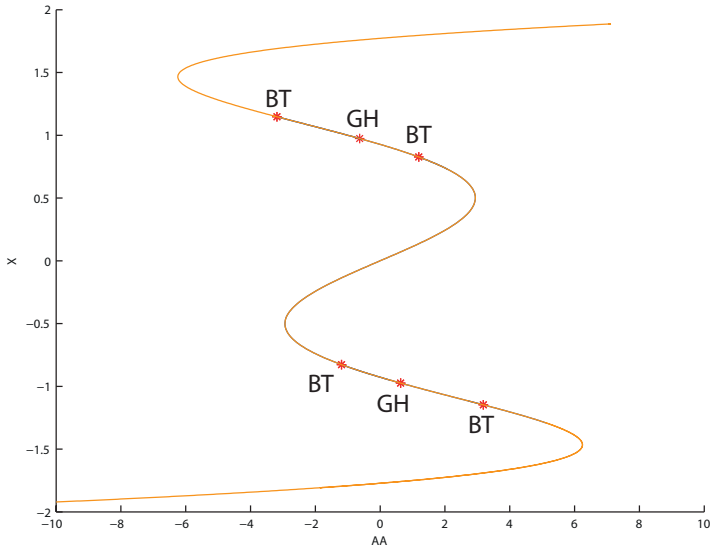

Figure 2.15: The Hopf curve obtain by two parameter variation a and b shown in the $x - a$ plane. The points labeled BT signify locations where a Bogdanov-Takens bifurcation has taken place. Points labeled GH are points where a generalised Hopf bifurcation has taken place.

2. The second and fifth bifurcations are labeled GH which represent Generalised Hopf (Bautin) bifurcations. These occur at

$$\mathbf{x} \approx \begin{bmatrix} -0.974004 \\ -0.665997 \end{bmatrix} \quad a \approx 0.632 \quad b \approx 0.513$$

and

$$\mathbf{x} \approx \begin{bmatrix} 0.974004 \\ 0.665997 \end{bmatrix} \quad a \approx -0.63 \quad b \approx 0.51$$

these are nondegenerate as they have nonzero second Lyapunov numbers given by

$$l_2 \approx -0.242 \quad \text{and} \quad l_2 \approx -0.2419903$$

respectively.

3. The third and fourth bifurcations are BT bifurcations occurring at

$$\mathbf{x} \approx \begin{bmatrix} -0.826905 \\ -0.638434 \end{bmatrix} \quad a \approx -1.19 \quad b \approx 3.16$$

and

$$\mathbf{x} \approx \begin{bmatrix} 0.826905 \\ 0.638434 \end{bmatrix} \quad a \approx 1.19 \quad b \approx 3.16$$

Both are nondegenerate with the normal form coefficients given by

$$\alpha_1 = 0.2493215, \quad \alpha_2 = 1.576846$$

and

$$\alpha_1 = -0.2493215, \quad \alpha_2 = -1.576846$$

respectively.

In the $a - b$ parameter plane we have Figure 2.16

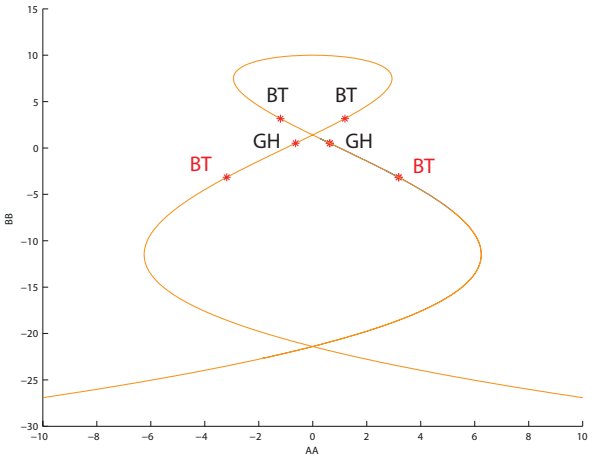

Figure 2.16: The Hopf curve with the degenerate BT bifurcations in red

Supercritical Hopf bifurcation and the Generalised Hopf bifurcation

Thus far it has been shown that Hopf bifurcations that occur when $\epsilon = 0.1$ and $b = 1$ is subcritical. The Hopf curve has also been shown for variation in the parameter b as well. It was shown that there are two nondegenerate generalised Hopf bifurcations that occur at the parameters (shown in Figure 2.17)

$$a \approx 0.632 \quad b \approx 0.513 \quad \text{and}$$
$$a \approx -0.63 \quad b \approx 0.513$$

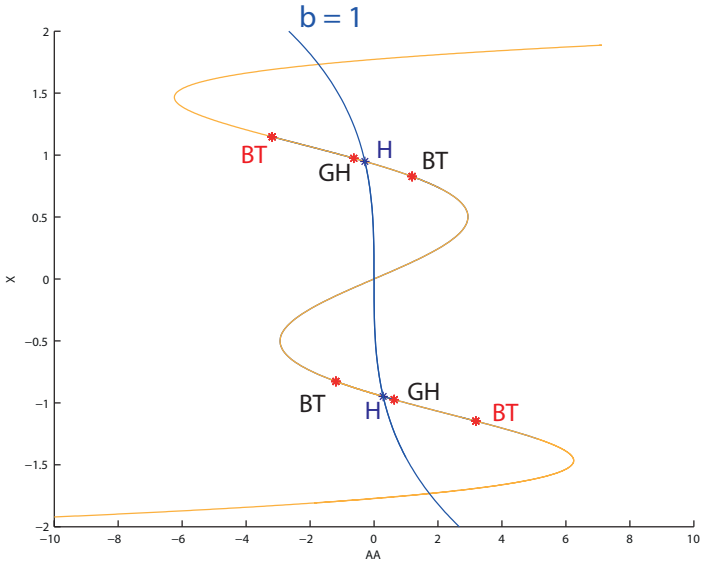

Figure 2.17: The Hopf curve (orange) shown when one varies both parameters a and b and the equilibrium curve when one varies a and keeps $b = 1$ (blue).

Generalised Hopf points, also referred to as Bautin points, are points where the first Lyapunov number is zero. Recalling that the sign of the first Lyapunov number determines if a bifurcating limit cycle from a Hopf bifurcation is stable or unstable and that a Hopf bifurcation is supercritical (subcritical) if the bifurcation limit cycle is stable(unstable). Then it should be clear that the generalized Hopf points are points at which the subcritical and supercritical branches of the Hopf bifurcation meet.

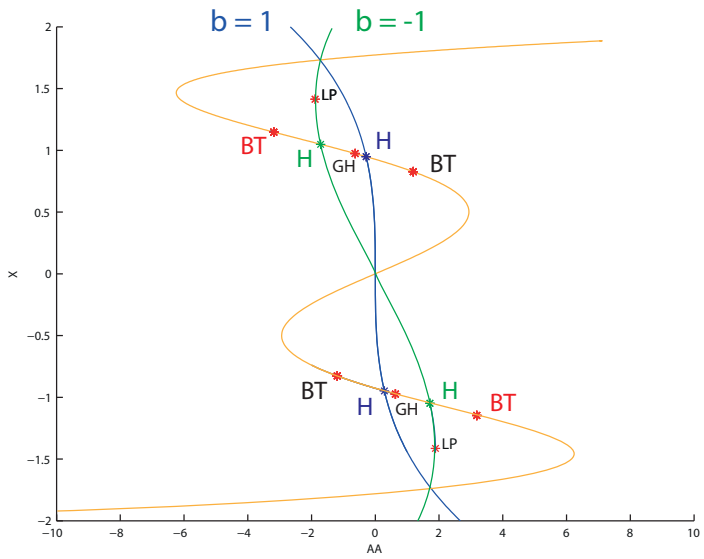

Figure 2.18: Hopf Curve (orange), equilibrium curves for $b = 1$ (blue) and $b = -1$ (green). The Generalised Hopf points GH divide the supercritical and subcritical branches of the Hopf curve.

The Hopf bifurcations shown on the green curve of Figure 2.18 occur at the points

$$\mathbf{x} = \begin{bmatrix} -1.048808 \\ -0.664246 \end{bmatrix}, \quad a = 1.713053, \qquad \text{with} \quad l_1 = -1.565675$$

and

$$\mathbf{x} = \begin{bmatrix} 1.048808 \\ 0.664246 \end{bmatrix}, \quad a = -1.713053, \qquad \text{with} \quad l_1 = -1.565672$$

making them both supercritical Hopf points. The points labeled LP shown in figure 2.18 represent *limit points* which are also known as saddle-node bifurcation points. Saddle-node bifurcations are codimension-1 bifurcations and occur when one has exactly one zero eigenvalue about the linearised system. This type of bifurcation occurs when two equilibrium points collide at a particular set of parameters and the nondegeneracy condition requires one to find a nonzero parameter α related to the order two terms of the taylor expansion of the systems vector field. For the particular cases shown in figure 2.18

we have

$$\mathbf{x} = \begin{bmatrix} -1.414212 \\ -0.471406 \end{bmatrix}, \quad \text{with} \qquad a = 1.885618, \qquad \text{with} \quad \alpha = 0.1111118$$

and

$$\mathbf{x} = \begin{bmatrix} 1.414212 \\ 0.471406 \end{bmatrix}, \quad \text{with} \qquad a = -1.885618, \qquad \text{with} \quad \alpha = 0.1111118$$

2.8 Chapter Summary

The following is a summary of the main results concerning the single FHN system, discussed in greater depth in the preceding chapter.

- The FHN system is a 2D set of ODEs,

$$\dot{x} = x - x^3/3 - y + I$$
$$\dot{y} = \epsilon(x + a - by)$$

  Derived from the quantiative electrophysiological Hodgkin-Huxley model. The variable x is a qualitative representation of a cells transmembrane potential, y represents the cells recovery (from action potential generation) variable. The parameter $\epsilon < 1$ controls the difference in timescale between the fast and slow dynamics in an action potential profile.

- The nullclines of the FHN system are given by

$$y = x - x^3/3 + I$$
$$y = \frac{x + a}{b}.$$

  The system parameters a and b effect the location of the y-nullcline. While the external current term I effects the x-nullcline in the system's phase space.

- All the equilibria $(\bar{x}, \bar{y})$ of the FHN system satisfy

$$b\bar{x}^3 + 3(1-b)\bar{x} + 3(a - bI) = 0$$
$$\bar{y} = \frac{\bar{x} + a}{b}.$$

  The number of equilibria in the system depends on the descriminant From the discriminant

$$D = -3^3 b \left\{ 9b(a - bI)^2 + 4(1-b)^3 \right\}$$

  If

  - $D < 0$ the system has 1 equilibrium
  - $D = 0$ the system has at least 1 equilibrium.

– $D > 0$ the sustem has 3 equilibiria.

- Equilibria that lay on the Left or Right branch of the x-nullcline are stable equilibria while equilibria found on the centre branch are unstable.

- The FHN system is a Lienard type system and as such it can be show that the system will have one unique limit cycle if

$$I = 0, \quad b \leq 1 \quad \text{and} \quad \epsilon b < 1$$

- Classical perturbation theory yields the fold points (points where the systems slow manifold loses stability) of the FHN system occur at

$$x_{\text{fold}} = \pm\sqrt{1 + I}.$$

  At these points trajectories leave the systems slow manifold and closely follow the system's fast foliation, which are curves

$$y = \text{constant}.$$

- The FHN system can produce limit cycles by undergoing a Hopf bifurcation. Hopf bifurcations occur at

$$\bar{x} = \sqrt{1 - \epsilon b}.$$

  The stability of the resulting limit cycle depends on the sign of the systems first Lyapunov number l

$$l = \frac{1}{2\omega^2}\left\{\frac{\epsilon\omega^3}{\omega^4 + \epsilon^2 b^2\omega^2} - \frac{2\epsilon^3 b\bar{x}^2\omega^3}{\left(\omega^4 + \epsilon^2 b^2\omega^2\right)^2}\right\}$$

  where,

$$\omega^2 = \epsilon - \epsilon^2 b^2 > 0 \quad \text{and} \quad \bar{x}^2 = 1 - \epsilon b > 0$$

  ϵ and b are real.

Chapter 3

Synchronisation of FHN systems.

3.1 Synchronisation in biological systems

The first well documented observation of synchronisation in physical systems was due to Christiaan Huygens, whom at the time was working on a method to accurately determine the longitude of a vessel for the purposes of maritime navigation.

(a) Christiaan Huygens

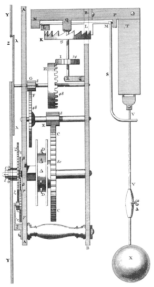

(b) Huygens Clock

Figure 3.1: Huygens and his pendulum clock. Schematic taken from his manuscript Horolgium Oscillorium published in 1673.

Huygens had invented the pendulum clock in 1657 and believed that with modification to withstand sea travel his pendulum clocks would be the answer. In a letter to his father, while briefly ill in his room, Huygens described that while observing two of his pendulum clocks, hung on a bean on his wall, that they would swing with the same frequency and 180° out of phase with each other. Furthermore when he disturbed one of the pendulums it would fall into the same anti phase state within half an hour and remain so indefinitely. This being the first documented observation of synchrony in physical systems, referred to as *mutual sympathy*. For further reading on this historical event the reader is referred to [16] and references therein.

3.1.1 The role of synchronisation in physiological organisms

Synchronisation has become a rich area of nonlinear dynamical research finding many applications in systems that are not traditionally studied in physics [134, 168]. Synchronisation and complex rhythmic processes are ubiquitous in living organisms and are central to life [65]. Most plants and animals posses accurate endogenous time-measuring machinery known as *circadian clocks*, whose mechanisms are an area of intensive study in molecular biology [204]. The early signs of a circadian clock came from experiments conducted by the French geophysicist and chronobiologist Jean-Jacques d'Ortous de Mairan in 1729. Jean de Mairan discovered that haricot bean plants have leaves that move up and down with the daily cycle of light and darkness [204].

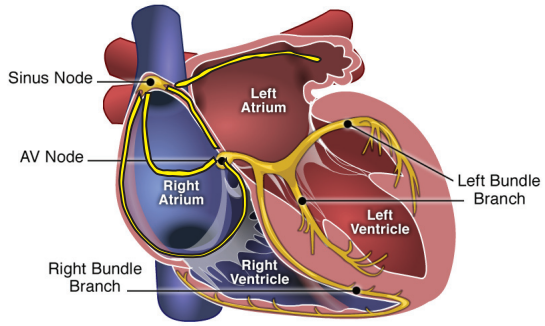

(a) The synchronous and well timed contraction of cardiomyocytes in the atria and ventricles results in effective pumping of blood through the circulatory system.

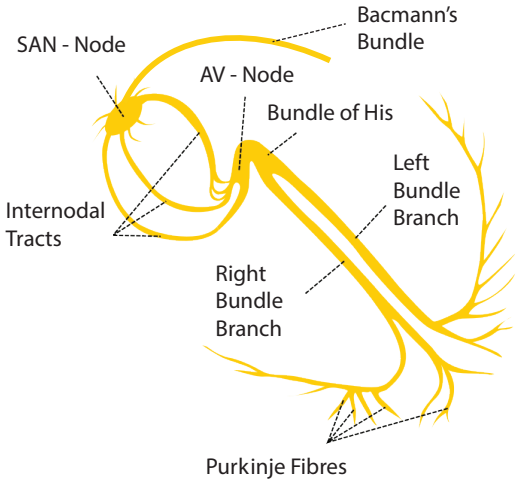

(b) The cardiac conduction system which transmits and delays the action potential signal throughout the cardiac tissue.

Figure 3.2: Synchrony in the cardiac conduction system is essential for the en mass contraction of myocardial cells.

More obvious signs of synchrony in living organisms include the rhythmic motion of walking and the coordination of human limbs, wake sleep patterns in mammals and the monthly menstrual cycle [65]. Rhythms such as wake sleep patterns are synchronised to the like dark cycle typically due to the sun, in the absence of this cycle shows that humans can fall into a default rhythm that is longer than the 24hour period. The effect has a multitude of effects on human physiology such as temperature fluctuation, changes in plasma phosphates and excess urinary electrolyte concentrations [117].

Less obvious rhythms that are present in living organisms which also depend on synchro-

nisation include the release of hormones, regulation of growth and metabolism and the digestion of food [65].

The heart is an organ which vitally depends on synchronisation for its function as has been described in an earlier chapter. The disturbance in the regular rhythms in a healthy adult can lead to fatality. Synchrony plays a vital role in the cardiac conduction system Figure 3.2.

However it is not only the loss of synchrony which causes negative effects on a living organism, synchrony can also produce undesirable effects on the functioning of an organism. An example of which is found in patients diagnosed with Parkinson's disease.

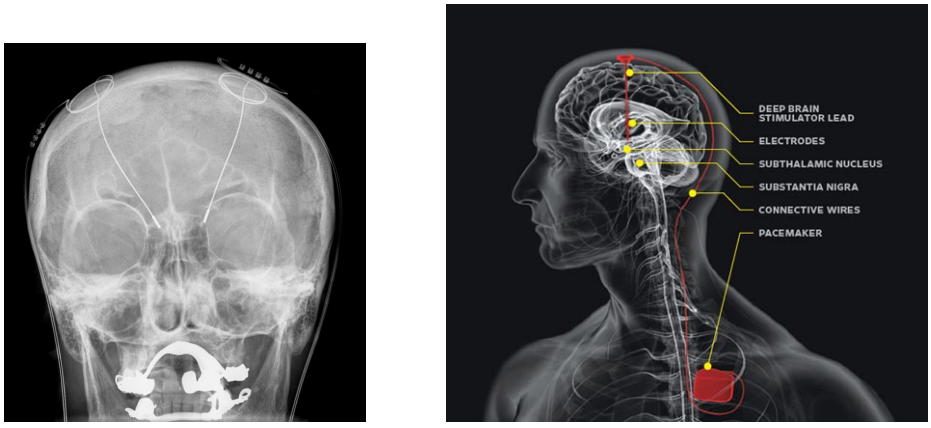

(a) An x-ray of a patient with an implanted brain pacemaker.

(b) A schematic of the brain pacemaker in relation to a human.

Figure 3.3: Deep brain stimulation has been shown to reduce the 5Hz tremor associated to patients suffering from Parkinson's.

Parkinson's disease is a progressive age-related neurodegenerative disorder, which is characterised by poverty of voluntary movements, slowness or involuntary movements, muscle rigidity and tremor of the limbs at rest. It has been found that humans with Parkinson's disease have abnormally high levels of synchronised neurons in the mid part of their brain, namely at the ganglia-cortical loop [70]. Such neurodegenerative disorders require an understanding of the synchronisation process underlying them in order to find effective treatments for them. One of the leading treatments of the tremors resulting from Parkinson's disease is that of Deep Brain Stimulation (DBS), where a brain pacemaker is surgically implanted within a patient and is used to controllably pulsate the affected areas [130], Figure 3.3. However the mechanism responsible for the the successes found by using DBS are still ill understood and as a result not optimal.

3.2 Chapter Aim and Context

The aim of this chapter is to define and use the property of synchronisation measures to characterise coupled neural cells. Synchronisation and FHN systems has been studied from a number of different perspectives in the literature.

Intensive area of study concerns synchronisation of externally driven FHN cells [55, 106, 91, 98], Synchronisation of FHN cells influenced by noise [9, 120, 90, 96, 174, 158, 2], and Control [142, 148, 186, 145]. The FHN system is also used in reaction-diffusion systems where one examines wave propagation across a continuous sheet of FHN cells. More recent work in this direction have focused on synchronisation and control [6], numerical investigation of the parameter dependencies in the resulting reaction diffusion system [33], and action potential propagation in chains of stimulated FHN cells [144].

In contrast the results in this chapter mainly concern systems that are not externally driven. This chapter focuses on the emergence and decline of synchronisation phenomena, intrinsic to a coupled set of excitable oscillators, with respect to factors such as coupling strength. Furthermore keeping the system of study restricted to small discrete networks not only allows for a clearer analytical treatment of coupled FHN systems but also relates synchronisation to conduction of action potentials, via feedback, from a single cell to another in a clear manner.

3.3 Defining Synchronisation

In order to put the following results concerning synchronisation of FHN systems into perspective it is important to define what is meant by "synchronisation" in this thesis. There are a number of definitions throughout the literature of what the synchronisation phenomena is, however in a general context the working definition used in favour here is that due to [134],

> Synchronisation is the adjustment of rhythms of oscillating objects due to their interaction.

Furthermore the aim will be to study **self sustained oscillators**.

Definition 3.3.1 (Self sustained oscillations)**.**
These are nondecaying stable oscillations that occur in autonomous dissipative systems.

In dissipative systems there is always energy lost to the environment, such as is the case in the real word be it due to friction, heat, conduction impurities, sound etc. Thus for oscillations to repeatedly occur in a dissipative system they must contain an internal energy source which counter balances this energy dissipation. This is precisely the case when looking at biological oscillators such as cardiac cells and neurons as they derive their energy from metabolic processes internal to the cell.

3.3.1 Definitions of synchrony

We begin with the definition of the strictest form of synchronisation.

Definition 3.3.2 (Complete Synchronisation (CS))**.** [131]
Given two oscillators with respective position vectors

$$\mathbf{x}_1(t) \quad \text{and} \quad \mathbf{x}_2(t)$$

and respective velocity vectors

$$\dot{\mathbf{x}}_1(t) \quad \text{and} \quad \dot{\mathbf{x}}_2(t).$$

Then the oscillations are said to be **completely synchronised** over the interval $[t_1, t_2]$ if and only if

$$\mathbf{x}_1(t) = \mathbf{x}_2(t) \quad \text{and} \quad \dot{\mathbf{x}}_1(t) = \dot{\mathbf{x}}_2(t), \forall t \in [t_1, t_2]$$

Complete synchronisation (CS) is a rather narrow definition of sync as it requires the systems involved to be completely homogenous[1] [166], that is to be made up of the same system of equations with identical parameter values and identical noise. As such it is an impractical definition of synchronisation for research concerned with biological systems.

For inhomogenous systems or systems that are influenced by external noise (which is often the case in real systems), the coupled systems may reach a state that is referred to here as a state of *imperfect complete synchronisation* and else where as *practical* or *disturbed synchronisation*.

[1] except for an initial phase difference

Definition 3.3.3 (Imperfect Complete Sychronisation (ICS))**.** [166, p. 5]

Given two oscillators with respective trajectories in phase space

$$\mathbf{x}_1(t) \quad \text{and} \quad \mathbf{x}_2(t)$$

The system is in **imperfect complete sycnhronisation** over the interval $[t_1, t_2]$ if

$$|\mathbf{x}_1(t) - \mathbf{x}_2(t)| < \epsilon$$

where ϵ is a small parameter such that

$$\epsilon << \sup |\mathbf{x}_1(t) - \mathbf{x}_2(t)|, \forall t \in [t_1, t_2]$$

Lastly it is useful to define a synchronous state that occurs when oscillators behave in a similar fashion up to a temporal translation.

Definition 3.3.4 (Lag Synchronisation (LS))**.** [18, p. 35]
Given position and velocity as stated in Definition 3.3.2, the two oscillators are said to be **lag synchronised** over the interval $[t_1, t_2]$ if $\exists\ \tau \in \mathbb{R}$, known as the *lag*, such that the approximate equalities $\mathbf{x}_1(t) \approx \mathbf{x}_2(t - \tau)$ and $\mathbf{y}_1(t) \approx \mathbf{y}_2(t - \tau)$ hold $\forall t \in [t_1, t_2]$.

Definitions 3.3.2, 3.3.3 and 3.3.4 are concerned with the coincidences of the amplitude and frequency of the oscillators involved. In both cardiac and neural systems however it is believed that the most important component of action potential propagation is *timing*. The assumption here is that neurons transmit binary information, firing (1) or not firing (0). For cardiac systems it is somewhat more transparent as the action potential directly causes contraction of the myocyte. Action potentials are transmitted by cells that elicit all-or-nothing responses much like integrate-fire oscillators. Both cardio-myocytes and neurons have a stimulus threshold. Stimuli above this threshold result in a complex set of ionic movements across the cell membrane which ultimately leads to relatively[2] large potential differences being generated across the cell. In such systems one would not be concerned with the amplitude of the elicited action potentials given that the APs produced are supratheshold should suffice.

In order to reach a definition of synchrony based on the timing of the potentials it is necessary to define a *phase* for action potentials themselves.

[2]relative to the threshold stimulus.

3.4 Synchrony in an electrically coupled system of FHN oscillators.

3.4.1 Electrically coupled FHN cells

To examine synchrony between two FHN cells it is necessary to introduce a coupling term within the original FHN system.

Definition 3.4.1 (Electrically coupled FHN cells)**.**
A system of n FHN cells are electrically coupled if they are of the form

$$\begin{aligned}\dot{x_i} &= x_i - x_i^3/3 - y_i + \sum_{i\neq j, j=1}^{n} g_{i,j}(x_i - x_j)\\ \dot{y_i} &= \epsilon_i(x_i + a_i - b_i y_i)\end{aligned}$$

where $i, j \in [1, n] \subset \mathbb{N}$ and $g_{i,j} \neq 0, \forall i$.

Notes concerning the Electrically coupled FHN system

The dynamics of the electrically coupled FHN system are rich, most notably the admission of chaos which is discussed in the subsequent chapter.

The diffusion coupling term is placed on the *voltage-like* variable x. Where the parameter $g_{i,j}$ represents the conductance of the voltage from cell j to cell i. The term $(x_i - x_j)$ is the voltage difference between cell i and cell j. This constant flow of communication from cell j to cell i, is representative of a *gap junction* connection between the cells, where cells have a physical connection between their cell membranes as described in earlier chapters. Such connections occur commonly between cardiomyocytes. Gap junction connections are also found between neurons, however they are not as common as synaptic connections which are discussed later.

3.4.2 Sync between two electrically coupled FHN cells

The two electrically coupled FHN system is given by

$$\begin{aligned}\dot{x_i} &= x_i - x_i^3/3 - y_i + \sum_{i\neq j, j=1}^{2} g_{i,j}(x_i - x_j) \qquad (3.4.2.1)\\ \dot{y_i} &= \epsilon(x_i + a - b y_i)\end{aligned}$$

Here we have chosen the parameters for both the cells to be the same except for the coupling strength which is allowed to be different. This introduces the least amount of inhomogeneity and allows an analytic treatment of the problem.
Define the "distance" between the two neurons as

$$r = \sqrt{(x_2 - x_1)^2 + (y_2 - y_1)^2} = \left(\Delta x^2 + \Delta y^2\right)^{1/2}$$

where for convenience of notation $\Delta x = (x_2 - x_1)$ and $\Delta y = y_2 - y_1$.

Complete synchronisation occurs if this distance tends toward zero at some finite point in time. To show that this occurs it is convenient to define $U = r^2$, whose derivative is given by

$$\dot{U} = 2r\dot{r}.$$

the derivative

$$\dot{r} = \left(\Delta x^2 + \Delta y^2\right)^{-1/2} \left(\Delta x \dot{\Delta x} + \Delta y \dot{\Delta y}\right)$$

and thus

$$\dot{U} = 2r\dot{r} = 2\left(\Delta x \dot{\Delta x} + \Delta y \dot{\Delta y}\right)$$

Substituting expressions $\dot{x_i}$ and $\dot{y_i}$ from (3.4.2.1) into our expression for $\dot{U}$ yields

$$r\dot{r} = \Delta x \left\{ \Delta x - \frac{1}{3}(x_2^3 - x_1^3) - \Delta y + g_{2,1}\Delta x + g_{1,2}\Delta x \right\} + \epsilon \Delta y \left\{ \Delta x - b\Delta y \right\}$$

The aim now is to find an upper bound for the product $r\dot{r}$ which linearises the problem at hand and ultimately solve for r. To achieve this one can examine the nonlinear terms that arise namely the product $(\Delta x)(x_2^3 - x_1^3)$

$$\begin{aligned}
(x_2 - x_1)(x_2^3 - x_1^3) &= x_2^4 - x_2 x_1^3 - x_1 x_2^3 + x_1^4 \\
&= \left(x_2^2 + x_2 x_1 + x_1^2\right)(x_2 - x_1)^2 \\
&= \left(\left(x_2 + \frac{x_1}{2}\right)^2 + \frac{3}{4}x_1^2\right)(x_2 - x_1)^2 \\
&= \left(\left(x_2 + \frac{x_1}{2}\right)^2 + \left(\frac{\sqrt{3}}{2}x_1\right)^2\right)(x_2 - x_1)^2 \geq 0
\end{aligned}$$

This inequality gives an upper bound to $r\dot{r}$ given by

$$r\dot{r} \leq \Delta x \left\{\Delta x - \Delta y + g_{2,1}\Delta x + g_{1,2}\Delta x\right\} + \epsilon \Delta y \left\{\Delta x - b\Delta y\right\}$$

multiplying through and grouping terms we have the inequality

$$r\dot{r} \leq (1 + g_{2,1} + g_{1,2})\Delta x^2 - \epsilon b \Delta y^2 + (\epsilon - 1)\Delta x \Delta y.$$

Making a switch to polar coordinates,

$$\begin{aligned} \Delta x &= r\cos(\theta) \\ \Delta y &= r\sin(\theta) \end{aligned}$$

produces a system which can be further bounded,

$$r\dot{r} \leq r^2(1 + g_{2,1} + g_{1,2})\cos^2(\theta) - \epsilon b r^2 \sin^2(\theta) + r^2(\epsilon - 1)\sin(\theta)\cos(\theta).$$

The trigonometric functions themselves have upper bounds as,

$$\begin{aligned} \left|\cos^2(\theta)\right| &= \left|\frac{1}{2}(\cos(2\theta) + 1)\right| \leq 1 \\ \left|\sin^2(\theta)\right| &= \left|\frac{1}{2}(1 - \cos(2\theta))\right| \leq 1 \\ \left|\sin(\theta)\cos(\theta)\right| &= \left|\frac{1}{2}\sin(2\theta)\right| \leq 1/2. \end{aligned}$$

This yields another upper bound for $r\dot{r}$ given by,

$$r\dot{r} \leq r^2(1 + g_{2,1} + g_{1,2}) - \epsilon b r^2 + \frac{r^2}{2}(\epsilon - 1).$$

and the differential equation bounding the synchronisation distance between the two FHN oscillators is given by

$$\dot{r} \leq \left(\frac{1}{2} + g_{2,1} + g_{1,2} + \epsilon\left(\frac{1}{2} - b\right)\right) r = \alpha r$$

where $\alpha = \dfrac{1}{2} + g_{2,1} + g_{1,2} + \epsilon\left(\dfrac{1}{2} - b\right)$. This is a first order ODE which can be solved to yield,

$$r_{upper}(t) = r(0)e^{\alpha t}$$

Thus choosing parameters such that $\alpha < 0$ guarantees that the coupled system will exponentially converge to a synchronous state.

Numerical simulation of synchrony between two inhonogenously coupled FHN oscillators

Imperfect complete synchrony between two FHN cells is guaranteed to occur between two cells if one chooses parameters such that

$$\frac{1}{2} + g_{2,1} + g_{1,2} + \epsilon\left(\frac{1}{2} - b\right) < 0$$

The result proven analytically in the preceding section can be demonstrated with the aid of numerics. Choosing parameters for the cells

$$b_1 = b_2 = b = 0.5, \quad a_1 = a_2 = a = 0.1 \quad \text{and} \quad \epsilon_1 = \epsilon_2 = \epsilon = 0.01$$

with no coupling

$$g_{i,j} = 0.$$

Results in two FHN cells which are in a state of independent self-sustaining oscillations.

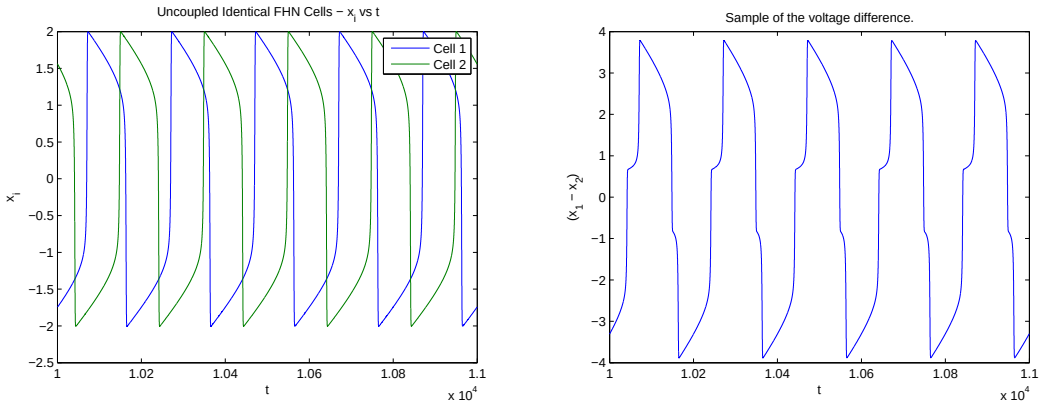

(a) The voltage time series of both uncoupled FHN oscillators.

(b) The voltage difference between the two uncoupled oscillators.

Figure 3.4: The uncoupled system, $a = 0.1$, $b = 0.5$, $\epsilon = 0.01$ and $g_{i,j} = 0$.

For the chosen system parameters the derived sync condition reduces to

$$g_{2,1} + g_{1,2} < -\frac{1}{2}$$

choosing the coupling strengths

$$g_{1,2} = -0.1 \quad \text{and} \quad g_{2,1} = -0.45$$

the system falls into a state of imperfect complete synchronisation

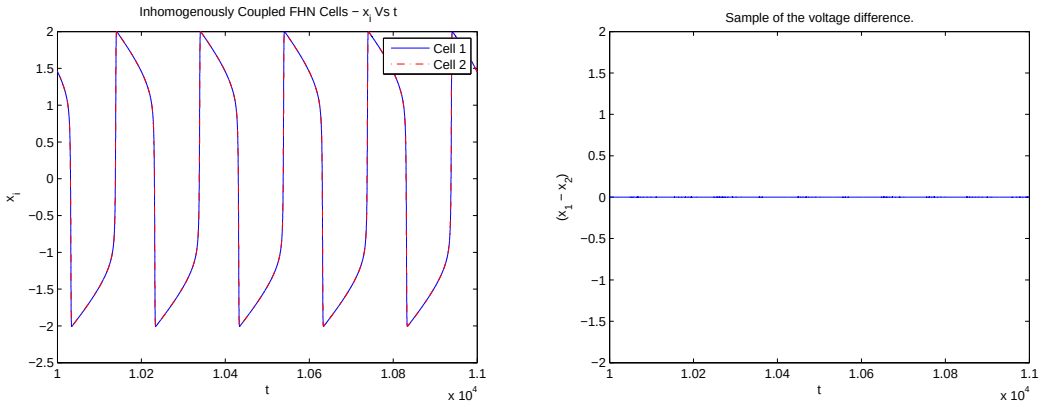

(a) The voltage time series of the coupled FHN oscillators.

(b) The voltage difference between the two coupled oscillators.

Figure 3.5: Sync in the inhomogenously coupled system $g_{2,1} = -0.45$ and $g_{1,2} = -0.1$.

with

$$|\boldsymbol{x}_1 - \boldsymbol{x}_2| < 3 \times 10^{-3}$$

Time varying coupling strength

The role of the coupling strengths, $g_{i,j}$, with regards to synchrony can be further appreciated if one allows the coupling strength to vary in time. From the numerical simulation it becomes clear that there are definite coupling strengths where the system falls into synchrony by examining the voltage difference between the two oscillators.

To achieve this the system parameters have been set to

$$a = 0.1, \quad b = 0.5, \quad \epsilon = 0.01 \quad \text{and} \quad g_{2,1} = -0.1 \quad g_{1,2} = -0.15.$$

The introduction of time varying coupling strength is simply achieved with the following

iterative process

$$g_{i,j} \leftarrow g_{i,j} + A\sin(\omega t)$$

and $g_{i,i} = 0$ ensuring there is no self coupling in the system. Here A is the amplitude of the coupling variation and ω is the frequency over which the coupling strength is to change. This frequency should be taken to be small enough compared to the natural frequency of the oscillators so as to allow the system to reach a state of synchrony before greatly changing the coupling strength. For the chosen system the time varying coupling term parameters they have been set to

$$A = 0.5 \quad \text{and} \quad \omega = 1 \times 10^{-3}.$$

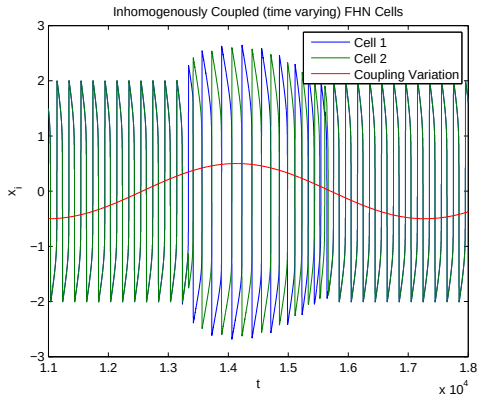

(a) The voltage time series of both FHN cells with time varying coupling strength

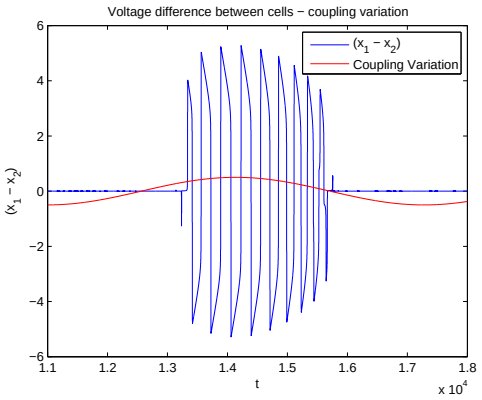

(b) The voltage difference between the two coupled oscillators.

Figure 3.6: Time varying coupling strength

As can be seen in Figure 3.6 the system moves from a state of imperfect complete sync to a state of *out of phase synchrony* when moving from negative coupling strengths to positive coupling strengths. Of further note is that the oscillations themselves even through are out of phase maintain a 1:1 firing patter, that is an AP response from cell i results in a single AP response from cell j. Thus the 1:1 firing pattern is still maintained even though the cells are firing out of phase with each other.

3.5 The Phase of an oscillator

Given a dissipative autonomous system of ODEs

$$\dot{\boldsymbol{x}} = f(\boldsymbol{x}), \qquad \boldsymbol{x} \in \mathbb{R}^n \quad (n \geq 2) \tag{3.5.0.2}$$

a nonconstant solution to (3.5.0.2), $\boldsymbol{x}(t)$ is said to be periodic if $\exists\ T > 0$ such that

$$\boldsymbol{x}(t) = \boldsymbol{x}(t+T).$$

Denote this periodic orbit as γ and an arbitrary point on γ as $\boldsymbol{x}_0$. In phase space this is an isolated trajectory, namely a *limit cycle*. A point moving along the curve γ represents oscillations of a self sustained oscillator.

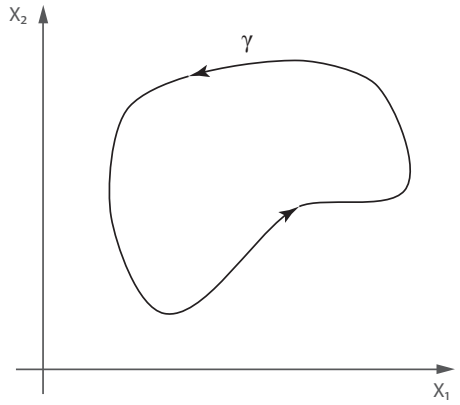

Figure 3.7: An example of a limit cycle γ in 2D phase space.

Any point on γ can be specified by the time θ since passing through $\boldsymbol{x}_0$. The variable χ is the phase of oscillation which is bounded by T. Typically one normalises the phase by a factor of $T/2\pi$, thus bounding the phase by 2π, the normalised phase is denoted by ϕ.

Since the limit cycle repeats itself every T time steps, it should be clear that the rate of change of the phase is a constant, i.e.

$$\frac{d\phi}{dt} = \omega_0$$

where ω_0 is known as the **natural frequency** of the oscillator. It is also possible to define a phase outside of γ with the notion of an *isochrone* [197]. Given that the limit cycle is stable any orbits starting from initial conditions within the limit cycles basin of attraction will converge to the limit cycle. To construct the isochrones begin with (3.5.0.2) containing a stable limit cycle orbit γ of period T. Stroboscopically observing the evolution of trajectories, with period T, one finds the isochrones with the mapping

$$\boldsymbol{x}(t) \to \boldsymbol{x}(t+T) \equiv \Phi(\boldsymbol{x})$$

Points $\boldsymbol{x}_0$ in the basin of attraction of the point $\boldsymbol{x} \in \gamma$ under the action of $\Phi(\boldsymbol{x})$, define an $(n-1)$ dimensional manifold known as isochrone which passes through the limit cycle at $\boldsymbol{x}$.

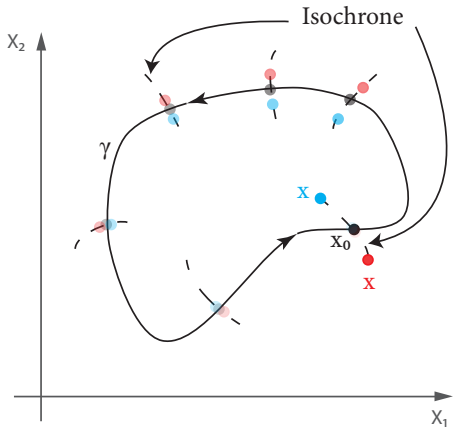

Figure 3.8: Isochrones associated the with limit cycle γ.

3.5.1 The phase of an FHN oscillator

The FHN system is a second order ODE and as such its dynamical behaviour is easily visualised using a phase plane diagram. A definition of phase is also easily made for a simple closed curve in whose dynamics are restricted on a phase plane. If a limit cycle is centered around the origin (otherwise a simple translation of the axis is needed) then a geometric phase can be defined as

$$\theta(t) = \arctan\left(\frac{x_2(t)}{x_1(t)}\right).$$

The phase for a chaotic oscillator however is somewhat more difficult to define. For attractors that exist in higher than 2-D space it is often possible to find a projection of the attractor onto a plane (x, y) such that the projection is reminiscent of a smeared limit cycle. One can then define a Poincare map attributing a 2π increase in phase with each successive intersection with the secant surface. If one can find such a Poincare map then it is also possible to define the phase according to the same rule above, ie $\theta = \arctan\left(\frac{y}{x}\right)$. In practice finding an appropriate Poincare section can be difficult.

Engineering fields such as signal processing have faced the problem of extracting information from noisy signals; be it temporal measurement, operation on or analysis of.

The *Hilbert transform* is a method of finding the phase and amplitude of a signal. It is particularly useful when dealing with experimental data or noisy data sets. The instantaneous phase and amplitude of a signal $s(t)$ can be found by examining its *analytic signal*

$$\zeta(t) = s(t) + i\boldsymbol{H}[s(t)] = A(t)e^{i\phi(t)}$$

where $\boldsymbol{H}[s(t)]$ is the Hilbert transform of the signal $s(t)$, $A(t)$ is the instantaneous amplitude and $\phi(t)$ is the instantaneous phase. Formally the Hilbert transform is found by evaluating the following indefinite integral

$$\begin{aligned}\boldsymbol{H}[s(t)] &= \frac{1}{\pi}\int_{-\infty}^{\infty}\frac{s(\tau)}{t-\tau}\,d\tau \\ &= \frac{1}{\pi}\int_{-\infty}^{\infty}\frac{s(t-\tau)}{\tau}\,d\tau\end{aligned}$$

This integrand however has a singularity at $t = \tau$. The Hilbert transform is more accurately defined as the Cauchy principal value of the above integral which is given by

$$\begin{aligned}\boldsymbol{H}[s(t)] &= \frac{1}{\pi}\lim_{\epsilon\to 0^+}\left(\int_{t-1/\epsilon}^{t-\epsilon}\frac{s(\tau)}{t-\tau}\,d\tau + \int_{t+\epsilon}^{t+1/\epsilon}\frac{s(\tau)}{t-\tau}\,d\tau\right) \\ &= \frac{1}{\pi}\lim_{\epsilon\to 0^+}\left(\int_{-1/\epsilon}^{-\epsilon}\frac{s(t-\tau)}{\tau}\,d\tau + \int_{\epsilon}^{1/\epsilon}\frac{s(t-\tau)}{\tau}\,d\tau\right)\end{aligned}$$

The evaluation of such an integral is computationally expensive, however it is possible to evaluate the Hilbert transform of a signal with two fourier transforms the algorithms of which are highly optimised [113].

From the analytic signal $\zeta(t)$ one can find the instantaneous phase of the oscillator, by translating the center of the closed curve in the $(s, \boldsymbol{H}(s))$ plane, as

$$\phi(t) = \arctan\left(\frac{\boldsymbol{H}(s(t))}{s(t)}\right).$$

Furthermore the instantaneous frequency $\omega(t)$ can also be found by taking the derivative of the phase with respect to time

$$\omega(t) = \frac{d}{dt}[\phi(t)]$$

3.5.2 Phase Synchronisation and the Order Parameter

Definition 3.5.1 (Phase Synchronization (PS))**.** Given the phase of two oscillators $\phi_1(t)$ and $\phi_2(t)$ respectively. The system is said to be phase synchronised if $\phi_1(t) \approx \phi_2(t)$.

There is a weaker form of synchronisation than PS that is also relevant to studies of biorhythms which concerns the frequency of oscillation. The frequency of an oscillator can be simply defined using its phase.
The average time rate of change of an oscillator's phase is known as its winding number

$$\Omega = \langle \dot{\phi(t)} \rangle = \lim_{T \to \infty} \frac{1}{T} \int_0^T \phi(t)\, dt \tag{3.5.2.1}$$

which we will use here as the intrinsic frequency of an oscillator within a system of coupled oscillators.

Definition 3.5.2 (Frequency Synchronisation)**.** Given two oscillators within a system with respective frequencies Ω_1 and Ω_2, the oscillators are said to be frequency synchronised if $\Omega_1 \approx \Omega_2$.

Thus far a number of definitions concerning synchronisation have been introduce; complete synchronisation (CS), imperfect complete synchronisation (ICS), phase synchronisation (PS) and frequency synchronisation (FS). There is a hierarchy concerning the strictness of these definitions of synchronisation represented by

$$\text{CS} \Rightarrow \text{ICS} \Rightarrow \text{PS} \Rightarrow \text{FS}$$

an important representation of phase synchronisation comes in the form of the *order parameter*.

The order parameter

An order parameter is a normalised parameter which indicates the degree of order within a system. Typically order parameters in the context of synchronisation takes a value of 0 to indicate a completely non synchronous state while a value of 1 indicates a completely synchronous state. One of the most extensively studied models of synchronisation is due to Kuramoto see [3] and references therein for a review. Following the Kuramoto scheme a collective amplitude $\rho(t)$ and phase $\psi(t)$ is defined using the phase of each of our oscillators $\phi_i(t)$ with the relation

$$\rho(t)e^{i\psi(t)} = \frac{1}{N} \sum_{i=1}^{N} e^{i\phi_i(t)}$$

where N is the number of coupled oscillators. Kuromoto originally defined the order parameter ρ as the time average of the collective phase

$$\rho \equiv \langle \rho(t) \rangle_t$$

For excitable systems however this order parameter leads to a certain level of ambiguity. There are two situations where one can find the system in perfect sync, the first is a dynamical one in which all the units fire synchronously $\rho = 1$ here means full sync. The other situation is a static one, which occurs when units are all at rest at a stable fixed point [171].

To discern the dynamical state from the static state it is useful to define the order parameter according to another order parameter also due to Kuramoto

$$\zeta = \left\langle \left| \rho(t) e^{i\psi(t)} - \langle \rho(t) e^{i\psi(t)} \rangle \right| \right\rangle$$

which removes the possible ambiguity.

Time Varying Coupling Strength phase and order parameter

Revisiting the inhomogenously coupled FHN Cells with time variation one can see the gain and loss of synchrony at a glance with the aid of the defined order parameter.

As before the system parameters for the electrically coupled system are chosen to be

$$a = 0.1, \quad b = 0.5, \quad \epsilon = 0.01 \quad \text{and} \quad g_{2,1} = -0.1 \quad g_{1,2} = -0.15.$$

the time varying coupling strength terms being modulated by

$$g_{i,j} : \begin{cases} g_{i,j} \leftarrow g_{i,j} + A \sin(\omega t) & \text{if } i \neq j \\ 0 & \text{otherwise} \end{cases}$$

and the periodic terms having parameters

$$A = 0.5 \quad \text{and} \quad \omega = 1 \times 10^{-3}.$$

After numerical integration of the coupled FHN system the analytic signal of each of the cell voltage variables are reconstructed using the Hilbert transform, $\phi(t) = \arctan\left(\frac{\boldsymbol{H}(s(t))}{s(t)}\right)$. After calculation of the phase of each oscillator from the analytic signals one finds the

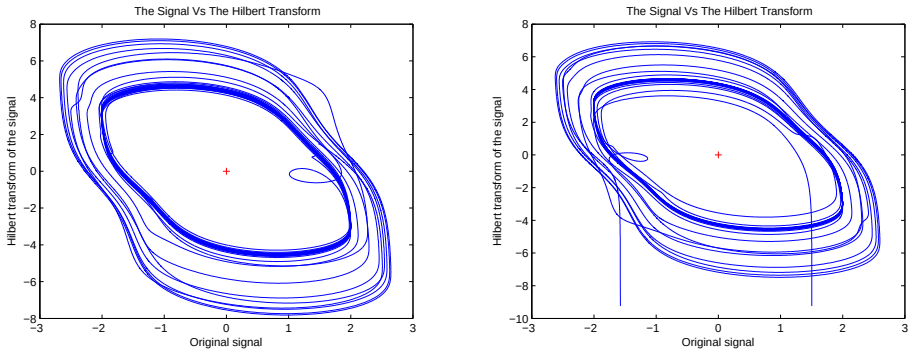

(a) Analytic Signal for Cell 1 (b) Analytic Signal for Cell 2.

Figure 3.9: Time varying coupling strength, analytic signal for cell 1 and cell 2 - used to ensure the curve is centered after appropriate translation to calculate the resulting phase of the oscillators.

order parameter $\rho(t)$ using Kuramoto's formulation

$$\rho(t)e^{i\psi(t)} = \frac{1}{N}\sum_{i=1}^{N} e^{i\phi_i(t)}$$

which here results in

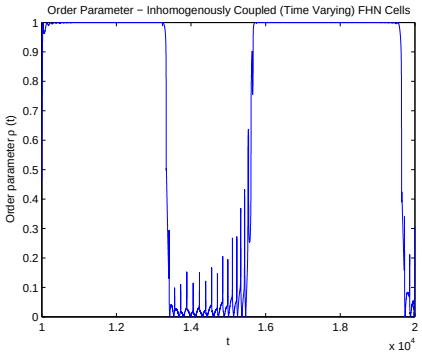

Figure 3.10: The order parameter for electrically coupled FHN cells with time varying coupling strengths.

The order parameter tells us that the system is in a state of synchronisation when $\rho = 1$ and a completely non synchronous state when $\rho = 0$. Further examining the onset and loss of complete sync with relation to the variation in coupling strength as shown in figure 3.11.

A striking feature of figure 3.11 is when the order parameter reaches $\rho = 1$ and when the synchronous state is lost again. The system shows that once it is in a state of synchrony there is a reluctance for the system to break the synchronous state. At a time of approximately 1.3×10^4 time units the system looses its state of synchrony at a coupling

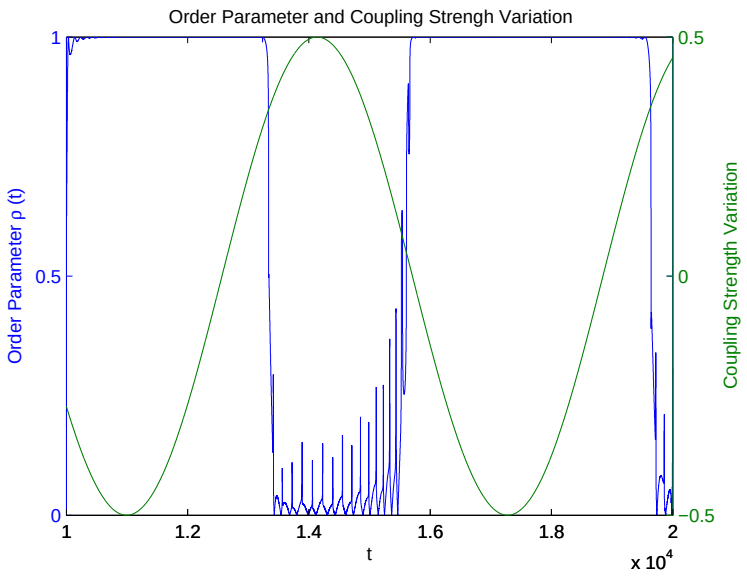

Figure 3.11: The order parameter for electrically coupled FHN cells with time varying coupling strengths and hysteresis.

adjustment of ≈ 0.3. At which point the synchrony is lost rapidly to a value of $\rho \approx 0$. On decreasing the coupling adjustment again the system is reluctant to reach a state of synchrony once more requiring a *negative* coupling strength (this being a phase attractive coupling strength) to reach a state of synchrony again. Here it is clear that the phase transitions from synchronous to non synchronous states possesses **hysteric** properties.

3.5.3 Synchronisation between inhomogenously coupled subsystems by means of nonlinear control

Here we examine the possibility of synchronising a system of coupled FHN cells (the subsystem) to another system of FHN cells (the main system) by means of a nonlinear control scheme. The aim here is to show that a semi-analytic approach can be used to force a network of cells undergoing one type of dynamic behaviour to the dynamical behaviour of another set of cells which have a different network structure[3]. Both the main and subsystems are composed of identical cells that are inhomogenously coupled. The coupling strengths however between the cells in the subsystem are here considered to be different to those of the main system. This introduces a certain level of inhomogeneity between the two systems.

[3]The network structure difference here refers to the coupling strengths between cells.

The main system is given by

$$\dot{x}_{(M,i)} = x_{(M,i)} - \frac{1}{3}x^3_{(M,i)} - y_{(M,i)} + \sum_{\substack{j\neq i \\ j\in \text{Neigh(i)}}} g_{i,j}(x_{(M,i)} - x_{(M,j)})$$

$$\dot{y}_{(M,i)} = \epsilon(x_{(M,i)} + a - by_{(M,i)}).$$

The subsystem is given by

$$\dot{x}_{(S,i)} = x_{(S,i)} - \frac{1}{3}x^3_{(S,i)} - y_{(S,i)} + \mu_{x_i}(t) + \sum_{\substack{j\neq i \\ j\in \text{Neigh(i)}}} h_{i,j}(x_{(S,i)} - x_{(S,j)})$$

$$\dot{y}_{(S,i)} = \epsilon(x_{(S,i)} + a - by_{(S,i)}) + \mu_{y_i}(t).$$

The μ_{x_i} and μ_{y_i} are the nonlinear control functions that are yet to be determined. The aim is to show that convergence to synchrony between the main and subsystem can be achieved with appropriately chosen $\mu(t)$ despite the systems being made up of different intercellular coupling strength. To achieve this one begins by examining the difference between the corresponding FHN cells and thus defining an *error signal* between the two systems,

$$E_{x_i} = x_{(M,i)} - x_{(S,i)}$$
$$E_{y_i} = y_{(M,i)} - y_{(S,i)}.$$

The rate of change of the error signals defined above can be written as

$$\dot{E}_{x_i} = (x_{(M,i)} - x_{(S,i)}) - \frac{1}{3}(x^3_{(M,i)} - x^3_{(S,i)}) - (y_{(M,i)} - y_{(S,i)}) + \\ + \sum_{\substack{j\neq i \\ j\in \text{Neigh(i)}}} (g_{i,j}(x_{(M,i)} - x_{(M,j)}) - h_{i,j}(x_{(S,i)} - x_{(S,j)})) - \mu_{x_i}(t)$$

$$\dot{E}_{y_i} = \epsilon((x_{(M,i)} - x_{(S,i)}) - b(y_{(M,i)} - y_{(S,i)})) - \mu_{y_i}(t).$$

We are free to choose the nonlinear control functions $\mu_*(t)$. Choosing

$$\begin{aligned}\mu_{x_i}(t) &= -\frac{1}{3}(x^3_{(M,i)} - x^3_{(S,i)}) + \kappa_{x_i}E_{x_i} \ldots \\ &\quad + \sum_{\substack{j\neq i \\ j\in \text{Neigh(i)}}} (g_{i,j}(x_{(M,i)} - x_{(M,j)}) - h_{i,j}(x_{(S,i)} - x_{(S,j)})) \\ \mu_{y_i}(t) &= \kappa_{y_i}E_{y_i},\end{aligned}$$

where the parameters denoted by κ are control constants, reduces the error system to

$$\begin{aligned}\dot{E}_{x_i} &= (1-\kappa_{x_i})E_{x_i} - E_{y_i} \\ \dot{E}_{y_i} &= \epsilon E_{x_i} - (\kappa_{y_i} + \epsilon b)E_{y_i}.\end{aligned}$$

This is a homogenous set of constant coefficient ordinary differential equations. It is also clear that the system has a fixed point at the origin. In order to synchronise the subsystem to the main system, we require the values of E_{x_i} and E_{y_i} tend to zero in finite time. In other words we require the fixed point at the origin of the *error* system defined above to be both the only fixed point and a stable fixed point. Rewriting the system in matrix form we have

$$\underbrace{\begin{pmatrix} \dot{E}_{x_1} \\ \dot{E}_{y_1} \\ \vdots \\ \dot{E}_{x_n} \\ \dot{E}_{y_n} \end{pmatrix}}_{\dot{\mathbf{E}}} = \underbrace{\begin{pmatrix} (1-\kappa_{x_1}) & -1 & \cdots & 0 & 0 \\ \epsilon & -(\kappa_{y_1}+\epsilon b) & \cdots & 0 & 0 \\ \vdots & \vdots & \ddots & \vdots & \vdots \\ 0 & 0 & \cdots & (1-\kappa_{x_n}) & -1 \\ 0 & 0 & \cdots & \epsilon & -(\kappa_{y_n}+\epsilon b) \end{pmatrix}}_{\mathbf{A}} \underbrace{\begin{pmatrix} E_{x_1} \\ E_{y_1} \\ \vdots \\ E_{x_n} \\ E_{y_n} \end{pmatrix}}_{\mathbf{E}}$$

One can solve this system in general with the aid of a matrix exponential however in practice this can be a difficult task. Finding the eigenvalues of the matrix **A** can be made a simpler task with the aid of tools such as **Maple** or **Mathematica**, if the number of cells in the system is kept small (≤ 3) for larger systems however one can use tools developed in the field of computational and numerical algebraic geometry which involve the *discriminant variety* and Gröbner basis [101].

Solution for the two cell system

Here the analysis is continued for a system of two cells which is tractable without being overly cumbersome. The system to solve is

$$\underbrace{\begin{pmatrix} \dot{E}_{x_1} \\ \dot{E}_{y_1} \\ \dot{E}_{x_2} \\ \dot{E}_{y_2} \end{pmatrix}}_{\dot{\mathbf{E}}} = \underbrace{\begin{pmatrix} (1-\kappa_{x_1}) & -1 & 0 & 0 \\ \epsilon & -(\kappa_{y_1}+\epsilon b) & 0 & 0 \\ 0 & 0 & (1-\kappa_{x_2}) & -1 \\ 0 & 0 & \epsilon & -(\kappa_{y_2}+\epsilon b) \end{pmatrix}}_{\mathbf{A}} \underbrace{\begin{pmatrix} E_{x_1} \\ E_{y_1} \\ E_{x_2} \\ E_{y_2} \end{pmatrix}}_{\mathbf{E}}$$

The system

$$\dot{\mathbf{E}} = \mathbf{A}\mathbf{E}$$

has solution

$$\mathbf{E} = \mathbf{x}e^{\lambda t}$$

where $\mathbf{x}$ is a vector of constants and λ is a scalar decay/growth coefficient. Now by substitution

$$\dot{\mathbf{E}} = \lambda \mathbf{x} e^{\lambda t} = \mathbf{A}\mathbf{E} = \mathbf{A}\mathbf{x}e^{\lambda t}$$

and division by $e^{\lambda t}$, results in the usual eigenvalue equation

$$\lambda \mathbf{x} = \mathbf{A}\mathbf{x}.$$

The eigenvalues and corresponding eigenvectors of $\mathbf{A}$ are found to be

$$\lambda_{1,2} = \frac{1}{2}\left\{a + b \pm \sqrt{(a-b)^2 - 4\epsilon}\right\}, \qquad \mathbf{x}_{1,2} = \begin{pmatrix} -\dfrac{2}{b - a \pm \sqrt{(a-b)^2 - 4\epsilon}} \\ 1 \\ 0 \\ 0 \end{pmatrix}$$

and

$$\lambda_{3,4} = \frac{1}{2}\left\{c + d \pm \sqrt{(c-d)^2 - 4\epsilon}\right\}, \qquad \mathbf{x}_{3,4} = \begin{pmatrix} 0 \\ 0 \\ 2 \\ -\dfrac{2}{d - c \pm \sqrt{(c-d)^2 - 4\epsilon}} \\ 1 \end{pmatrix}$$

where

$$a = 1 - \kappa_{x_1}, \quad b = -(\kappa_{y_1} + \epsilon b), \quad c = 1 - \kappa_{x_2} \quad \text{and} \quad d = -(\kappa_{y_2} + \epsilon b).$$

In order to achieve the synchronisation of the subsystem to the main system using the proposed nonlinear control signals it is necessary for the error signal $\mathbf{E}$ to exponentially decay to zero. As the ODEs governing $\mathbf{E}$ has a unique fixed point at the origin, the only requirement is for the derived eigenvalues λ_* to be negative and real.

Numerical simulation for the $n = 2$ case

To see the synchronisation of the subsystem to the master system we take the following parameters

$$a = 1.23, \quad \epsilon = 0.1 \quad \text{and} \quad b = 0.06.$$

The main system has the following *adjacency matrix*[4]

$$g = \begin{pmatrix} 0 & 1 \\ 1 & 0 \end{pmatrix}$$

and the subsystem is subject to the adjacency matrix h

$$h = \begin{pmatrix} 0 & 0.3 \\ 0.7 & 0 \end{pmatrix}.$$

The uncoupled systems (no nonlinear control signal present) have the following oscillatory profiles, Figure 3.12

[4]An adjacency matrix is simply a matrix representation of the coupling strengths of a network of elements, typically used in the literature of network systems.

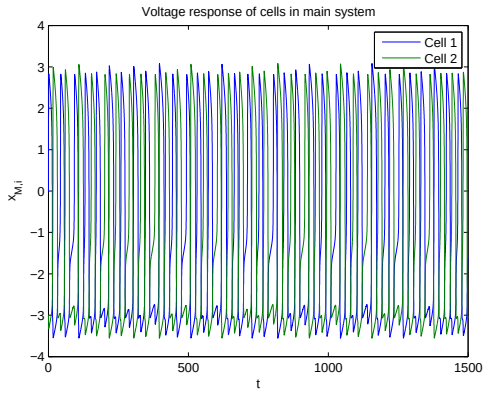

(a) The main system's voltage responses.

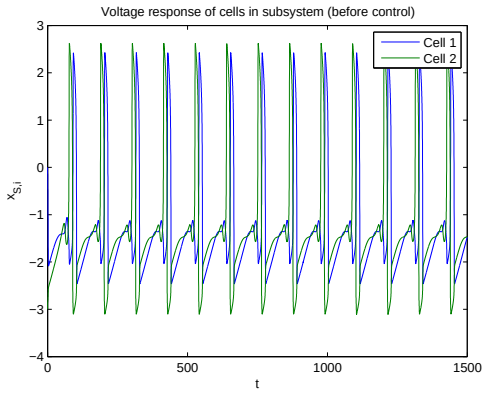

(b) The subsystem's voltage responses.

Figure 3.12: Time Series responses of the main and subsystem before implementation of the nonlinear control signal.

The main system has a chaotic[5] high frequency firing response while the subsystem is undergoing regular 1:1 oscillations with a smaller frequency than that of the main system.

Applying the control signals outlined earlier with control parameters

$$\kappa_{x_1} = \kappa_{x_2} = 4 \quad \text{and} \quad \kappa_{y_1} = \kappa_{y_2} = .4$$

results in an error system with repeated eigenvalues

$$\lambda_{1,3} \approx -0.45$$
$$\lambda_{2,4} \approx -2.96.$$

Thus the fixed point at the origin of the error system is a stable node and one is guaranteed synchrony between the main system and the subsystem.

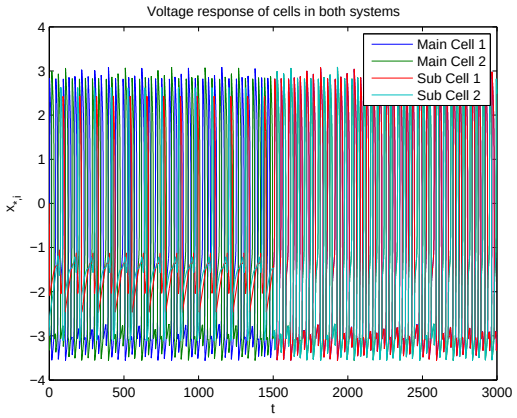

Figure 3.13: Voltage response of the cells in the main system and cells in the subsystem. The control signal is initiated at $t = 1500$.

The control signal is applied to the subsystem at $t = 1500$, Figure 3.13.

[5]This chaotic system will be introduced to the reader in subsequent chapters.

The analytic signals are constructed for each of the cells in order to define their phase, shown in Figure 3.14.

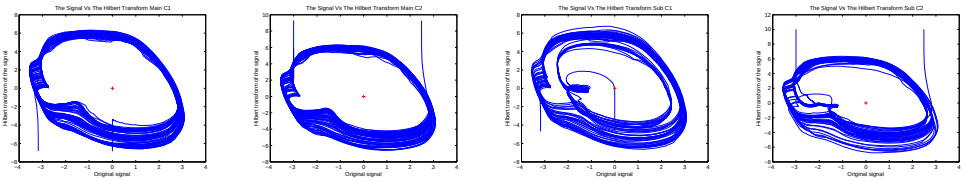

(a) Main Cell 1 Analytic signal. (b) Main Cell 2 Analytic signal. (c) Sub Cell 1 Analytic signal. (d) Sub Cell 2 Analytic signal.

Figure 3.14: Analytic signals of each cell in each system.

After defining the phase the order parameter is computed, clearly showing, Figure 3.15, the onset of synchrony after the control signal is initiated at $t = 1500$.

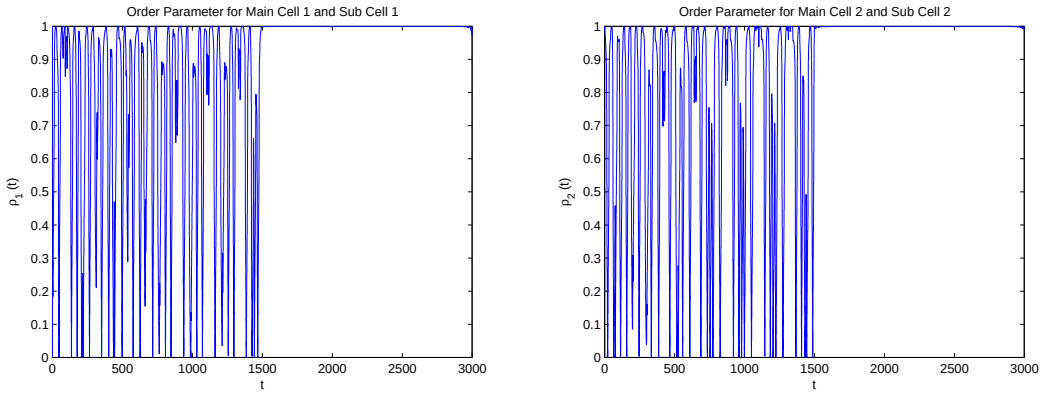

(a) Order parameter for main cell 1 and sub cell 1. (b) Order parameter for main cell 2 and sub cell 2.

Figure 3.15: Order parameter showing the onset of synchrony after implementation of the control signal.

3.6 Sinusoidally Forced FHN Cell and Wenckenbach Rhythms

Arrhythmias, irregular rhythms, in heart cells can lead to ineffective pumping of blood through the cardiovascular system in living organisms. One type of arrhythmia named after the Dutch atonomist Karl Frederick Wenckebach, named the Wenckenbach phenomenon, is characterised by improper conduction of action potentials from the atria to the ventricles. In patients suffering from Wenckenbach type rhythmic behaviour M contractions of the atria leads to N contractions of the ventricles where $N < M$. In the

medical literature Wenckenbach rhythms are categorised under second-degree atrioventricular block and manifest in two types

- **Type 1**: Considered a nonfatal arrythmia and is typically due to defects at the atrioventricular node.
- **Type 2**: Is considered a more serious form of arrhythmia which can lead to sudden cardiac death. Arrhythmias are usually due to defects in the Bundle of His-Purkinje system.

To gain insight into these arrhythmia we introduce a sinusoidal current term into the voltage like variable of the FHN system. The model is

$$\begin{aligned} \dot{x} &= x - x^3/3 - y + A\cos(\omega t) \\ \dot{y} &= \epsilon(x + a - by). \end{aligned} \tag{3.6.0.1}$$

System (3.6.0.1) is not in autonomous form as the $\dot{x}$ equation contains time dependant terms, one can rewrite (3.6.0.1) as

$$\begin{aligned} \dot{x} &= x - x^3/3 - y + A\cos(\psi) \\ \dot{y} &= \epsilon(x + a - by) \\ \dot{\psi} &= \omega. \end{aligned} \tag{3.6.0.2}$$

Equation (3.6.0.2) is a set of three autonomous coupled ordinary differential equations. The dynamics of this system compared to that of the unforced FHN system is richer in that it can admit chaotic dynamics[6]. The aim will be to find Weckenbach rhythms as well as more complex chaotic rhythms on variation of the frequency (ω) of forcing.

3.6.1 Numerical treatment of the forced FHN system

The cardiac conduction system is composed of cells capable of producing autonomous self sustained oscillations, as described earlier. Picking parameters that produce typical suprathreshold action potential like oscillations[7] in the unforced system, such as

$$\epsilon = 0.05, \quad a = 0.1 \quad \text{and} \quad b = 0.5$$

[6]Chaos can not appear in the unforced FHN system due to the Poincare-Bendixon theorem, which states that trajectories governed by a 2D system of ODEs will either converge to an equilibrium point or a limit cycle.

[7]These are parameters that admit stable limit cycles and not equilibrium points.

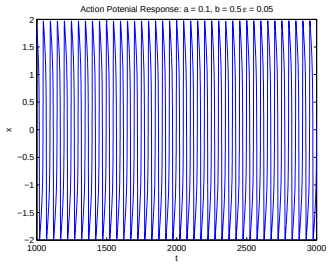

(a) Action Potential Time series of unforced FHN system.

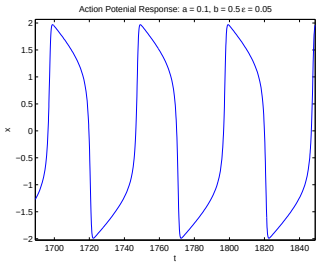

(b) Action Potential Time series (zoom) of unforced FHN system.

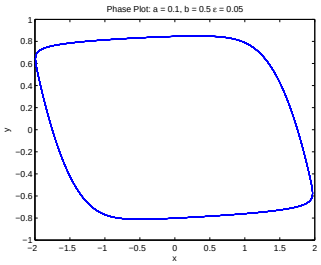

(c) Phase space plot of unforced FHN system.

Figure 3.16: The unforced FHN system, $a = 0.1$, $b = 0.5$ and $\epsilon = 0.05$.

Defining a Poincaré section

$$\Sigma : x = 0, \quad \text{and} \quad \dot{y} < 0$$

gives us a return map which catches the action potential crossing zero during its repolarisation. From the return times the unforced oscillations have a period of

$$T_{\text{Cell}} = 50.13 \pm 0.03$$

thus the natural frequency of the firing cell without forcing is

$$\omega_0 \approx 0.02$$

Introducing the external current with

$$A = 0.25$$

and using the forcing frequency as a bifurcation parameter, we have the bifurcation plot shown in figure 3.17 after taking the Poincaré section.

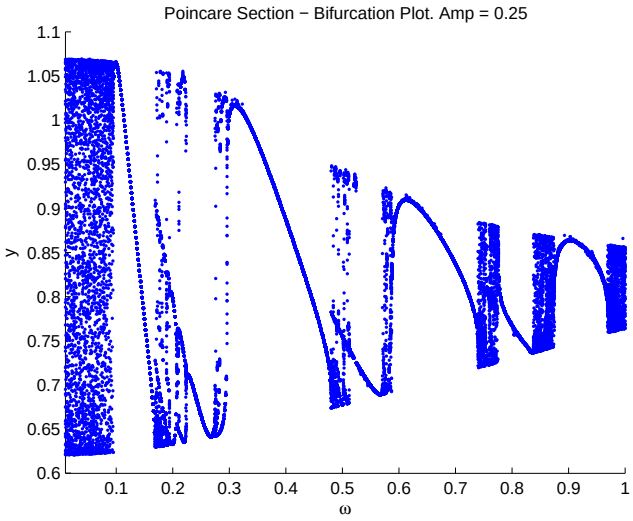

Figure 3.17: Bifurcation plot on variation of the forcing frequency ω

The bifurcation plot clearly shows bands of complex dynamical behaviour at the low frequency scale giving way to regular behaviour that once again leads to complex bands. Taking a narrower look at the bifurcation plot gives further insight into the transition from regular-complex-regular behaviour in the forced system

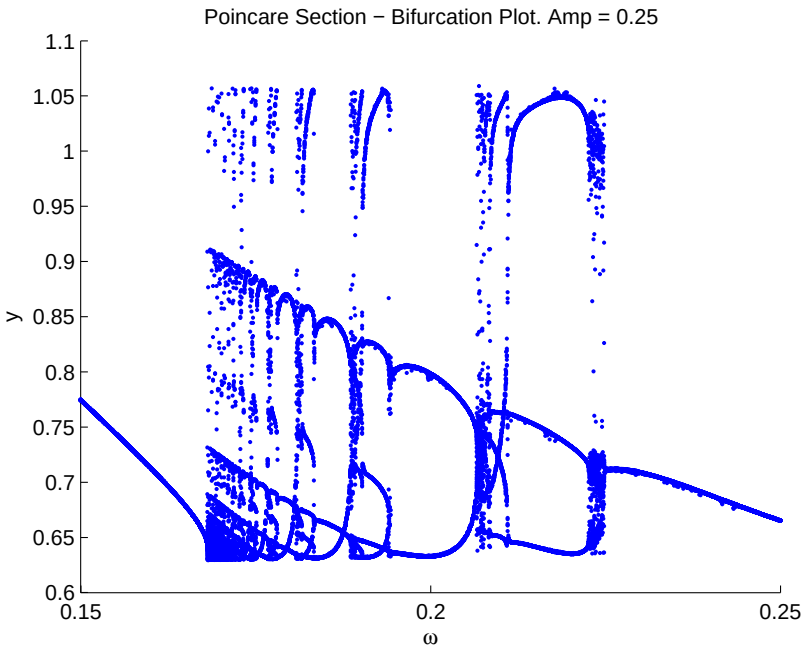

Figure 3.18: Bifurcation plot on variation of the forcing frequency $\omega = 0.15$ to $\omega = .25$.

Looking for Wencheback rhythms it is useful to examine the regions of figure 3.18 where the rhythmic behaviour is not extremely complex, these being the frequencies where the cell punctures the Poincaré surface in only 1, 2 or 3 places and making a direct comparison to the frequency of the forcing term.

1:1 Cell response to $\omega = 0.16$

With $\omega = 0.16$ the forcing term has a period of

$$T_{\text{Force}} = \frac{2\pi}{0.16} \approx= 39.37$$

which has a frequency

$$\omega_{\text{force}} = 0.0255.$$

The resulting action potentials have the following form
From the Poincaré map the forced cell has period and frequency of

$$T_{\text{Cell}} \approx 39.27 \quad \text{and} \quad \omega_{\text{Cell}} = 0.0255$$

We thus have 1:1 phase locking and frequency synchronisation between the forcing term

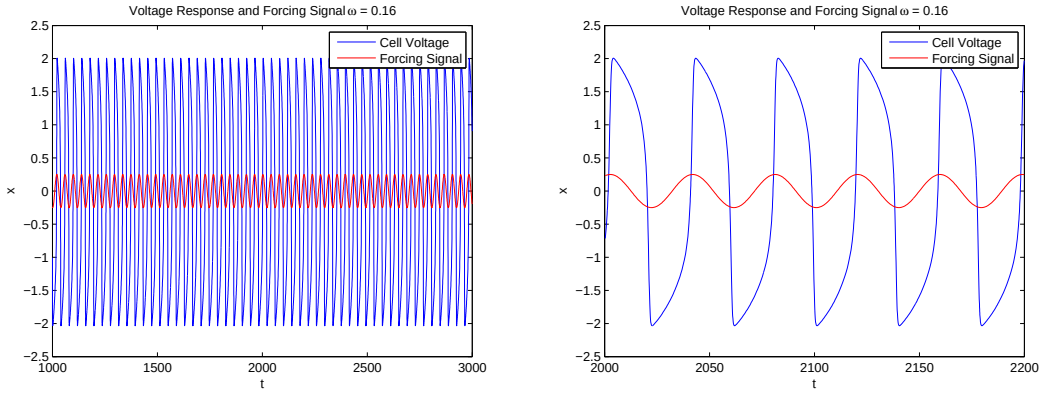

(a) Long Term action potential response.

(b) Zoom of the action potentials and the forcing current

Figure 3.19: Voltage response of the forced FHN system with $A = 0.25$, $\omega = 0.16$, $a = 0.1$, $b = 0.5$ and $\epsilon = 0.05$.

and the action potential response.

3:2 Cell response to $\omega = 0.2$

At this frequency of forcing figure 3.18 shows that the Poincaré surface is punctured in two places a doubly folded limit cycle in phase space. Which is indeed the case as is shown in the figure

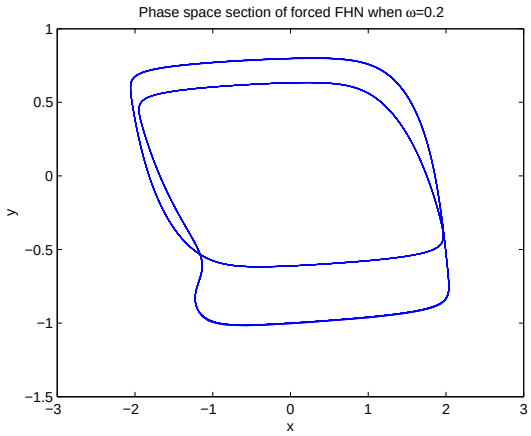

Figure 3.20: Cross section of the phase space for the forced FHN system with $A = 0.25$, $\omega = 0.2$, $a = 0.1$, $b = 0.5$ and $\epsilon = 0.05$.

The action potential profiles reflect this showing that there are consecutive doublets of action potentials being elicited by the forced cell.

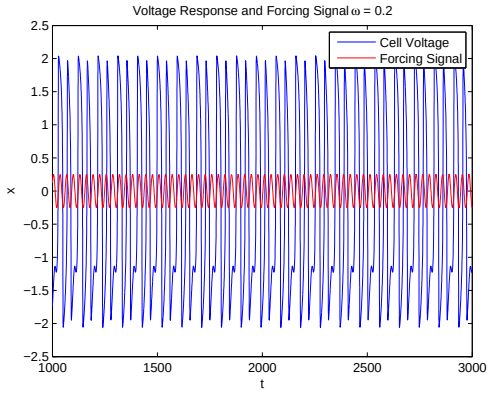

(a) Long Term action potential response.

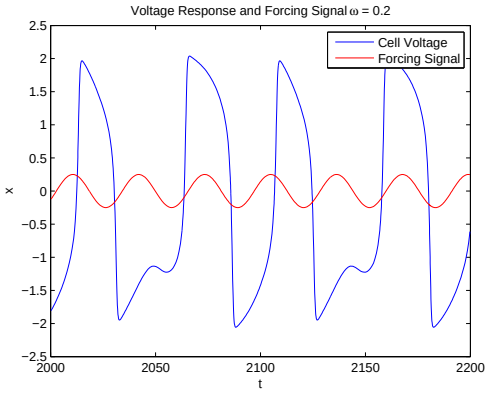

(b) Zoom of the action potentials and the forcing current

Figure 3.21: Voltage response of the forced FHN system with $A = 0.25$, $\omega = 0.2$, $a = 0.1$, $b = 0.5$ and $\epsilon = 0.05$.

The forcing frequency for $\omega = 0.2$ is

$$\omega_{\text{force}} = 0.0318$$

With the cell producing an action potential firing at a frequency of

$$\omega_{\text{Cell}} \approx 0.0213.$$

From the frequency ratios we have

$$\frac{\omega_{\text{force}}}{\omega_{\text{Cell}}} \approx \frac{3}{2}$$

which shows a 3:2 phase locking response and the presence of of a Wenckebach rhythm.

4:3 Cell response to $\omega = 0.185$

Figure 3.18 implies there is a triply folded limit cycle in phase space for this forcing frequency, which is the case
with action potential responses as shown in the figure.
The frequency of the forcing term and the frequency of the cell's action potential response are found to be

$$\omega_{\text{force}} = 0.0294 \quad \text{and} \quad \omega_{\text{Cell}} \approx 0.0222$$

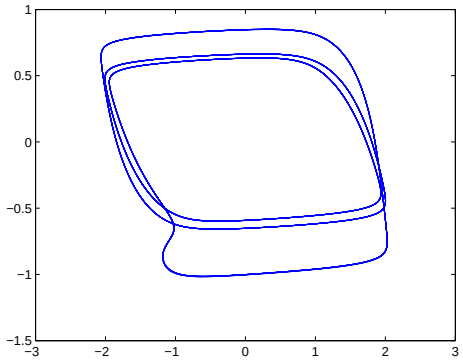

Figure 3.22: Cross section of the phase space for the forced FHN system with $A = 0.25$, $\omega = 0.185$, $a = 0.1$, $b = 0.5$ and $\epsilon = 0.05$.

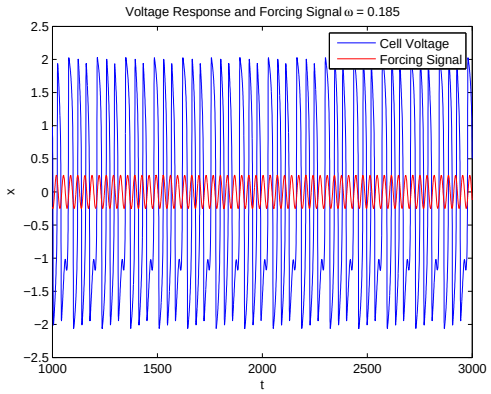

(a) Long Term action potential response.

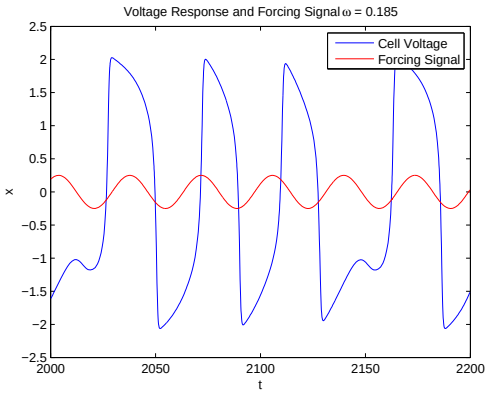

(b) Zoom of the action potentials and the forcing current

Figure 3.23: Voltage response of the forced FHN system with $A = 0.25$, $\omega = 0.185$, $a = 0.1$, $b = 0.5$ and $\epsilon = 0.05$.

resulting in a 4:3 phase locking response.

$$\frac{\omega_{\text{force}}}{\omega_{\text{Cell}}} = \frac{0.0294}{0.0222} \approx 1.3333$$

3.6.2 Phase Locking and Arnold Tongues in the forced FHN

Continuing the analysis one finds bands of frequencies over which the Wenckenbach rhythms of various phase locking regimes are expressed

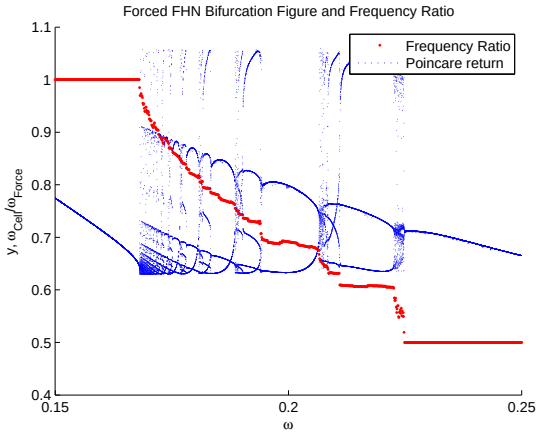

Figure 3.24: The phase locked regions and the frequency ratio $\frac{\omega_{\text{cell}}}{\omega_{\text{Force}}}$

A number of illustrated Wenchebach rhythms are indicated in figure 3.25, the cells voltage responses are shown for typical simulations within the indicated frequency bands for illustration.

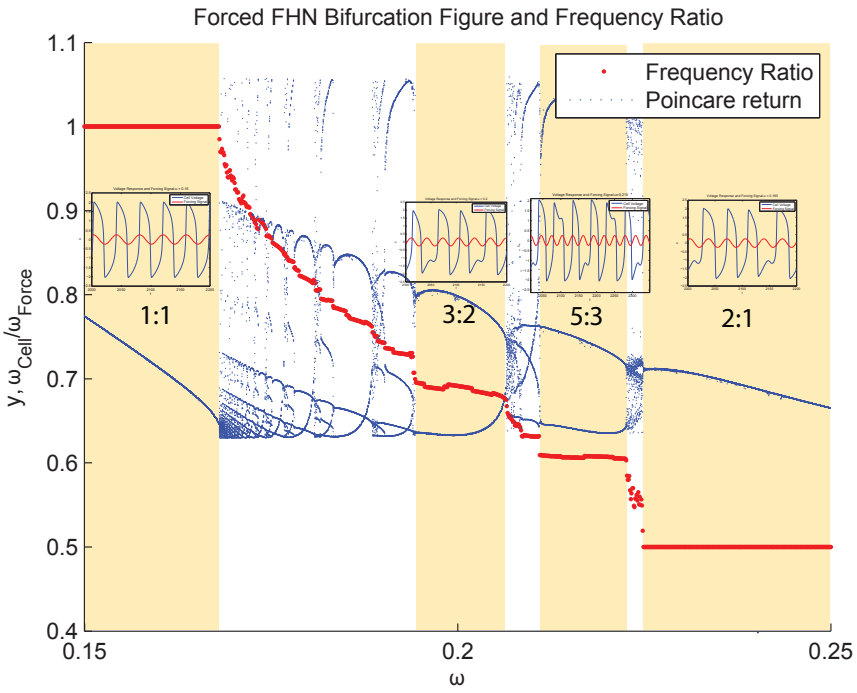

Figure 3.25: The phase locked regions and the frequency ratio $\frac{\omega_{\text{cell}}}{\omega_{\text{Force}}}$

Arnold Tongues

Thus far there has been no treatment of the effect that the amplitude of the forcing term has on the forced FHN cell. With stronger amplitude of the forcing term one finds a greater tendency of the FHN cell to entrail its oscillations with the cosine wave. This phenomena is best represented by a plot of the systems phase locking regions as a function of the amplitude and frequency of the external force. Such regions are commonly referred to as Arnold Tongues.

Finding the boundaries of a system's Arnold Tongues is a rather computationally intensive task. It involves scanning a two parameter phase space, integrating the system of ODEs to be examined and calculating the frequency of the oscillator (using a Poincaré map or otherwise) and deciding if the system is phase locked at each point of the parameter space.

The basic algorithm for finding the boundaries of an Arnold tongue are as follows:

1. Set all initial conditions for the FHN system of ODEs
2. Find the natural frequency of the unforced system
    - Using Peak Detection Methods
    - Integrate the system with an adaptive Runge-Kutta algorithm. Calculate the Power Spectrum using a fast fourier transform and approximate the frequency at the peak energy.
3. Set the locking mode, e.g 1:1, 2:1 etc.
4. Set the forcing frequency to the appropriate multiple of the oscillators natural frequency.
5. Set the amplitude of the forcing term.
6. Find the upper bound of the Arnold tongue boundary
    - Pick a large forcing frequency (compared to the multiple of the natural frequency) such that the system is not phase locked at this upper frequency.
    - Run a bisection root finding algorithm to find the boundary point.
        - Integrate the system and use peak detection to find the frequency of the resulting forced system.

- If the system is not phased locked return a +1 (forcing frequency upper bound) to the bisection method. If it is locked return a -1 (forcing frequency lower bound).
- Continue this narrowing of the upper and lower bound, by taking the midpoint between the upper and lower estimate and testing it for phase locking, for a set number of iterations, typically 1×10^3.

• Return the resulting frequency.

7. Find the lower bound for the Arnold tongue boundary

   This is performed in an almost identical manner to finding the upper bound.

8. Increase the amplitude of the forcing term and repeat the search for the upper and lower boundary of the Arnold Tongue at this amplitude.

The advantage of finding the frequency of the forced oscillator using a peak detection algorithm over a Poincaré section, is computational speed. Finding when a system passes through the Poincaré surface involves interrupting the integrator and having it listen to a number of events testing each one of them at every iteration of the integrator. After finding the return times and storing them, which takes memory and time, it is still necessary to find the frequencies from the return times again adding to the computational effort. The fourier power spectrum on the other hand is very efficient since it depends on taking an appropriate combination of fast fourier transforms which are very well optimised for computational tasks.

Furthermore using a root finding algorithm instead of the simply iterating through every frequency until one no longer has a phase locking response greatly reduces the number of iterations one must take in order to estimate the Arnold tongue boundary. The bisection method also continuously increases the accuracy of the frequency at which the boundary occurs when the distance between the upper and lower estimate tends to zero.

Using the power spectrum to estimate the frequency has the disadvantage of not giving the user a guaranteed proper 'frequency' for the oscillator, the oscillations may in fact be chaotic making the period infinite which leads to no proper definition of frequency, this also being an issue when looking at Poincaré sections. What can be said however is that there is locking between the external forcing terms and the *dominant* frequency of the FHN cells power spectrum, which can be of use when examining chaotic oscillations.

Taking the forced FHN system given by Equation (3.6.0.1) with parameters[8]

$$a = 0.1, \quad b = 0.5 \quad \text{and} \quad \epsilon = 0.01$$

The 1:1 Arnold tongue is found and plotted in figure 3.26.

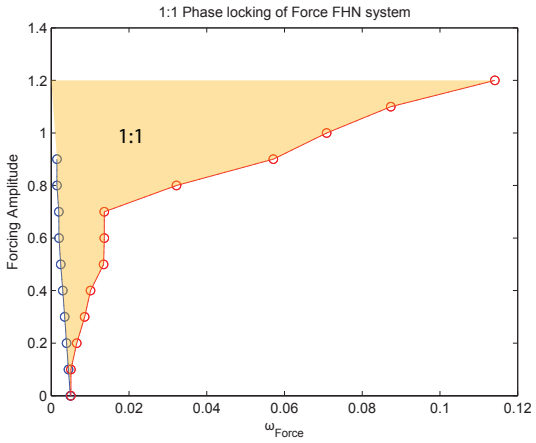

Figure 3.26: The 1:1 Arnold Tongue for the forced FHN system.

The 1:1 Arnold tongue shows that forcing the system with larger amplitudes of forcing leads to wider frequency ranges that the 1:1 locking regime is expressed over. Looking for higher order locking terms one finds

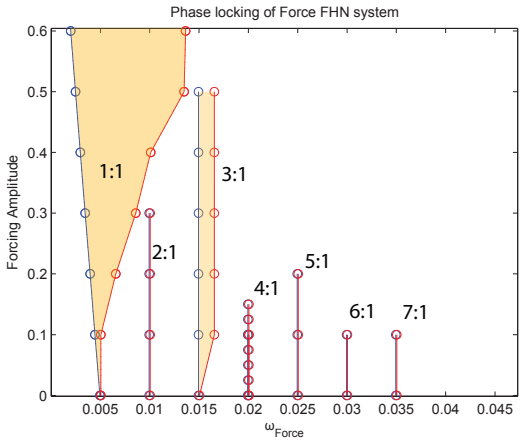

Figure 3.27: Higher order Arnold Tongues for the forced FHN system.

The root finding algorithm fails to find the boundaries of the higher order phase locking regimes. The starting point for the algorithm depends on bracketing the upper (lower)

[8]Reducing the value of epsilon to $\epsilon = 0.01$ from $\epsilon = 0.05$stiffens the ODEs costing more computational time while making the transition between fast a slow dynamics more marked.

boundary between the appropriate multiple of the cells unforced natural frequency and a relatively large (small) frequency. In the FHN system however the Arnold tongues are not centered about multiples of the cells natural frequency for larger amplitudes of the forcing term. This can be seen with a more intensive study of the forcing terms parameter space, a coarse grained figure is shown in Figure 3.28

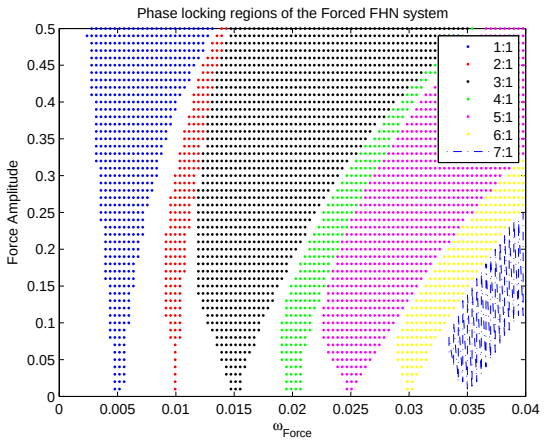

Figure 3.28: The $N:1$ Arnold Tongues for the forced FHN system

The higher order locking regions can be found if one again opts for finer detail in the parameter space, finding $2:X$ and $3:X$ rhythms which are shown in Figure 3.29.

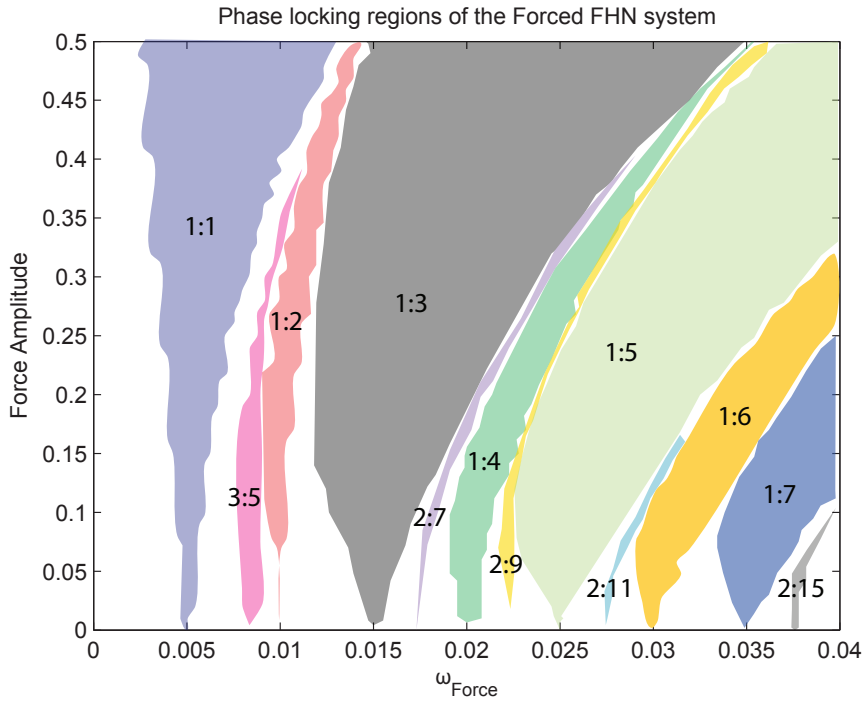

Figure 3.29: The higher order Arnold Tongues for the forced FHN system

3.7 Frequency Sync In the Master-Slave Electrically coupled FHN system

A natural extension to the results concerning the sinusoidally forced FHN cell, is an analysis of a master-slave coupled FHN system.

The two cell Master-Slave FHN system is given by the following 4D set of coupled ODEs

$$\begin{aligned} \dot{x_{\mathrm{M}}} &= x_{\mathrm{M}} - x_{\mathrm{M}}^3/3 - y_{\mathrm{M}} \\ \dot{x_{\mathrm{S}}} &= x_{\mathrm{S}} - x_{\mathrm{S}}^3/3 - y_{\mathrm{S}} + g_{\mathrm{M,S}}\,(x_{\mathrm{S}} - x_{\mathrm{M}}) \\ \dot{y_{\mathrm{M}}} &= \epsilon(x_{\mathrm{M}} + a_{\mathrm{M}} - b_{\mathrm{M}} y_{\mathrm{M}}) \\ \dot{y_{\mathrm{S}}} &= \epsilon(x_{\mathrm{S}} + a_{\mathrm{S}} - b_{\mathrm{S}} y_{\mathrm{S}}). \end{aligned} \tag{3.7.0.1}$$

Master slave coupling such as the one described here can be considered simplified models of the interaction of cardiac pacemaker cells[9] with the bulk myocardium and the interaction of neural pacemaker cells[10] with cells awaiting action potential signals.

3.7.1 Self sustained master and excitable slave: Variation of Coupling Strength

In contrast to the forced FHN system here the analysis begins with a self sustained FHN cell (the master) and a FHN cell at equilibrium (the slave). Before coupling the systems together, typical action potential profiles for the self sustained FHN system have the appearance of those shown in figure 3.30(a)

$$\text{Parameters: } a_{\mathrm{M}} = 0.1, \quad b_{\mathrm{M}} = 0.5 \quad \text{and} \quad \epsilon_{\mathrm{M}} = 0.01$$

which possesses a stable limit cycle shown in figure 3.30(b).
The parameters for the slave cell are chosen such that it posses a stable equilibrium point, here

$$\text{Parameters: } a_{\mathrm{S}} = 0.7, \quad b_{\mathrm{S}} = 0.5 \quad \text{and} \quad \epsilon_{\mathrm{S}} = 0.01$$

which possesses a stable equilibrium point at

$$\bar{x} = -1.0328 \quad \bar{y} = -0.6656.$$

[9] For example in the sinoatrial node.
[10] The circadian cells.

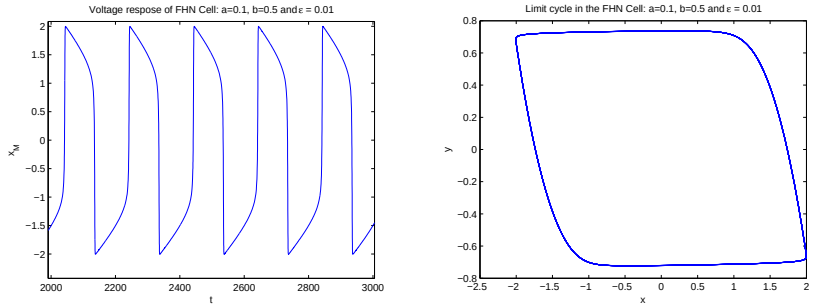

(a) Action potential profile (b) Action potential profile

Figure 3.30: Action potential profile and limit cycle of the self sustained FHN master cell with $a_{\mathrm{M}} = 0.1, \quad b_{\mathrm{M}} = 0.5 \quad \text{and} \quad \epsilon_{\mathrm{M}} = 0.01.$

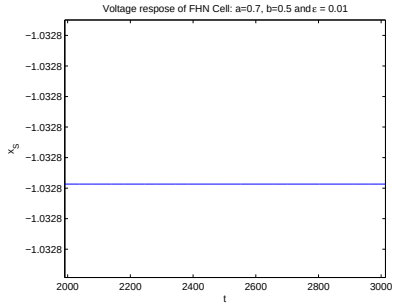

Figure 3.31: Action potential profile of the uncoupled $g_{\mathrm{M,S}} = 0$ FHN Slave cell at equilibrium with $a_{\mathrm{S}} = 0.7, \quad b_{\mathrm{S}} = 0.5 \quad \text{and} \quad \epsilon_{\mathrm{S}} = 0.01.$

Bifurcation in the Master-Slave system due to changes in coupling strength

In order to characterise the slave cells response to the master cell's oscillations a Poincaré surface is used in a similar fashion to that used in the force FHN system. Taking a section of the 4D system in the (x_S, y_S) plane and looking at punctures through the surface

$$\Sigma : \quad x_S = 0 \quad \text{and} \quad \frac{dy_s}{dt} < 0.$$

defines a firing event in the slave cell to have occurred whenever the voltage like variable passes through $x = 0$ in the negative direction. Computation can be memory and processor intensive as transient phenomena must be allowed to decay making for longer integration times. Allowing the coupling strength to vary from $g_{M,S} = -1$ attractive coupling[11] and $g_{M,S} = +1$ repulsive coupling[12] in increments of 0.01, one finds a course bifurcation diagram shown in figure 3.32(a). The frequency ratio between the firing cell and the slave cell shown in figure 3.32(b) shows the regions over which the system is frequency synchronised.

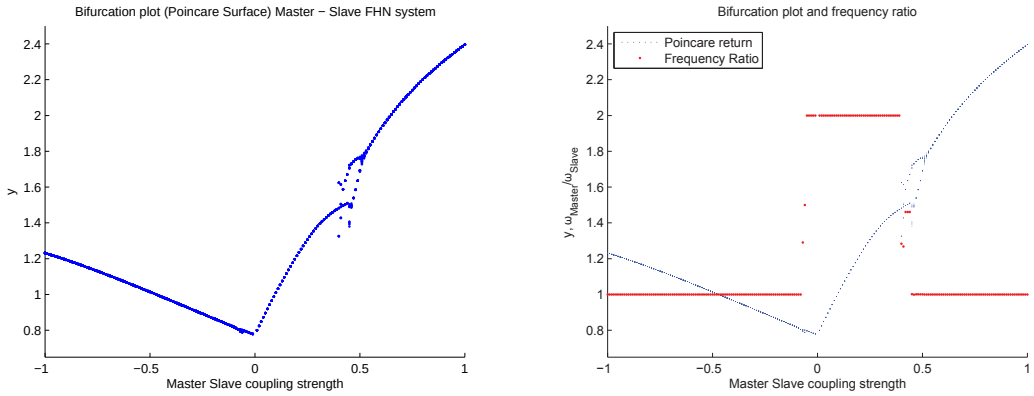

(a) Bifurcation plot.

(b) Frequency ratio plot.

Figure 3.32: Coarse bifurcation plot of the master slave coupled FHN system on variation of the coupling strength.

From figure 3.32(a) one can see that there are a number of irregularities over the $g_{M,S} \in (-0.2, 0.6)$ which warrant finer detail. These namely are regions where the slave cell transitions from a 1:1 frequency response to a 2:1 frequency response and viceversa.

[11]Named attractive as negative coupling strengths as cells are drawn together. Negative coupling strengths are those that are most close in nature to gap junctions, allowing (relatively) positive currents from one cell to cause a positive current input into the coupled cell. Here the coupling strength is limited to unity implying that the maximum voltage like stimulus the FHN cell can have is complete conduction of the voltage difference. Thus ruling out amplification of the voltage difference by the coupling junction

[12]Named repulsive as positive coupling strengths between cells tend to put cells in an anti-phase state. Such coupling strengths serve as a basic model of inhibitive synapses between neurons.

Transition from 1:1 to 2:1 frequency response

Figure 3.32(b) shows a transition from 1:1 frequency locking to 2:1 frequency locking over the attractive coupling strength

$$g_{\mathrm{M,S}} \in (-0.1 - 0.05).$$

After reduction of the coupling strength incremental step size to 0.0001 the finer structure within the bifurcation plot at the transition can be seen more clearly in figure 3.33.

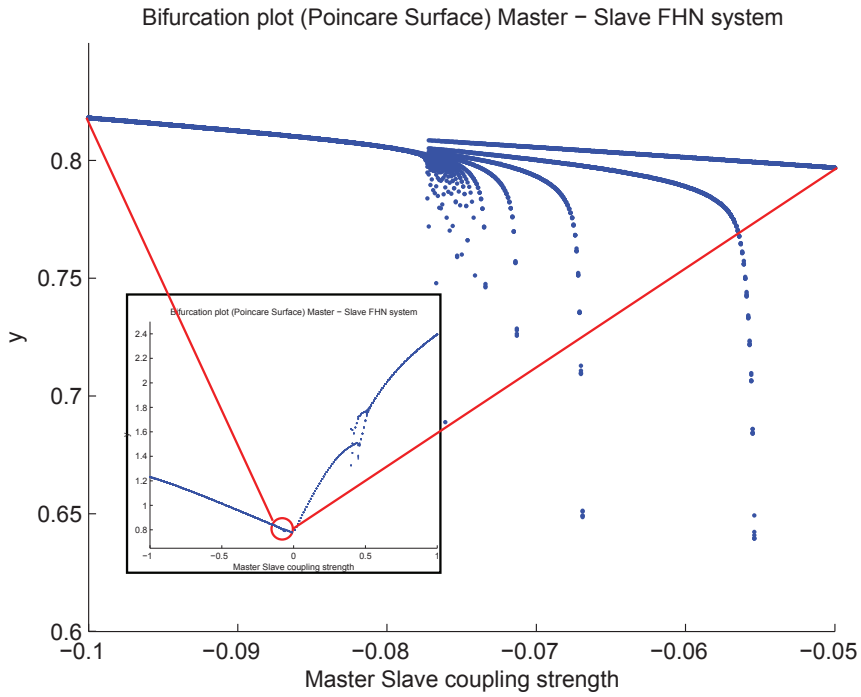

Figure 3.33: Bifurcation figure of zoomed in region. Inset graph shows the large scale bifurcation diagram shown in figure 3.32(a)

The frequency synchronised regions over this transition are shown in figure 3.34.

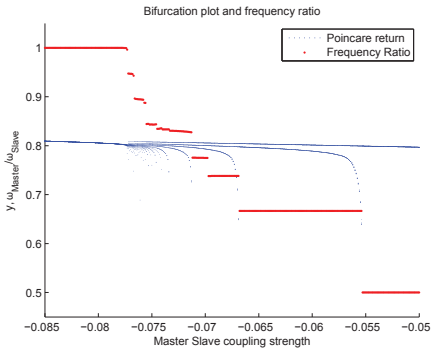

Figure 3.34: Bifurcation diagram is in blue while the frequency ratio is in red. The frequency ratio has been inverted here for ease of visualisation.

The transition over from 1:1 to 2:1 frequency locking regions shows a **devils staircase** like structure, typical action potential responses have been included in figure 3.35 for reference.

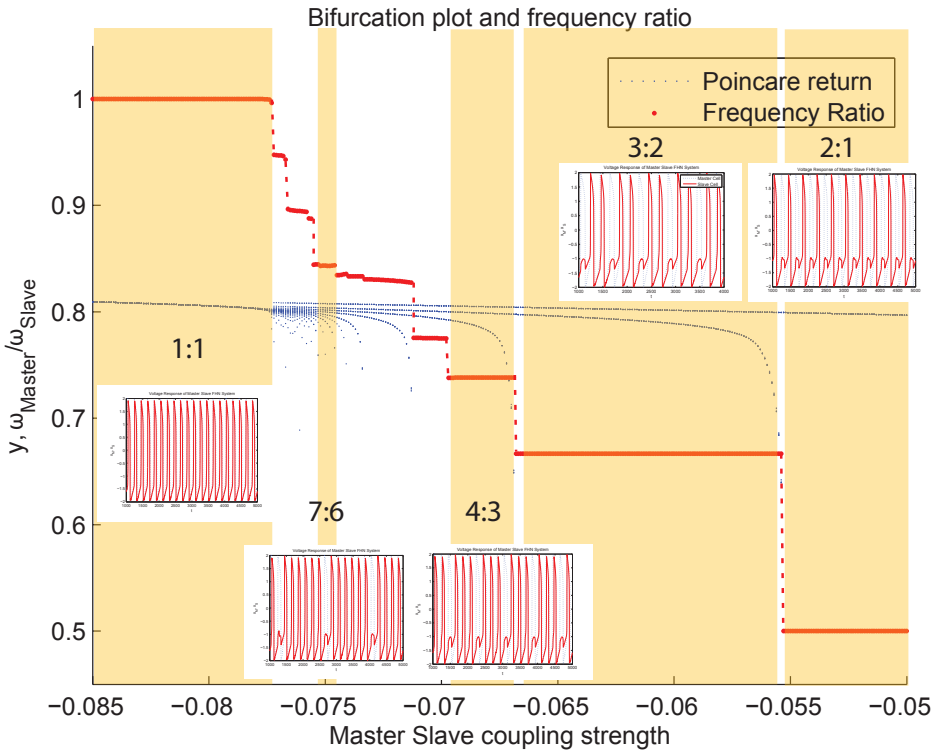

Figure 3.35: The devils staircase like structure and the action potential responses for the frequency synchronised transition from 1:1 to 2:1 locking in the attractively coupled master slave FHN system.

Transition from 2:1 to 1:1 frequency response

The transition from a 2:1 frequency ratio to a 1:1 frequency ratio can be seen in figure 3.32(b) occurring over the repulsive coupling strength interval

$$g_{\mathrm{M,S}} = (0.35, 0.52)$$

A close look at this bifurcation region is shown in figure 3.36

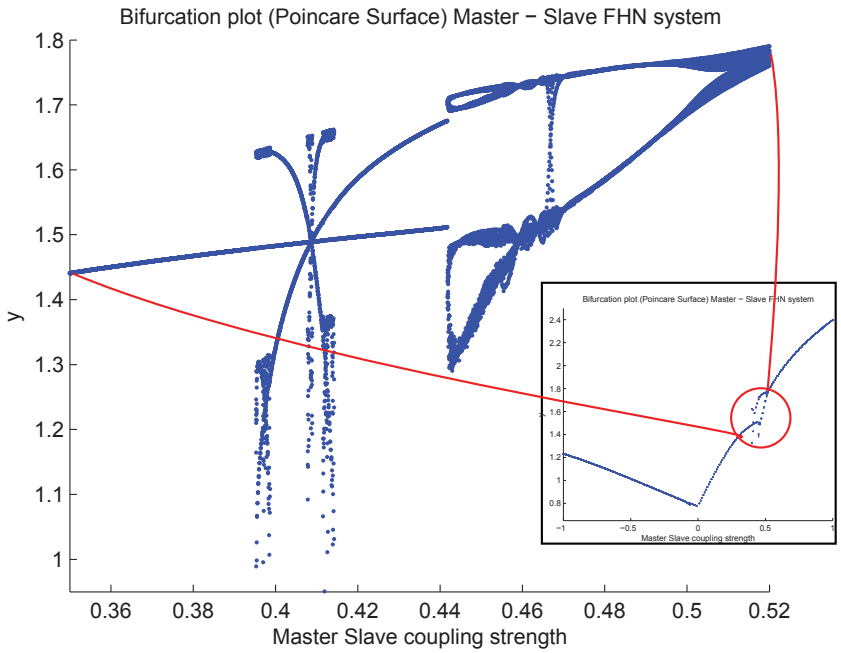

Figure 3.36: Bifurcation figure over the 2:1 to 1:1 frequency locking transition. Here the coupling strength increment is set to 0.0001.

The frequency synchronised regions over this coupling strength are shown in figure 3.37

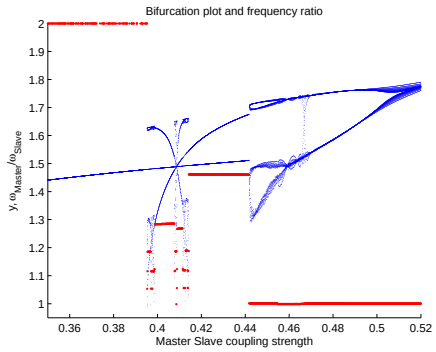

Figure 3.37: The frequency locking regions over the 2:1 to 1:1 transition.

In contrast to the attractive coupled system the transition does not follow a devils staircase like structure.

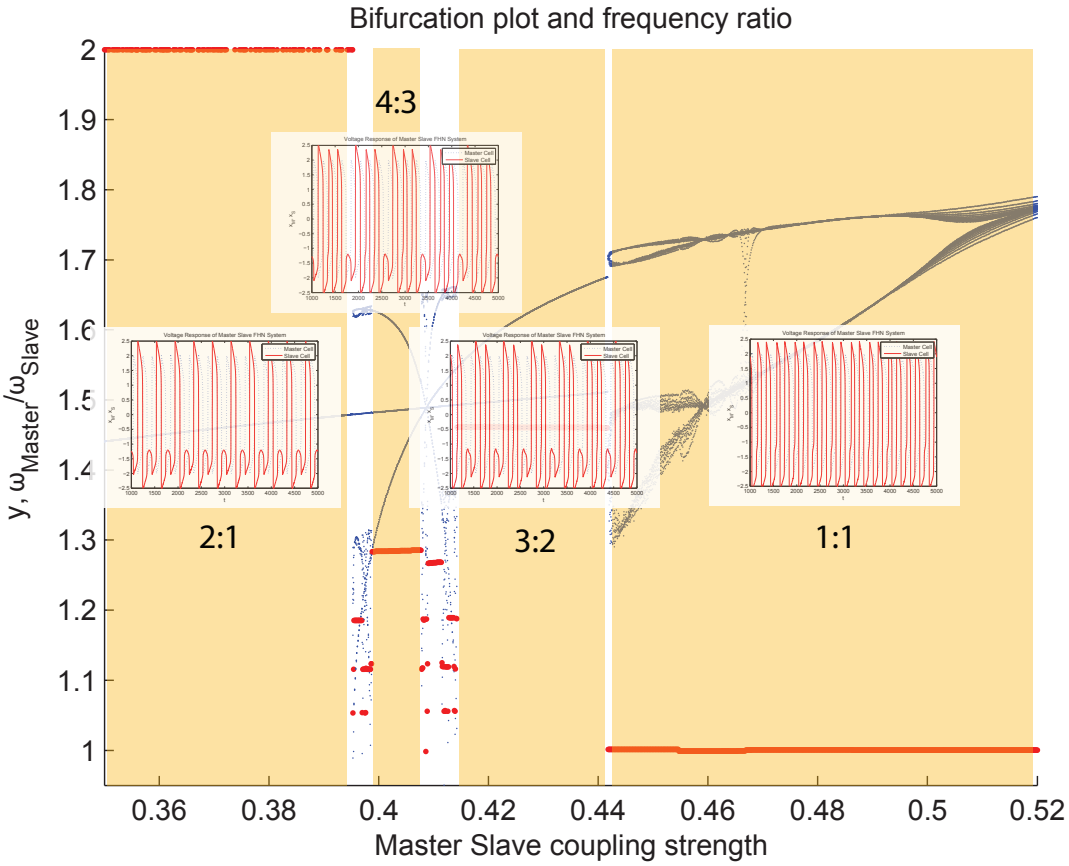

Figure 3.38: Regions of frequency synchronisation over the transition from 2:1 to 1:1 locking in the repulsively coupled master slave FHN system. Typical action potential profiles are included as reference.

Of note concerning repulsive coupling strengths in the master slave system is the type of phase synchrony that is present, namely **anti-phase syncrhonisation** between the master and the slave cell. This can be clearly seen (Figure 3.39) when examining coupling strengths $g_{\mathrm{M,S}} > 0.44$ where one has a 1:1 firing response between master and slave cells.

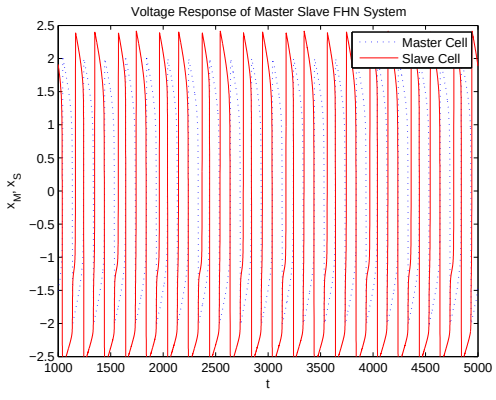

Figure 3.39: Anti-phase syncrhonisation between cells couple in a master slave system.

3.7.2 Arnold Tongues in the Self Sustained Master and Excitable Slave System.

In order to examine the Arnold tongues of the Master Slave FHN system it is necessary to have a means to adjust the frequency of the driving master system.

Frequency dependence of the FHN system on the parameter ϵ.

The single cell FHN system

$$\dot{x} = x - x^3/3 - y$$
$$\dot{y} = \epsilon(x + a - by)$$

undergoes a Hopf bifurcation for appropriately chosen values of the parameter a and b, which is independent of the parameter ϵ. The limit cycle resulting from the supercritical Hopf bifurcation results in stable self sustained oscillations in the system. The parameter ϵ controls the rate at which phase space trajectories transition from along the systems slow manifold, which results in changes in the frequency, and to a lesser extent the shape, of the limit cycle trajectories.

Taking

$a = 0.1, \quad b = 0.5 \quad \text{and} \quad \epsilon \in (0.001, 0.1)$

and recording the cell's frequency results in the relationship shown in Figure 3.40. Figure 3.40 depicts a typical frequency Vs. ϵ graph, which can be seen if one examines the cells frequency for various values of b (provided a stable limit cycle exists for the chosen parameters).

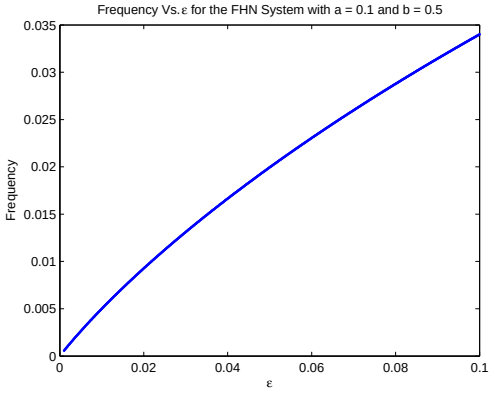

Figure 3.40: FHN cell frequency response as a function of ϵ, taking $a = 0.1$ and $b = 0.5$.

The loglog plot shown in figure 3.41(b) suggest that the frequency of the limit cycle formed during a supercritical Hopf bifurcation in the FHN system follows a power law.

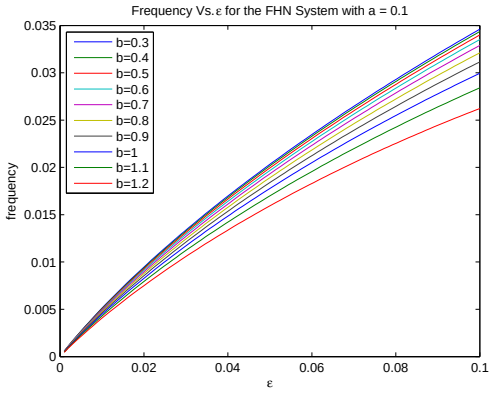

(a) FHN cell frequency response on variation of the parameters b and ϵ

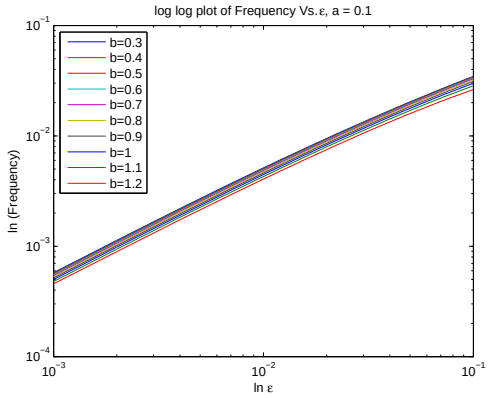

(b) log-log plot of figure 3.41(a)

Figure 3.41: The frequency of the FHN cell follows a power law relationship with the parameter ϵ.

Arnold Tongues in the Master Slave FHN system

As noted in the previous sections there is a relationship between the parameter ϵ and the frequency of the limit cycle created in the FHN system. To examine the Arnold tongues of the master slave FHN system an excitable slave cell is electrically coupled to a self sustained master cell. The two control parameters are the coupling strength $g_{\mathrm{M,S}}$ and the parameter ϵ for the master cell which controls the frequency at which the slave cell will be forced.

After extensive simulations over both attractive and repulsive coupling strengths

$$g_{\mathrm{M,S}} \in [-1, 1]$$

and master cell frequencies over the parameter range

$$\epsilon_{\mathrm{M}} \in [0.001, 0.1].$$

The frequency synchronised regions are shown in figure 3.42 for the master slave system (3.7.0.1) with parameters

$$a_{\mathrm{M}} = 0.1, \quad a_{\mathrm{S}} = 0.7, \quad b_{\mathrm{M}} = b_{\mathrm{S}} = 0.5 \quad \text{and} \quad \epsilon_{\mathrm{S}} = 0.01.$$

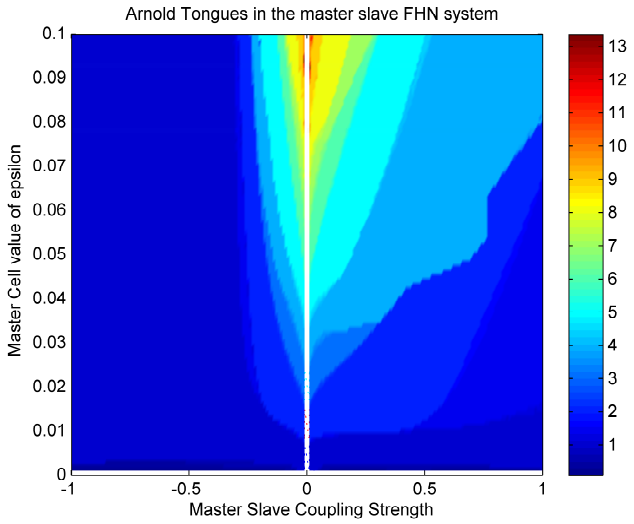

Figure 3.42: 2D view of the frequency synchronised regions of the Master Slave FHN system

The highest Master Freq : Slave Frequency responses occur in the relatively weak coupling strength interval $|g_{\mathrm{M,S}}| < 0.5$ as can be seen in figure 3.43,

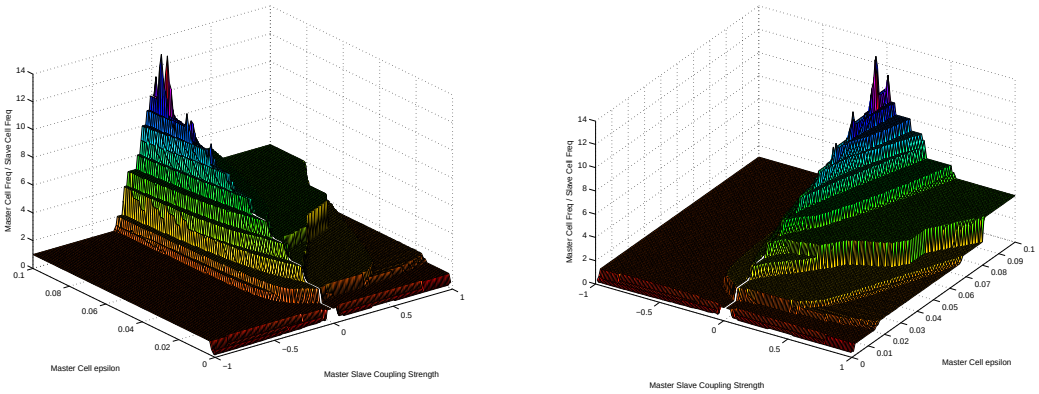

(a) 3D (left) view of the Arnold Tongues present in master slave couple system

(b) 3D (right) view of the Arnold Tongues present in master slave couple system

Figure 3.43: 3D view of the frequency synchronised regions of the Master Slave FHN system

Although figure 3.43 shows a rich structure of frequency locking regions between the master and slave cells the only frequency locking regions that are clearly visible are of the form

$$M : N \qquad \text{where } M \geq N$$

implying that 1 action potential response from the master cell only gives forth to 1 or

more action potential responses from the slave. This however is not the case as for very low frequency oscillatory behaviour of the master cell (corresponding to small values of ϵ_{M}) one finds frequency ratios of the form

$$M : N \qquad \text{such that } M \leq N$$

which can be seen in a more intensive parameter sweep at smaller values of ϵ, shown in figure 3.44.

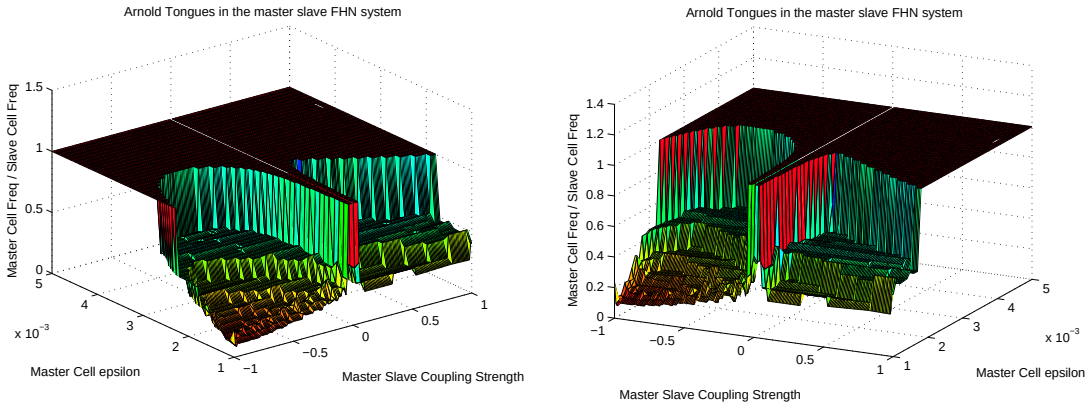

(a) 3D (left) view of the Arnold Tongues present in master slave couple system

(b) 3D (right) view of the Arnold Tongues present in master slave couple system

Figure 3.44: 3D view of the frequency synchronised regions of the Master Slave FHN system, for small values of $\epsilon \in [0.001, 0.05]$.

Bursting behaviour in the Master Slave FHN system

Bursting behaviour in neurons can be found in the central nervous system of mammals in neocortical pyramidal neurons [196] and has been linked to the reward circuit in the brain, addiction learning and memory [34].

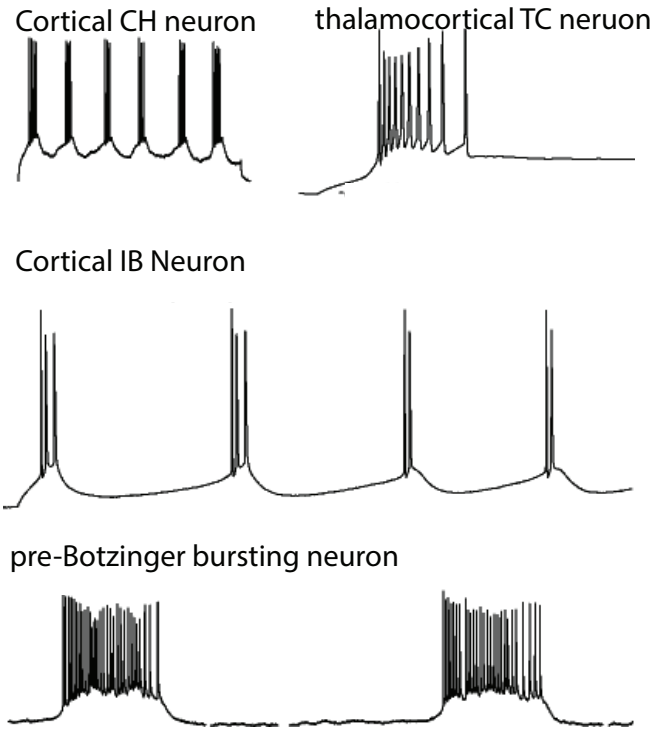

Figure 3.45: Examples of bursting action potentials from in vitro experiments on neural cells, figure adapted from [86]

Although certain neurons are capable of bursting behaviour on their own, there exist a multitude of neurons which produce bursting behaviour due to forcing; such as those found in the vocal sequencing of songbirds [54] and weakly electric fish [47].

Action potential bursting is the term given to a series of action potentials occurring in quick succession followed by a period of quiescence.

The bursting behaviour in the master slave FHN system occurs when the master cell which is driving the the slave cell produces an action potential response that is on a much longer timescale than the intrinsic action potential behaviour of the slave. The result of the master cells long action potential on the slave cell is a prolonged period of current input into the slave cell. The long plateaux present in the master cell's action potential effectively acts as a constant bias current on the slave cell. The slave cell is

unable to maintain the long plateaux response of the master cell as it's recovery variable (which dictates if the cell is able to produce an action potential or not) does not full return to its recovery, before having to produce another action potential. The result is a series of smaller action potentials in the slave system without a return to its rest state. An example of this behaviour can be seen in figure 3.46.

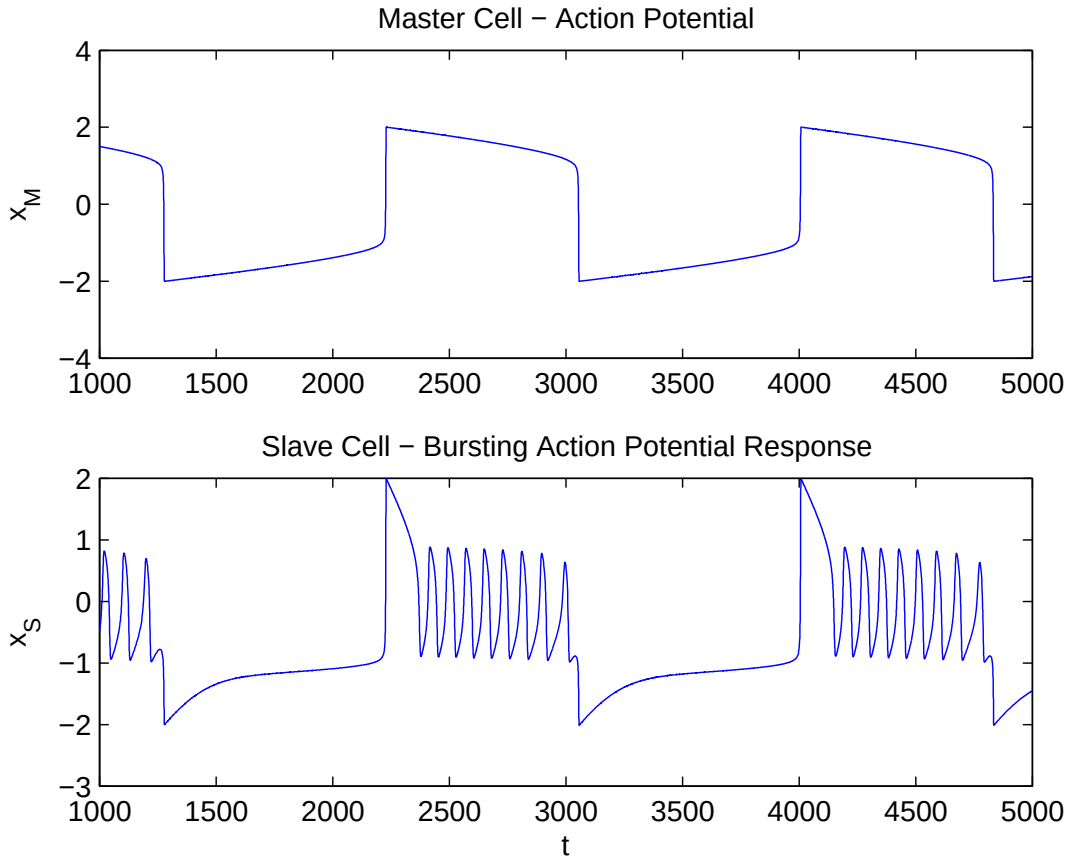

Figure 3.46: Bursting in the Master Slave FHN system. Parameters: $a_M = 0.1$, $a_S = 0.7$, $b_M = b_S = 0.5$, $\epsilon_M = 0.005$, $\epsilon_S = 0.01$ and $g_{M,S} = -0.8$ (attractive coupling).

Interestingly the same bursting response is not present in the repulsive ($g_{\mathrm{M,S}} < 0$) regime. Instead for parameter differences such that $\frac{\epsilon_{\mathrm{M}}}{\epsilon_{\mathrm{S}}} < 0.1$ one finds the usual anti-phase synchrony with the exception that firing patterns of the form

$$M \text{ Firings of the master cell} : N \text{ Firings of the save cell}, \qquad \text{such that } M < N$$

are readily found. Examples of which are shown in figure 3.47

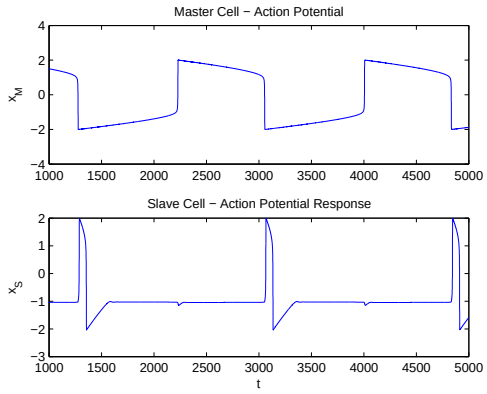

(a) Action potential response with $g_{\mathrm{M,S}} = 0.01$

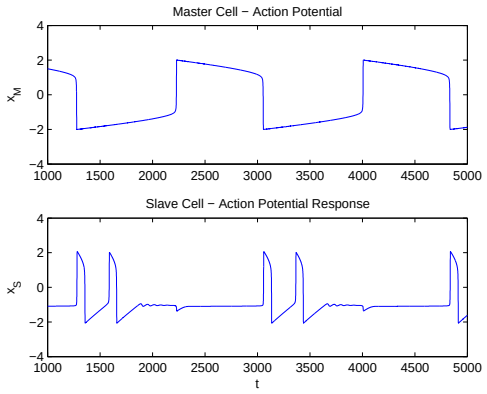

(b) Action potential response with $g_{\mathrm{M,S}} = 0.05$

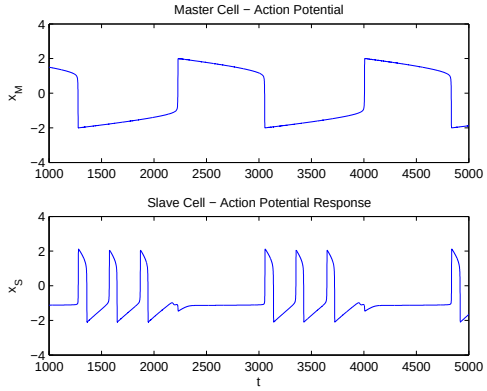

(c) Action potential response with $g_{\mathrm{M,S}} = 0.08$

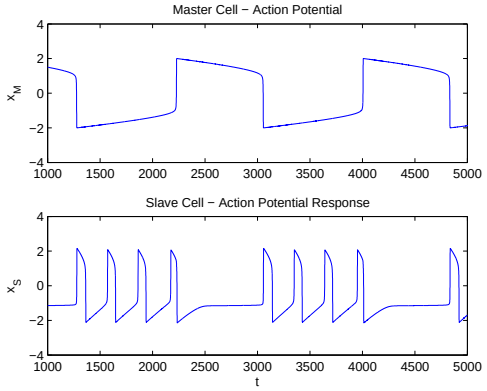

(d) Action potential response with $g_{\mathrm{M,S}} = 0.1$

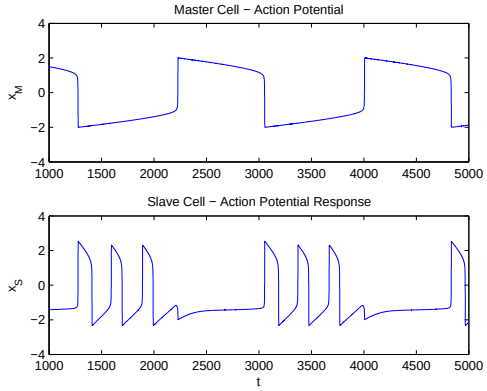

(e) Action potential response with $g_{\mathrm{M,S}} = 0.35$

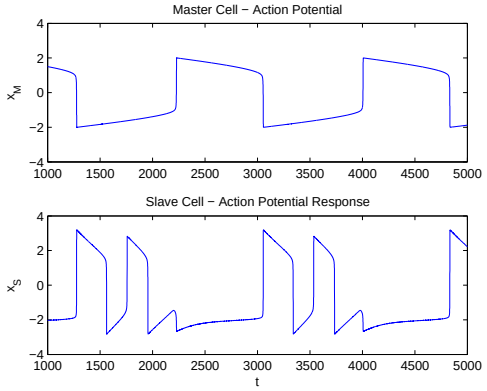

(f) Action potential response with $g_{\mathrm{M,S}} = 1$

Figure 3.47: Multiple action potential responses in the phase repulsive FHN system. Parameters are $a_M = 0.1$, $a_S = 0.7$, $b_M = b_S = 0.5$, $\epsilon_M = 0.001$, $\epsilon_S = 0.01$ and the repulsive coupling strengths indicated in the sub figure captions.

3.8 Chapter Summary

A summary of the results concerning synchronisation of FHN systems is here presented.

- A system of n FHN cells are electrically coupled (gap-junction like coupling), the model taking the form

$$\dot{x_i} = x_i - x_i^3/3 - y_i + \sum_{i \neq j, j=1}^{n} g_{i,j}(x_i - x_j), \qquad \dot{y_i} = \epsilon_i(x_i + a_i - b_i y_i)$$

  where $i, j \in [1, n] \subset \mathbb{N}$ and $g_{i,j}$ is the coupling strength imposed on cell i. The coupling imposed on cell i's voltage like variable and is dependent on the "potential difference" between cell i and cell j, i.e. $(x_i - x_j)$.

- Two electrically coupled cells with parameters $\epsilon_1 = \epsilon_2 = \epsilon$, $a_1 = a_2 = a$, $b_1 = b_2 = b$ and inhomogeneous coupling strengths is analytically shown to fall into a state of imperfect complete synchrony provided

$$\frac{1}{2} + g_{2,1} + g_{1,2} + \epsilon\left(\frac{1}{2} - b\right) < 0$$

- An appropriate definition for the phase, ϕ, of a coupled FHN oscillator is introduced in terms of the *Hilbert Transform*, a technique taken from the field of Engineering, namely signal processing. Furthermore an order parameter ρ and a collective phase ψ for N FHN oscillators is defined as

$$\rho(t)e^{i\psi(t)} = \frac{1}{N}\sum_{i=1}^{N} e^{i\phi_i(t)}$$

- On variation of the coupling strength between two electrically coupled FHN cells it is shown that the phase transition from a synchronous state to an asynchronous state posses hysteric properties.

- Semi-analytical methods are used to show that a system of n identical FHN systems (electrically coupled to one another inhomogeneously) can be syncrhonised to another system of n identical FHN cells (with a different set of intracellular electrically coupling strengths) by means of a nonlinear control scheme.

- The Arnold tongues for a sinusoidally forced FHN system are numerically explored and discussed. It is also shown that the $m : n$ firing response represented by the Arnold tongues can be found as an emergent property natural to a master-slave system of FHN systems without forcing.

Chapter 4

Emergent Chaos in Coupled FHN systems.

4.1 Chaos in biological systems

The role of chaos in neural systems is not currently fully understood however it has been hypothesised since the 1980s that cognitive functions depend on them, such as those involved in olfactory system, perception and more generally as a ground state for the neural perceptual apparatus [161]. Intensive studies have been conducted both experimentally and theoretically into the presence of chaotic behaviour in the brain, with experimental findings proving to be difficult to produce though present [97]. The primary difficulties with finding chaos experimentally are due to the level of noise associated with measurements concerning neural activity. The debate on the presence of chaos vs measurement noise in the brain is still an active one, leading to much work concerning measures of different types of complexity found in neural dynamics, the reader is referred to [60] and references therein for details.

Cardiac systems are more amenable in the detection of chaos, in the form of heart rate variability (HRV). Interestingly it has been shown that patients with a lower HRV are more susceptible to cardiac arrhythmias [105]. There are a multitude of tools that allow clinical physicians and researchers to study HRV, with comparative studies having being conducted in transplant patients [94], however there are discrepancies between the various measures of chaos; correlation dimension, return maps and Lyapunov exponents can give rise to conflicting results when looking at chaotic models of HRV [185] suggesting that there are significant difficulties. Investigation of nonlinear dynamical behaviour, inclusive of chaos, in cardiac systems remains active amongst theorists investigating the mechanism of the different arrhythmias of the heart, a review of which can be found in [31]. There

is a focus on finding new methods of analysing the risk a patient has of suffering from arrhythmias such as sudden cardiac death [64] and finding a means to implement findings in a clinical setting, though difficult [66].

4.2 Chapter Objective and Model Outline

The focus of this chapter is in the emergence of chaotic dynamics due to communication between nonchaotic subunits, without external forces. Chaotic firing patterns have been observed in experiments conducted on bursting neurons [97], there are a number of models that can be used in order to study this behaviour from mappings such as those due to Aihara [4]

$$y(t+1) = ky(t) - \alpha f(y(t)) + a$$

where for example the function $f(y(t))$ is a chaotic map such as the logistic function

$$f(y(t)) = \frac{1}{1+\exp(-y(t))/\epsilon}$$

and k, α, a are parameters known as the decay factor, scaling factor of refractoriness, and the external current respectively.

Sets of ODEs can produce inherent bursting behaviour, such as those found in the Hindmarsh-Rose (HR) model [76] of a bursting neuron

$$\begin{aligned}
\dot{x} &= y + ax^2 - x^3 - z + I \\
\dot{y} &= 1 - bx^2 - y \\
\dot{z} &= r(s(x - x_r) - z)
\end{aligned}$$

where the parameters a, b, r are related to ion channel kinetics, I is the external current and s and x_r are two further parameters that can be varied.
Unlike the 3-dimensional HR model the FHN system of equations can not admit chaotic solutions unless acted upon by an external force. This being due to the Poincare-Bendixon theorem the 2-dimensional set of ODEs making up the FHN system can not give rise to a strange attractor. Thus the FHN system has no intrinsic means of producing chaotic dynamics. By coupling FHN systems together one produces a system (with dimension greater than 3) which may admit chaotic dynamics. Such chaotic solutions are due to the passage of information between the constituent FHN systems. Making chaos an emergent

phenomenon that is directly consequent on the cells interacting with one another.

The objective of this chapter are to show

- Chaos is present in attractive/repulsive/mixed electrically (gap junction - like) coupled FHN systems.
- Chaos is present in chemically coupled (synapse-like) coupled FHN systems.
- The chaotic solutions can be found in both homogenous and inhomogenous parameter regimes within parameter regimes that maintain the integrity of biophysical interpretation.

Within the literature chaos in Fitzhugh-Nagumo systems has previously been reported. These reports are typically of chaos found when FHN cells are forced by an external current [141, 121]. Choas in couple FHN systems has also been found if one introduces time variation in gap junction conduction properties between couple cells [145]. Studies have also been conducted on the control of space-clamped chaotic FHN systems [190].

Chaotic firing patterns in FHN cells have also found application in robotic AI, in [8] the authors find that chaotic FHN cells can be used to produce a 'dancing' response in robots to music stimulus.

Most relevant to the following work are the chaotic results reported in [59], where the authors successfully find chaotic parameters in an electrically coupled system of FHN cells without the use of a time varying current. The authors report chaos for a system of homogenous FHN cells which show a diffusion like coupling term and find that the chaotic solutions integrity is maintained even with increasing system size. Unlike the work in [59] the aim here is to show that chaotic solutions in coupled FHN cells is possible in homogenous and inhomogenous systems be they electrically coupled in an attractive, repulsive or mixed manor, or if they are coupled with a synaptic-like (chemical) coupling term.

4.2.1 The bidirectionally Electrically coupled FHN system.

In the model neurons are coupled together bidirectional with a simple linear *diffusive coupling* term. Let $\mathbf{N}$ be a set of nodes in our graph with $i, j \in \mathbf{N}$ and $\{i, j\} \in \mathbf{E}$ be the set of directed edges in the graph

$$\begin{aligned} \dot{x_i} &= x_i - \frac{1}{3}x_i^3 - y_i + \sum_{j||\{i,j\}\in\mathbf{E}} g_{ij}\left(x_i - x_j\right), \\ \dot{y_i} &= \epsilon_i(x_i + a_i - b_i y_i) \end{aligned} \tag{4.2.1.1}$$

The g_{ij} are the coupling strengths between coupled neurons in the graph. If $g_{ij} > 0$ then node i is repulsively dependent on the voltage difference between itself and node j, and increase/decrease in the voltage of node j causes a decrease/increase in voltage in node i, this will be refereed to as 'phase repulsive' coupling. For $g_{ij} < 0$ node i is attractively dependent on the voltage difference between itself and node j, an increase/decrease in the voltage of node j causes an increase/decrease of voltage in node i, this will be referred to as 'phase attractive' coupling. This model has been explored in previous chapters showing complex rhythmic behaviour, here the emphasis is placed on chaotic behaviour.

4.2.2 The chemically coupled FHN system

Synaptic coupling between neurons involves transmission of electrical signals through chemical transmitters. Synaptic connections are not direct electrical connections between neurons, which is the case with gap-junctions. The chemical synapse behaves as a *pulse* coupling between the neurons which has a timescale of it's own. The model used can be found adapted from [102, 44, 189]

$$\begin{aligned} \dot{x_i} &= x_i - \frac{1}{3}x_i^3 - y_i + \sum_{j||\{i,j\}\in\mathbf{E}} g_{ij}s_j\left(x_i - v\mathrm{Syn}_i\right), \\ \dot{y_i} &= \epsilon_i(x_i + a_i - b_i y_i) \\ \dot{s_i} &= \frac{1}{\epsilon_i}\beta_i\alpha(x_i)(1 - s_i) - \frac{s_i}{\tau\mathrm{Syn}} \\ \alpha(x_i) &= \frac{\alpha_0}{1 + \exp(-x_i/V_{\mathrm{shp}})} \end{aligned}$$

where g is now the adjacency matrix holding the maximal synaptic conductance for each edge of the graph, τSyn is the time scale over which the synapse is active, $v\mathrm{Syn}_i$ is the synaptic reverse potential and α is the activation rate. $s \in [0,1] \subset \mathbb{R}$ is the synaptic coupling variable. The synaptic coupling equation can be reduced [189] to

$$\dot{s_i} = \beta\mathcal{H}(x_i)(1 - s_i) - \delta\epsilon_i s_i$$

where $\mathcal{H}$ is the heaviside function and the parameters β and δ are the activation and decay rate of the synapse respectively.

4.2.3 Finding and Characterising Chaos

In order to find parameters which produce chaotic dynamics it is essential to firstly have a measure of chaos in the system. A system is said to be chaotic if it

- Exhibits exponential sensitivity to initial conditions.
- Forms a dense set of periodic orbits in its phase space.

One typically examines the largest *Lyapunov exponent*, denoted Λ, of the system under study taking a **positive Lyapnuov exponent as being a signature of chaos**.

Numerical calculation of Lyapunov exponents

- The Largest Lyapunov Exponent - using secondary trajectories.
- Wolf Algorithm - to calculate the Lyapunov Spectrum.

Numerical Calculation of the Largest Lyapunov Exponent .

Given a set of coupled ODEs

$$\dot{\mathbf{x}} = f(\mathbf{x}, \alpha)$$

where $\mathbf{x} \in \mathbb{R}^n$ are the system variables and $\alpha \in \mathbb{R}^m$ are the systems parameters. The maximum Lyapunov exponent λ_M (shortened to λ) is a measurement of the *rate of separation* of two trajectories in phase space that are initially infinitesimally separated from one another.

Given an initial point $\mathbf{x}_0$ and a neighboring point $\mathbf{x}_1$ and denoting the initial separation as

$$d_0 = |\mathbf{x}_1 - \mathbf{x}_0|$$

and the separation after a time t is denoted

$$d_t = |\mathbf{x}_1(t) - \mathbf{x}_0(t)|$$

the maximum Lyapunov exponent is defined as

$$\lambda = \lim_{t \to 0} \lim_{d_0 \to 0} \frac{1}{t} \ln \left(\frac{d_t}{d_0} \right)$$

The Lyapunov exponent measures the divergence of nearby trajectories as

$$d_t \approx \exp(\lambda t) d_0$$

The algorithm is as follows

1. Solve the ode system with initial condition $\mathbf{x}_0$ allowing the trajectory to reach the attractor.
2. Take the point that is on the attractor and define this point as $\mathbf{x}_0$.
3. Pick a neighboring point in phase space which is a small distance away (ensuring the distance is larger than the accuracy of the machine) label it $\mathbf{x}_1$.
4. Track the orbits originating from $\mathbf{x}_0$ and $\mathbf{x}_1$ simultaneously in time for a time step δt.
5. Compute the distance between the two orbits at this time.
6. Store the value of $\frac{1}{\delta t} \ln\left(\frac{d_1}{d_0}\right)$.
7. Computer the running average of $\frac{1}{\delta t} \ln\left(\frac{d_1}{d_0}\right)$
8. Adjust the secondary orbit so that it again is a distance d_0 from the primary orbit which is now at $\mathbf{x}_0(\delta t)$. This adjustment is made along the line of separation between $\mathbf{x}_0(\delta t)$ and $\mathbf{x}_1(\delta t)$.
9. Redefine $\mathbf{x}_0(\delta t) \to \mathbf{x}_0$ and $\mathbf{x}_1(\delta t) \to \mathbf{x}_1$, repeat 4 to 8 until the running average stabilises. Typically over a time $T >> \delta t$.

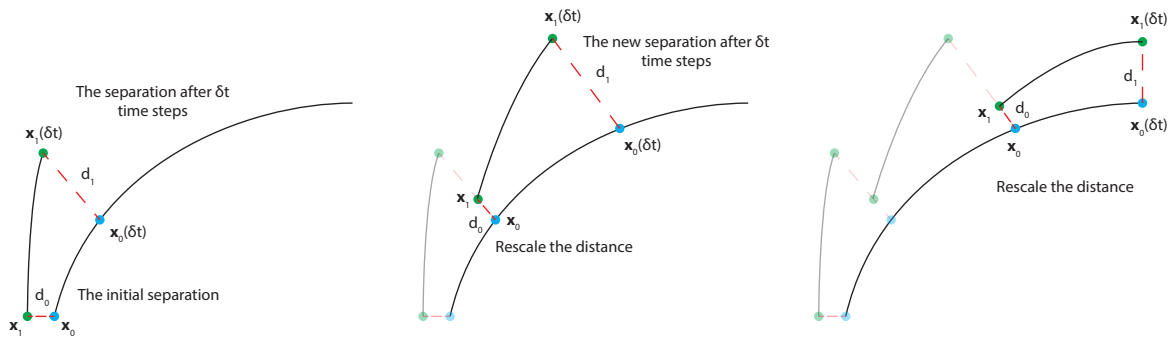

Figure 4.1: Rescaling the secondary trajectory after every δt time steps.

Numerical Calculation of the Lyapunov Spectrum .

For an $n-$dimensional system there are in fact n Lyapunov exponents. To see this it is useful to consider the evolution of an $n-$sphere of initial conditions perturbed from a point $\mathbf{x}_0$ on the chaotic attractor. During the time evolution of the sphere of initial conditions the sphere is stretched and compressed into an $n-$dimensional ellipsoid. Letting

$$d_k(t), \quad k = 1, 2, \ldots, n$$

denote the length of the k^{th} principal axis of the ellipsoid at time t, the expansion will follow

$$d_k(t) \approx d_k(0) \exp(\lambda_k t)$$

where λ_k is a Lyapunov exponent.

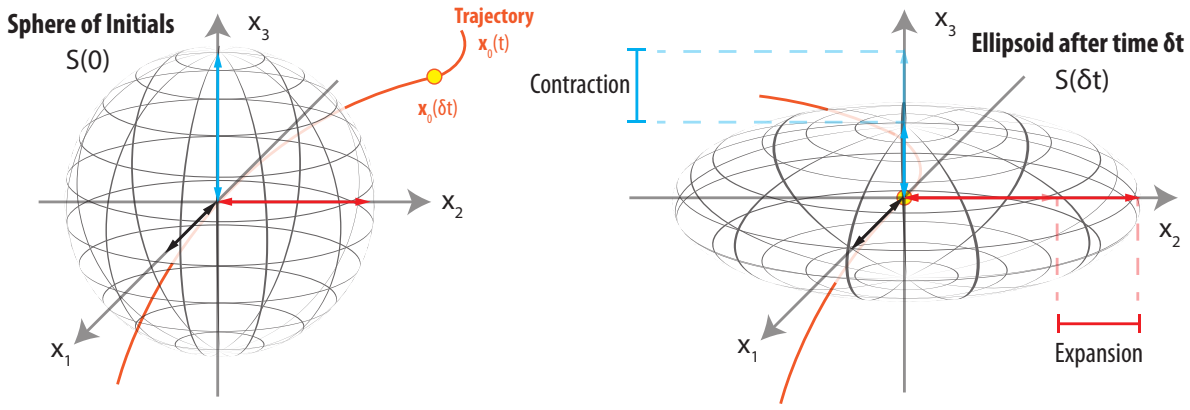

Figure 4.2: Evolution from a sphere to an ellipsoid. x_1 is in the tangential direction of the flow, with zero expansion of contraction (zero Lyapunov exponent). x_2 is an expansion direction (positive Lyapunov exponent). x_3 is a contraction direction (negative Lyapunov exponent).

The collection of Lyapunov exponents λ_k yields the *Lyapunov spectrum* for the system

$$\Lambda = [\lambda_1, \lambda_2, \ldots, \lambda_n]$$

Computation of Lyapunov spectra was conducted using Wolf's algorithm [200] with a Gram-Schmidt orthonormalisation process. Wolf's algorithm involves solving the ode

system[1]

$$\mathbf{x} = f(\mathbf{x}, \alpha)$$

and its associated linearised system, often referred to as the tangent system, given by

$$\mathbf{T} = J(\mathbf{x}, \alpha)\mathbf{T}$$

where $\mathbf{T}$ is an $n-$dimensional vector and J is the $n \times n$ Jacobian matrix associated with $f(\mathbf{x}, \alpha)$. The perturbation from the trajectory on the attractor is measured by following the evolution of $n-$orthogonal vectors which evolve in time according to the linearised system.

A key step to find the spectrum is to reorthogonalise the $n-$orthogonal vectors after every δt time steps where $\delta t < |\frac{1}{\lambda_{max}}|$. Without a reothogonalisation all of vectors evolving with respect to the linearised system will eventually move to point in the direction of greatest increase, leaving only an estimate of the largest Lyapunov exponent for the system. The reorthogonalisation process is conducted as follows

1. Record the length of the first ($k = 1$) of the $n-$orthogonal vectors (this will be the direction of greatest divergence).
2. By computing the inner product between the $k = 1$ vector and the remaining $k = 2, \ldots, n$ vectors: remove the component of the $k = 1$ vector from all of the other vectors. This leaves only the second largest divergence direction for the remaining vectors to converge towards.
3. Repeat this process removing the $k = 2$ component from the $k = 3, \ldots, n$ vectors, recording the length of the $k = 2$ vector.
4. Continue this process of removing the components of the vectors found higher up in the hierarchy from all the n orthogonal vectors.
5. Record the running sum of the log of the lengths of each of the orthogonal vectors.
6. Renormalise the vectors.

The orthonormal set of vectors

$$\mathbf{e}_1, \mathbf{e}_2, \ldots, \mathbf{e}_n$$

[1]where $\mathbf{x} \in \mathbb{R}^n$ is the state space vector holding the $n-$dimensial system's variables α is a vector holding the system parameters.

initially taken to be the standard basis for $\mathbb{R}^n$ evolve according to the linearised system. The Gram-Schmidt process involves taking

$$\mathbf{u}_1 = \mathbf{e}_1(\delta t), \qquad \text{The vector } \mathbf{e}_k \text{ after } \delta t \text{ time steps.}$$

and then,

$$\mathbf{u}_k = \mathbf{e}_k(\delta t) - \sum_{i=1}^{k-1} \frac{\langle \mathbf{u}_i, \mathbf{e}_k(\delta t) \rangle}{\langle \mathbf{u}_i, \mathbf{u}_i \rangle} \mathbf{u}_i.$$

Finally renormalisation all the vectors simply involves

$$\mathbf{e}_k = \frac{\mathbf{u}_k}{|\mathbf{u}_k, \mathbf{u}_k|}$$

and the vectors are ready for the next step of integration.
This process of tracking orbits and the expansions of orthogonal vectors in the linearised system is continued until the mean value of the computed λ_k no longer varies. The resulting spectrum will consists of the Lyapunov exponents in decreasing order of size one of which being zero[2].

Finding Chaotic parameters

One can treat finding chaotic parameters in a given system of differential equations as an optimization problem, where one is trying to maximise the systems largest Lyapunov exponent. Here the method of *simulated annealing* is briefly described.

Annealing is a concept taken from thermodynamics and is used to change the properties of metals through a process of heating and cooling. Annealing with solids occurs when a solid is heated and allowed to slowly cool until it reaches its minimum lattice energy state, leaving a regular lattice which is free from defects and is associated with superior structural integrity compared to an untreated solid. A system in thermal equilibrium at a temperature T has its energy distributed probalistically according to the Boltzmann distribution

$$P(E) = \exp\left(-\frac{E}{kT}\right).$$

[2]The zero exponent is the exponent derived from the orthonormal vector which lies in the direction of the trajectory on the attractor. As such there will be no relative divergence from the trajectory in this direction. This zero exponent must appear in ODE systems whose exponents are calculated in this manner, however Poincare section methods would not have such a zero exponent, see[24]. This zero exponent can also serve as an estimate to the error in computing the spectrum.

This probability suggests that at large values of T the system has a uniform probability of being at any given energy state. However at smaller values of T it only has a small probability of being at a higher energy state. Simulated annealing (SA) works upon this principal.

Conventional global optimisation algorithms work in the following manner; given an objective function $Y(\mathbf{x})$ that one wishes to minimize (maximize) given control of the input vector $\mathbf{x}$ then one accepts a change to the input vector $\mathbf{x}$

$$\begin{cases} \mathbf{x}^0 \to \mathbf{x}^1, & \text{Accept this change} \\ Y^0 \to Y^1, & \text{if } Y^0 > Y^1, \qquad (Y^0 < Y^1) \end{cases}$$

Under SA the above criteria is also adhered to like most conventional optimisation algorithms. SA however has a further acceptance/rejection policy. If one finds that

$$\begin{cases} \mathbf{x}^0 \to \mathbf{x}^1, & \text{leads to} \\ Y^0 \to Y^1, & \text{such that } Y^0 < Y^1, \qquad (Y^0 > Y^1) \end{cases}$$

then the change from $\mathbf{x}^0 \to \mathbf{x}^1$ should *not be instantly rejected*, instead it should be rejected with a probability, given by a Boltzman distribution

$$P(\Delta Y) = \exp\left(-\frac{\Delta Y}{\overline{Y}}\right)$$

Where the "change in energy" is analogous to the *change in the objective function*, "Boltzmann's constant" is taken to be unity and the "temperature" is taken to be the *average value of the objective function* at a number of points[3]. This probabilistic approach to optimisation makes SA a stochastic optimisation algorithm.

The change in the input parameters $\mathbf{x}$ from

$$\mathbf{x}^0 \to \mathbf{x}^1$$

is conducted with a random walk. The random perturbation of $\mathbf{x}^0$ depends on the parameter constraints for the components of the input parameters which are the components of $\mathbf{x}$. Typically one takes the midpoint of the interval which one wants to constrain the

[3]Before beginning the simulated annealing process one must have an initial temperature for the system. This is found by taking a number of arbitrary values for $\mathbf{x}$ within the parameter constraints that are desired, evaluating the objective function at these arbitrary $\mathbf{x}_i$ and taking their mean

parameter within and use this as the mean for a normal distribution[4]. One performs this same sampling for every parameter which makes up the input vector $\mathbf{x}$ in order to choose a new value $\mathbf{x}^1$.

If the change from $\mathbf{x}^0 \to \mathbf{x}^1$ minimises (maximises) the objective function it is accepted, otherwise one produces a random number between $R \in [0,1] \subset \mathbb{R}$ and accept the change $\mathbf{x}^0 \to \mathbf{x}^1$ if

$$R \leq \exp\left(-\frac{\Delta Y}{\overline{Y}}\right)$$

After this initial iteration and having made a move from $\mathbf{x}^0 \to \mathbf{x}^1$ one must perform a *cooling* of the system. Thus we no longer define the temperature as $\overline{Y}$ but introduce the cooling

$$T \to \alpha T$$

where $\alpha \in (0.8, 0.99) \subset \mathbb{R}$.

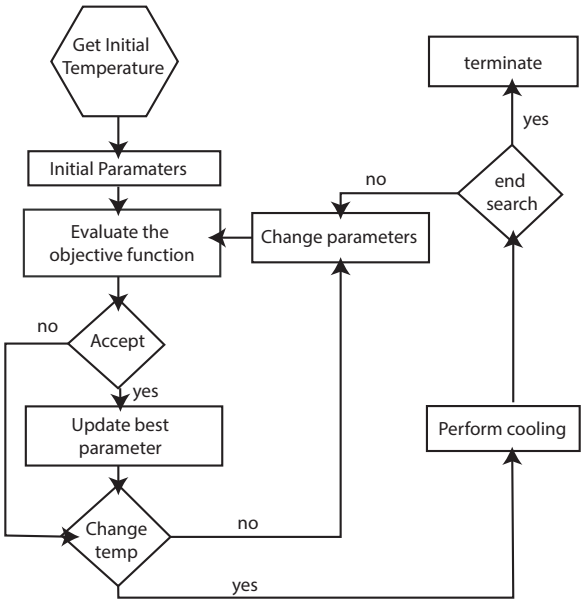

Figure 4.3: Flow chart describing the SA algorithm

[4]The standard deviation of the normal distribution is chosen such that 99% (3σ) of all random sample values from the distribution will lie between the constraints for the parameter of interest

4.2.4 Chaos in Electrically Coupled FHN Cells

In this section chaos is reported in, attractive, repulsive and mixed $N = 2$ and $N = 3$ electrically coupled FHN cells. The parameters, here and in all the subsequent cases, which lead to chaotic solutions are found using a simulated annealing optimisation algorithm. Furthermore each of the parameters are tested around a local neighbourhood about the reported values and the following results are found to be representative of those locally perturbed cases.

The two cell electrically coupled system is given by

$$\begin{aligned}
\dot{x_1} &= x_1 - \frac{1}{3}x_1^3 - y_1 + g_{12}\left(x_1 - x_2\right), \\
\dot{x_2} &= x_2 - \frac{1}{3}x_2^3 - y_2 + g_{21}\left(x_2 - x_1\right), \\
\dot{y_1} &= \epsilon_1(x_1 + a_1 - b_1 y_1) \\
\dot{y_2} &= \epsilon_2(x_2 + a_2 - b_2 y_2).
\end{aligned} \tag{4.2.4.1}$$

The coupling strength for these systems is restrained to

$$-1 \leq g_{ij} \leq 1, \quad \text{with} \quad g_{ii} = 0.$$

The case where $|g_{ij}| = 1$ implies full transmission ($g_{ij} = -1$ being) of an action potentials from cell j and i. Furthermore the timescale parameter is taken to be $\epsilon = 0.1$. The ODE system becomes progressively stiffer as $\epsilon \to 0$, making error free (numerical) integration of the ODE system increasingly difficult.

The three cell electrically coupled system

$$\begin{aligned}
\dot{x_1} &= x_1 - \frac{1}{3}x_1^3 - y_1 + g_{12}\left(x_1 - x_2\right) + g_{13}\left(x_1 - x_3\right) \\
\dot{x_2} &= x_2 - \frac{1}{3}x_2^3 - y_2 + g_{21}\left(x_2 - x_1\right) + g_{23}\left(x_2 - x_3\right), \\
\dot{x_3} &= x_3 - \frac{1}{3}x_2^3 - y_3 + g_{31}\left(x_3 - x_1\right) + g_{32}\left(x_3 - x_2\right), \\
\dot{y_1} &= \epsilon_1(x_1 + a_1 - b_1 y_1) \\
\dot{y_2} &= \epsilon_2(x_2 + a_2 - b_2 y_2) \\
\dot{y_3} &= \epsilon_3(x_3 + a_3 - b_3 y_3).
\end{aligned} \tag{4.2.4.2}$$

Phase Repulsive Electrical Coupling

Repulsive coupling between electrically coupled FHN cells effectively behaves as a means of periodically kicking a cell. Repulsive coupling also has a tendency to push cells into a state of antiphase synchrony, where the peak of one cell's action potential response coincides with the trough of another cell's action potential. In such systems there is a spring like tension between the cells. The further the action potentials are from one another the stronger the repulsion, the cells however are bounded in the period of time they are capable of producing an action potential response. After producing an action potential the system must return to a state of quiescence before becoming capable of

producing another action potential response. During this period of quiescence the cell is in a refractory state making it unable to respond to stimulus. Here we report chaotic dynamics for small systems (2 and 3 neurons) that are phase repulsively coupled.

For repulsive coupling we require

$$g_{ij} > 0 \quad \text{and} \quad g_{ii} = 0.$$

Chaos in homogenous cells with phase repulsive coupling

System Label	System Parameters
xxxxx	$g = \begin{pmatrix} g_{11} & g_{12} \\ g_{22} & g_{21} \end{pmatrix}$ $a = [a_1, a_2]$ $b = [b_1, b_2]$ $\epsilon = [\epsilon_1, \epsilon_2]$
E2HR1	$g = \begin{pmatrix} 0 & 1 \\ 1 & 0 \end{pmatrix}$ $a = [1.23, 1.23]$ $b = [0.06, 0.06]$ $\epsilon = [0.1, 0.1]$

Two homogenous FHN cells with electrically repulsive coupling strengths. The computed Lyapunov spectrum

$$\Lambda = \begin{pmatrix} 0.016 \\ 0.000 \\ -2.044 \\ -7.939 \end{pmatrix}$$

shows that there is a positive exponent in the system.

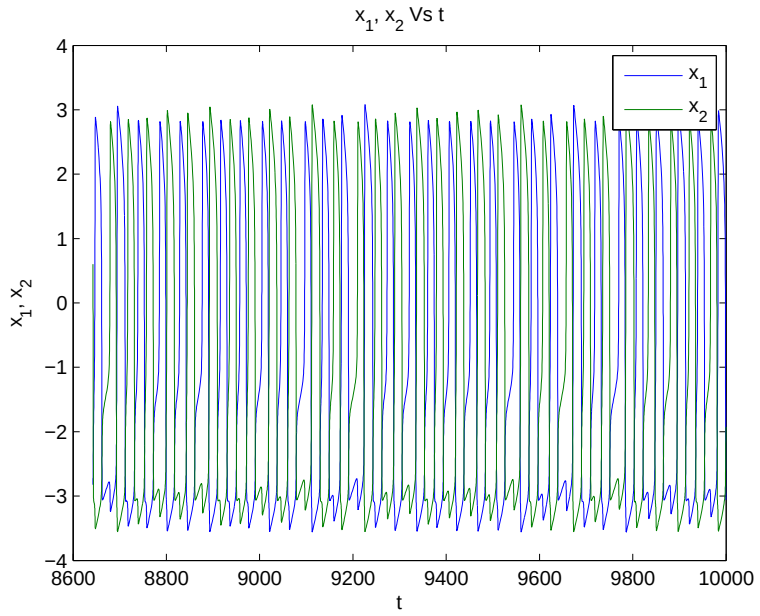

Figure 4.4: Voltage Time Series Plots of system E2HR1 undergoing chaotic dynamics.

Three homogenous FHN cells with electrically repulsive coupling strengths.

Lyapunov spectrum

System Label	**System Parameters**		$\Lambda =$
E3HR1	$g = \begin{pmatrix} 0 & 1 & 1 \\ 1 & 0 & 1 \\ 1 & 1 & 0 \end{pmatrix}$	$a = [0.2, 0.2, 0.2]$ $b = [0.2, 0.2, 0.2]$ $\epsilon = [0.1, 0.1, 0.1]$	$\begin{pmatrix} 0.009 \\ 0.000 \\ -0.025 \\ -1.471 \\ -7.750 \\ -10.516 \end{pmatrix}$

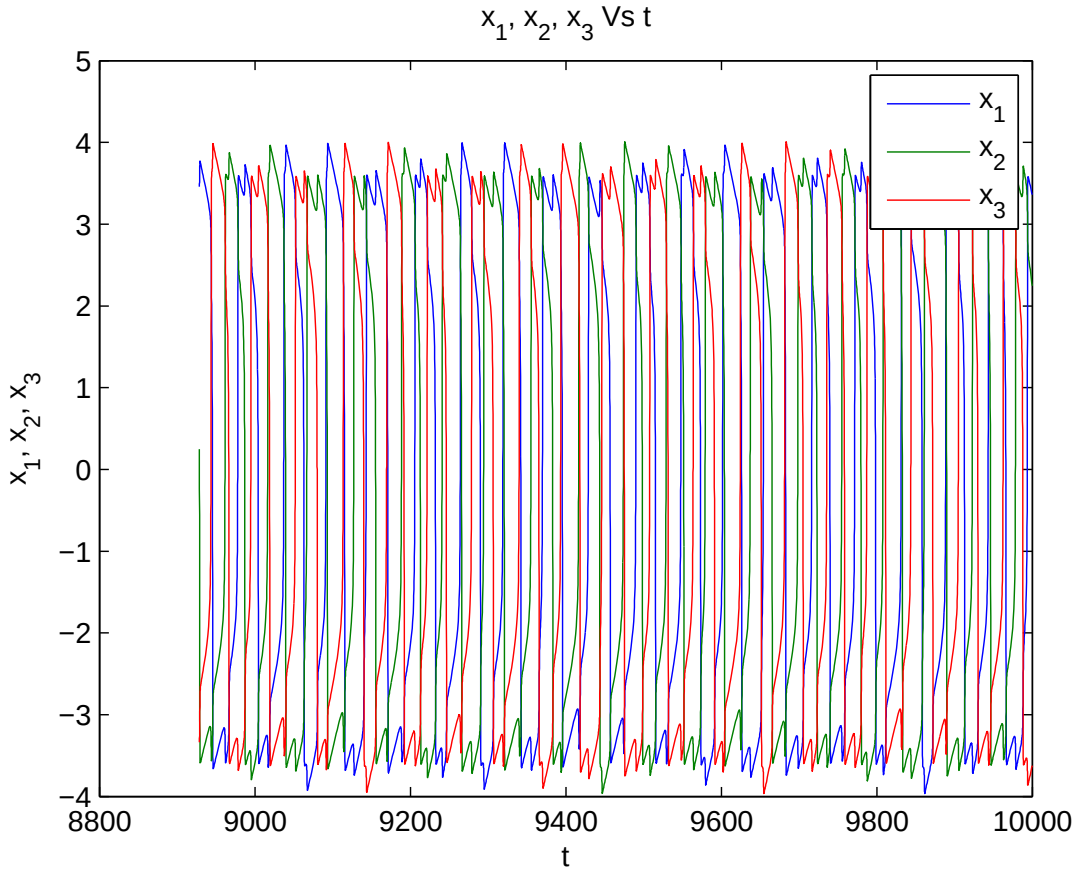

Figure 4.5: Voltage Time Series Plots of system E3HR1 undergoing chaotic dynamics.

Both systems shown (E2HR1 and E3HR1) above consist of completely homogenous neurons, that is for every pair of cells indexed i and j

$$a = a_i = a_j, \quad b = b_i = b_j, \quad \epsilon = \epsilon_i = \epsilon_j, \quad \text{and} \quad g = g_{ij} = g_{ji}$$

the only difference is in terms of the initial conditions given to each of the neurons. The voltage like variables time series in both cases shows that the system falls into an antiphase synchrony. The peak of one cell's action potential coincides with the trough of another.

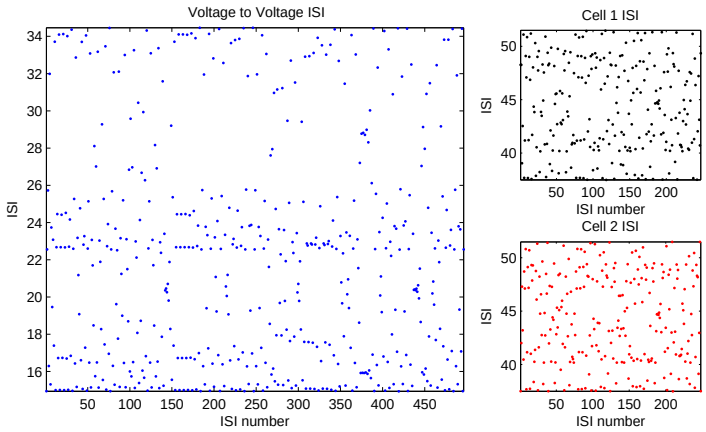

Figure 4.6: Inter spike intervals of E2HR1. Large figure shows the inter spike interval between both cells.

The chaotic process in these examples doesn't effect the order in which the cells fire however there is a marked variability in the inter-spike intervals. The inter-spike interval is one of the leading candidates by which the mechanism for information encoding[177] and processing is mediated in the brain [146, 157]. While HRV (Heart Rate Variability) has seen connections between depressive disorders[165], a possible indicator for the suitability of a candidate to undergo anesthesia before surgery [29] and a measure for recovery of patients suffering from arrhythmia [172].

Figures 4.6 and 4.7, show the the inter spike interval between the two cells in the E2HR1 system and the distribution of those spiking intervals respectively. The large figure shows the spiking intervals between consecutive spikes of both of the cells action potential time series' superimposed, while the smaller figures show the inters pike intervals for each of the individual cells.

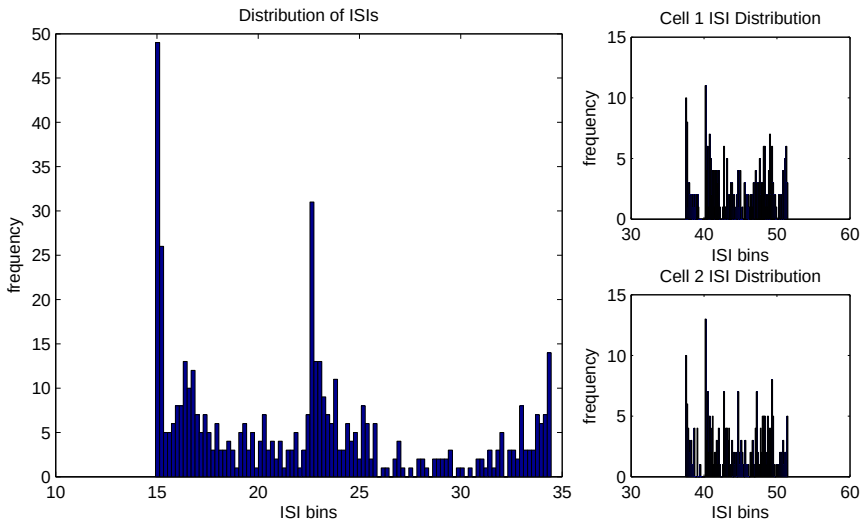

Figure 4.7: Distribution of inter spike intervals of E2HR1.

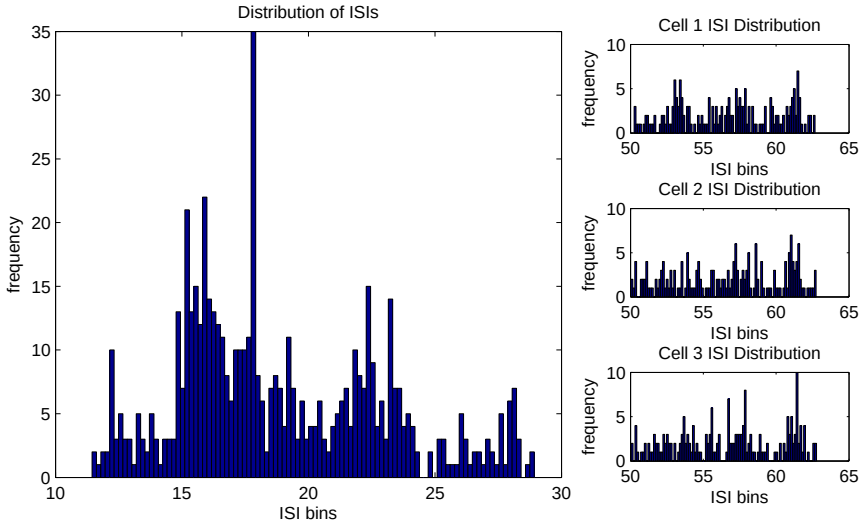

Figure 4.8: Distribution of inter spike intervals of E3HR1.

Phase Attractive Electrical Coupling

Attractive coupling between homogenous oscillators typically leads to in phase synchronised oscillations. Given two oscillators, A and B, an increase in A causes and increase in B while a decrease in A causes a decrease in B (the same influence is exerted by oscillator B on A when the oscillators are bidirectionally coupled). This push and pull dynamic often leads to both cells falling completely in line with each other. There is however obvious limitations to achieving synchrony when the oscillators are inhomogeneous. Two different oscillators are limited[5] by their own intrinsic dynamical behaviour and are in-

[5] An assumption here is that interactions are of similar magnitude to the intrinsic oscillatory behaviour of the oscillators themselves.

capable of producing *perfect* synchrony with one another. Here we show that even under the strict condition of homogeneity between FHN cells with attractive coupling to one another one can find dramatically chaotic behaviour emerging from the system.

The ODE systems are the same as those state in (4.2.4.1) and (4.2.4.1), examining attractive coupling implies

$$g_{ij} < 0 \quad g_{ii} = 0$$

while the homogeneity constraint is to take

$$a = a_i = a_j, \quad b = b_i = b_j, \quad \epsilon = \epsilon_i = \epsilon_j, \quad \text{and} \quad g = g_{ij} = g_{ji}$$

Chaos in homogenous cells with phase attractive coupling

System Label	**System Parameters**
E2HA1	$g = \begin{pmatrix} 0 & -0.6 \\ -0.6 & 0 \end{pmatrix}$ $a = [0, 0]$ $b = [-0.8, -0.8]$ $\epsilon = [0.1, 0.1]$

The computed Lyapunov spectrum

$$\Lambda = \begin{pmatrix} 0.0122 \\ 0.000 \\ -0.891 \\ -2.905 \end{pmatrix}$$

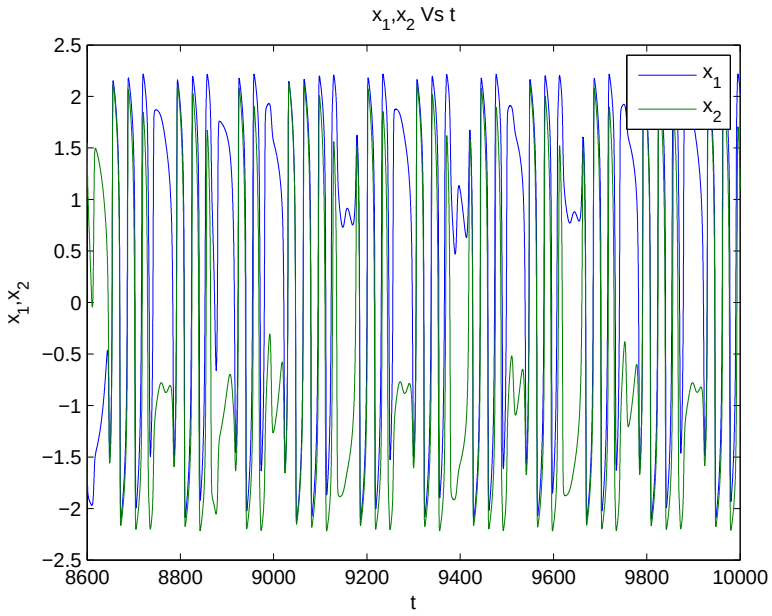

Figure 4.9: Voltage Time Series Plots of system E2HA1 undergoing chaotic dynamics.

Examining the inter spike intervals for this system using a Poincare section we have

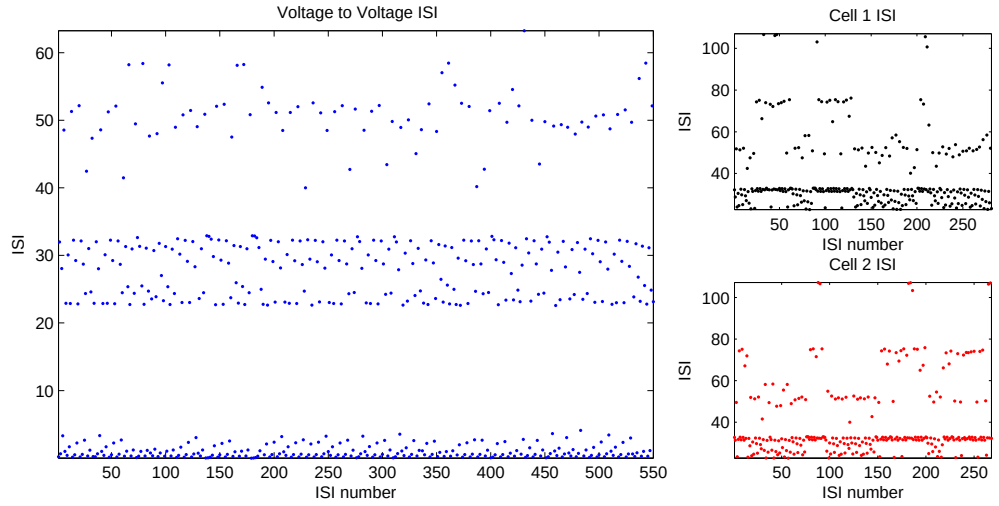

Figure 4.10: Inter spike intervals of E2HA1. Large figure shows the inter spike interval between both cells.

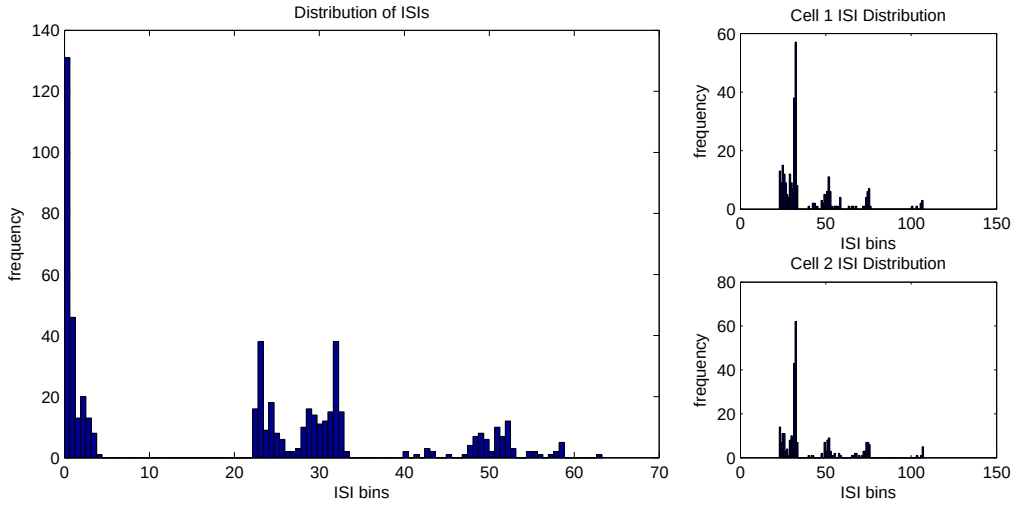

Figure 4.11: Distribution of inter spike intervals of E2HA1.

System Label	System Parameters		Lyapunov spectrum
E3HA1	$g = \begin{pmatrix} 0 & -1 & -1 \\ -1 & 0 & -1 \\ -1 & -1 & 0 \end{pmatrix}$	$a = [0, 0, 0]$ $b = [-1, -1, -1]$ $\epsilon = [0.1, 0.1, 0.1]$	$\Lambda = \begin{pmatrix} 0.013 \\ 0.005 \\ 0.000 \\ -0.572 \\ -2.253 \\ -3.374 \end{pmatrix}$

The presence of two positive Lyapunov exponents tells us that the system is *hyperchaotic*.

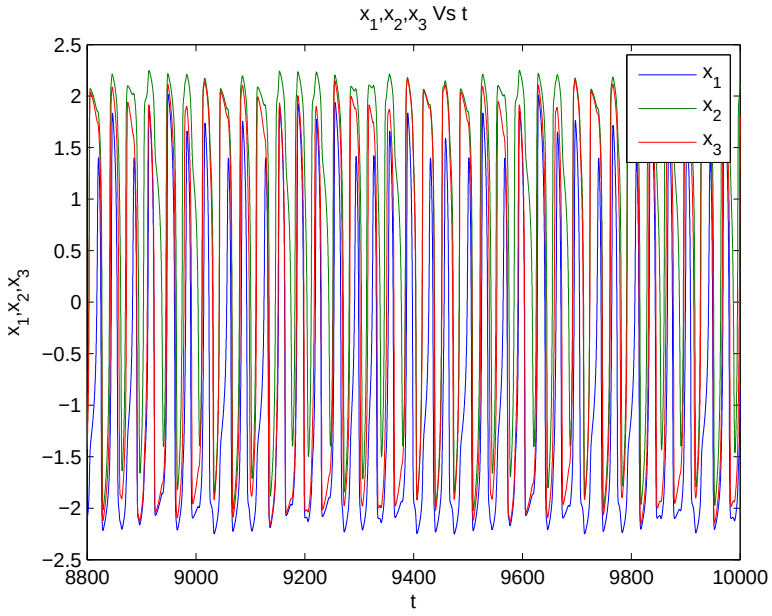

Figure 4.12: Voltage Time Series Plots of system E3HA1 undergoing chaotic dynamics.

Examining the inter spike intervals of the system we have Figure 4.13 and Figure 4.14.

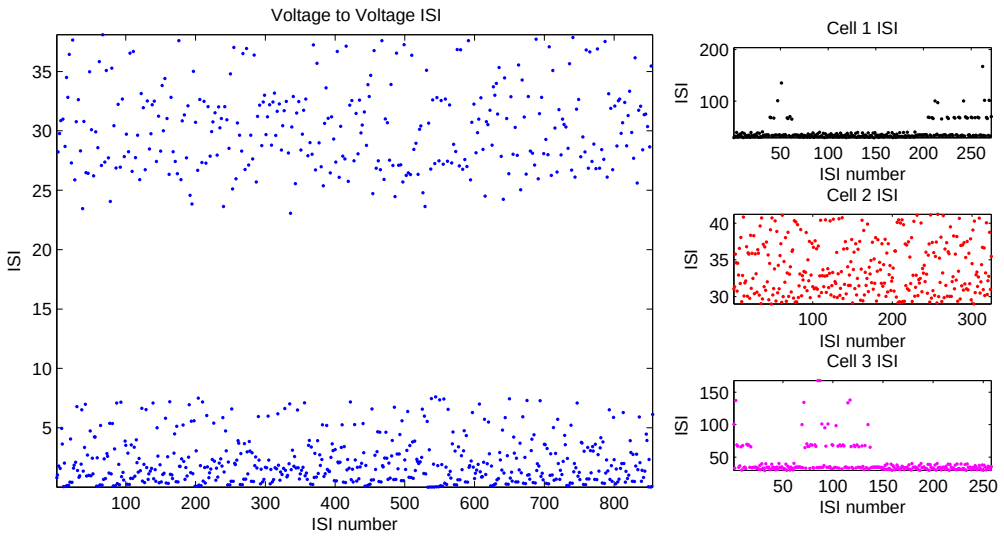

Figure 4.13: Inter spike intervals of E3HA1. Large figure shows the inter spike interval between three cells.

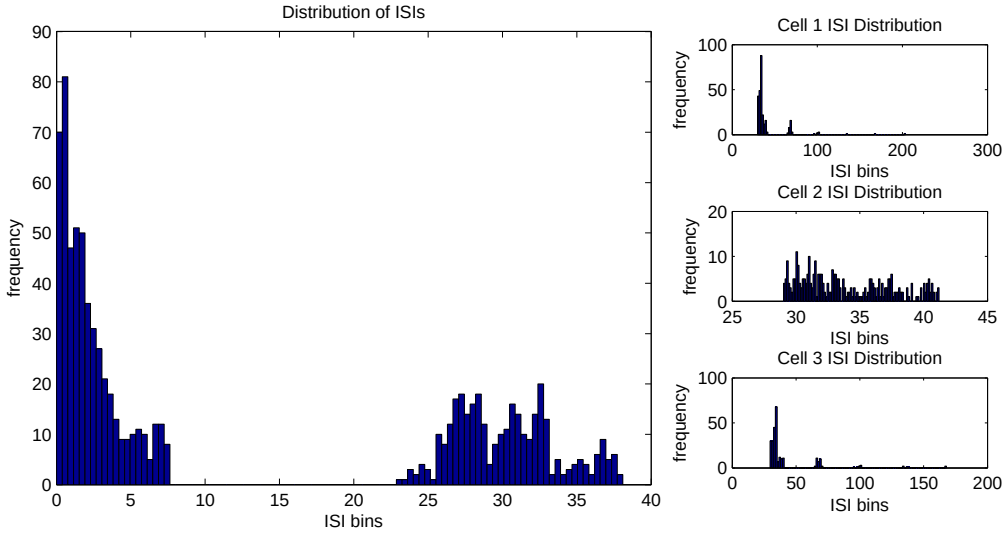

Figure 4.14: Distribution of inter spike intervals of E3HA1.

Mixed Electrical Coupling

Mixed coupling types introduces heterogeneity into the system. In such systems a number of cells are repulsively coupled to its neighbours while others are attractively coupled. This introduces a push pull dynamic where attractive cells are moving toward a synchronous state with it's neighbour and the repulsive cells are attempting to move to an anti-phase regime. The push pull dynamic is akin to the stretch-fold nature of a chaotic attractor making it less surprising that one finds chaos in such systems.

The restraint on systems (4.2.4.1) and (4.2.4.1), is

$$\text{sgn}(g_{ij}) \neq \text{sgn}(g_{nm}), \quad \text{for at least one set of } ij \text{ and } nm.$$

System Label	**System Parameters**		Lyapunov spectrum
E2IM1	$g = \begin{pmatrix} 0 & 1 \\ -0.2 & 0 \end{pmatrix}$	$a = [.7, .6]$ $b = [.7, .4]$ $\epsilon = [0.1, 0.1]$	$\Lambda = \begin{pmatrix} 0.022 \\ 0.000 \\ -0.196 \\ -1.018 \end{pmatrix}$

System Label	**System Parameters**		Lyapunov spectrum
E3IM1	$g = \begin{pmatrix} 0 & 0.1 & 0.7 \\ 0.15 & 0 & 1 \\ 0.21 & -0.29 & 0 \end{pmatrix}$	$a = [0, 0.53, 0.2]$ $b = [0.4, 0.17, 1]$ $\epsilon = [0.1, 0.1, 0.1]$	$\Lambda = \begin{pmatrix} 0.025 \\ 0.000 \\ -0.188 \\ -0.226 \\ -2.496 \\ -4.107 \end{pmatrix}$

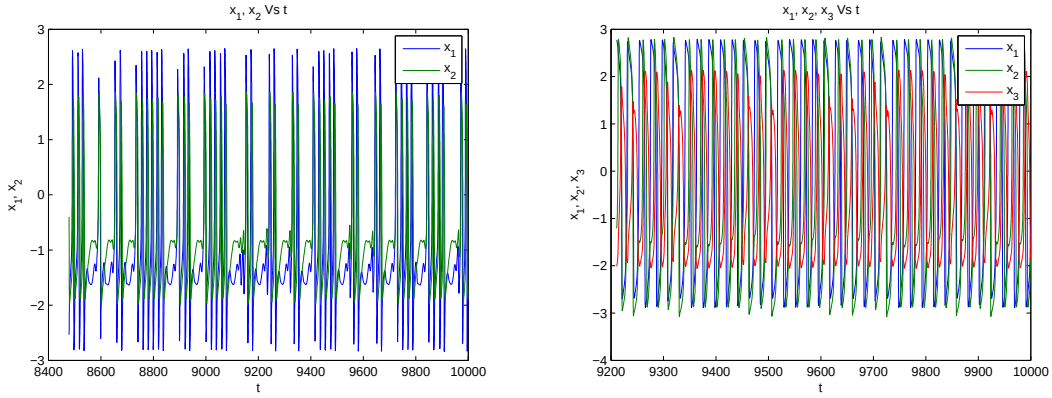

(a) E2IM1 Timeseries

(b) E3IM1 Timeseries

Figure 4.15: Voltage Time Series Plots of system E2IM1 and E31M1 undergoing chaotic dynamics.

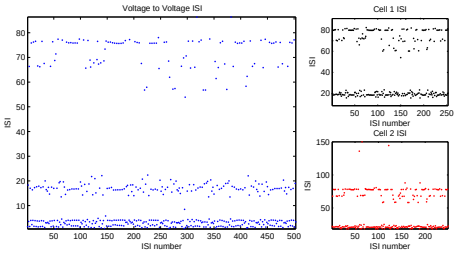

(a) E2IM1 Inter Spike Intervals.

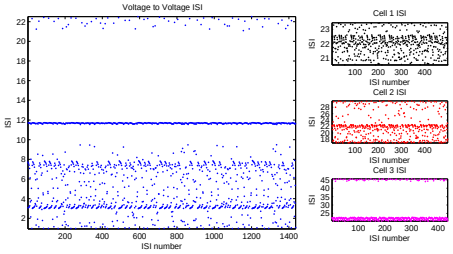

(b) E3IM1 Inter Spike Intervals.

Figure 4.16: Inter spike intervals of E2IM1 and E3IM1.

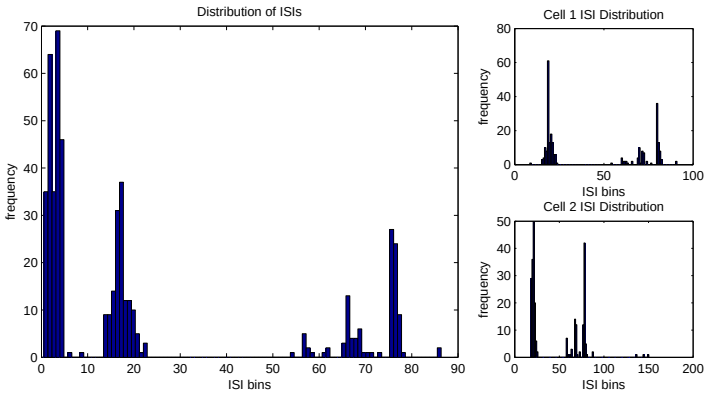

(a) Distribution of inter spike intervals of E2IM1.

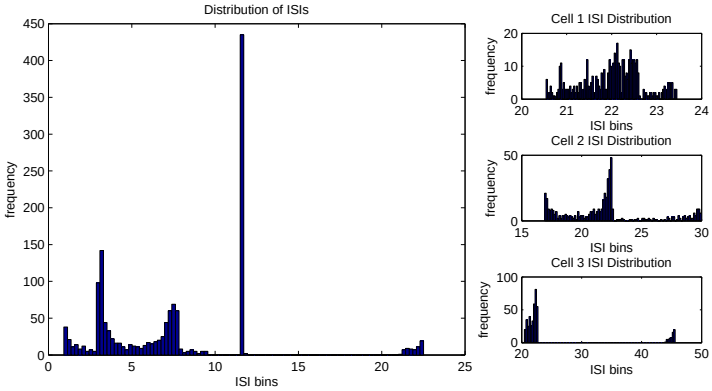

(b) Distribution of inter spike intervals of E3IM1.

Figure 4.17: Distribution of inter spike intervals for mixed electrical coupling.

4.2.5 Chaos in Chemically Coupled FHN Cells

In this section chaos is reported in a system of $N = 2$ and $N = 3$ synaptically coupled FHN cell.s

The two cell synaptically coupled system FHN system is given by

$$\begin{aligned}
\dot{x_1} &= x_1 - \frac{1}{3}x_1^3 - y_1 + g_{12}s_2\left(x_1 - v\mathrm{Syn}_1\right) \\
\dot{x_2} &= x_2 - \frac{1}{3}x_2^3 - y_2 + g_{21}s_1\left(x_2 - v\mathrm{Syn}_2\right) \\
\dot{y_1} &= \epsilon_1(x_1 + a_1 - b_1 y_1) \\
\dot{y_2} &= \epsilon_2(x_2 + a_2 - b_2 y_2) \\
\dot{s_1} &= \beta\mathcal{H}(x_1)(1 - s_1) - \delta\epsilon_1 s_1 \\
\dot{s_2} &= \beta\mathcal{H}(x_2)(1 - s_2) - \delta\epsilon_2 s_2 \qquad (4.2.5.1)
\end{aligned}$$

A number of simplifications are introduced to (4.2.5.1)-(4.2.4.2). The parameter

$$\epsilon = 0.1$$

In order to keep the differential equations from becoming very *stiff* for numerical integration. The parameters

$$v\mathrm{Syn}_i = 0, \forall i$$

Giving every synapse in the system the same reverse potential and reducing the dimension of the parameter space. Due to the discontinuity of the heaviside function, $\mathcal{H}(x)$, the calculation of they Lyapunov spectrum, which involves the system's Jacobian and hence the derivative of the heaviside function, runs into difficulty.

The three cell chemically coupled system

$$\begin{aligned}
\dot{x_1} &= x_1 - \frac{1}{3}x_1^3 - y_1 + g_{12}s_2\left(x_1 - v\mathrm{Syn}_1\right) + g_{13}s_3\left(x_1 - v\mathrm{Syn}_1\right) \\
\dot{x_2} &= x_2 - \frac{1}{3}x_2^3 - y_2 + g_{21}s_1\left(x_2 - v\mathrm{Syn}_2\right) + g_{23}s_3\left(x_3 - v\mathrm{Syn}_2\right) \\
\dot{x_3} &= x_3 - \frac{1}{3}x_3^3 - y_3 + g_{31}s_1\left(x_3 - v\mathrm{Syn}_3\right) + g_{32}s_2\left(x_3 - v\mathrm{Syn}_3\right) \\
\dot{y_1} &= \epsilon_1(x_1 + a_1 - b_1 y_1) \\
\dot{y_2} &= \epsilon_2(x_2 + a_2 - b_2 y_2) \\
\dot{y_3} &= \epsilon_3(x_3 + a_3 - b_3 y_3) \\
\dot{s_1} &= \beta\mathcal{H}(x_1)(1 - s_1) - \delta\epsilon_1 s_1 \\
\dot{s_2} &= \beta\mathcal{H}(x_2)(1 - s_2) - \delta\epsilon_2 s_2 \\
\dot{s_3} &= \beta\mathcal{H}(x_3)(1 - s_3) - \delta\epsilon_3 s_3 \qquad (4.2.5.2)
\end{aligned}$$

As a compromise the heaviside function is approximated with a hyperbolic tangent function, namely

$$\mathcal{H}(x) \approx \frac{1}{2}\left(1 + \tanh(Ax)\right)$$

where $A >> 1$ is taken to be sufficiently large, in the following results $A = 100$. Furthermore the parameter

$$\tau_{\mathrm{Syn}_i} = \delta_i \epsilon_i$$

is used to reduce the number of operations and τ_{Syn_i} is 'interpretable' as the timescale of the synapse.

Chaos in 2 and 3 Chemically coupled Cells

System Label	**System Parameters**		Lyapunov spectrum
C2HA1	$g = \begin{pmatrix} 0 & 0.2 \\ 0.2 & 0 \end{pmatrix}$	$a = [0.71, 0.71]$ $b = [0.4, 0.4]$ $\epsilon = [0.1, 0.1]$ $\beta = [1, 1]$ $\tau_{syn} = [1/1.2, 1/1.2]$ $V_{syn} = [0, 0]$	$\Lambda = \begin{pmatrix} 0.013 \\ 0.000 \\ -0.055 \\ -0.191 \\ -1.179 \\ -1.719 \end{pmatrix}$

System Label	**System Parameters**		Lyapunov spectrum
C3HA1	$g = \begin{pmatrix} 0 & 0.2 & 0.2 \\ 0.2 & 0 & 0.2 \\ 0.2 & 0.2 & 0 \end{pmatrix}$	$a = [-0.5, -0.5, -0.5]$ $b = [1, 1, 1]$ $\epsilon = [0.1, 0.1, 0.1]$ $\beta = [1, 1, 1]$ $\tau_{syn} = [1/1.2, 1/1.2, 1/1.2]$ $V_{syn} = [0, 0, 0]$	$\Lambda = \begin{pmatrix} 0.018 \\ 0.000 \\ -0.058 \\ -0.263 \\ -0.461 \\ -0.884 \\ -5.630 \\ -9.192 \\ -10.944 \end{pmatrix}$

Comparing the oscillatory behaviour of the voltage like variable when using the hyperbolic tangent function approximation to that of the Heaviside function shows that even during chaotic motion the difference is negligible for system C2HA1 while much of the characteristics in system C3HA1 is kept.

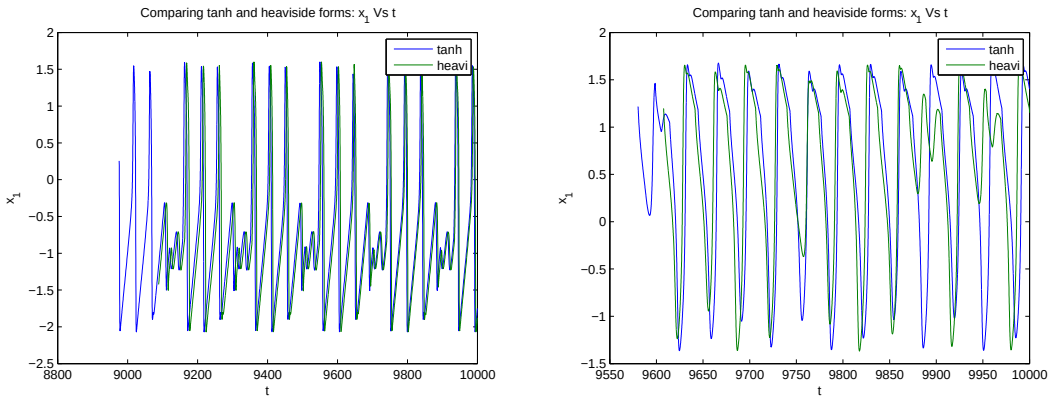

(a) Comparison for system C2HA1 (b) Comparison for system C3HA1

Figure 4.18: Typical comparison of oscillations using a hyperbolic tangent approximation to the heaviside function

The time series plot of C2HA1 shows that both cells fall into out of phase 3 spike regime, each cell dropping an action potential when it's neighbour produces it's third AP.

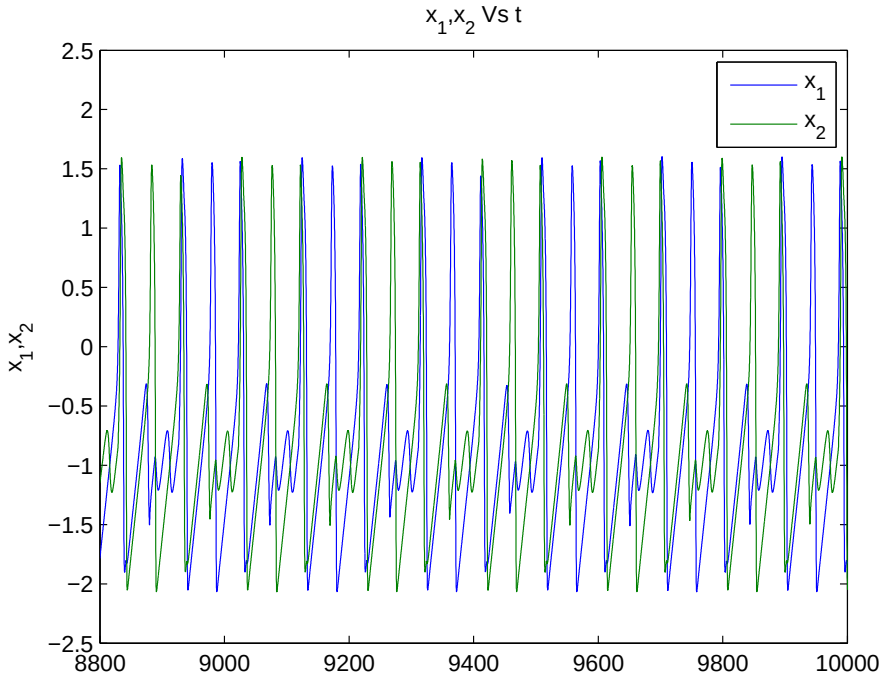

Figure 4.19: Voltage time series of C2HA1, showing out of phase action potential triplets of action potential.

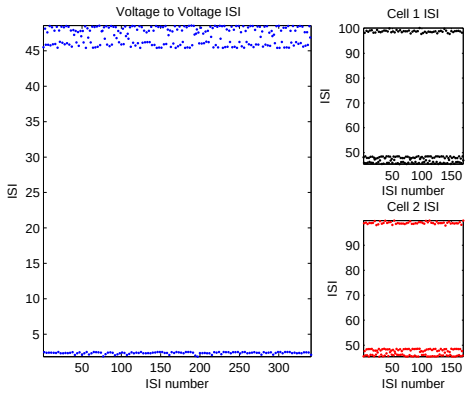

(a) C2HA1 Inter Spike Intervals.

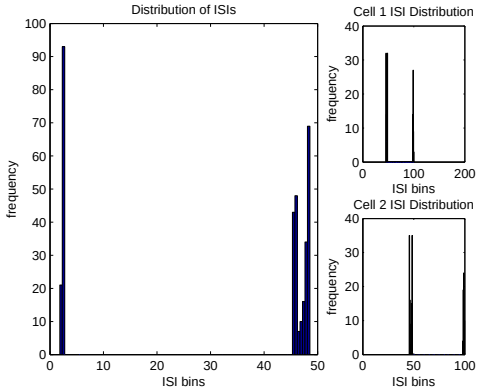

(b) Distribution of inter spike intervals of C2HA1 Inter Spike Intervals.

Figure 4.20: Inter spike intervals of C2HA1 and their distribution.

In a homogenous system of three chemically coupled FHN cells one can find rich dynamical behaviour. The time series shows two of the cells have a phase like behaviour while the third is completely out of phase with the other two.

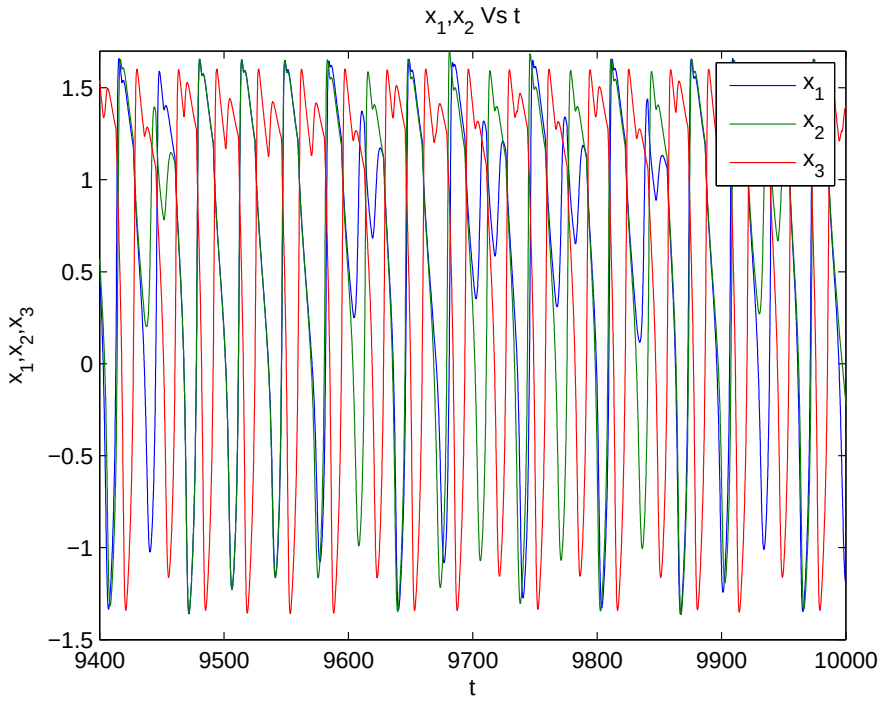

Figure 4.21: Voltage time series of C3HA1. The homogenous cells showing in and out of phase behaviour.

The inter spike intervals of C3HA1 shows a rich variety in spiking times, with one of the cells producing action potentials that have a plateaux which is twice as long as the other

two cells.

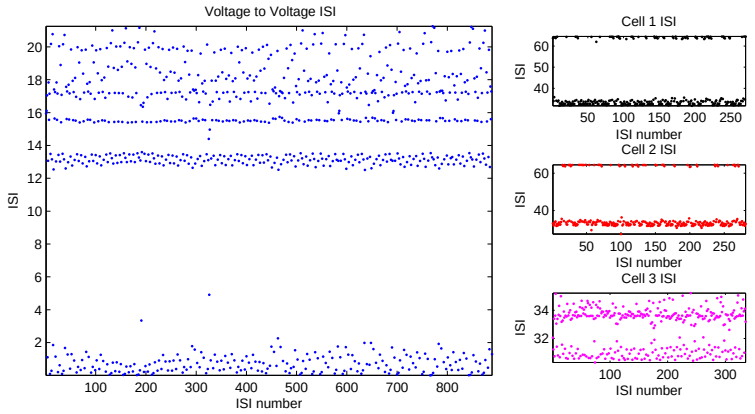

(a) C3HA1 Inter Spike Intervals.

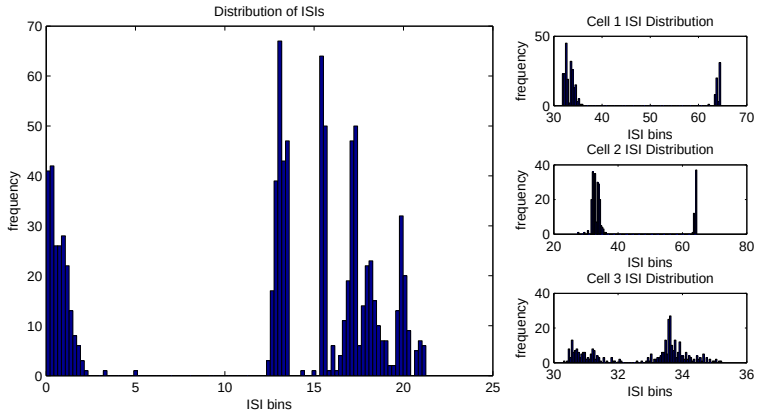

(b) Distribution of inter spike intervals of C3HA1 Inter Spike Intervals.

Figure 4.22: Inter spike intervals of C3HA1 and their distribution.

Conclusions and Future Research

This thesis is concerned with the study of cardiac and neural cells. The majority of this thesis is concerned with the rhythmic disorders and the emergence of these disorders as an inherent result of the most basic characteristics of cardiac and neural cells.

One of the primary aims was to show that biological oscillators which posses refractory periods and action potential like wave forms can undergo a complex and rich change in dynamical attributes when coupled.

The FHN system[57] is an ideal candidate for this line of research as it is a reduced model for excitable cells derived from the quantitative Hodgkin-Huxley model[77] of a neuron. As a 2D system of ODEs the FHN system is itself unable to intrinsically produce chaotic behaviour, which can be found in vitro neurons and cardiomyocytes, however it itself possess many of the properties that action potentials produced by neurons and cardiac cells have.

I show some of the bifurcation structure of a single FHN cell with a mixture of both analytical methods and computational methods from nonlinear dynamical systems theory. Paying particular attention to parameter regions where an FHN cell has a transition from equilibrium and quiescence to oscillations. These parameter regions in which the system can produce limit cycles give a qualitative view of a phase portrait of a full model of a cardiac cell or a neuron. The bifurcation analysis conducted on the single cell later serves as an important means of constraining the analysis of coupled cells to regions of parameter space where cells are excitable or oscillating self sustainably.

I show that introduction of a linear coupling term between FHN cells which qualitatively behaves as a gap junction between excitable cells produces in phase and anti-phase synchronous regimes. Excitable cells such as neurons and cardiac cells do not produce waves in a traditional sense as they do not interfere with one another, the action potentials do not have a superposition principle. Instead action potentials behave as triggers to

neighbours; if a neighbour is not in a refractory state and the coupling is large enough for a supratheshold potential to be transmitted then a neighbouring cell will elicit an action potential response. Methods from the study of synchronisation theory introduce a number of useful dynamical measures of dynamical behaviour that can be used to quantify the emergent dynamics of the coupled system. I define an order phase variable by means of a Hilbert transform that can be used in vitro experiments for analysis of cell-cell interactions, needing only a measurement of the action potential signal. The phase variable in turn allows the definition of an order parameter to quantify the synchrony of a system in terms of the relative times at which the constituent cells produce action potentials.

I analytically find and show a sufficient condition for the emergence of synchrony between FHN cells coupled electronically with inhomogeneous coupling strengths and verify the result numerically showing a particular instance. Furthermore it is shown that varying the coupling strength between neighbouring cells that once in a synchronous or non-synchronous state coupled cells can show a reluctance to make a transition from synchronous to asynchronous (or viceversa) behaviour. The coupled system is a hysteretic system in this respect; variation of the strength of coupling between the cells shows that it is not only important what coupling strength is currently being imposed on the system but also what the coupling strength was imposed on the system while varying the coupling strength and looking for transitions from synchrony to asynchrony.

With rhythmic disorders an immediate question that arises is: how can the rhythms be controlled? In this thesis I show analytically that identical electrically coupled FHN cells which are inhomogeneously coupled can be synchronised to another, separate, set of identical neurons that possess a different coupling strength structure. By means of nonlinear control signals applied to the constituent FHN cells that are to be controlled the system can be forced into a synchronous state relative to a second system of FHN cells. This result is illustrated for a system of two two-cell systems both analytically and numerically. This shows that at least for systems of cells that have had their conduction pathways compromised it is theoretically possible to adjust their action potential responses with respect to an uncompromised system of cells with a cell by cell control sequence. Ideally however such a control mechanism would not need to be administered to *all* the constituent cells but rather to *key* cells within the network structure.

For coupled FHN cells I investigate the frequency locking regions of a master-slave system as a function of the coupling strength from master to slave. For repulsive coupling strengths the FHN system shows a rich variety of frequency responses over relatively nar-

row coupling strengths. Such frequency locking regions have implications for Wenchenbach rhythms in cardiac systems where contractions of the atria do not always lead to contraction of the ventricles. I show that between action potential generating cells it is not simply a complete block of conduction between cells that can cause action potentials to be dropped but more simply functioning junctions with relatively small changes in repulsive coupling strengths can lead to dramatic changes in relative frequency responses between the cells. These results are illustrated with numerical simulations drawing from the techniques earlier developed in studying the synchrony between cells. Additionally bursting behaviour which individual neurons can themselves exhibit, can be generated as an emergent property of a system of master-slave coupled cells whose activity timescales differ by an order of magnitude. This suggests that bursting signals need not be a direct result of intrinsic bursting in a cell and can be generated as an emergent property in a coupled system.

Finally in this thesis I show that coupled FHN cells can produce chaotic dynamics when they are electrically or chemically coupled together. The chaos present in the system is an emergent phenomenon directly resulting from communication between the cells. Chaotic firing patterns in forced neurons have been found both experimentally and theoretically [5]. In this thesis the chaos reported is not that of a forced system which can be found in [32]. The chaotic dynamics, which each individual cell is incapable of producing, is a result of coupling the cells together. This suggests that in real neural or cardiac systems where one finds chaotic behaviour one may have success in successfully eliminating or enhancing the chaotic signals by targeting the conductivity of the gap junctions and synapse between cells rather than the intrinsic properties of the cells themselves.

There are a multitude of topics to examine in the future. Most notable are topics in nonlinear control and complex networks. A means to control the synchrony of a group of coupled FHN cells by simply influencing a small subset of the cells in a system would make for a more practical basis for medical implementation. There are a number of challenges that such a study would entail, firstly one must find a means of finding the most influential cells in a network which are the most likely targets for network control and then one must find a combination of nonlinear control signals to administer a desired control throughout the network.

The role of the network structures found in cardiac and neural systems is also an open problem. This thesis has shown that a number of emergent properties can occur when coupling cells together in an all-to-all or master-slave regime. In reality however car-

diac and more so neural networks are made up of neurons connected in complex network structures. These structures have small-world and scale-free type characteristics that are found in communication networks such as the internet, social networks and even collaboration networks between researchers. The study of such systems is vitally important in terms of the structure of the internet but also in understanding how neural systems are assembled. The neural system is a system capable of learning, optimising and restructuring all of which lead to evolving network structures. These ideas will be important to investigate when one is interested in neural plasticity.

Examining complex networks of dynamical nodes is still in its infancy and will require new developments in mathematics and new approaches in dynamical systems theory to adequately, identify, characterise and control dynamical systems that live on a complex network whose functional properties are a result of the systems topology.

Appendix A

FHN slow manifold expansion in terms of the small parameter

Here we find an expression for the slow manifold of the FHN system when ϵ is a small parameter. We follow the formulation found in [63, p 74].
The FHN system after transformation to slow time $\tau = \epsilon t$ is given by

$$\epsilon \dot{x}_\tau = f(x, y) = x - \frac{x^3}{3} - y + I$$
$$\dot{y}_\tau = g(x, y) = x + a - by$$

The aim is to find a function

$$y = Y(x, \epsilon)$$

which is locally a slow invariant manifold of the slow time FHN system. The slow manifold takes the following form

$$Y(x, \epsilon) = Y_0(x) + \epsilon Y_1(x) + \epsilon^2 Y_2(x) + \mathcal{O}\left(\epsilon^3\right)$$

where the functions $Y_i, \quad i = 0, 1, 2$ are to be determined. From [63, p 75-76] these functions are found by looking at the invariance property

$$\frac{\partial Y}{\partial x} f(x, Y) = \epsilon g(x, Y)$$

using it in the Taylor series expansion of $f(x,y)$ to yield

$$\left(\frac{\partial Y_0}{\partial x}+\epsilon\frac{\partial Y_1}{\partial x}+\epsilon^2\frac{\partial Y_2}{\partial x}\right)\left[f(x,Y_0)+(\epsilon Y_1+\epsilon^2 Y_2)\frac{\partial f}{\partial y}+\frac{1}{2!}\left(\epsilon Y_1+\epsilon^2 Y_2\right)^2\frac{\partial^2 f}{\partial y^2}\right]$$
$$=\epsilon g(x,Y_0)+\epsilon(\epsilon Y_1+\epsilon^2 Y_2)\frac{\partial g}{\partial y}+\frac{\epsilon}{2!}\left(\epsilon Y_1+\epsilon^2 Y_2\right)^2\frac{\partial^2 g}{\partial y^2}$$

Solving the above by order we have at $\mathcal{O}(\epsilon^0)$

$$\frac{\partial Y_0}{\partial x}f(x,Y_0(x))=0 \iff y=Y_0(x)$$

at order $\mathcal{O}(\epsilon^1)$

$$\epsilon\frac{\partial Y_1}{\partial x}f(x,Y_0(x))+\epsilon Y_1\frac{\partial Y_0}{\partial x}\frac{\partial f}{\partial y}=\epsilon g(x,Y_0)$$

we have $f(x,Y_0(x))=0$ and thus

$$Y_1(x)=\frac{g(x,Y_0(x))}{\frac{\partial Y_0}{\partial x}\frac{\partial f}{\partial y}}$$

at order $\mathcal{O}(\epsilon^2)$ we have

$$Y_2(x)\frac{\partial Y_0}{\partial x}\frac{\partial f}{\partial y}+\frac{Y_1^2(x)}{2}\frac{\partial Y_0}{\partial x}\frac{\partial^2 f}{\partial y^2}+Y_1(x)\frac{\partial Y_1}{\partial x}\frac{\partial f}{\partial y}+\frac{\partial Y_2}{\partial x}f(x,Y_0(x))=Y_1(x)\frac{\partial g}{\partial y}.$$

Again since $f(x,Y_0(x))=0$ we have

$$Y_2(x)=\frac{Y_1(x)\frac{\partial g}{\partial y}(x,Y_0(x))-\frac{Y_1^2(x)}{2}\frac{\partial Y_0}{\partial x}\frac{\partial^2 f}{\partial y^2}(x,Y_0(x))-Y_1(x)\frac{\partial Y_1}{\partial x}\frac{\partial f}{\partial y}(x,Y_0(x))}{\frac{\partial Y_0}{\partial x}\frac{\partial f}{\partial y}(x,Y_0(x))}.$$

For the slow time FHN system we thus have,

$$Y_0(x)=x-\frac{x^3}{3}+I$$

The $\mathcal{O}(\epsilon)$ term requires a number of derivatives,

$$\frac{\partial Y_0}{\partial x} = 1 - x^2, \qquad \frac{\partial f}{\partial y} = -1$$

and thus

$$Y_1(x) = \frac{x + a - bx + \frac{bx^3}{3} + bI}{(1 - x^2)\,(-1)}$$

which can be written more compactly as

$$Y_1(x) = \frac{(1-b)x - \dfrac{bx^3}{3} + a + bI}{x^2 - 1}.$$

Finally the $\mathcal{O}(\epsilon^2)$ term requires the derivatives

$$\frac{\partial g}{\partial y} = -b, \quad \frac{\partial Y_0}{\partial x} = 1 - x^2, \quad \frac{\partial^2 f}{\partial^2 y} = 0, \quad \frac{\partial f}{\partial y} = -1$$

$$\frac{\partial Y_1}{\partial x} = \frac{(1-b) - bx^2}{x^2 - 1} + \frac{2\left\{\dfrac{bx^4}{3} - (1-b)x^2 - (a + bI)x\right\}}{(x^2-1)^2}$$

After a little simplification one can write

$$Y_2(x) = -\frac{1}{9}\frac{(3x - 3xb - bx^3 + 3a + 3Ib)\,(4bx^4 - 12bx^2 + 3x^2 + 6ax + 6Ibx + 3)}{(x^2-1)^4}$$

The slow manifold equation for the FHN system is given by

$$y = Y_0(x) + \epsilon Y_1(x) + \epsilon^2 Y_2(x) + \mathcal{O}(\epsilon^3)$$

where,

$$Y_0(x) = x - \frac{x^3}{3} + I$$

$$Y_1(x) = \frac{(1-b)x - \frac{bx^3}{3} + a + bI}{x^2 - 1}$$

$$Y_2(x) = -\frac{1}{9}\frac{(3x - 3xb - bx^3 + 3a + 3Ib)\,(4bx^4 - 12bx^2 + 3x^2 + 6ax + 6Ibx + 3)}{(x^2-1)^4}$$

Appendix B

The FHN cell in second order form

B.1 The single cell

Beginning with the FHN system

$$\dot{x} = x - \frac{1}{3}x^3 - y + I \tag{B.1.0.1}$$

$$\dot{y} = \epsilon(x + a - by) \tag{B.1.0.2}$$

we can differentiate the equation for $\dot{x}$ to obtain

$$\ddot{x} = \dot{x} - x^2\dot{x} - \dot{y} + \dot{I}$$

assuming that the external current is a constant we have $\dot{I} = 0$. The aim is to completely write this system in terms of x and its derivatives and thus we eliminate the $\dot{y}$ term using (**??**),

$$\begin{aligned}\ddot{x} &= \dot{x} - x^2\dot{x} - \dot{y} \\ &= \dot{x} - x^2\dot{x} - \epsilon x - \epsilon a + \epsilon by.\end{aligned}$$

On rearranging (B.1.0.1) we find that

$$y = x - \dot{x} - \frac{1}{3}x^3 + I.$$

Thus,

$$\ddot{x} = \dot{x} - x^2\dot{x} - \epsilon x - \epsilon a + \epsilon b x - \epsilon b\dot{x} - \frac{\epsilon b}{3}x^3 + \epsilon b I.$$

Finally we have the second order ODE given by

$$\ddot{x} = (1 - \epsilon b - x^2)\dot{x} + \left(\epsilon b - \epsilon - \frac{\epsilon b}{3}x^2\right)x + \epsilon b I - \epsilon a \tag{B.1.0.3}$$

B.2 The electrically coupled system

The system of N electrically coupled FHN cells is given by

$$\dot{x_i} = x_i - \frac{1}{3}x_i^3 - y_i + I_i + \sum_{\substack{j=1 \\ j\neq i}}^{N} g_{ij}\left(x_i - x_j\right) \tag{B.2.0.4}$$

$$\dot{y_i} = \epsilon_i(x_i + a_i - b_i y_i) \tag{B.2.0.5}$$

Again it can be useful to write this in terms of coupled second order ODE systems and proceed to differentiate (B.2.0.4) and obtain

$$\ddot{x_i} = \dot{x_i} - x_i^2\dot{x_i} - \dot{y_i} + \dot{I_i} + \sum_{\substack{j=1 \\ j\neq i}}^{N} g_{ij}\left(\dot{x_i} - \dot{x_j}\right).$$

As before we look at the case where the external currents are constant and so $\dot{I_i} = 0$ for all i and use (B.2.0.5) to eliminate the $\dot{y_i}$ and find

$$\ddot{x_i} = \dot{x_i} - x_i^2\dot{x_i} - \epsilon_i x_i - \epsilon_i a_i + \epsilon_i b_i y_i + \sum_{\substack{j=1 \\ j\neq i}}^{N} g_{ij}\left(\dot{x_i} - \dot{x_j}\right).$$

Rearrangement of (B.2.0.4) yields an expression for y_i,

$$y_i = x_i - \dot{x}_i - \frac{1}{3}x_i^3 + I_i + \sum_{\substack{j=1 \\ j\neq i}}^{N} g_{ij}\left(x_i - x_j\right)$$

Now the set of coupled second order equations can be written as

$$\ddot{x}_i = \dot{x}_i - x_i^2\dot{x}_i - \epsilon_i x_i - \epsilon_i a_i + \epsilon_i b_i \left(x_i - \dot{x}_i - \frac{1}{3}x_i^3 + I_i + \sum_{\substack{j=1 \\ j\neq i}}^{N} g_{ij}\left(x_i - x_j\right) \right) + \sum_{\substack{j=1 \\ j\neq i}}^{N} g_{ij}\left(\dot{x}_i - \dot{x}_j\right)$$

and finally we have

$$\begin{aligned} \ddot{x}_i = (1 - \epsilon_i b_i - x_i^2)\dot{x}_i + \left(\epsilon_i b_i - \epsilon_i - \frac{\epsilon_i b_i}{3}x_i^2\right) x_i + \epsilon_i b_i I_i - \epsilon_i a_i + \\ + \sum_{\substack{j=1 \\ j\neq i}}^{N} g_{ij}\left(x_i - x_j\right) + \sum_{\substack{j=1 \\ j\neq i}}^{N} g_{ij}\left(\dot{x}_i - \dot{x}_j\right) \end{aligned} \tag{B.2.0.6}$$

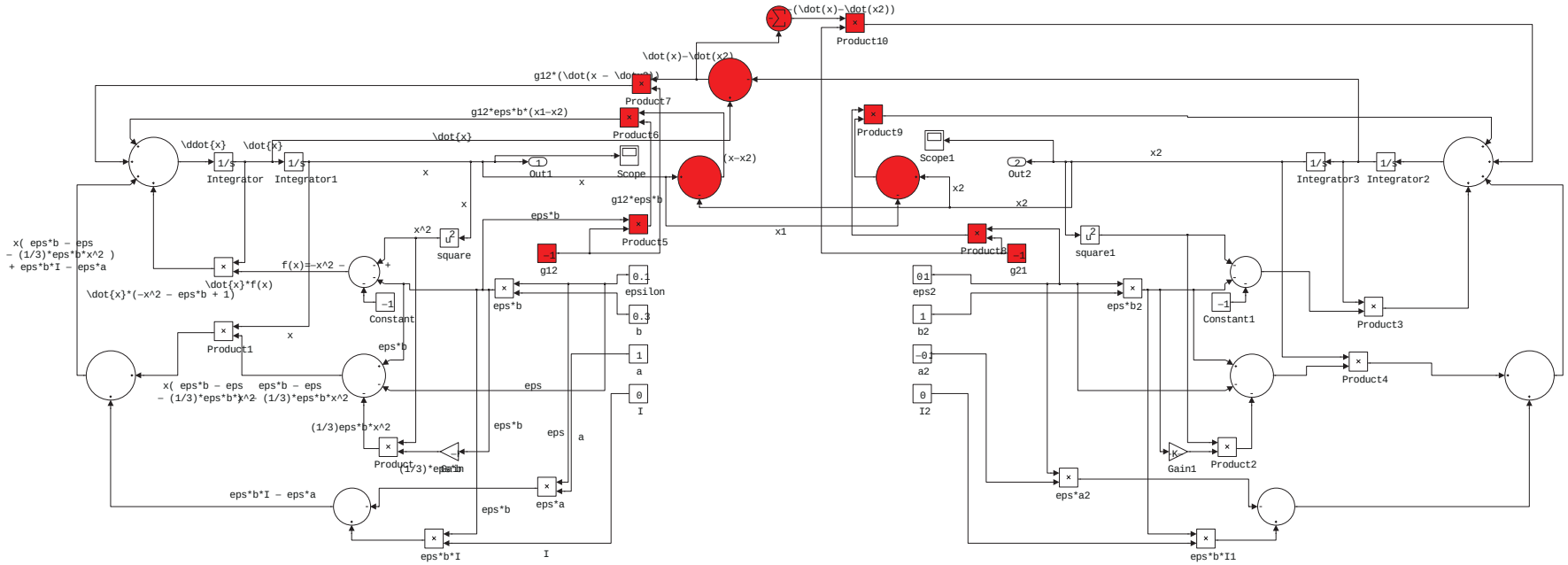

Figure B.1: The Simulink schematic for two electrically coupled FHN cells.

Bibliography

[1] A gradient model of cardiac pacemaker myocytes. *Progress in Biophysics and Molecular Biology*, 85(2-3):301 – 323, 2004.

[2] J. A. Acebrón, A. R. Bulsara, and W.-J. Rappel. Noisy fitzhugh-nagumo model: From single elements to globally coupled networks. *Phys. Rev. E*, 69:026202, Feb 2004.

[3] Juan A. Acebrón, L. L. Bonilla, Conrad J. Pérez Vicente, Félix Ritort, and Renato Spigler. The kuramoto model: A simple paradigm for synchronization phenomena. *Reviews of Modern Physics*, 77(1):137–185, 2005.

[4] K. Aihara, T. Takabe, and M. Toyoda. Chaotic neural networks. *Physics Letters A*, 144(67):333 – 340, 1990.

[5] Kazuyuki Aihara, Gen Matsumoto, and Yuhji Ikegaya. Periodic and non-periodic responses of a periodically forced hodgkin-huxley oscillator. *Journal of Theoretical Biology*, 109(2):249 – 269, 1984.

[6] B. Ambrosio and M.A. Aziz-Alaoui. Synchronization and control of coupled reactiondiffusion systems of the fitzhughnagumo type. *Computers & Mathematics with Applications*, 64(5):934 – 943, 2012. ¡ce:title¿Advanced Technologies in Computer, Consumer and Control¡/ce:title¿.

[7] V.I Arnold and Richard A. Silverman. *Ordinary Differential Equations*. The MIT Press, 10 edition, 1998.

[8] Jean-Julien Aucouturier, Yuta Ogai, and Takashi Ikegami. Making a robot dance to music using chaotic itinerancy in a network of fitzhugh-nagumo neurons. In Masumi Ishikawa, Kenji Doya, Hiroyuki Miyamoto, and Takeshi Yamakawa, editors, *Neural Information Processing*, volume 4985 of *Lecture Notes in Computer Science*, pages 647–656. Springer Berlin Heidelberg, 2008.

[9] J.P. Baltanas and J.M. Casado. Bursting behaviour of the fitzhugh-nagumo neuron model subject to quasi-monochromatic noise. *Physica D: Nonlinear Phenomena*, 122(14):231 – 240, 1998.

[10] L C Barrio, T Suchyna, T Bargiello, L X Xu, R S Roginski, M V Bennett, and B J Nicholson. Gap junctions formed by connexins 26 and 32 alone and in combination are differently affected by applied voltage. *Proceedings of the National Academy of Sciences*, 88(19):8410–8414, 1991.

[11] Luis C. Barrio, Ana Revilla, Juan M. Goméz-Hernandez, Marta de Miguel, and Daniel González. Chapter 8: Membrane potential dependence of gap junctions in vertebrates. In Carnillo Peracchia, editor, *Gap Junctions Molecular Basis of Cell Communication in Health and Disease*, volume 49 of *Current Topics in Membranes*, pages 175 – 188. Academic Press, 1999.

[12] P. J. Basser et al. In vivo fibre tractography using dt-mri data. *Magnetic Resonance in Medicine*, 44:625–632, 2000.

[13] Peter J. Basser, James Mattiello, and Denis LeBihan. Estimation of the effective self-diffusion tensor from the nmr spin echo. *Journal of Magnetic Resonance Series B*, 103:247–254, 1994.

[14] Mark F. Bear, Barry W. Connors, and Michael A. Paradiso. *Neuroscience: Exploring the Brain*. Lippincott Williams & Wilkins, third edition, February 2006.

[15] G. W. Beeler and H. Reuter. Reconstruction of the action potential of ventricular myocardial fibres. *The Journal of Physiology*, 268(1):177–210, 1977.

[16] Matthew Bennett, Michael F. Schatz, Heidi Rockwood, and Kurt Wiesenfeld. Huygens's clocks. *Proceedings of the Royal Society of London. Series A: Mathematical, Physical and Engineering Sciences*, 458(2019):563–579, 2002.

[17] O. Bernus, R. Wilders, C. W. Zemlin, H. Verschelde, and A. V. Panfilov. A computationally efficient electrophysiological model of human ventricular cells. *American Journal of Physiology - Heart and Circulatory Physiology*, 282(6):H2296–H2308, 2002.

[18] S. Boccaletti, J. Kurths, G. Osipov, D. L. Valladares, and C. S. Zhou. The synchronization of chaotic systems. *Physics Reports*, 366:1–101, August 2002.

[19] Vladimir E. Bondarenko, Gyula P. Szigeti, Glenna C. L. Bett, Song-Jung Kim, and Randall L. Rasmusson. Computer model of action potential of mouse ventricular

myocytes. *American Journal of Physiology - Heart and Circulatory Physiology*, 287(3):H1378–H1403, 2004.

[20] K.F. Bonhoeffer. Activation of passive iron as a model for the excitation in nerve. *The Journal of General Physiology*, September.

[21] M. R. Boyett, H. Zhang, A. Garny, and A. V. Holden. Control of the pacemaker activity of the sinoatrial node by intracellular ca2+. experiments and modelling. *Philosophical Transactions of the Royal Society of London. Series A: Mathematical, Physical and Engineering Sciences*, 359(1783):1091–1110, 2001.

[22] M.R. Boyett and B.R. Jewell. Analysis of the effects of changes in rate and rhythm upon electrical activity in the heart. *Progress of Biophysics and Molecular Biology*, 36(1):1–52, 1980.

[23] S. M. Breedlove, N. V. Watson, and M. R. Rsenzweig. *Biological Psychology: An Introduction to Behavioral, Cognitive, and Clinical Neuroscience*. Sinauer Associates, Inc., sixth edition, March 2010.

[24] Reggie Brown, Paul Bryant, and Henry D. I. Abarbanel. Computing the lyapunov spectrum of a dynamical system from an observed time series. *Phys. Rev. A*, 43:2787–2806, Mar 1991.

[25] F. Buchholtz, N. Schinor, and F. W. Schneider. Stochastic nonlinear dynamics: Hown many ion channels are in a single neuron. *The Journal of Physical Chemisty B*, 106(19):5086–5090, 2002.

[26] Feliksas F. Bukauskas, Claudia Elfgang, Klaus Willecke, and Robert Weingart. Heterotypic gap junction channels (connexin26 - connexin32) violate the paradigm of unitary conductance. *Pflügers Archiv European Journal of Physiology*, 429:870–872, 1995.

[27] Candido Cabo and Penelope A. Boyden. Electrical remodeling of the epicardial border zone in the canine infarcted heart: a computational analysis. *American Journal of Physiology - Heart and Circulatory Physiology*, 284(1):H372–H384, 2003.

[28] William A. Catterall. From ionic currents to molecular mechanisms: The structure and function of voltage-gated sodium channels. *Neuron*, 26:13–25, 2000.

[29] Dmitri Chamchad, Valerie A. Arkoosh, Jay C. Horrow, Jodie L. Buxbaum, Igor Izrailtyan, Lev Nakhamchik, Dirk Hoyer, and J. Yasha Kresh. Using heart rate

variability to stratify risk of obstetric patients undergoing spinal anesthesia. *Anesthesia & Analgesia*, 99(6):1818–1821, 2004.

[30] Junjie. Chen et al. Regional ventricular wall thickening reflects changes in cardiac fibre and sheet structure during contraction: quatification with diffusion tensor mri. *American Journal of Physiology: Heart and Circulatory Physiology*, 289(5):H1898–H1907, 2005.

[31] Elizabeth M Cherry, Flavio H Fenton, and Robert F Gilmour. Mechanisms of ventricular arrhythmias: A dynamical systems-based perspective. *American Journal of Physiology - Heart and Circulatory Physiology*, 2012.

[32] Mo-Hong Chou and Yu-Tuan Lin. Exotic dynamic behavior of the forced fitzhugh-nagumo equations. *Computers & Mathematics with Applications*, 32(10):109 – 124, 1996.

[33] Konstantinos Chrysafinos, Sotirios P. Filopoulos, and Theodosios K. Papathanasiou. Error estimates for a fitzhughnagumo parameter-dependent reaction-diffusion system. *ESAIM: Mathematical Modelling and Numerical Analysis*, 47:281–304, 1 2013.

[34] Donald C Cooper. The significance of action potential bursting in the brain reward circuit. *Neurochemistry International*, 41(5):333 – 340, 2002.

[35] Steven R. Coppen, Emmanuel Dupont, Stephen Rothery, and Nicholas J. Severs. Connexin45 expression is preferentially associated with the ventricular conduction system in mouse and rat heart. *Circulation Research*, 82(2):232–243, 1998.

[36] Steven R. Coppen, Riyaz A. Kaba, Deborah Halliday, Emmanuel Dupont, Jeremy N. Skepper, Suzy Elneil, and Nicholas J. Severs. Comparison of connexin expression patterns in the developing mouse heart and human foetal heart. *Molecular and Cellular Biochemistry*, 242:121–127, 2003.

[37] Steven R. Coppen, Itsuo Kodama, Mark R. Boyett, Halina Dobrzynski, Yoshiko Takagishi, Haruo Honjo, Hung-I Yeh, and Nicholas J. Severs. Connexin45, a major connexin of the rabbit sinoatrial node, is co-expressed with connexin43 in a restricted zone at the nodal-crista terminalis border. *Journal of Histochemistry & Cytochemistry*, 47(7):907–918, 1999.

[38] Linda S. Costanzo. *BRS Physiology (Board Review Series)*. Lippincott Williams & Wilkins, fourth edition, July 2006.

[39] Marc Courtemanche, Rafael J. Ramirez, and Stanley Nattel. Ionic mechanisms underlying human atrial action potential properties: insights from a mathematical model. *American Journal of Physiology - Heart and Circulatory Physiology*, 275(1):H301–H321, 1998.

[40] Charles R. Craig and Robert E. Stitzel. *Modern Pharmacology With Clinical Applications*. Lippincott Williams & Wilkins, sixth edition, June 2003.

[41] Cristiane del Corsso et al. Transfection of mammalian cells with connexins and measurement of voltage sensitivity of their gap junctions.

[42] S. S. Demir, J. W. Clark, C. R. Murphey, and W. R. Giles. A mathematical model of a rabbit sinoatrial node cell. *American Journal of Physiology - Cell Physiology*, 266(3):C832–C852, 1994.

[43] Semahat S. Demir, John W. Clark, and Wayne R. Giles. Parasympathetic modulation of sinoatrial node pacemaker activity in rabbit heart: a unifying model. *American Journal of Physiology - Heart and Circulatory Physiology*, 276(6):H2221–H2244, 1999.

[44] Bin Deng, Jiang Wang, and Xile Wei. Effect of chemical synapse on vibrational resonance in coupled neurons. *Chaos: An Interdisciplinary Journal of Nonlinear Science*, 19(1):013117, 2009.

[45] Thomas Desplantez, Deborah Halliday, Emmanuel Dupont, and Robert Weingart. Cardiac connexins cx43 and cx45: formation of diverse gap junction channels with diverse electrical properties. *Pflügers Archiv European Journal of Physiology*, 448(4):363–375, 2004.

[46] Stefan Dhein and Habo J. Jongsma. Forming the network - gap junctions in the cardiovascular system.

[47] Brent Doiron, Carlo R. Laing, Andr Longtin, and Leonard Maler. Ghostbursting: A novel neuronal burst mechanism. *Journal of Computational Neuroscience*, pages 5–25, 2002.

[48] Socrates Dokos, Branko Celler, and Nigel Lovell. Ion currents underlying sinoatrial node pacemaker activity: A new single cell mathematical model. *Journal of Theoretical Biology*, 181(3):245 – 272, 1996.

[49] Socrates Dokos, Branko Celler, and Nigel Lovell. Vagal control of sinoatrial rhythm: a mathematical model. *Journal of Theoretical Biology*, 182(1):21 – 44, 1996.

[50] Declan A. Doyle, Joao Morais Cabral, Richard A. Pfuetzner, Anling Kuo, Jacqueline M. Gulbis, Steven L. Cohen, Brian T. Chait, and Roderick MacKinnon. The structure of the potassium channel: Molecular basis of k+ conduction and selectivity. *Science*, 280(5360):69–77, 1998.

[51] Y. E. Earm and D. Noble. A model of the single atrial cell: Relation between calcium current and calcium release. *Proceedings of the Royal Society of London. Series B, Biological Sciences*, 240(1297):pp. 83–96, 1990.

[52] Sergio Elenes, Agustin D. Martinez, Mario Delmar, Eric C. Beyer, and Alonso P. Moreno. Heterotypic docking of cx43 and cx45 connexons blocks fast voltage gating of cx43. *Biophysical journal*, 81(3):1406 – 1418, 2001.

[53] L. P. Endresen, K. Hall, J. S. Hye, and J. Myrheim. A theory for the membrane potential of living cells. *European Biophysics Journal*, 29(2):90–103, 2000.

[54] MICHALE S. FEE, ALEXAY A. KOZHEVNIKOV, and RICHARD H.R. HAHNLOSER. Neural mechanisms of vocal sequence generation in the songbird. *Annals of the New York Academy of Sciences*, 1016(1):153–170, 2004.

[55] Mario Feingold, Diego L. Gonzalez, Oreste Piro, and Hector Viturro. Phase locking, period doubling, and chaotic phenomena in externally driven excitable systems. *Phys. Rev. A*, 37:4060–4063, May 1988.

[56] Charles ffrench Constant, Holly Colognato, and Robin J. M. Franklin. The mysteries of myelin unwrapped. *Science*, 304(5671):688–689, 2004.

[57] Richard Fitzhugh. Impulses and physiological states in theoretical models of nerve membrane. *Biophysical Journal*, July.

[58] Jeffrey J. Fox, Jennifer L. McHarg, and Robert F. Gilmour. Ionic mechanism of electrical alternans. *American Journal of Physiology - Heart and Circulatory Physiology*, 282(2):H516–H530, 2002.

[59] G. Gaier and M. Muller. Excitable chaos in diffusively coupled fitzhugh-nagumo equations. *Revista Mexicana De Fisica*, 50(5):422–426, 2004.

[60] J. Gao, J. Hu, and W. W. Tung. Complexity measures of brain wave dynamics. *Cognative Neurodynamics*, 5(2):171 – 182, 2011.

[61] S. H. Gilbert, A. P. Benson, P. Li, and A.V. Holden. Regional localisation of left ventricular sheet structure: integration with current models of cardiac fibre, sheet

and band structure. *European Journal of Cardio-Thoracic Surgery*, 32(2):231–249, 2007.

[62] Gina and Sosinsky. Chapter 1: Gap junction structure: New structures and new insights. In Carnillo Peracchia, editor, *Gap Junctions Molecular Basis of Cell Communication in Health and Disease*, volume 49 of *Current Topics in Membranes*, pages 1–22. Academic Press, 1999.

[63] Jean-marc Ginoux. *Differential Geometry Applied to Dynamical Systems*. World Scientific Publishing Company, 1 edition, April 2009.

[64] L. Glass, C. Lerma, and A. Shrier. New methods for the analysis of heartbeat behavior in risk stratification. *Frontiers in Physiology*, 2(88), 2011.

[65] Leon Glass. Synchronization and rhythmic processes in physiology. *Nature*, 410:277–284, 2001.

[66] Leon Glass. Introduction to controversial topics in nonlinear science: Is the normal heart rate chaotic. *CHAOS*, 19(2):028501, 2009.

[67] R.G. Gourdie, C. R Green, and N. J. Severs. Gap junction distribution in adult mammalian myocardium revealed by an anti-peptide antibody and laser scanning confocal microscopy. *Journal of Cell Science*, 99:42–55, 1991.

[68] Joseph L. Greenstein and Raimond L. Winslow. An integrative model of the cardiac ventricular myocyte incorporating local control of ca2+ release. *Biophysical Journal*, 83(6):2918 – 2945, 2002.

[69] Arthur C. Guyton and John E. Hall. *Textbook of medical physiology*. Saunders, eleventh edition, 2005.

[70] Constance Hammond, Hagai Bergman, and Peter Brown. Pathological synchronization in parkinson's disease: networks, models and treatments. *Trends in Neurosciences*, 30(7):357 – 364, 2007.

[71] Andrew L. Harris. Connexin channel permeability to cytoplasmic molecules.

[72] Andrew L. Harris. Emerging issues of connexin channels: biophysics fills the gap.

[73] Jean-Claude Hervé, Pauline Phelan, Roberto Bruzzone, and Thomas W. White. Connexins, innexins and pannexins: Bridging the communication gap. *Biochimica et Biophysica Acta (BBA) - Biomembranes*, 1719(1-2):3–5, 2005.

[74] D. W. Hilgemann and D. Noble. Excitation-contraction coupling and extracellular calcium transients in rabbit atrium: Reconstruction of basic cellular mechanisms. *Proceedings of the Royal Society of London. Series B, Biological Sciences*, 230(1259):pp. 163–205, 1987.

[75] Bertil. Hille. *Ion Channels of Excitable Membranes*. Sinauer Associates, third edition, 2001.

[76] J. L. Hindmarsh and R. M. Rose. A model of neuronal bursting using three coupled first order differential equations. *Proceedings of the Royal Society of London. Series B. Biological Sciences*, 221(1222):87–102, 1984.

[77] A. L. Hodgkin and A. F. Huxley. A quantitative description of membrane current and its application to conduction and excitation in nerve. *The Journal of Physiology*, 117(4), August.

[78] Hyunsuk Hong and Steven. H. Strogatz. Kuramoto model of coupled oscillators with positive and negative coupling parameters: An example of conformist and contrarian oscillators. *Physical Review Letters*, 106(054102):1–4, 2011.

[79] Matthew G. Hopperstad, Miduturu Srinivas, and David C. Spray. Properties of gap junction channels formed by cx46 alone and in combination with cx50. *Biophysical journal*, 79(4):1954–1966, 2000.

[80] E. W. Hsu, A. L. Muzikant, S. A. Matulevicius, R. C. Penland, and C. S. Heriquez. Magnetic resonance myocardial fibre-orientation mapping with direct histological correlation. *American Journal of Physiology: Heart and Circulatory Physiology*, 274(5):H1627–H1634, 1998.

[81] Marjorie Letitia Hubbard, Wenjun Ying, and Craig S. Henriquez. Effect of gap junction distribution on impulse propagation in a monolayer of myocytes: a model study. *Europace*, 9(suppl 6):vi20–vi28, 2007.

[82] Thomas J. Hund and Yoram Rudy. Rate dependence and regulation of action potential and calcium transient in a canine cardiac ventricular cell model. *Circulation*, 110(20):3168–3174, 2004.

[83] Thomas J. Hund and Yoram Rudy. Rate dependence and regulation of action potential and calcium transient in a canine cardiac ventricular cell model. *Circulation*, 110(20):3168–3174, 2004.

[84] T.J Hund and Y. Rudy. Determinants of excitability in cardiac myocytes: Mechanistic investigation of memory effect. *Biophysical Journal*, 79(6):3095–3104, 2000.

[85] Vivek Iyer, Reza Mazhari, and Raimond L. Winslow. A computational model of the human left-ventricular epicardial myocyte. *Biophysical Journal*, 87(3):1507 – 1525, 2004.

[86] Eugene M. Izhikevich. *Dynamical Systems in Neuroscience: The Geometry of Excitability and Bursting*. The MIT Press, 1 edition, January 2010.

[87] M. Saleet Jafri, J. Jeremy Rice, and Raimond L. Winslow. Cardiac ca2+ dynamics: The roles of ryanodine receptor adaptation and sarcoplasmic reticulum load. *Biophysical Journal*, 74(3):1149 – 1168, 1998.

[88] M. J. Janse and R. H. Anderson. Specialized internodal atrial pathways. fact or fiction? *European Journal of Cardiology*, 2:117–136, 1974.

[89] Dominic Jordan and Peter Smith. *Nonlinear Ordinary Differential Equations: An Introduction for Scientists and Engineers*. Oxford University Press, USA, 2007.

[90] Takashi Kanamaru, Takehiko Horita, and Yoichi Okabe. Theoretical analysis of array-enhanced stochastic resonance in the diffusively coupled fitzhugh-nagumo equation. *Phys. Rev. E*, 64:031908, Aug 2001.

[91] Daniel T. Kaplan, John R. Clay, Timothy Manning, Leon Glass, Michael R. Guevara, and Alvin Shrier. Subthreshold dynamics in periodically stimulated squid giant axons. *Phys. Rev. Lett.*, 76:4074–4077, May 1996.

[92] Arnold M. Katz. *Physiology of the Heart*. Lippincott Williams & Wilkins, fourth edition, November 2005.

[93] James Keener and James Sneyd. *Mathematical Physiology*. Springer, corrected edition, October 1998.

[94] L.M. Khadra, T.J. Maayah, and H. Dickhaus. Detecting chaos in hrv signals in human cardiac transplant recipients. *Computers and Biomedical Research*, 30(3):188 – 199, 1997.

[95] Hassan K. Khalil. *Nonlinear Systems*. Prentice Hall, 3 edition, December 2001.

[96] Hiroyuki Kitajima and Jurgen Kurths. Synchronized firing of fitzhugh–nagumo neurons by noise. *Chaos: An Interdisciplinary Journal of Nonlinear Science*, 15(2):023704, 2005.

[97] Henri Korn and Philippe Faure. Is there chaos in the brain? ii. experimental evidence and related models. *Comptes Rendus Biologies*, 326(9):787 – 840, 2003.

[98] Tanya Kostova, Renuka Ravindran, and Maria Schonbek. Fitzhughnagumo revisited: Types of bifurcations, periodical forcing and stability regions by a lyapunov functional. *International Journal of Bifurcation and Chaos*, 14(3):913, 2004.

[99] Yasutaka Kurata, Ichiro Hisatome, Sunao Imanishi, and Toshishige Shibamoto. Dynamical description of sinoatrial node pacemaking: improved mathematical model for primary pacemaker cell. *American Journal of Physiology - Heart and Circulatory Physiology*, 283(5):H2074–H2101, 2002.

[100] Yuri A. Kuznetsov. *Elements of Applied Bifurcation Theory.* Springer, 2 edition, 1998.

[101] Daniel Lazard and Fabrice Rouillier. Solving parametric polynomial systems. *J. Symb. Comput.*, 42(6):636–667, 2007.

[102] Xiumin Li, Jiang Wang, and Wuhua Hu. Effects of chemical synapses on the enhancement of signal propagation in coupled neurons near the canard regime. *Phys. Rev. E*, 76:041902, Oct 2007.

[103] D. S. Lindblad, C. R. Murphey, J. W. Clark, and W. R. Giles. A model of the action potential and underlying membrane currents in a rabbit atrial cell. *American Journal of Physiology - Heart and Circulatory Physiology*, 271(4):H1666–H1696, 1996.

[104] Cecilia W. Lo. Role of gap junctions in cardiac conduction and development : Insights from the connexin knockout mice. *Circulation Research*, 87(5):346–348, 2000.

[105] Federico Lombardi. Chaos theory, heart rate variability, and arrhythmic mortality. *Circulation*, 101(1):8–10, 2000.

[106] A. Longtin. Synchronization of the stochastic fitzhugh-nagumo equations to periodic forcing. *Il Nuovo Cimento D*, 17(7-8):835–846, 1995.

[107] CH Luo and Y Rudy. A model of the ventricular cardiac action potential. depolarization, repolarization, and their interaction. *Circulation Research*, 68(6):1501–1526, 1991.

[108] CH Luo and Y Rudy. A dynamic model of the cardiac ventricular action potential. i. simulations of ionic currents and concentration changes. *Circulation Research*, 74(6):1071–1096, 1994.

[109] Peter W. Macfarlane et al. *Comprehensive Electrocardiology*. Springer, second edition, November 2010.

[110] Jaakko Malmivuo and Robert Plonsey. *Bioelectromagnetism: Principles and applications of Bioelectric and Biomagnetic Fields*. Oxford University Press, 1995.

[111] Matteo E. Mangoni, Achraf Traboulsie, Anne-Laure Leoni, Brigitte Couette, Laurine Marger, Khai Le Quang, Elodie Kupfer, Anne Cohen-Solal, Jos Vilar, Hee-Sup Shin, Denis Escande, Flavien Charpentier, Jol Nargeot, and Philippe Lory. Bradycardia and slowing of the atrioventricular conduction in mice lacking cav3.1/1g t-type calcium channels. *Circulation Research*, 98(11):1422–1430, 2006.

[112] G. Marmont. Studies on the axon membrane; a new method. *The Journal of Cellular Physiology*, 34(4), December.

[113] L. Jr. Marple. Computing the discrete-time analytic signal via fft.

[114] Satoshi Matsuoka, Nobuaki Sarai, Shinobu Kuratomi, Kyoichi Ono, and Akinori Noma. Role of individual ionic current systems in ventricular cells hypothesized by a model study. *The Japanese Journal of Physiology*, 53(2):105–123, 2003.

[115] Donald C. Michaels, Dante. R. Chialvo, Edward P. Matyas, and Jose Jalife. Dynamics of synchronization in the sinoatrial node. *Annals of the New York Academy of Sciences*, 591:154–165, 1990.

[116] Donald C. Michaels, Edward P. Matyas, and Jose Jalife. Dynamical interactions and mutual synchronization of sinoatrial node pacemaker cells. a mathematical model. *Circulation Reasearch*, 58:706–720, 1986.

[117] J.N. Mills, D.S. Minors, and J.M. Waterhouse. The circadian rhythms of human subjects without timepieces or indication of the alternation of day and night. *The Journal of Physiology*, 240(3):567–594, 1974.

[118] R. E Mirollo and S. H. Strogatz. Synchronization of pulse-coupled biological oscillators. *SIAM Journal of Applied Mathematics*, 50:1645–1662, 1990.

[119] J. Nagumo, S. Arimoto, and S. Yoshizawa. An active pulse transmission line simulating nerve axon. *Proceedings of the IRE*, 50.

[120] Alexander Neiman, Lutz Schimansky-Geier, Ann Cornell-Bell, and Frank Moss. Noise-enhanced phase synchronization in excitable media. *Phys. Rev. Lett.*, 83:4896–4899, Dec 1999.

[121] Le Hoa Nguyen and Keum-Shik Hong. Synchronization of coupled chaotic fitzhugh-nagumo neurons via lyapunov functions. *Mathematics and Computers in Simulation*, 82(4):590 – 603, 2011.

[122] D. Noble, D. DiFrancesco, and J. C. Denyer. *Ionic mechanisms in normal and abnormal cardiac pacemaker activity: J.W. Jacklet Neuronal and Cellular Oscillators.*

[123] D. Noble and S. J. Noble. A model of sino-atrial node electrical activity based on a modification of the difrancesco–noble (1984) equations. *Proceedings of the Royal Society of London. Series B, Biological Sciences*, 222(1228):pp. 295–304, 1984.

[124] D. NOBLE, S. J. NOBLE, G. C. L. BETT, Y. E. EARM, W. K. HO, and I. K. SO. The role of sodium - calcium exchange during the cardiac action potentiala. *Annals of the New York Academy of Sciences*, 639(1):334–353, 1991.

[125] D. Noble, A. Varghese, P. Kohl, and P. Noble. Improved guinea-pig ventricular cell model incorperating a diadic space, i_{Kr} and i_{Ks}, and length- and tension-dependent processes. *The Canadian Journal of Cardiology*, 14(1):123–134, 1998.

[126] C. Nordin. Computer model of membrane current and intracellular ca2+ flux in the isolated guinea pig ventricular myocyte. *American Journal of Physiology - Heart and Circulatory Physiology*, 265(6):H2117–H2136, 1993.

[127] A. Nygren, C. Fiset, L. Firek, J. W. Clark, D. S. Lindblad, R. B. Clark, and W. R. Giles. Mathematical model of an adult human atrial cell : The role of k+ currents in repolarization. *Circulation Research*, 82(1):63–81, 1998.

[128] Yuri V. Panchin. Evolution of gap junction protiens - the pannexin alternative.

[129] Sandeep V. Pandit, Robert B. Clark, Wayne R. Giles, and Semahat S. Demir. A mathematical model of action potential heterogeneity in adult rat left ventricular myocytes. *Biophysical Journal*, 81(6):3029 – 3051, 2001.

[130] Joel S. Pearlmutter and Jonathan W. Mink. Deep brain stimulation.

[131] Louis M. Pecora and Thomas L. Carroll. Synchronization in chaotic systems. *Phys. Rev. Lett.*, 64:821–824, Feb 1990.

[132] Pauline Phelan. Innexins members of an evolutionary conserved family of gap-junction protiens.

[133] Arkady Pikovsky, Michael Rosenblum, and Kurths Jurgen. *Synchronization: A Universal Concept in Nonlinear Sciences*. Cambridge University Press, November 2001.

[134] Arkady Pikovsky, Michael Rosenblum, and Kurths J´urgen Kurths. *Synchronization A universal concept in nonlinear sciences*. Cambridge University Press, first edition, May 2003.

[135] B. Van Der Pol. The heartbeat condifered as a relaxation oscillator and an electrical mode of the heart. *The London Edinburgh and Dublin Philosophical Magazine and Journal of Science*, 7(6):763–775, 1928.

[136] B. Van Der Pol. Le battement du coeur considr comme oscillation de relaxation et un modle lectronique du coeur. *L'Onde electrique*, 7:365–392, September 1928.

[137] Victor. V Prasolov and Dimitry Leites. *Polynomials (Algorithms and Computation in Mathematics, Vol. 11)*. Springer, 1 edition, November.

[138] Leo Priebe and Dirk J. Beuckelmann. Simulation study of cellular electric properties in heart failure. *Circulation Research*, 82(11):1206–1223, 1998.

[139] Jos L. Puglisi and Donald M. Bers. Labheart: an interactive computer model of rabbit ventricular myocyte ion channels and ca transport. *American Journal of Physiology - Cell Physiology*, 281(6):C2049–C2060, 2001.

[140] Mindaugas Rackauskas, Maria M. Kreuzberg, Mindaugas Pranevicius, Klaus Willecke, Vytas K. Verselis, and Feliksas F. Bukauskas. Gating properties of heterotypic gap junction channels formed of connexins 40, 43, and 45. *Biophysical journal*, 92(6):1952–1965, 2007.

[141] S. Rajasekar and M. Lakshmanan. Bifurcation, chaos and suppression of chaos in fitzhugh-nagumo nerve conduction model equation. *Journal of Theoretical Biology*, 166(3):275 – 288, 1994.

[142] S. Rajasekar, K. Murali, and M. Lakshmanan. Control of chaos by nonfeedback methods in a simple electronic circuit system and the fitzhugh-nagumo equation. *Chaos, Solitons & Fractals*, 8(9):1545 – 1558, 1997. ¡ce:title¿Controlling Chaos¡/ce:title¿.

[143] Rafael J. Ramirez, Stanley Nattel, and Marc Courtemanche. Mathematical analysis of canine atrial action potentials: rate, regional factors, and electrical remodeling. *American Journal of Physiology - Heart and Circulatory Physiology*, 279(4):H1767–H1785, 2000.

[144] Irmantas Ratas and Kestutis Pyragas. Pulse propagation and failure in the discrete fitzhugh-nagumo model subject to high-frequency stimulation. *Phys. Rev. E*, 86:046211, Oct 2012.

[145] Muhammad Rehan and Keum-Shik Hong. Lmi-based robust adaptive synchronization of fitzhughnagumo neurons with unknown parameters under uncertain external electrical stimulation. *Physics Letters A*, 375(15):1666 – 1670, 2011.

[146] Daniel S. Reich, Ferenc Mechler, Keith P. Purpura, and Jonathan D. Victor. Interspike intervals, receptive fields, and information encoding in primary visual cortex. *The Journal of Neuroscience*, 20(5):1964–1974, 2000.

[147] V.L. Roger. Heartdisease and stroke statistics – 2011 update. *Circulation: American Heart Associateion*, 123:e18–e209, 2011.

[148] Michael G. Rosenblum and Arkady S. Pikovsky. Controlling synchronization in an ensemble of globally coupled oscillators. *Phys. Rev. Lett.*, 92:114102, Mar 2004.

[149] Alexander. S. et al. Guide to receptors and channels (grac), 3rd edition. *British Journal of Pharmacology*, 153:S1–S209, 2008.

[150] Nobuaki Sarai, Satoshi Matsuoka, Shinobu Kuratomi, Kyoichi Ono, and Akinori Noma. Role of individual ionic current systems in the sa node hypothesized by a model study. *The Japanese Journal of Physiology*, 53(2):125–134, 2003.

[151] Stanley J. Sarnoff. Myocardial contractility as described by ventricular function curves; observations on starling's law of the heart. *Physiological Reviews*, 35(1):107–122, January 1955.

[152] Karin Schirrmacher, S.V Ramanan, Kerry Cronin, Elizabeth Peterson, and Peter R Brink. Voltage sensitivity of gap junction currents in rat osteoblast-like cells. *Biochimica et Biophysica Acta (BBA) - Biomembranes*, 1327(1):89 – 96, 1997.

[153] E. Schneidman, W. Bialek, and M. Berry. An information theoretic approach to the functional classification of neuron. *Advances of Neural Information Processing Systems*, 15:197–204, 2002.

[154] D.F. Scollan, Alex Holmes, Raimond Winslow, and John Forder. Histological validation of myocardial microstructure obtained from diffusion tensor magnetic resonance imaging. *American Journal of Physiology: Heart and Circulatory Physiology*, 275(6):H2308–H2318, 1998.

[155] Nicholas J. Severs, Stephen Rothery, Emmanuel Dupont, Steven R. Coppen, Hung-I Yeh, Yu-Shien Ko, Tsutomu Matsushita, Riyaz Kaba, and Deborah Halliday. Immunocytochemical analysis of connexin expression in the healthy and diseased cardiovascular system. *Microscopy Research and Technique*, 52(3):301–322, 2001.

[156] Thomas R. Shannon, Fei Wang, Jos Puglisi, Christopher Weber, and Donald M. Bers. A mathematical treatment of integrated ca dynamics within the ventricular myocyte. *Biophysical Journal*, 87(5):3351 – 3371, 2004.

[157] Jonathan Y. Shih, Craig A. Atencio, and Christoph E. Schreiner. Improved stimulus representation by short interspike intervals in primary auditory cortex. *Journal of Neurophysiology*, 105(4):1908–1917, 2011.

[158] Yuji Shinohara, Takashi Kanamaru, Hideyuki Suzuki, Takehiko Horita, and Kazuyuki Aihara. Array-enhanced coherence resonance and forced dynamics in coupled fitzhugh-nagumo neurons with noise. *Phys. Rev. E*, 65:051906, May 2002.

[159] D.C. Sigg, P.A Laizzo, Y-F. Xiao, and B. He. *Cardiac Electrophysiology Methods and Models*. Springer, first edition, 2010.

[160] Alexander M. Simon and Daniel A. Goodenough. Diverse functions of vertebrate gap junctions. *Trends in Cell Biology*, 8(12):477–483, 1998.

[161] C. A. Skarda and W. J. Freeman. How brains make chaos in order to make sense of the world. *Behavioral and Brain Sciences*, 10(2):161–195, 1987.

[162] Richard S. Snell. *Clinical Neuroanatomy*. Lippincott Williams & Wilkins, seventh edition, January 2009.

[163] Goran Söhl and Klaus Willecke. Gap junctions and the connexin protein family. *Cardiovascular Research*, 62(2):228–232, 2004.

[164] Madison S. Spach, J. Francis Heidlage, Paul C. Dolber, and Roger C. Barr. Electrophysiological effects of remodeling cardiac gap junctions and cell size : Experimental and model studies of normal cardiac growth. *Circulation Research*, 86(3):302–311, 2000.

[165] Nicolas J Stapelberg, Ian Hamilton-Craig, David L Neumann, David HK Shum, and Harry McConnell. Mind and heart: Heart rate variability in major depressive disorder and coronary heart disease - a review and recommendations. *Australian and New Zealand Journal of Psychiatry*, 46(10):946–957, 2012.

[166] Andrzei Stefanski. *Determining Thresholds of Complete Synchronization, and Application*. World Scientific Publishing Company, first edition, June 2009.

[167] Lawrence Steinman. Multiple sclerosis: a two-stage disease. *Nature Immunology*, 2:762–764, 2001.

[168] Steven Strogatz. *Sync: The Emerging Science of Spontaneous Order*. Hyperion, first edition, March 2003.

[169] K. H. W. J. ten Tusscher, D. Noble, P. J. Noble, and A. V. Panfilov. A model for human ventricular tissue. *American Journal of Physiology - Heart and Circulatory Physiology*, 286(4):H1573–H1589, 2004.

[170] K. H. W. J. ten Tusscher and A. V. Panfilov. Alternans and spiral breakup in a human ventricular tissue model. *American Journal of Physiology - Heart and Circulatory Physiology*, 291(3):H1088–H1100, 2006.

[171] C. J. Tessone, A. Scirè, R. Toral, and P. Colet. Theory of collective firing induced by noise or diversity in excitable media. *Physical Review E*, 75(1):016203, 2007.

[172] Marjaana Tiainen, Hannu J. Parikka, Markku A. Makijarvi, Olli S. Takkunen, Seppo J. Sarna, and Risto O. Roine. Arrhythmias and heart rate variability during and after therapeutic hypothermia for cardiac arrest. *Critical Care Medicine*, 37(7):403–409, 2009.

[173] Andrey N. Tikhonov. Systems of differential equations containing small parameters in the derivatives. *Mathematical Sbornik*, 31(73)(3):575–586, 1952.

[174] Ral Toral, C Masoller, Claudio R Mirasso, M Ciszak, and O Calvo. Characterization of the anticipated synchronization regime in the coupled fitzhughnagumo model for neurons. *Physica A: Statistical Mechanics and its Applications*, 325(12):192 – 198, 2003. ¡ce:title¿Stochastic Systems: From Randomness to Complexity¡/ce:title¿.

[175] Mark L. Trew et al. Cardiac electrophysiology and tissue structure: bridging the scale gap with a joint measurement and modelling paradigm. *Experimental Physiology*, 91(2):355–370, 2006.

[176] E B Trexler, M V Bennett, T A Bargiello, and V K Verselis. Voltage gating and permeation in a gap junction hemichannel. *Proceedings of the National Academy of Sciences*, 93(12):5836–5841, 1996.

[177] Yasuhiro Tsubo, Yoshikazu Isomura, and Tomoki Fukai. Power-law inter-spike interval distributions infer a conditional maximization of entropy in cortical neurons. *PLoS Comput Biol*, 8(4):e1002461, 04 2012.

[178] D. Ungar and FM Hughson. Snare protein structure and function. *Annual Reviews of Cell and Developmental Biology*, 19:493–517, 2003.

[179] Vinzenz M. Unger, Nalin M. Kumar, Norton B. Gilula, and Mark Yeager. Three-dimensional structure of a recombinant gap junction membrane channel.

[180] Toon A.B. van Veen, Harold V.M. van Rijen, and Tobias Opthof. Cardiac gap junction channels: modulation of expression and channel properties. *Cardiovascular Research*, 51(2):217–229, 2001.

[181] Richard D. Veenstra. Size and selectivity of gap junction channels formed from different connexins. *Journal of Bioenergetics and Biomembranes*, 28(4):327–337, 1996.

[182] V. Veliov. A generalization of the tikhonov theorem for singularly perturbed differential inclusions. *Journal of Dynamical and Control Systems*, 3(3):291–319, 1997.

[183] E. E. Verheijick et al. Pacemaker synchronization of electrically coupled rabbit sinoatrial node cells. *Journal of general Physiology*, 111(1):95–112, 1998.

[184] Sander Verheule, Marjan J. A. van Kempen, Pascal H. J. A. te Welscher, Brenda R. Kwak, and Habo J. Jongsma. Characterization of gap junction channels in adult rabbit atrial and ventricular myocardium. *Circulation Research*, 80(5):673–681, 1997.

[185] K. Vibe, J-M. Vesin, and E. Pruvot. Chaos and heart rate variability. *Engineering in Medicine and Biology Society, 1995., IEEE 17th Annual Conference*, 2:1481–1482, 1995.

[186] Jiang Wang, Zhen Zhang, and Huiyan Li. Synchronization of fitzhughnagumo systems in {EES} via h_∞ variable universe adaptive fuzzy control. *Chaos, Solitons & Fractals*, 36(5):1332 – 1339, 2008.

[187] Linda R. Watkins and Steven F. Maier. Beyond neurons: Evidence that immune and glial cells contribute to pathological pain states. *Physiological Reviews*, 82(4):981–1011, 2002.

[188] Stephen Waxman. *Clinical Neuroanatomy*. McGraw-Hill Medical, twenty sixth edition, July 2009.

[189] M. Wechselberger. Existence and bifurcation of canards in r3 in the case of a folded node. *SIAM Journal on Applied Dynamical Systems*, 4(1):101–139, 2005.

[190] Du Qu Wei, Xiao Shu Luo, Bo Zhang, and Ying Hua Qin. Controlling chaos in space-clamped fitzhughnagumo neuron by adaptive passive method. *Nonlinear Analysis: Real World Applications*, 11(3):1752 – 1759, 2010.

[191] R Werner, E Levine, C Rabadan-Diehl, and G Dahl. Formation of hybrid cell-cell channels. *Proceedings of the National Academy of Sciences*, 86(14):5380–5384, 1989.

[192] PJ Whitehouse, DL Price, RG Struble, AW Clark, JT Coyle, and MR Delon. Alzheimer's disease and senile dementia: loss of neurons in the basal forebrain. *Science*, 215(4537):1237–1239, 1982.

[193] Stephen Wiggins. *Introduction to Applied Nonlinear Dynamical Systems and Chaos*. Springer, 2003.

[194] R. Wilders et al. Model clamp and its application to synchronization of rabbit sinoatrial node cells. *American journal of Physiology Heart and Circulatory Physiology*, 271(5):H2168–H2182, 1996.

[195] R. Wilders, H.J. Jongsma, and A.C. van Ginneken. Pacemaker activity of the rabbit sinoatrial node. a comparison of mathematical models. *Biophysical Journal*, 60(5):1202 – 1216, 1991.

[196] Stephen R Williams and Greg J Stuart. Mechanisms and consequences of action potential burst firing in rat neocortical pyramidal neurons. *The Journal of Physiology*, 521(2):467–482, 1999.

[197] Arthur T. Winfree. *The Geometry of Biological Time*. Springer, second edition, June 2001.

[198] Raimond L. Winslow, Jeremy Rice, Saleet Jafri, Eduardo Marbn, and Brian O'Rourke. Mechanisms of altered excitation-contraction coupling in canine tachycardia-induced heart failure, ii : Model studies. *Circulation Research*, 84(5):571–586, 1999.

[199] Francis X Witkowski, L. Joshua Leon, Patricia A. Penkoske, Wayne R. Giles, Mark L. Spano, William L. Ditto, and Arthur T. Winfree. Spatiotemporal evolution of ventricular fibrillation. *Nature*, 392:78–82, 1998.

[200] A. Wolf, J. B. Swift, H. L. Swinney, and J. A. Vastano. Determining Lyapunov exponents from a time series. *Physica D Nonlinear Phenomena*, 16:285–317, July 1985.

[201] Gary Yellen. The voltage-gated potassium channels and their relatives. *Nature*, 419:35–42, 2002.

[202] H. Zhang, A. V. Holden, I. Kodama, H. Honjo, M. Lei, T. Varghese, and M. R. Boyett. Mathematical models of action potentials in the periphery and center of the rabbit sinoatrial node. *American Journal of Physiology - Heart and Circulatory Physiology*, 279(1):H397–H421, 2000.

[203] HENGGUI ZHANG, ARUN V. HOLDEN, DENIS NOBLE, and MARK R. BOYETT. Analysis of the chronotropic effect of acetylcholine on sinoatrial node cells. *Journal of Cardiovascular Electrophysiology*, 13(5):465–474, 2002.

[204] Mauro Zordan, Rodolfo Costa, Giuseppe Macino, Chiaki Fukuhara, and Gianluca Tosini. Circadian clocks: What makes them tick? *Chronobiology International*, 17(4):433–451, 2000.